Springer Theses
Recognizing Outstanding Ph.D. Research

Yanrong Zhang

Study on Microstructure and Rheological Properties of Cement-Chemical Admixtures-Water Dispersion System at Early Stage

Springer

Springer Theses

Recognizing Outstanding Ph.D. Research

Aims and Scope

The series "Springer Theses" brings together a selection of the very best Ph.D. theses from around the world and across the physical sciences. Nominated and endorsed by two recognized specialists, each published volume has been selected for its scientific excellence and the high impact of its contents for the pertinent field of research. For greater accessibility to non-specialists, the published versions include an extended introduction, as well as a foreword by the student's supervisor explaining the special relevance of the work for the field. As a whole, the series will provide a valuable resource both for newcomers to the research fields described, and for other scientists seeking detailed background information on special questions. Finally, it provides an accredited documentation of the valuable contributions made by today's younger generation of scientists.

Theses are accepted into the series by invited nomination only and must fulfill all of the following criteria

- They must be written in good English.
- The topic should fall within the confines of Chemistry, Physics, Earth Sciences, Engineering and related interdisciplinary fields such as Materials, Nanoscience, Chemical Engineering, Complex Systems and Biophysics.
- The work reported in the thesis must represent a significant scientific advance.
- If the thesis includes previously published material, permission to reproduce this must be gained from the respective copyright holder.
- They must have been examined and passed during the 12 months prior to nomination.
- Each thesis should include a foreword by the supervisor outlining the significance of its content.
- The theses should have a clearly defined structure including an introduction accessible to scientists not expert in that particular field.

More information about this series at http://www.springer.com/series/8790

Yanrong Zhang

Study on Microstructure and Rheological Properties of Cement-Chemical Admixtures-Water Dispersion System at Early Stage

Doctoral Thesis accepted by
Tsinghua University, Beijing, China

Springer

Author
Dr. Yanrong Zhang
School of Civil Engineering
Beijing Jiaotong University
Beijing
China

Supervisor
Associate Prof. Dr. Xiang-Ming Kong
Department of Civil Engineering
Tsinghua University
Beijing
China

ISSN 2190-5053 ISSN 2190-5061 (electronic)
Springer Theses
ISBN 978-981-10-4569-1 ISBN 978-981-10-4570-7 (eBook)
DOI 10.1007/978-981-10-4570-7

Library of Congress Control Number: 2017946672

Printed on acid-free paper

This Springer imprint is published by Springer Nature
The registered company is Springer Nature Singapore Pte Ltd.
The registered company address is: 152 Beach Road, #21-01/04 Gateway East, Singapore 189721, Singapore

Supervisor's Foreword

As Yan-Rong Zhang's supervisor during her Ph.D. program, it is my pleasure to write this foreword for her dissertation, accepted for publication within the Springer Theses book series.

Dr. Zhang started her Ph.D. program in August 2009 at the Department of Civil Engineering in Tsinghua University. During her Ph.D. program, she exhibited high self-motivation, outstanding ingenuity and persistent diligence. She received a number of scholarships and awards over the course of the four year Ph.D. program in Tsinghua University and one visiting year in University College London (UCL), among which most valuable ones include the National Scholarship of China and CSC (China Scholarship Council) Research Student Visiting Awards in UCL that was awarded to only two students each year with great academic potential. She has also been actively participating in international academic activities by presenting her work at several international conferences. In January 2015, she graduated with top honors from Tsinghua University.

This dissertation was designed to establish the correlation between the rheological properties and microstructure of fresh cement pastes. The workability and/or the rheological properties of fresh concrete is one of the most important properties of concrete both for casting at initial stage and even for performance during long-term service. In recent years, the rheological properties of fresh concrete could be tuned in a wide range in virtue of the advanced chemical admixture technology. Water soluble superplasticizers like polycarboxylate type superplasticizer, water dispersible admixtures such as polymer latexes and asphalt emulsions were within the scope of investigation as chemical admixtures. On the other hand, rheology is highly related to the microstructure of the mixtures. Therefore, the rheological properties and the microstructure of fresh cement pastes containing various chemical admixtures are the two main focuses of this research by using different microscopes for characterization of microstructure of fresh cement pastes and rheometer for rheological investigation. Adsorption of the admixtures on cement and retardation effects on cement hydration were given particular emphasis. In addition, the impacts of these admixtures on properties of hardened cementitious materials such like pore structure and permeability of hardened cement pastes were

also discussed, as it is believed that they are also related to the microstructure of fresh cement pastes.

The results of this dissertation bring a new insight into the working mechanisms of chemical admixtures in cementitious materials and lay a theoretical foundation for further development of chemical admixture technology as well as for the practical applications of chemical admixtures in concrete industry.

Beijing, China
May 2017

Associate Prof. Dr. Xiang-Ming Kong

Abstract

Superplasticizer has become one of the key components in modern concrete. Polymer latex is often used as cement mortars modifier to improve properties such as flexural strength, water proofing and so on. Cement asphalt mortar consisting of Portland cement and asphalt as co-binders, serves as a vibration-absorbing layer in the slab track system of railroad structures. Superplasticizers, polymer latexes and asphalt emulsions are regarded as chemical admixtures in this thesis. Their addition has substantially changed the workability of cement-based materials. However, fundamental research on their effects and working mechanisms largely lags behind industry development and engineering application, which has become the neck bottle for further development of new chemical admixtures and cement-based composites with higher performance.

Rheological properties are major elements of the workability of cement-based materials and closely related to the microstructure. This thesis aims at revealing the correlation of rheological properties with microstructure of cement-based materials. Superplasticizers, polyacrylate latexes and asphalt emulsions, which differ in molecular/particle size from nanometer to micron, were employed to study their effects on the rheological properties of fresh cement pastes (FCPs) and working mechanism. Fluidity, yield stress and plastic viscosity of FCPs at various superplasticizer to cement ratios (Sp/Cs), water to cement ratio (W/Cs), temperature (T) and elapsed time (t) were measured. The viscoelastic properties were also estimated by a microrheometer. Optical microscope was used to directly observe the microstructure of FCPs and the correlation of microstructure with fluidity of FCPs was established. Polymers with different molecular structures were chosen to investigate their adsorption by total organic carbon, zeta potential tests and their retardation effects by isothermal calorimetry, in order to disclose their working mechanisms. Based on the microstructure observation and the working mechanism of chemical admixtures, a generalized microstructure model was proposed. Relative hydration degree was introduced to indicate the evolution of rheological properties and two models were developed. Rheological equations including Sp/C, W/C, T and t were also deduced. The effects of chemical admixtures on the pore structure and impermeability of hardened cement pastes were elucidated.

Results indicate that chemical admixtures change the rheological behaviors through the disassembly of flocculated cement grains by their adsorption. The addition of latexes and asphalt emulsions could increase the volume fraction of solid phase and further affect the rheological properties. As a reactive system, FCP undergoes a continuous change on the microstructure due to hydration and consequently the rheological properties continuously develop over time. The changes of rheological properties with T and t originate from the development of hydration degree. Moreover, the stability of latex and asphalt emulsion also results in the changes of rheological properties.

The main contributions of this thesis are summarized as follows. 1) The effects of W/C, Sp/C, T and t on the rheological behaviors of FCPs were investigated and were formulated into two rheological equations. 2) The microstructure of FCPs was analyzed quantitatively, and the correlation of microstructure with rheological properties was established. 3) The adsorption behaviors of polycarboxylate polymers with different functional groups and their effects on cement hydration were elucidated. 4) The different working mechanism of NSF from that of PCE superplasticizer was revealed. 5) Relative hydration degree was introduced to indicate the coupled effects of the temperature and time on rheological properties. 6) A conceptual microstructure-rheology model was developed. All of these new findings may lend theoretical supports to the development of new chemical admixtures and new cement-based composites with higher performance.

Keywords Superplasticizer · Polyacrylate latex · Asphalt emulsion · Microstructure of fresh cement paste · Rheological properties

Publications and Key Presentations Arising from this Research

Articles in Referred Journals

[1] Zhang Y.R., Kong X.M., Lu Z.B., et al. Effects of the charge characteristics of polycarboxylate superplasticizers on the adsorption and the retardation in cement pastes. Cement and Concrete Research, 2015, 67: 184–196.

[2] Zhang Y.R., Kong X.M. Correlations of the dispersing capability of NSF and PCE type superplasticizers and their impacts on cement hydration with the adsorption in fresh cement pastes. Cement and Concrete Research, 2015, 69: 1–9.

[3] Zhang Y.R., Kong X.M., Gao L., et al. In-situ measurement of viscoelastic properties of fresh cement paste by a microrheology analyzer. Cement and Concrete Research 2016, 79: 291–300.

[4] Zhang Y.R., Kong X.M., Hou S.S., et al. Study on the rheological properties of fresh cement asphalt paste. Construction and Building Material, 2012, 37(1): 534–544.

[5] Zhang Y.R., Kong X.M. Influences of superplasticizer, polymer latexes and asphalt emulsions on the pore structure and impermeability of hardened cementitious materials. Construction and Building Materials, 2014, 53(28): 392–402.

[6] Zhang Y.R., Kong X.M., Gao L., et al. Characterization of the mesostructural organization of cement particles in fresh cement paste. Construction and Building Materials, 2016, 124: 1038–1050.

[7] Zhang Y.R., Kong X.M. Influences of PCE superplasticizer on the pore structure and the impermeability of hardened cementitious materials. Journal of Advanced Concrete Technology, 2014, 12: 443–455.

[8] Zhang Y.R., Kong X.M., Gao L., et al. Microstructure model of fresh cement paste in the presence of superplasticizer. ZKG International, 2015, 68(10): 36–46.

[9] Zhang Y.R., Kong X.M., Gao L., et al. Rheological behaviors of fresh cement pastes with polycarboxylate superplasticizer. Journal of Wuhan University of Technology, Materials Science, 2016, 31(2): 286–299.

[10] Zhang Y.R., Kong X.M., Gao L., et al. Variations of yield stress of fresh cement pastes in the presence of superplasticizer highlighted by a hydration index. Journal of Materials in Civil Engineering, 2017, 29(2): 1–12.

[11] Zhang Y.R., Kong X.M., Cao E.X., et al. Effects of temperatures on flowability of fresh cement asphalt pastes and cement hydration. Journal of the Chinese Ceramic Society, 2010, 38(11): 156–161. (in Chinese)

[12] Zhang Y.R., Kong X.M., Gao L. Microstructure and flowability of fresh cement pastes in varied dispersion media. 2016, 44(8): 1103–1108. (in Chinese)

Articles in Refereed Proceedings

[1] Zhang Y.R., Kong X.M. In situ measurement of viscoelastic properties of fresh cement paste by a microrheology analyzer. The 14th International Congress on the Chemistry of Cement, Beijing, China, 2015.10.

[2] Zhang Y.R., Kong X.M., Wang J.X. Rheological properties of fresh cement pastes with polycarboxylate superplasticizers. 1st International RILEM Conference on Rheology and Processing of Construction Materials, Paris, France, 2013.09.

[3] Zhang Y.R., Kong X.M. Correlations between adsorption and dispersing capability, impact on cement hydration of PCE and PNS type superplasticizers in fresh cement pastes. The 8th International Symposium on Cement & Concrete (ISCC2013), Nanjing, China, 2013.09.

[4] Zhang Y.R., Kong X.M., Zhang Z.L. Influences of chemical admixtures with different sizes on pore structure and impermeability of the hardened cement. Asian Symposium on Polymers in Concrete, Istanbul, Turkey, 2012.10.

Acknowledgements

I would like to express my utmost gratitude to my supervisor Prof. Xiang-Ming Kong for all his invaluable help and endless encouragement throughout this research.

My sincere thanks also go to Prof. Pei-Yu Yan, Prof. Jun Zhang, Prof. Ke-Fei Li, Prof. Ya Wei and Prof. Qiang Wang for their helpful valuable assistance and advice throughout the years. My thanks also go to Prof. Yun Bai in University College London (UCL) and Jian-Guo Han for their help in providing valuable data for this research.

This work was made possible through funding provided by the National Natural Science Foundation of China (No. 51173094 and No. 50802050), whose generous support I would like to acknowledge. I would also like to thank the Chinese Scholarship Council and University College London for providing the funding that enabled me to visit UCL during my Ph.D. program.

A part of this research was undertaken in participation with industry, I would therefore like to thank Antai Technology Company who kindly offered their equipment, support and feedback, especially, Yang Chang and Ming Li.

My gratitude and wishes go to all my Ph.D. room colleagues, whose dedication to their work I greatly admire and friendship throughout the years I sincerely appreciate, and to all my extended family for their constant support.

Finally, I would like to thank my parents and my fiance, Zhen-Hua Wei for the tremendous amount of help, support and patience, especially during the past few months.

Contents

Abbreviations and Symbols

A/C	Mass ratio of asphalt to cement
AA	Acrylic acid
AAE	Anionic asphalt emulsion
AFM	Atomic force microscopy
Afm	Calcium aluminate monosulphate
Aft	Ettringite
AMPS	2-acrylamido-2-methylpropane sulfonic acid
APS	Ammonium persulfate
AW	Adsorption water
C-A	Cement-air
CAE	Cationic asphalt emulsion
CAM	Cement asphalt mortar
C-E	Cement-ethanol
C-EW	Cement-ethanol and water
C-E + C-W	Cement-ethanol and cement-water
C-W	Cement-water
C-W-A	Cement-water-asphalt
C-W-L	Cement-water-latex
C-W-N	Cement-water-NSF superplasticizer
C-W-P	Cement-water-PCE superplasticizer
Dc	Critical dosage
Dpd	Fractal dimension of particle spatial distribution
Dsp	Dosage of superplasticizer
DWS	Diffusing wave spectroscopy
EEW	Released entrapped water by superplasticizers
EI	Elastic index
ESEM	Environmental scanning electron microscope
EW	Entrapped water
FCP	Fresh cement paste
FTIR	Fourier transform infrared spectrum

FW	Free water
HCP	Hardened cement paste
HPC	High performance concrete
HW	Hydration water
L/C	Mass ratio of latex to cement
LS	Light scattering
MAPTAC	[3-(methacryloylamino) propyl] trimethyl ammonium chloride
MIP	Mercury intrusion porosimetry
MPEGMA	Methyl polyethylene glycol methacrylate
MSD	Mean square displacement
MVI	Macroscopic viscosity index
NSF	Naphthalene formaldehyde condensates
P/C	Mass ratio of polymer to cement
PAA	Poly(acrylic acid)
PAM	Amphoteric co-polymers
PAS	Co-polymers containing $-COO^-$ groups and $-SO_3^-$ groups
PCE	Polycarboxylate
PDI	Polydispersity
PMAPTAC	Poly ([3-(methacryloylamino) propyl] trimethyl ammonium chloride)
PSSS	Poly (sodium p-styrene sulfonate)
REW	Remaining entrapped water
Rf	Retention factor
RI	Refractive index
SEC	Size exclusion chromatography
SEM	Scanning electron microscope
SMAS	Sodium methyl acryl sulfonate
Sp/C	Mass ratio of superplasticizer to cement
SSS	Sodium p-styrene sulfonate
TEM	Transmission electron microscope
TOC	Total organic carbon
XRD	X-ray diffraction
W/C	Mass ratio of water to cement
G	The elastic modulus of spring in Maxwell model
η	The viscosity of dashpot in Maxwell model
G'	Storage modulus
G''	Loss modulus
τ_0	Yield stress
μ_p	Plastic viscosity
ϕ	Volume fraction of solid phase
ϕ_M	Maximum volume fraction of solid phase
t	Elapsed time
T	Temperature

Chapter 1
Introduction

1.1 Research Background

Concrete is regarded as a key material to satisfy the requirements in the global housing and modern infrastructure (Wu and Lian 1999). Currently, the annual global cement production has reached 4.0 billion tons and the corresponding concrete production is more than 10 billion cubic meters (China Cement Information Center 2014). With the increasing amount of infrastructure projects over the world, especially in developing countries, the production of cement and concrete is expected to increase at a stable rate per year.

Compared with other building materials, concrete is characterized with the advantages of ample raw materials and low cost etc. More importantly, it is featured as superior workability, mechanical properties and durability. Currently, high performance concrete (HPC) has been widely used in the construction industry for its excellent properties (Aïtcin 2011). The excellent properties of HPC are closely associated with the incorporation of chemical admixtures, especially the superplasticizers and polymer latexes. By adding superplasticizers, the rheological properties of fresh cementitious materials can be significantly improved (Bian and Shen 2006; Kasami et al. 1979; Malhotra 1989, 1999; Miao et al. 2009). This not only can satisfy the construction requirements, but also can help to achieve at the higher strength and durability for its lower water to cement ratio (W/C) (Gagn et al. 1996; Gao et al. 2001; Houst et al. 2008; Swamy 1989). Polymer latexes are often used as cement mortars and concrete modifiers, which can improve the properties of mortars and concrete, such as adhesion, fracture toughness, flexural strengths, crack resistance and waterproof (Barluenga and Hernández-Olivares 2004; Huang et al. 1999; Kong et al. 2013a, b; Li and Kong 2009; Ohama 1987; Saija 1995; Wang et al. 2005; Wang et al. 2008a, b, c, d, e; Yang et al. 2009; Ye et al. 2012). Thus, chemical admixtures have become indispensable components for HPC besides cement, water and aggregates (Qian et al. 2002).

Y. Zhang, *Study on Microstructure and Rheological Properties of Cement-Chemical Admixtures-Water Dispersion System at Early Stage*, Springer Theses, DOI 10.1007/978-981-10-4570-7_1

Additionally, cement asphalt mortar (CAM) can be used as the cushion layer between the track slab and the concrete bed of ballastless slab track structures for high speed railways (Hu et al. 2012; Liu et al. 2011, 2012a, b; Wang et al. 2011). It is one type of inorganic-organic composite material, which consists of Portland cement, asphalt emulsion, water, fine aggregates and other admixtures (Kong et al. 2010a, b; Liu et al. 2009; Zhang et al. 2010). With its high elasticity and suitable toughness, hardened CAM serves as a vibration-absorbing layer in the slab track structure during operation; its properties impose a significant influence on the slab track performance. In reality, CAM is mixed on site and casted into a relatively narrow space; thus, fresh CAM must possess adequate workability to ensure the successful construction (Cao et al. 2012; Kong et al. 2011; Wang et al. 2008a, b; Yang et al. 2010a, b). Furthermore, the workability of fresh CAM also affects the strength and durability of hardened CAM considerably. As an essential component, asphalt emulsion can greatly influence the properties of fresh CAM and hardened CAM.

To sum up, it is the incorporation of various chemical admixtures in concrete and the asphalt emulsion in CAM that fundamentally brings about the improvement on the properties of cement mortars and concrete (hereinafter referred to as cementitious materials), particularly on the workability. Workability is considered as one of the most important properties of cementitious materials because it directly influences the construction process of fresh cementitious materials and even the mechanical properties and durability of hardened ones. The workability is an assembly of several properties such as fluidity, plasticity, stability and cohesion (Huang and Xie 1984). There is an extensive research working on the workability through evaluating the rheological properties of blank fresh cementitious materials (Banfill 1994; Flatt et al. 2004; Hu and de Larrard 1996; Huang 1980; Schwartzentruber et al. 2006). Nevertheless, due to the presence of various chemical admixtures in HPC, the rheology theory of traditional cementitious materials may no longer be suitable for the modern cementitious materials (Banfill 2003; Li and Kong 2009; Zhang et al. 2012). For a long time, the scientific research has been significantly lagged behind the development of industry, so that the influence mechanism of various chemical admixtures and asphalt emulsion on the rheological properties and workability of cementitious materials has not been fully investigated and clarified so far, which has become a main obstacle to both further development of chemical admixture technology and the practical applications of chemical admixtures in the HPC. Therefore, it is necessary, both practically and scientifically, to carry out an in-depth research on the fundamental theory about the interactions between cement and chemical admixtures as well as asphalt emulsions and on the rheological properties of fresh cementitious materials, with the aim of developing new chemical admixtures with more efficient and robust performance and further improving the workability of HPC.

In this research, superplasticizers, polymer latexes and asphalt emulsions are chosen to investigate their effects on rheological properties of fresh cementitious materials. These polymers, which are widely used in cementitious materials, have different molecular/particle sizes and dosages in practice. Superplasticizers usually

have a hydraulic radius of 5–20 nm in aqueous solution and the common dosage is lower than 1%. The particle size of polymer latexes ranges from 100 to 1000 nm and the usual dosage is from 1 to 10%, while the particle size of asphalt emulsions is in the range of 1–10 μm with the dosage in CAM of more than 20%. We need to emphasize that chemical admixtures usually refer to the chemical substances added in cementitious materials to dramatically improve the properties of materials with the dosage of less than 5%. Although the content of asphalt in CAM is relatively larger, its mechanism is believed to have characteristics in common with that of superplasticizers and polymer latexes. Thus, asphalt emulsion is regarded as a special type of chemical admixture in this research. Moreover, aggregates in concrete and cement mortars could be regarded as chemically inert and seldom be affected by the chemical admixtures (Kong et al. 2013a, b; Sheinn et al. 2002). Hence, cement pastes were employed in this research to investigate the impacts of chemical admixtures on the rheological properties. The fresh cement pastes with chemical admixtures are defined as the Cement-Chemical admixtures-Water dispersion system, while the ones with superplasticizers, polymer latexes and asphalt emulsions respectively correspond to Cement-Superplasticizer-Water system, Cement-Latex-Water system and Cement-Asphalt-Water system in this research.

Furthermore, from a microscopic point of view, all these macroscopic properties of fresh cementitious mixtures are primarily determined by their microscopic structure (Barnes and Hutton 1989; Xu 1989). Much research has been dedicated to studying the microstructure of fresh cement paste (FCP) by means of microscopy and granulometry technique or establishing model, but the obtained information is far from being satisfied due to the low resolution and the limited measuring area of a regular microscope as well as the lacks of firm validations from experimental data (Autier et al. 2013; Wang et al. 2008a, b, c, d, e, 2013; Zhang et al. 2013). Quantitative characterization on the microstructure of FCPs remains as a challenge and the clear correlation of microstructure with rheological behaviors of FCPs has not been established.

From the above, we know that in order to essentially investigate the effects of chemical admixtures on the workability of fresh cementitious materials, it is necessary to conduct an in-depth research on the rheological properties and microstructure of Cement-Chemical admixtures-Water dispersion system as well as the inner correlation between them.

1.2 Objectives and Significances

This research aims at revealing the correlation of rheological properties with microstructure of FCPs. Superplasticizers, polyacrylate latexes and asphalt emulsions, which differ in molecular/particle size from nanometer to micron, were incorporated into the FCPs to evaluate their effects on rheological properties and the relevant working mechanisms.

(1) Fluidity, yield stress and plastic viscosity of FCPs at various superplasticizer to cement ratios (Sp/Cs), water to cement ratios (W/Cs), temperature (T) and elapsed time (t), were measured to discuss the rheological properties of FCPs containing various chemical admixtures. The viscoelastic properties were also measured by a microrheometer.
(2) Morphologi G3 with a high response sensitivity and resolution was employed to systematically explore the structural organization of cement grains in different dispersion media and to establish the correlation of mesostructure with macroscopic rheological properties. Meanwhile, environmental scanning electron microscope (ESEM) was adopted to qualitatively analyze the mesostructure of FCPs in the presence of superplasticizers, latexes and asphalt emulsions.
(3) Organic monomers possessing different charges, their corresponding homo-polymers and two series of self-synthesized comb-shaped co-polymers with varied charging groups in the backbone were chosen to investigate their adsorption behaviors in cement pastes and the impacts on cement hydration with the aim of analyzing the essence of adsorption and retardation. Furthermore, the adsorption behaviors of superplasticizers, latexes and asphalt emulsions and their impacts on cement hydration were discussed, for which, their working mechanisms were revealed.
(4) Based on the microstructure observation and the working mechanisms of chemical admixtures, a generic multi-scale microstructure model of FCPs was proposed. The relative hydration degree was introduced to indicate the evolution of rheological properties, based on which, and two models were further developed. Rheological equations including Sp/C, W/C, T and t were also deduced.
(5) The effects of superplasticizers, polymer latexes and asphalt emulsions on the pore structure of hardened cement pastes (HCPs) and the impermeability of hardened mortars were analyzed and the working mechanisms of chemical admixtures with different sizes were elucidated.

With the achievement of above objectives, this research is expected to bring novel insights into the act mode of chemical admixtures on the workability of cementitious materials and lay a theoretical basis for the further development of new superplasticizers and HPC with more efficient and robust performance. Additionally, by integrating the effects of all these influencing factors and deducing microstructural and rheological models, the current theory of rheology and microstructure of FCPs can be improved and enriched.

1.3 Literature Review

This research was intended to be conducted from four aspects: (1) the rheological properties of FCPs; (2) the microstructure of FCPs; (3) the working mechanisms of chemical admixtures; (4) the pore structure and impermeability of HCPs. For these

four aspects, an extensive literature review has been conducted. Based on the review, specific issues in existing literatures and the research gaps can be clearly identified.

1.3.1 Rheological Properties

First of all, as the starting point and the important background of this research, the basic knowledge on the rheology of suspension dispersion system was summarized. The current research on the rheological properties of FCPs was also comprehensively analyzed with an identification of existing problems.

1.3.1.1 Basic Theory of Rheology

In 1929, Professor Bingham founded the Society of Rheology. Since then, rheology has formally become an independent sub-discipline. Rheology involves the science of flow and deformation of all types of matter, which is subordinated to the mechanics but is theoretically different from it. In rheology, the focus is on correlating the microstructure of matters with their properties from the viewpoints of relative movement of particles in matters. Meanwhile, the concepts of the viscous flow, elastic deformation and plastic deformation of matter responding to external forces belong to the research scope of rheology, which are used to confirm the quantitative relationships of stress and time-dependent deformation of matter under external forces. The research on rheology was originated from 19th century. After a large amount of theoretical and experimental work on rheology during the past years, rheology has become a mature discipline and been widely applied in industry (Castro et al. 2013; Murray 2011; Rao 2014).

Fluids are a special subject in the research on rheology, whose flow behaviors and deformation under external forces at a certain temperature, humidity and pressure could be described by the relationship of shear stress (τ) and shear rate ($\dot{\gamma}$). According to the different relationships, the fluids could be classified into multiple types, as shown in Fig. 1.1 (Shi and Wu 2009).

(1) Newtonian fluids

Newtonian fluids are associated with easy deformation and the constant viscosity (η) at a fixed temperature regardless of shear rate. Their rheological properties are described by the equation $\tau = \eta\dot{\gamma}$. Newtonian fluids are considered as ideal viscous fluids, in which the particles are independent, namely there are no interactions between particles. Usually, an extremely diluted suspension dispersion system is regarded as the Newtonian fluid.

(2) Generalized Newtonian fluids

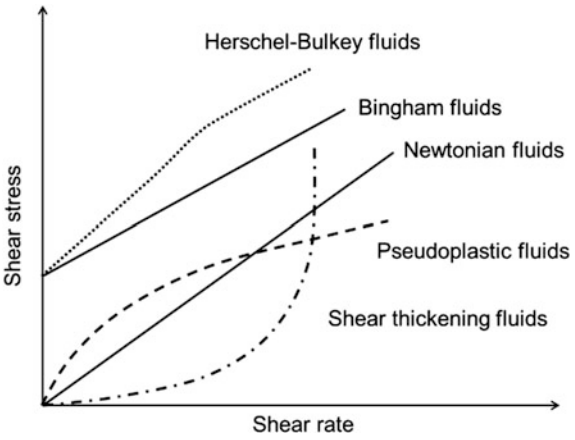

Fig. 1.1 Rheological curves of several typical fluids

Plastic fluids, pseudoplastic fluids and shear thickening fluids are concerned.

Plastic fluids: their shear stress versus shear rate flow curves have shown the existence of a yield stress (τ_0) by requiring an intercept on the shear stress axis. These indicate that the fluids cannot flow when the shear stress is lower than the yield stress but flows at higher stresses. During flow process, if the viscosity is constant and independent to the shear rate, their rheological properties could be described by Bingham equation $\tau = \tau_0 + \eta_p \dot{\gamma}$, where η_p denotes to the plastic viscosity. Plastic fluids are also referred to Bingham fluids. If the viscosity is a power law function of shear rate, the rheological properties are described by the Herchel–Bulkley equation $\tau = \tau_0 + K\dot{\gamma}^\mathrm{n}$, where k and n are the consistency and rate index respectively.

Pseudoplastic fluids: they are characterized as the easy deformation and the decreased viscosity with the increase of shear rate. Their rheological properties are described by the equation $\tau = K\dot{\gamma}^\mathrm{n}(0 < \mathrm{n} < 1)$. In industry, oil paint, printing ink and coating are considered as pseudoplastic fluids.

Shear thickening fluids: they are characterized as the easy deformation and the increased viscosity with the growth of shear rate. Their rheological properties are described through the equation $\tau = K\dot{\gamma}^\mathrm{n}(\mathrm{n} > 1)$.

(3) Viscoelastic fluids

They refer to the fluids that respond to external forces in a manner intermediately between an elastic solid and a viscous fluid. In the flow, the viscous deformation is unrecoverable and meanwhile consumes energy while the elastic deformation is recoverable and stores energy (Jin and Hua 1991). The shear stress is linearly proportional with the shear rate at a tiny deformation or deformation rate, otherwise visible non-linear relationship will happen. Due to the limited measuring methods on the rheological properties of non-linear viscoelastic properties, current research mainly focuses on the linear characteristics of viscoelastic fluids (Jiang 2004).

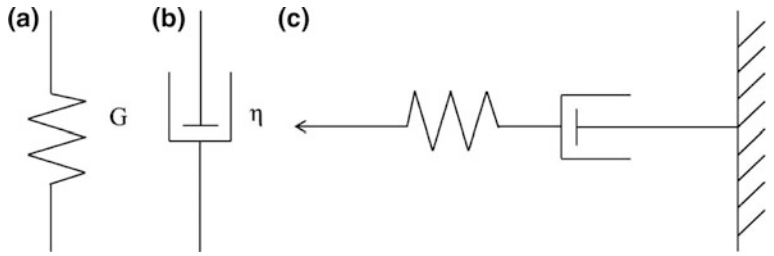

Fig. 1.2 Hookean spring (**a**), Newtonian dashpot (**b**) and Maxwell model (**c**)

The viscous feature of linear viscoelastic fluids could be described by the Newtonian raw while the elastic feature is characterized by the Hook's raw, i.e., $\tau_1 = \eta\dot{\gamma}_1$, $\gamma_2 = \tau_2/G$. γ_1 and γ_2 correspond to the viscous and elastic deformation, η represents the dynamic viscosity coefficient and G denotes the shear modulus. If the Hookean spring is connected with the Newtonian dashpot in series as shown in Fig. 1.2c, namely Maxwell model, we have $\gamma = \gamma_1 + \gamma_2$, $\tau = \gamma_2 G = \eta\dot{\gamma}_1$. The viscoelastic properties of Maxwell fluids can be simulated by the Maxwell model. In order to compare the elastic and viscous properties of viscoelastic fluids, relaxation time $t = G/\eta$ is introduced to represent the viscoelasticity (Gu and Pan 1994).

(4) Thixotropic Fluids

Under a certain shear rate, the viscosity of thixotropic fluids is time-dependent. For positive thixotropic fluids, their viscosity diminishes with the elapsed time under a constant external force. On the contrary, the viscosity of negative thixotropic fluids gradually increases with the time.

Much research on the rheology has been dedicated to establishing the constitutive equations between the stress history and the strain history of fluids according to the numerous theoretical and experimental work. However, due to the complexity of various fluids, no single model can be considered versatile or accurate enough to cover the whole range fluid characteristics (Yahia and Khayat 2001). This becomes even more complex when the flow geometry, gap between shearing surfaces, and their friction capacity also vary. Consequently, several different rheological models have been developed and listed below (Papo 1988):

(a) Voigt Model: $\varepsilon(\mathrm{t}) = \frac{\sigma}{E}\left(1 - \mathrm{e}^{-\frac{E}{\eta}t}\right)$

(b) Maxwell Model: $\eta \cdot \frac{d_\varepsilon}{d_t} = \sigma + \frac{G}{\eta} \cdot \frac{d_\sigma}{d_t}$

(c) Power Law Model: $\tau = K\dot{\gamma}^{\mathrm{n}}$

(d) Ellis Model: $\frac{\eta}{\eta_0} = 1 + \left(\frac{\tau}{\tau_{1/2}}\right)^{\alpha-1}$

(e) Carreau Model: $\frac{\eta_0 - \eta_\infty}{\eta - \eta_\infty} = \left[1 + (\lambda\dot{\gamma})^2\right]^{(n-1)/2}$

(f) Bingham Model: $\tau = \tau_0 + \eta_p\dot{\gamma}$

(g) Reversed Bingham Model: $\tau = \tau_0 + \eta_p\dot{\gamma} + c\dot{\gamma}^2$
(h) Herchel–Bukley Model: $\tau = \tau_0 + K\dot{\gamma}^n$
(i) Casson Model: $\sqrt{\tau} = \sqrt{\tau_0} + \sqrt{\eta_p}\sqrt{\dot{\gamma}}$
(j) Sisko Model: $\eta = \eta + \eta_p\dot{\gamma}^{n-1}$
(k) Willianmson Model: $\eta = \frac{\eta_0}{1+(K\dot{\gamma})^n}$

In these models, $\sigma, \varepsilon, \tau, \dot{\gamma}, \eta, \eta_p, \eta_\infty, \eta_0$, K, n and c are referred to as the stress, strain, shear stress, shear rate, apparent viscosity, plastic viscosity, viscosity at infinite shear rate, viscosity at zero shear rate, consistency, rate index, and a regression constant, respectively. In the remainder of the text, plastic viscosity is presented by the μ_p.

By substituting the measured curves of shear stress-shear rate into the above constitutive equations, the corresponding rheological parameters can be calculated to analyze the rheological properties of fluids. For Newtonian fluids and generalized Newtonian fluids, the static rheometer has been widely used to measure the shear stress and shear rate of fluids (Barnes and Nguyen 2001; Clayton et al. 2003; Nguyen and Boger 1992; Roussel et al. 2005). With regard to the viscoelastic fluids, the oscillatory shear tests (dynamic rheometer) in low frequency are conducted to monitor the variation of strain with sine stress. According to Eq. (1.1), the loss and storage moduli could be obtained to estimate the elastic and viscous characteristics of fluids (Schultz and Struble 1993; Sun et al. 2006; Valič 2000). $G' < G''$ indicates that the viscous behavior is pronounced. Oppositely, $G' > G''$ means that the elastic behavior is becoming the dominant feature. As for the thixotropic fluids, thixotropic loops in the shear stress-shear rate curves are measured by increasing the shear rate from 0 to a certain value and then drop to 0 (Assaad et al. 2003; Roussel 2006, 2007). Larger area of the loops indicates stronger thixotropic properties of fluids.

$$G^* = \frac{\sigma}{\varepsilon} = G' + iG'' = \frac{\sigma_0}{\varepsilon_0}\cos\delta + i\frac{\sigma_0}{\varepsilon_0}\sin\delta = \frac{\sigma_0}{\varepsilon_0}\cos\delta + i\omega\eta' \tag{1.1}$$

where σ_0 and ε_0 are the maximum stress and maximum strain respectively. δ denotes the lag angel, ω refers to as the angular frequency and η' means the in-phase viscosity (Labouret et al. 1998).

1.3.1.2 Rheological Properties of Suspension Dispersion System

Being for a long time, numerous existing research has been conducted on the rheological properties of various fluids from the aspects of developing experimental methods, analyzing experimental data, discussing the effects of various factors and deducing constitutive models. Basically, the rheological properties of fluids are mainly determined by their microstructures.

Different from liquids and solutions, suspensions contain a large number of particles in the systems, thus their rheological properties are intensively dependent on the particles including their size, shape, amounts and the interactions between particles as well as the hydrodynamics around particles (Dai 2005). When particles are added in the liquids and function as dispersion phase, the streamline of liquids flows around the particles under the condition of laminar flow, which will increase the resistance of flow and change the velocity distribution and viscosity. At low content of particles, steaming only involves the influence of particles on the continuous phase (i.e., dispersion medium). In the case of high content of particles existing, the distance between particles is shortened and thus the interactions between particles will also be affected by steaming. As well known, there are four types of interaction forces between particles in the suspension dispersion system, including the Van der Waals forces, electrostatic forces, Brownian motion forces, and viscosity forces (Bremmell et al. 1998; Yoshioka et al. 1997). These interaction forces are able to change the viscosity of the system by methods of impacting the viscosity of continuous phase. When the contact and friction among particles are increased, the flow resistance will become stronger, and consequently, the viscosity of system becomes larger. This means that the viscosity of suspension dispersion system is not only dependent on the content of dispersion phase, but also on the interactions between particles. On the other hand, the interactions between particles will produce a strong network structure in the system, which is able to stand external forces to some extents, namely yield stress (Scales et al. 1998). As for the viscoelastic properties of suspension dispersion system, the particle interaction is also an important influencing factor (Zhang 2001).

To sum up, the microstructure of suspension dispersion system is closely related to the rheological properties. The information on the microstructure can be obtained by analyzing the rheological properties of system. Conversely, the rheological properties can be modified by adjusting the microstructure of system. In the literatures on rheological properties, two key rheological parameters, yield stress and plastic viscosity are frequently involved and numerous empirical and/or theoretical models were developed to semi-quantitatively and even quantitatively describe the correlation of rheological properties with microstructure.

Viscosity Model

(1) On the assumption that an extremely diluted suspension is a non-compressible Newtonian fluid, rigid spheres of mono size without solvation effect act as the dispersion phase, there is no slipping between sphere surface and dispersion medium, and the size of sphere is much larger than the molecular size of dispersion medium, the relationship between the viscosity of the system η and volume fraction of dispersion phase ϕ could be described by Einstein equation, in which η_0 is the viscosity of dispersion medium (Einstein 1956).

$$\eta = \eta_0(1+0.5\phi)(1+\phi+\phi^2+\ldots)^2 \approx \eta_0(1+2.5\phi) \tag{1.2}$$

(2) When the concentration of dispersion phase in the above suspension becomes larger, Eq. (1.2) is not suitable any more. It was modified to the following equation by Goodwin, in which the constant k is related to the agglomeration degree of particles and their interaction forces (Goowin 1975).

$$\eta = \eta_0(1+2.5\phi+k\phi^2) \tag{1.3}$$

(3) With the further increase of the dispersion phase concentration, Brinkma et al. (1952) amended Eq. (1.2) into Eq. (1.4). Meanwhile, Vand et al. (1948) proved that Eq. (1.5) was more accurate than Eq. (1.4) to predict the viscosity of concentrated suspensions based on the experimental data. Additionally, an empirical equation Eq. (1.6) with high accuracy was also proposed by Tomas (1965).

$$\eta = \eta_0(1-\phi)^{-2.5} \tag{1.4}$$

$$\eta = \eta_0 \exp\left[\left(2.5\phi+2.7\phi^2\right)/(1-0.609\phi)\right] \tag{1.5}$$

$$\eta = \eta_0[1+2.5\phi+10.05\phi^2+0.00273\exp(16.6\phi)] \tag{1.6}$$

(4) When non-spherical particles with mono size act as the dispersion phase of suspension, a shape index or an equivalent diameter will be introduced to describe the size of these particles. At very low concentration, the viscosity of the suspension could be expressed by Eq. (1.7).

$$\eta = \eta_0(1+k\phi). \tag{1.7}$$

in which k denotes the shape index of particles. For spherical particles, oval particles with the ratio of macro to minor axis of 4 and sheet particles with the ratio of length to thickness of 12.5, their shape indices are 2.5, 4.8, 12.5 and 53 respectively. In the case of especial shape, e.g. rigid needle-like, the relative viscosity could be calculated by the Eq. (1.8) (Shen and Wang 1991).

$$\frac{\eta}{\eta_s} = 1+\left(2.5+\frac{J^2\phi}{16}\right) \tag{1.8}$$

where η_s is the viscosity of suspensions with spherical particles and J is the ratio of macro to minor axis.

Based on the Eqs. (1.7) and (1.8), it is known that a larger shape index and J lead to higher viscosity of suspensions. Additionally, for the particles with solvation effects, their size also impacts the viscosity of suspensions (Mewis and Wagner 2009).

(5) When the rigid spheres of multi sizes act as the dispersion phase of suspension, the viscosity of suspensions could be calculated by the semi-empirical equations Eqs. (1.9) and (1.10) (Frankel and Acrivos 1967).

$$\eta/\eta_0 = \frac{9}{8}\left[\frac{\left(\frac{\phi}{\phi_M}\right)^{\frac{1}{2}}}{1-\left(\frac{\phi}{\phi_M}\right)^{\frac{1}{2}}}\right] \tag{1.9}$$

$$\eta/\eta_0 = \left[1+\frac{3}{4}\left(\frac{\frac{\phi}{\phi_M}}{1-\frac{\phi}{\phi_M}}\right)\right]^2 \tag{1.10}$$

in which, ϕ_M refers to the volume fraction at geometrical maximum packing of solid phase, namely maximum volume fraction.

(6) When non-spherical particles with multi sizes act as the dispersion phase of suspension, relative movements between two particles were taken into account by Krieger and Dougherty and the following semi-empirical/theoretical K-D equation was proposed (Krieger and Dougherty 1959).

$$\eta/\eta_0 = \left[1-\frac{\phi}{\phi_M}\right]^{-[\eta]\phi_M} \tag{1.11}$$

in which, $[\eta]$ is intrinsic viscosity.

(7) When the bimodally distributed and polydispersed rigid spheres act as the dispersion phase, the viscosity of suspensions is determined by the Eq. (1.12) (Probstein et al. 1994).

$$\eta/\eta_0 = \left[1-\frac{\phi_1}{\phi_{M1}}\right]^{-[\eta_1]\phi_{M1}} \times \left[1-\frac{\phi_2}{\phi_{M2}}\right]^{-[\eta_2]\phi_{M2}} \tag{1.12}$$

In the aforementioned models, K-D is most commonly used for viscosity investigations of suspensions, which establishes the correlation of viscosity with three variables including volume fraction of solid phase, maximum volume fraction and the viscosity of dispersion medium. Thus, it is clear to reach at a conclusion that all the influential factors such as the mean particle size, size distribution, particle shape, temperature and shear rate impact the viscosity of suspensions through altering the above three variables in K-D equation. However, the interactions among particles that are also essential for viscosity are not considered in K-D equation, which may result in some deflections when predicting the viscosity of suspensions.

Yield Stress Model

Many studies have shown that yield stress is closely related to the inter-particle forces, the volume fraction, particle size, and size distribution. Considerable attentions have been paid to predicting and modelling the yield stress of suspensions as a function of particle size, interaction energy, and volume fraction of solids (Zhou et al. 1999). The following will introduce the relevant models of yield stress.

(1) Rumpf model (Rumpf 1962): when the mono-size particles with stable surface charge characteristics act as the dispersion phase of suspensions, the inter-particle forces are determined by the volume fraction ϕ, the coordination number on the surface of particles K, the combining forces H and the particle size d.

$$\tau = \frac{\phi \mathrm{HK}}{\pi \mathrm{d}^2} \tag{1.13}$$

(2) Prakash model (Kapur et al. 1997): in the case of suspensions containing two-sized particles, the inter-paticle forces are expressed by Eq. (1.14).

$$\tau = \frac{0.011}{\pi} \frac{\mathrm{A}\phi^2 \frac{36}{\pi}}{[9.5\mathrm{h}_0 \exp(-4.5\phi)]^2} \sum_{\mathrm{j}} \frac{\mathrm{S_j}}{\mathrm{X_j}} \sum_{\mathrm{i}} \mathrm{S_i} \times \left[\frac{\mathrm{X_i}}{(\mathrm{X_j} + \mathrm{X_i}) - \sqrt{\mathrm{X_j^2} + 2\mathrm{X_i X_j}}} \right] \tag{1.14}$$

(3) Scales model (Scales et al. 1998): for the polydisperse suspensions, the inter-particle forces are expressed by Eq. (1.15).

$$\tau = \frac{\mathrm{F}(\phi)}{\left(\sum \mathrm{x_{vi}} \mathrm{d_i}\right)^2} = \frac{\mathrm{K}\left(\frac{\phi}{1-\phi}\right)^{3.2}}{\left(\sum \mathrm{x_{vi}} \mathrm{d_i}\right)^2} \tag{1.15}$$

(4) Yodel model (Flatt and Bowen 2006, 2007): Flatt and Bowen deduced a model for the yield stress of particulate suspensions that incorporates microstructural parameters and relates the physical parameters (particle size, size distribution, maximum packing fraction, minimum separation distance at contact) to the shear stress required to break down the attractive network sufficiently for it to yield.

$$\tau_{\mathrm{y}} = \frac{\mathrm{m_1}}{\phi_{\mathrm{m}}} \frac{\phi^2(\phi - \phi_0)}{(\phi_{\mathrm{m}} - \phi)} \mathrm{m_1} = \frac{0.15 \times \mathrm{u_{k,k}} \times \mathrm{A_0}}{\pi^4 H^2} \times \frac{f_{\sigma,\Delta}}{R_{V,50}} \tag{1.16}$$

where $\mathrm{A_0}$ is the hamaker constant, ϕ_0 is a percolation threshold, $u_{\mathrm{k,k}}$ denotes a normalization factor that changes the size distribution, $R_{\mathrm{v},50}$ refers to the median volume radius, H is the minimum separation distance between particles and $f_{\sigma,\Delta}$

corresponds to a particle size distribution function. In this model, a number of parameters, such as volume fraction of solids, particle size, particle size distribution, maximum packing, percolation threshold, are taken into account. The model is proved to predict the dependence of yield stress of concentrated suspensions on volume fraction accurately (Flatt 2004).

1.3.1.3 Rheological Properties of Fresh Cementitious Materials

Fresh cementitious materials have been regarded as highly concentrated polydisperse suspensions with multiple phases. Aggregates are dispersed in the cement pastes while cement grains are dispersed in water. Different from the normal inert suspensions, cementitious materials are featured with chemical activity due to the hydration reaction of cement grains. With the progressing cement hydration, a fresh cementitious material gradually evolves from a viscous fluid to a viscoelastic semi-solid and finally becomes an elastic solid due to the production of hydration products. This evolution plays an essential role in workability of cementitious materials, because superior workability is always required throughout the construction process to ensure the successful construction. Thus, extensive research has been conducted on the workability of fresh cementitious materials, specifically, by evaluating their rheological properties to achieve the aim of ascertaining the key factors influencing the workability from an academic point of view (Banfill 2006; Yahia and Khayat 2001).

Nowadays, rheology of cementitious materials has become an indispensable component in concrete disciplines. It mainly focuses on three aspects: (1) the rheological types and models of fresh cement pastes, cement mortars and concrete, (2) the evolution essence of viscosity, elasticity and plasticity from a microstructural point of view, (3) the effects of varied factors on the rheological properties, particularly the chemical admixtures.

1. **Rheology models**

Practical observation demonstrates that fresh cementitious materials are yield stress fluids where the material can support shear stress without flowing at $\tau < \tau_0$ but flows at higher stress (Barnes 1999). The shear stress-shear rate curve is dependent on the composition of cement pastes and the test accessory used in the test, so that different mathematical models have been developed and are selectively applied according to flow curves (Papo 1988). Researchers generally agree that Herchel-Bulkley model can adequately describe their nonlinear flow behaviors of cementitious materials (Domone and Thurairatnam 1988; Ferraris et al. 2001; Ferraris and Gaidis 1992; Nehdi et al. 1997; Struble et al. 1998). The main drawback, however, is that a tedious procedure is required to determine the three model parameters (Heywood and Cheng 1984). Casson model allows a quick testing of experimental data and determination of the two parameters. This model has been successfully applied to a diverse range of other materials such as food

products, mineral suspensions, polymer suspensions, and composites. In some cases, however, it has been reported that the linear relationship was only identified in the high shear rate region (Blair 1966). Bingham model is the simplest model but commonly used for rheological investigations on cement pastes. With only two intrinsic rheological parameters included, yield stress τ_0 and plastic viscosity μ_p, Bingham model could roughly describe the rheological properties of cement paste in certain cases (Aiad 2003; Axelsson and Gustafson 2006; Roussel et al. 2007; Wallevik 2006).

2. **Rheology properties**

Currently, slump test of fresh concrete and mini-cone test of fresh cement pastes are two simple and effective methods to reach at a rough view on the rheological properties of cementitious materials. Academically speaking, the two parameters with specific physical significance, yield stress and plastic viscosity, are able to reveal the rheology essence of cementitious materials from a microstructure point of view.

In the theory of rheology of cementitious materials, it is believed that yield stress is caused by the cohesion forces and static friction forces of cement grains, which reflects the number of contacting points and the contacting strength in the structure network of cement grains. Cohesion forces are dependent on the particle size, numbers and shape. More contacting points can enhance the static friction forces and cohesion forces, which further increases the yield stress. On the other hand, plastic viscosity refers to the resistance between two adjacent layers during flowing and reflects the capability to flow to some extent. The cohesion forces and dynamic friction forces are contributable to the resistance during flowing.

For fresh cement pastes, the cohesion forces of cement grains mainly originate from Van der Waals forces and electrostatic attractive forces (Flatt 2004; Morris 2009; Struble and Sun 1995). Flatt (2004) and Kauppi et al. (2003) calculated these forces to predict the yield stress and plastic viscosity. After the contact of cement grains with water, various ions are quickly dissolved from the mineral phases of cement grains into the aqueous phase, consequently developing a heterogeneous charge distribution on the surface of hydrating cement grains. This mosaic structure results in the formation of flocculated cement grains that entrap a large quantity of mixing water (Struble and Sun 1995). Meanwhile, due to the chemical activity of cement grains, hydration reaction brings significant effects on the rheological properties of fresh cement pastes. Along with the progressing cement hydration, the content of mixing water is diminished and more hydration products are formed, which effectively increases the number and strength of contacting points. As a consequence, the yield stress and plastic viscosity of fresh cement pastes gradually grow with the elapsed time. Rößler et al. (2008) pointed that the transformation of particle shape, from sphere to rodlike during cement hydration, resulted in an increment of plastic viscosity but a decrement of yield stress.

Previous research reported that the elastic feature of fresh cement pastes is primarily dependent on the network structure in the pastes caused by the

inter-particle crosslinking (Bellotto 2013; Ferrandis and Leveque 2003; Martini and Nehdi 2009; Papo and Piani 2004a, b; Schultz and Struble 1993). During cement hydration, by creating new links among cement grains, the newly formed hydrates would increase the inter-particle crosslinking and thus lead to a stronger "network structure". Correspondingly, the elasticity of FCPs becomes more pronounced. When cement hydration steps into induction period, an evident transformation of viscoelastic properties will occur (Grasley and Lange 2007; Nachbaur et al. 2001; Subramaniam et al. 2005; Subramaniam and Wang 2010; Wang et al. 2010).

3. **Influencing factors**

Apart from the cement-to-aggregate ratio, the workability of cementitious materials is primarily determined by the rheological properties of cement pastes. Influencing factors of the rheological properties include cement types, grinding history during cement manufacturing, W/C, mixing conditions, testing time and temperature as well as the use of SCMs and superplasticizers, etc. (Ferraris et al. 2001; Petit et al. 2005; Rubio-Hernández et al. 2013; Sheinn et al. 2002). In this section, four important influencing factors were discussed.

(1) Water to cement ratio

Water to cement ratio actually reflects the volume fraction of dispersion phase in suspension dispersion system. At a higher W/C, the distance between the cement grains and flocculated structures is larger. In the first minutes of cement-water contact, the crosslinking of cement grains and flocculated structures is not obvious. With the progressing cement hydration, more newly formed hydrates are produced to create new links among cement grains. Compared with lower W/C, more hydration products are required at higher W/C, in order to achieve a stronger inter-particle crosslinking. Hence, in the premise of constant cement type, the yield stress and plastic viscosity of fresh cement pastes as well as their growing rates are reduced at higher W/C. Flatt and Struble respectively introduced Yodel model and K-D equation into the cementitious materials to describe the relationships between rheological parameters and the volume fraction of dispersion phase (Flatt and Bowen 2006; Struble and Sun 1995).

(2) Time

Rheological properties usually present continuously ascending trends with elapsed time due to the progressing cement hydration. Hakansson et al. (1992) and Shroff et al. (1996) did much research on the variations of yield stress and plastic viscosity with hydrating time, in which three types of curve shape including the linear growth, power function growth and exponential growth were observed. In practice, fluidity retention over a certain period of time is a key element of concrete workability in order to ensure sufficient construction time. However, the development of rheological parameters with time is not considered in the current rheological models. Previous studies demonstrate that for a fixed cement paste, the rheological models with elapsed time could be expressed by the variations of rheological

parameters with time in a linear, power or exponential manner (Struble and Lei 1995; Umlauf 1993).

(3) Temperature

The effects of temperature on the rheological properties are dependent on the changed dissolution rate of mineral phases and the hydration rate under varied temperatures (Nehdi and Al Martini 2009; Petit et al. 2005, 2006, 2007, 2009; Romano and Pileggi 2012). A higher temperature usually accelerates the dissolution and hydration rate. This means that new links among cement grains will be created more rapidly and the crosslinking of network structure will be strengthened due to the consumption of much water and the production of hydration products. As a result, the yield stress and plastic viscosity of fresh cementitious materials generally ascend evidently with the growth of temperature. Apart from the dispersion phase of cement grains, the dispersion medium is also affected by temperature. For example, a lower temperature brings about larger viscosity of dispersion medium. Thus, the coupled effects are responsible for the variations of the rheological properties of FCPs with temperatures. If the effects of dispersion medium are dominant, the yield stress and plastic viscosity decrease at elevated temperatures. Vice versa.

(4) Chemical admixtures

The chemical admixtures can alter the rheological properties of cementitious materials from three perspectives (Chandra and Björnström 2002; Cyr M et al. 2000; Golaszewski and Szwabowski 2004; Papo and Piani 2004b; Rahman et al. 2014): (a) changing the rheological models; (b) impacting the initial rheological properties and the development of rheological properties with elapsed time; (c) affecting the thixotropy of paste. In practice, the effects of chemical admixtures on the rheological properties are rather complicated due to the variety of chemical admixtures used in the cementitious materials. The difference on the interactions between various chemical admixtures with varied molecular sizes and cement grains may lead to the distinct working mechanisms of chemical admixtures. In this research, three types of chemical admixtures with varied sizes, i.e., superplasticizers, polymer latexes and asphalt emulsions, are employed to investigate their different effects on the rheological properties of cementitious materials. The state-of-art of their working mechanisms will be reviewed in detail in the next section.

It has been widely accepted that the incorporation of superplasticizers can effectively assemble the flocculated structures and retard the cement hydration, which can consequently enhance the initial fluidity and fluidity retention of fresh cementitious materials. A larger dosage of superplasticizers usually results in a lower yield stress and plastic viscosity as well as their lower growth rates with time. However, some researchers claimed that the plastic viscosity would increase in the presence of excessive superplasticizers (Cyr and Mouret 2003; Faroug et al. 1999; Felekoğlu et al. 2007). Ravi and Sutton (1990) investigated the effects of temperature on the rheological properties and found that the effects of temperature on the

FCPs with superplasticizers were completely different from that on the blank FCPs. For example, an elevated temperature led to a decrement of the plastic viscosity in the presence of superplasticizers (Schmidt et al. 2014). These contradictory phenomena demonstrate that in the case of FCPs with superplasticizers, the effects of temperature on rheological properties are not only related to the cement hydration but also associated with the superplasticizer types, dosages and their interactions with cement grains. On the other hand, FCPs with polymer latexes present superior fluidity retention but different initial fluidity (Allan 1997; Li and Kong 2009). As for asphalt emulsion, Wang (2008) and Wang et al. (2008a, b, c, d, e) examined the effects of mixture components on the workability of FCPs and found that a higher asphalt content was beneficial to increasing the initial fluidity and fluidity retention but might cause a serious separation of components.

To sum up, many researchers have contributed on the topic of rheological properties of blank fresh cement pastes, for which, many findings and conclusions have been reached. For the FCPs with chemical admixtures, although a large number of studies have been found in existing literatures concerning several topics, including the effects of the mixture composition and the environmental factors on the rheological properties as well as the working mechanism of each influencing factor, limited research has been found on the synergistic mechanism of these influencing factors from the microstructure point of view. Thus, a few of contradictory phenomena have not been well investigated and explained so far. Moreover, rheological models incorporating all the aforementioned factors are poorly researched and only a few studies of FCPs without chemical admixtures are found in the literatures with the aim of predicting the required properties of the mixtures to be cast. The fact of research lacking in above topics has posed a certain difficulty against deeply understanding the rheological properties of FCPs with chemical admixtures.

1.3.2 Microstructure of Fresh Cement Pastes

From the microscopic point of view, all these macroscopic properties of fresh cementitious mixtures are primarily determined by the microscopic structure (Barnes and Hutton 1989; Xu 1989). The microstructure refers to the particle size, morphology, organization structure of cement grains in the suspension systems and the hydration products. Being for a long time, researchers believe that the desired fluidity could be achieved by properly modifying the microstructure of the pastes. This motivates many researchers to investigate the microstructure of FCPs as well as its correlation with the macroscopic rheological properties.

The observation of FCPs by microscopes is a direct way to analyze the microstructure of FCPs including the morphologies of cement grains and the flocculated structures as well as the dispersion state of cement grains. The analysis of the microscopic images by image processing software can help to collect quantitative information on different granular populations like the shape index, size

distribution and so on. Furthermore, laser granulometry has also been applied in the quantitative analysis of the mesostructure of cement pastes. Scanning electron microscopy (SEM) and transmission electron microscope (TEM) are adopted to observe the morphology of hydration products at early stage and to analyze the crystal structure and element composition of the hydrates based on an equipped energy dispersive X-ray spectroscopy in the TEM and a selected area electron diffraction (SAED) technique (Aitcin 2000; Zingg et al. 2008).

Optical microscopes and ESEM have been frequently used to observe the mesostructure of cement suspensions focusing on the granular morphology and the characteristics of the flocculated structures (Aitcin 2000; Autier et al. 2013, 2014; Han 2012; Wang et al. 2013; Zhang et al. 2013). These flocculated structures are found to be a 3-D network structure with entrapped water in them. In the presence of superplasticizers, the flocculated structures are disassembled and cement grains present a superior dispersion state. Autier et al. (2013) characterized the dispersion state of cement grains by using a morpho-granulometric approach based on the complementarity of SEM and laser granulometry, in which dispersion indices were introduced to characterize the mesostructural variations caused by the inclusion of superplasticizers. However, the particle size results provided by laser granulometry were not consistent with the results indicated by the images presented in SEM, i.e., some agglomerates appeared in the particle size distribution curve were not observed in microscopy. Meanwhile, the dispersion indices could identify the influence of the superplasticizers but not to the influence of molecular architectures. The different influences of the molecular architectures were eventually distinguished by an indirect characterization approach of mesostructural organization in term of behavior settling (Phase separation Index) (Autier et al. 2014).

Wang et al. (2008a, b) considered a cement paste as a Menger sponge with fractal structure and figured out the fractal dimension of particle size distribution to quantitatively characterize the flocculated structures. Results indicated that larger fractal dimension corresponded to a lower fluidity of FCPs. But it did not present obvious variations when different dosages of superplasticizers were added into the pastes. It is supposed that there must be some vital information missing in the case of characterizing the microstructure using dispersion indices or particle size fractal dimension.

On the other hand, a few studies concerning the microstructure models of FCPs have been found in the literatures. Cao et al. (2012) established a microstructural model of FCPs containing mono-sized particles based on the working mechanism of superplasticizers. Zhang et al. (2013) proposed multi-level flocculated structures of blank FCP. Flatt (2004) proposed a microstructure model of fresh concrete based on a homogenisation approach. However, these models either fail to take into account of the effects of superplasticizers on the microstructure or lack firm validations from experimental data.

In the presence of polymer latexes, the microstructure of FCPs has been well documented. The adsorption of polymer particles on cement surface and the film formation of polymer latexes could be clearly observed under ESEM (Dimmig 2002; Kong et al. 2010a, b; Su 1995; Su et al. 1996). Ohama (1987) divided the

microstructural evolution of FCPs containing polymer latexes into three stages: (1) the adsorption of polymer particles on cement surface; (2) the agglomeration of polymer particles caused by the reduction of water in the process of hydration; (3) the formation of a continuous polymer film as the water among polymer particles is fully consumed by cement hydration. Similarly, Yang et al. (2010a, b) reported the formation and evolution of microstructure of cement asphalt binder with ESEM.

As described above, the qualitative research on the microstructure of FCPs is far from being satisfied due to the low resolution and the limited measuring area of a regular microscope while the accurately quantitative characterization on the microstructure of FCPs remains a challenge. Moreover, due to the lack of reasonable microstructural models, a clear correlation of microstructure with rheological behaviors of FCPs has not been established.

1.3.3 Working Mechanism of Chemical Admixtures

1.3.3.1 Superplasticizers

The invention and usage of superplasticizers are regarded as the third revolution in the field of concrete technology (Kong et al. 2010a, b). Superplasticizers, also known as superfluidizers, water reducers or high-range water reducers, are practically used to achieve higher fluidity of fresh cementitious materials at low water to cement ratio, which further enhances the strength and durability of hardened ones. Nowadays, superplasticizers have become one of indispensable components in most HPC (Qian et al. 2002).

In 1935, the first generation water reducer lignosulfonate (LS), a biopolymer, was invented by Master Builder Technology, providing 5–10% water reduction. In 1962, the appearance of melamine and naphthalene formalaldehyde condensates (NSF) signified another major milestone in the development of superplasticizers, which provide 10–25% water reduction. In the 1980s and 1990s, new types of polymers, comb-shaped polycarboxylate (PCE) superplasticizers were introduced successfully and up to 40% of water reduction can be achieved. With the appearance of superplasticizers, the working mechanism of superplasticizers has drawn increasing attentions aiming at developing new types of superplasticizers with more efficient and robust performance. However, the detailed mechanism of superplasticizers has not been clarified so far and some fundamental questions concerning the mechanism have not been answered yet.

Adsorption of Superplasticizers

After the contact of cement with water, quick dissolution of mineral phases as well as hydration starts immediately. Various ions (K^+, Na^+, Ca^{2+}, OH^-, SO_4^{2-}) diffuse

from the mineral phases of cement grains to the aqueous phase and meanwhile a part of Ca^{2+} is adsorbed on the surface of cement grains to form a Ca^{2+} rich layer. The Ca^{2+} rich layer moves with cement grains and is referred to as stern layer while the other ions free moving in the aqueous phase form diffusion layer. The interface between stern layer and diffusion layer denotes shear plane and the potential difference between the shear plane and aqueous phase is defined as zeta potential (Kim et al. 2000). It is well known that Portland cement mainly consists of four mineral phases including C_3S, C_2S, C_3A and C_4AF. When cement grains contact with water, the fast dissolution and the early hydration of mineral phases build surface charges on cement grains. Silicate phases are found to possess negative charges whereas aluminate hydrates are usually positively charged. The zeta potential of cement pastes is determined by the four mineral phases. Actually, due to the difference of cement components, testing conditions and methods, various zeta potential values of FCPs from positive to negative ones have been reported in the literatures (Plank and Gretz 2008; Plank and Hirsch 2007; Wang 2006), which definitely imposes difficulty to understand the adsorption of superplasticizers on cement surface.

On the other hand, the continuous hydration of cement grains further leads to the uncertainty of adsorption sites of superplasticizers on cement surface. There are no specific conclusions so far that the adsorption of chemical admixtures is on the surface of mineral phases or on the hydration products at very early stage. Plank et al. (2006) described the synthesis of a series of composite layered double hydroxides (LDH) based on the intercalations of PCE polymers containing ethylene oxide side chains of different lengths and found that basal spacing of the PC-LDH composite materials was dependent on the side chain length. As a consequence, it was supposed that in addition to being adsorbed on the cement surface and remaining in the aqueous phase, a part of the superplasticizers added in the FCPs was intercalated into the hydrates. For the part of being adsorbed superplasticizers, their adsorption behaviors on cement surface are entirely different (Yoshioka et al. 2002). Anionic superplasticizers could be easily adsorbed on the surface of positive charged aluminate phases and hydrates in a considerable amount. By contrast, their adsorption on silicate phases with negative charges is difficult and thus the adsorption amount is limited. Moreover, Jolicoeur and Simard (1998) pointed that the driving force of adsorption mainly lay in the electrostatic attractive forces, hydrogen bond and chelating effects between the charged functional groups in the superplasticizer molecules and the mineral phases of cement grains. Uchikawa et al. (1992) estimated the microstructure and the composition of the adsorption layer of chemical admixtures on the surface of clinker minerals by the mean of in-lens FESEM, ESCA-imaging, AES and AFM and found that the admixtures were partially adsorbed to the interstitial phase in a thick layer, forming characteristic three dimensional surface structure. An admixture having a functional group producing a complex salt with Ca^{2+} could be adsorbed on the cement surface and decreased the concentration of Ca^{2+} in liquid phase at early age. Plank and Kong also concluded that PC superplasticizers bearing $–COO^-$ groups were adsorbed on

cement surface through both electrostatic forces and the complexation bonding between $–COO^-$ and Ca^{2+} (Li and Kong 2009; Plank and Sachsenhauser 2009).

The adsorption of superplasticizers on cement grains usually follows a typical Langmuir monolayer adsorption model (Banfill et al. 2007; Hsu et al. 1999; Krstulović et al. 1994; Peng et al. 2005; Plank and Sachsenhauser 2006), namely a linear increase at low dosages and then a plateau at adsorption saturation. But a few studies pointed that the adsorption of superplasticizers on aluminate phases well fitted the Langmuir model whilst their adsorption on the silicates exhibited a linear increase trend and no plateau was found in the adsorption curves (Yoshioka et al. 2002). For a fixed cement grain, the adsorption of superplasticizers on it is largely governed by the molecular architectures of superplasticizers such as the types and amounts of the charged functional groups in the backbone of molecules, the density and length of side chains and so on. Burgos-Montes et al. (2012) found that the traditional admixtures such as lignosulfonate and sulfonated naphthalene-type superplasticizers had high adsorption values on cement and they supposed that the adsorption was related to the charge density and the configuration of the adsorbed molecules. In the premise of the same molecular weight and side chain density, some researchers adjusted the amounts of the charged functional groups in the backbone of molecules and confirmed that more charged functional groups caused a larger adsorption amount of superplasticizers on cement surface (Burge et al. 1999; Zingg et al. 2008; Ran et al. 2010; Winnefeld et al. 2007). Zingg et al. (2008) reported a positive correlation of side chain length with the adsorption amounts whilst Yamada et al. (2000) reached a completely opposite conclusion. Ran et al. (2009a, b) believed that the side chain length had slight effects on the adsorption amount of superplasticizers as the number of $–COO^-$ was constant. In addition, a few researchers reported that higher molecular weight of PCE influenced a larger adsorption amount (Ferrari et al. 2000; Ran et al. 2009a, b; Winnefeld et al. 2007). More specifically, Winnefeld et al. (2007) investigated the effects of superplasticizers with varied structures and found that PCEs with higher molecular weight, lower side chain density and shorter side chains were favorable to a high adsorption amount on cement surface. Pourchet et al. (2012) reported that not only the number of the carboxyl groups, but also their repartition along the polymer backbone would significantly affect the adsorption behaviors of the carboxyl groups containing polymers.

The adsorption rate of superplasticizers is also related to their molecular architectures. For example, more charged functional groups and shorter length of side chain lead to a rapider adsorption of superplasticizers on cement surface. The adsorbed superplasticizers may have two different regimes according to their coverage degree on cement surface, which has been validated theoretically and experimentally (Giraudeau et al. 2009). At low surface coverage, adsorbed superplasticizer molecules are independent of each other and we have the so-called mushroom regime, like in a dilute solution where the polymers have a coil conformation. When the surface coverage increases, the molecules overlap and a brush regime is established. The probability of this transition between the two regimes can be evaluated by using the Gay-Raphaël approach. Houst et al. (2005) estimated the

thickness of adsorbed layer by atomic force microscopy (AFM). The polymer conformation in solution was shown to be similar to that of the adsorbed layer thickness measured by AFM. The adsorbed layer thickness of polycarboxylate polymers was about half of the Rg and Rh values, indicating the molecules were flattened in their adsorbed state. For the lignosulfonates the situation was less clear and although the adsorbed layer thickness was often lower than the Rg, suggesting that the macromolecules had a more branched comb-like structure than a spherical micro gel structure. Giraudeau et al. (2009) developed a model of adsorbed polymers in a configuration of a flexible chain of hemispheric cores and the interlayer space scaled with twice the hemispheric radius.

On the other hand, the adsorption characteristics of superplasticizers on cement surface are also influenced by temperature. An elevated temperature usually leads to a decreased adsorption amount (Griesser 2002). Yamada et al. (1999) pointed that the concentration of sulphate ions was higher at elevated temperatures, which was unbeneficial to the adsorption of superplasticizers. Contrastively, Schmidt et al. (2014) measured a higher adsorption amount of PCE superplasticizers on cement surface at elevated temperatures and claimed that was caused by the enhanced dissolution of mineral phases and subsequently the more adsorption sites.

Adsorption-Dispersion-Rheology

Although many researchers have made efforts in exploring the relationship between the adsorption of superplasticizers and the dispersion of cement grains, the conclusions drawn from the existing research are still debatable. A few studies have demonstrated that a larger adsorption amount of superplasticizers will reach a superior dispersion state and subsequently lead to a larger fluidity of FCPs (Ran 2007). On the contrary, some researchers found that at the same dosage of superplasticizers in FCPs, higher adsorption amounts on cement surface suggested there was a lower concentration of remaining superplasticizers in aqueous solution, leading to an inferior dispersion state of cement grains and lower fluidity of FCPs (Liu 2005; Wang 2006). Moreover, several research concluded that the dispersion function of superplasticizers was determined by the thickness and conformation of the adsorbed layer instead of adsorption amounts (Houst et al. 2008; Plank and Sachsenhauser 2006; Uchikawa et al. 1992).

The superplasticizers added into a cement paste can be divided into three parts: integrated in the hydration products such as Afm and C–S–H gel, adsorbed onto the surface of cement grains as well as hydration products and remaining in the aqueous phase (Flatt and Houst 2001). It has been widely accepted that the dispersing capability of superplasticizers is closely linked to their adsorption on the surface of cement while the superplasticizers remaining in the aqueous phase continuously complement the consumed part to ensure stronger fluidity retention of FCPs.

Being for a long time, it has been believed that the dispersing function of superplasticizers in cement pastes is achieved through adsorbing on cement surface and changing the zeta potential of FCPs. When superplasticizers bearing anionic

groups are added in the pastes, they could be adsorbed on the surface of positively charged mineral phases and decrease the zeta potential of FCPs from positive to negative values. As a consequence, the electrostatic repulsion between cement grains is created and cement grains are well dispersed in the pastes. In the presence of NSF superplasticizers, lower zeta potential of FCPs corresponds to higher fluidity of FCPs (Kodama and Okazawa 1992). Nevertheless, Chandra and Björnström (2002) compared the effects of different types of superplasticizers on the fluidity of FCPs and found that PCE superplasticizers more significantly increased the fluidity of FCPs than NSF although the zeta potential of pastes with PCE was higher (Jolicoeur and Simard 1998). Houst et al. (1999, 2008) reported that PCE with long side chain presented stronger dispersion capability although its adsorption amount was obviously lower than that of NSF. This is due to the reason that NSF enhances the dispersion of cement grains only by electrostatic repulsion, whereas PCE favors the dispersion by the combined effects of electrostatic and steric repulsion. PCE polymers have a backbone chain with ionic groups and grafted side chains of varied length. The backbone chain is adsorbed on the cement surface while the side chains extend into the solution increasing the effective layer thickness. The steric repulsion is closely linked to the thickness of adsorbed layer. Therefore, it is supposed that the length and density of side chains also play essential roles in dispersing the cement grains. Yamada et al. (2000) indicated that PCE superplasticizers with shorter backbone chain and longer side chains presented higher dispersability and short dispersability retention. Ran et al. (2009a, b) proposed that at low W/C, the dispersability of superplasticizers with longer side chains was visibly higher, but the effects of side chains length were slight at high W/C. Ohta et al. (2000) have stated some semi-quantitative structure/dispersability relationships of superplasticizers and also proposed that polymers presented superior dispersaibility as the length of side chain n was 12. In addition, several studies have shown that the dispersabiliy and dispersabiliy retention of PCE superplasticizers are reduced at elevated temperatures, which may originate from the effects of temperature on cement hydration and the adsorption behaviors of superplasticizers (Petit et al. 2005, 2006, 2007, 2009, 2010; Romano and Pileggi 2012; Schmidt et al. 2014).

Effects of Adsorption on Cement Hydration

Adding superplasticizers into FCPs has a significant influence on the hydration kinetics of cement, generally leads to a prolonged induction period and a lowered maximum exothermic rate in the acceleration period of the cement hydration, which is the so-called retardation effects (Borget et al. 2005; Sakai et al. 2006; Shin et al. 2008).

Pourchet et al. (2006, 2007) investigated the effects of PCE superplasticizers on the hydration of C_3S and C_3A-CS system and concluded that the presence of PCE effectively reduced the dissolution rates of C_3S and C_3A as well as the precipitation rate of hydration products. Moreover, Sarkar and Aimin (1992) and Zingg et al.

(2008) reported the effects of superplasticizers on the morphology of hydration products and found that the sizes of Aft and Afm were diminished by adding superplasticizers, and meanwhile, the hydrates presented a superior distribution state in the pastes.

Mollah et al. (2000) proposed that the influences of superplasticizers on cement hydration might originate from three aspects: (1) the adsorbed superplasticizer layers hindered the diffusion of water and ions at the cement-solution interface; (2) the Ca^{2+} ions in aqueous solution might be chelated by the $–COO^-$ groups in PCE molecules and thus the nucleation and precipitation of hydrates were inhibited; (3) better dispersion of cement grains caused by superplasticizers changed the growth kinetics and the morphology of hydrate phases. It is widely accepted that the retardation effects of superplasticizers are related to the adsorption amounts of superplasticizers on cement surface. A higher adsorption amount usually results in a stronger retardation effect on cement hydration. Zingg et al. (2008) and Pourchet et al. (2012) established the correlation of the retardation effects with the backbone charge density and the number of $–COO^-$ groups in the adsorbed PCE molecules. Contrastively, Yamada et al. (2000) reported that higher concentrations of the carboxylic and sulfonic groups remaining in the aqueous phase could more effectively delay the setting of cement pastes. This demonstrates that those non-adsorbed PCE molecules play an important role in the retardation effects. The clear explanation of inner mechanism is still not clear.

To sum up, extensive research has been carried out for better understanding and explaining the structure-property relationship of superplasticizers in the context of investigating the effects of polymer architectures on the adsorption, zeta potential, rheological and hydration behaviors of cement pastes. However, there are still unsolved questions with regard to the specific mechanism through which superplasticizers affect the rheological properties of FCPs and cement hydration. For example, what are the adsorption behaviors on cement surface for different types of superplasticizer, such as NSF and PCE? How are the enhancement of the fluidity of FCPs and the retardation effects dependent on the dosages of superplasticizers? Can the enhancement of the fluidity and the retardation infinitely grow with the dosages? Moreover, there is so far no study exploring the effects of the various functional groups and the charge species of backbone in PCE molecules on the adsorption and cement hydration. Therefore, it is necessary to conduct an in-depth investigation to further elucidate the working mechanism of superplasticizers in cement paste, which is expected to lay a theoretical basis for the development of new superplasticizers with more efficient and robust performance.

1.3.3.2 Polymer Latexes

Polymer latexes are often used as cement mortars and concrete modifiers to improve mortars and concrete properties such as adhesion, fracture toughness, flexural strengths, crack resistance and waterproof. Previous studies have shown that after the mixing of cement with polymer latexes, cement grains begin to hydrate and

meanwhile the polymer particles gradually agglomerate together because the water in the latexes is consumed by cement hydration. Finally, unhydrated cement, hydrates and polymers are compactly connected with each other, forming a monolithic structure with improved mechanical and durability characteristics. Polymer modified concrete and mortars have already been used in various applications in the construction industry such as the pavement materials, decoration materials, waterproof materials, repairment materials and so on (Anagnostopoulos and Anagnostopoulos 2002; Ohama 1997; Zhong and Chen 2002).

In addition to influencing the properties of hardened cement pastes, the inclusion of polymer latexes affects the rheological properties of FCPs. Some researchers hold a view that the presence of latexes in the paste could effectively enhance the fluidity of FCPs due to the plasticizing effects of the surfactant in latexes, the lubricating effects of spherical polymer particles and some air bubbles caused by the surfactant and stabilizer in latexes. However, Allan (1997) found the presence of polymers led to an obvious decrement of fluidity in term of increasing yield stress and apparent viscosity. Li and Kong (2009) reported that with the addition of polymer latexes, the fluidity of FCPs increased in the beginning but dropped later on. So far, much work focuses on the properties of hardened polymer-modified pastes whereas quite a few researchers pay attention to the fresh ones. The working mechanism of polymer latexes on affecting rheological properties remains unrevealed.

1.3.3.3 Asphalt Emulsions

Cement-asphalt mortar (CAM), a kind of inorganic–organic composite material, has been widely used as the cushion layer between the track slab and the concrete bed of ballastless slab track structures in high speed railways. As a grouting material, fresh CAM must possess adequate workability to ensure a successful construction as well as the improved strength and durability of hardened CAM. However, current research mainly focuses on the estimation of workability and rheological properties of fresh CAM, few studies have explored the influencing mechanism of asphalt emulsion on the rheological properties, even though this topic is highly important to the scientific and engineering fields.

1.3.4 Pore Structure and Impermeability of Hardened Cement Pastes

With the development of cement hydration, the modification in the microstructure of FCPs by the addition of chemical admixtures will be persistently extended to the formation of the microstructure in the hardened cement pastes (HCPs), further influencing the properties of HCPs.

Existing research has been conducted on investigating the effects of superplasticizers on the pore structure and the impermeability (Arandigoyen and Alvarez 2007; Gu et al. 1994; Khatib and Mangat 1999; Puertas et al. 2005; Sakai et al. 2006; Xu et al. 2000). Many of them have agreed that the pore structure has been refined when adding superplasticizers. It is believed that the pore structure is associated with the coagulated structure of FCPs. By adding superplasticizers, the cluster size of aggregated cement grains in FCPs was decreased, which can further decrease the pore size of hardened ones (Arandigoyen and Alvarez 2007; Sakai et al. 2006). On the contrary, the addition of superplasticizers has also been found to increase or exert no influence on the porosity and the permeability of cement pastes, mortars or concrete (Gu et al. 1994; Khatib and Mangat 1999; Puertas et al. 2005; Xu et al. 2000). As a matter of fact, the above-mentioned contradictory phenomena are observed for specimens with different W/Cs and different types of superplasticizers. To conclude, at low W/C, superplasticizers generally lead to smaller porosity and pore size (Khatib and Mangat 1999; Sakai et al. 2006), whilst the incorporation of superplasticizers at high W/C has no obvious effects on the refinement of pore structure and the improvement of impermeability (Gu et al. 1994; Khatib and Mangat 1999; Puertas et al. 2005; Xu et al. 2000). It is well known that W/C has significant effects on the microstructure and the pore structure (Cook and Hover 1999). Thus, it can be deduced that the effective mechanism of superplasticizers may differ in different W/Cs in the pastes.

Generally, adding polymer latexes is beneficial to the reduction of pore size and the improvement of impermeability of hardened cementitious materials. Ohama et al. (1991) revealed oxygen diffusion resistance of the polymer-modified mortars was larger than that of unmodified mortars, and was markedly increased with an increase in polymer to cement ratio. Moreover, Gao et al. (2002) found that the pore volume and the pore size of latex-modified cement pastes tended to become smaller with an increase in latex to cement ratio because the capillary pores of the HCPs were filled in with the polymer particles or the polymer membranes formed by agglomeration of the polymer particles. Meanwhile, the polymer latex film could effectively compact the interfacial zones between fine aggregates and cement pastes, and improve the impermeability of hardened mortars (Beeldens et al. 2005; Czarnecki and Schorn 2007; Knapen and Van 2009; Zhang et al. 2011). As for CAM, the covering of hydrophobic asphalt emulsions on cement grains could increase the impermeability of CAM to some extents (Song et al. 2006).

The three polymers, which are widely used in cementitious materials, are available with different particle sizes. Although much research on the cement mortars with superplasticizers, polymer latexes and asphalt emulsions have been conducted, few studies dwell on their impacts on the pore structure and the impermeability from the viewpoints of microstructure in the fresh state of cement pastes, especially their different impacts originating from the particle size. Specifically, the formation of the pores may be affected by adding these polymers due to their impacts on the rheological properties of fresh pastes, cement hydration, and the shrinkage of hardened pastes. Furthermore, the type of polymers with

varied particle sizes also plays an important role in changing the pore structure and the impermeability.

As chemical admixtures are gaining an increasing importance in many applications including concrete and mortars, it is both practically and scientifically necessary to confirm the impacts of various chemical admixtures on the pore structure and the impermeability of hardened cementitious materials and to elucidate the inner mechanism from the viewpoints of microstructure in the fresh state of cement pastes.

1.4 Summary

This research is divided into eight chapters as below:

(1) This chapter Introduction. The research background, research significance, literature reviews and research contents were introduced in detail. More importantly, several specific problems in existing literatures and the research gaps were clarified in this chapter.
(2) Chapter 2 Methodology. In this chapter, the relevant raw materials used for experiments, preparation of specimens and measuring methods were described.
(3) Chapter 3 Rheological properties of FCPs. The effects of superplasticizers, polymer latexes and asphalt emulsions on the rheological properties of fresh cement pastes were discussed in this chapter. Moreover, the working mechanisms of these admixtures were proposed.
(4) Chapter 4 Mesostructure of FCPs. The organization structure of cement grains in suspensions and the mesostructure of FCPs containing various chemical admixtures were observed by using a combination of various microscopies. Additionally, the relationship between the mesostructure and the rheological properties of FCPs was established in this chapter.
(5) Chapter 5 Working mechanism of chemical admixtures. On the basis of the essence of adsorption and retardation of polymers, the working mechanisms of superplasticizers, latexes and asphalt emulsions in tuning the rheological properties of FCPs were elucidated.
(6) Chapter 6 Microstructural and rheological models. A microstructural model, two rheological evolution models and rheological parameter models with incorporation of important influencing factors were deduced, based on the mesostructure observation and the working mechanisms of chemical admixtures.
(7) Chapter 7 Pore structure of HCPs and impermeability of mortars. The impacts of various chemical admixtures on the pore structure and the impermeability were discussed and the mechanism was clarified from the viewpoints of microstructure in the fresh state of cement pastes in this chapter.

(8) Chapter 8 Conclusions. All the research contributions were summarized and highlighted in this chapter. Limitations were pointed out and future works in the related topics were proposed as well.

References

Aiad I (2003) Influence of time addition of superplasticizers on the rheological properties of fresh cement pastes. Cem Concr Res 33(8):1229–1234
Aïtcin PC (2000) Cements of yesterday and today: concrete of tomorrow. Cem Concr Res 30 (9):1349–1359
Aïtcin PC (2011) High performance concrete. CRC Press, Boca Raton
Allan ML (1997) Rheology of latex-modified grouts. Cem Concr Res 27(12):1875–1884
Anagnostopoulos CA, Anagnostopoulos AC (2002) Polymer-cement mortars for repairing ancient masonries mechanical properties. Constr Build Mater 16(7):379–384
Arandigoyen M, Alvarez JI (2007) Pore structure and mechanical properties of cement-lime mortars. Cem Concr Res 37(5):767–775
Assaad J, Khayat KH, Mesbah H (2003) Assessment of thixotropy of flowable and self-consolidating concrete. ACI Mater J 100(2):99–107
Autier C, Azéma N, Boustingorry P (2014) Using settling behaviour to study mesostructural organization of cement pastes and superplasticizer efficiency. Colloids Surf A 450:36–45
Autier C, Azema N, Taulemesse JM et al (2013) Mesostructure evolution of cement pastes with addition of superplasticizers highlighted by dispersion indices. Powder Technol 249:282–289
Axelsson M, Gustafson G (2006) A robust method to determine the shear strength of cement-based injection grouts in the field. Tunn Undergr Space Technol 21(5):499–503
Banfill PFG (1994) Rheological methods for assessing the flow properties of mortar and related materials. Constr Build Mater 8(1):43–50
Banfill PFG (2003) The rheology of fresh cement and concrete—a review. In: Proceedings of 11th international cement chemistry congress, Durban, South Africa, pp 1–13
Banfill PFG (2006) Rheology of fresh cement and concrete. Rheol Rev 2006:61
Banfill PFG, Bowen P, Flatt RJ et al (2007) Improved superplasticisers for high performance concrete: the SUPERPLAST project. In: Abstract CD ROM of the twelfth international congress on the chemistry of cement
Barluenga G, Hernández-Olivares F (2004) SBR latex modified mortar rheology and mechanical behaviour. Cem Concr Res 34(3):527–535
Barnes HA (1999) The yield stress—a review or ‘παντα ρει’—everything flows? J Nonnewton Fluid Mech 81(1):133–178
Barnes HA, Hutton JF (1989) An introduction to rheology. Elsevier, Amsterdam
Barnes HA, Nguyen QD (2001) Rotating vane rheometry-a review. J Nonnewton Fluid Mech 98 (1):1–14
Beeldens A, Van Gemert D, Schorn H et al (2005) From microstructure to macrostructure: an integrated model of structure formation in polymer-modified concrete. Mater Struct 38(6):601–607
Bellotto M (2013) Cement paste prior to setting: a rheological approach. Cem Concr Res 52:161–168
Bian R, Shen J (2006) Review of polycarboxylate superplasticizer: synthetic methods and research. Fine Chem 23(2):179–182
Blair GWS (1966) The success of Casson’s equation. Rheol Acta 5(3):184–187

Borget P, Galmiche L, Le Meins JF et al (2005) Microstructural characterisation and behaviour in different salt solutions of sodium polymethacrylate-g-PEO comb copolymers. Colloids Surf A 260(1):173–182
Bremmell KE, Jameson GJ, Biggs S (1998) Polyelectrolyte adsorption at the solid/liquid interface: interaction forces and stability. Colloids Surf A 139(2):199–211
Brinkman HC (1952) The viscosity of concentrated suspensions and solutions. J Chem Phys 20 (4):571
Burge TA, Krapf-Huber A, Sulser U et al (1999) Dispersing agent for high-flow or self-compacting concrete: U.S. Patent 5919300
Burgos-Montes O, Palacios M, Rivilla P et al (2012) Compatibility between superplasticizer admixtures and cements with mineral additions. Constr Build Mater 31:300–309
Cao EX, Zhang YR, Kong XM (2012) Microstructure model of fresh cement paste with superplasticizer. Concrete 8:37–161 (in Chinese)
Castro A, Bergenståhl B, Tornberg E (2013) Effect of heat treatment and homogenization on the rheological properties of aqueous parsnip suspensions. J Food Eng 117(3):383–392
China Cement Information Center. [EB/OL][20140731]. http://www.ccement.com/news/content/7538953450084.html (in Chinese)
Chandra S, Björnström J (2002) Influence of superplasticizer type and dosage on the slump loss of Portland cement mortars—part II. Cem Concr Res 32(10):1613–1619
Clayton S, Grice TG, Boger DV (2003) Analysis of the slump test for on-site yield stress measurement of mineral suspensions. Int J Miner Process 70(1):3–21
Cook RA, Hover KC (1999) Mercury porosimetry of hardened cement pastes. Cem Concr Res 29 (6):933–943
Cyr M, Legrand C, Mouret M (2000) Study of the shear thickening effect of superplasticizers on the rheological behaviour of cement pastes containing or not mineral additives. Cem Concr Res 30(9):1477–1483
Cyr M, Mouret M (2003) Rheological characterization of superplasticized cement pastes containing mineral admixtures: consequences on self-compacting concrete design. ACI Spec Publ 217:241–256
Czarnecki L, Schorn H (2007) Nanomonitoring of polymer cement concrete microstructure. Restor Build Monum 13(3):141–152
Dai XN (2005) Rheological study on LDHs klaolinite suspensions. Shandong University, Shandong (in Chinese)
Dimmig A (2002) Einflqsse von Polymeren auf die Mikrostruktur und die Dauerhaftigkeit kunststoffmodifizierter Mfrtel (PCC). Ph.D. thesis, Bauhaus-Universit, Weimar
Domone PL, Thurairatnam H (1988) The effect of water/cement ratio, plasticizers and temperature on the rheology of cement grouts. Adv Cem Res 1(4):195–206
Einstein A (1956) Investigations on the theory of the Brownian movement. Courier Dover Publications, New York
Faroug F, Szwabowski J, Wild S (1999) Influence of superplasticizers on workability of concrete. J Mater Civ Eng 11(2):151–157
Felekoğlu B, Türkel S, Baradan B (2007) Effect of water/cement ratio on the fresh and hardened properties of self-compacting concrete. Build Environ 42(4):1795–1802
Ferrandis JY, Leveque G (2003) In situ measurement of elastic properties of cement by an ultrasonic resonant sensor. Cem Concr Res 33(8):1183–1187
Ferrari G, Cerulli T, Clemente P et al (2000) Influence of carboxylic acid-carboxylic ester ratio of carboxylic acid ester superplasticizer on characteristics of cement mixtures. ACI Spec Publ 195:505–520
Ferraris CF, Gaidis JM (1992) Connection between the rheology of concrete and rheology of cement paste. ACI Mater J 89(4):388–393
Ferraris CF, Obla KH, Hill R (2001) The influence of mineral admixtures on the rheology of cement paste and concrete. Cem Concr Res 31(2):245–255
Flatt RJ, Bowen P (2006) Yodel: a yield stress model for suspensions. J Am Ceram Soc 89 (4):1244–1256

Flatt RJ, Bowen P (2007) Yield stress of multimodal powder suspensions: an extension of the YODEL (Yield Stress YODEL). J Am Ceram Soc 90(4):1038–1044
Flatt RJ, Houst YF (2001) A simplified view on chemical effects perturbing the action of superplasticizers. Cem Concr Res 31(8):1169–1176
Flatt RJ, Martys N, Bergström L (2004) The rheology of cementitious materials. MRS Bull 29 (05):314–318
Flatt RJ (2004) Towards a prediction of superplasticized concrete rheology. Mater Struct 37 (5):289–300
Frankel NA, Acrivos A (1967) On the viscosity of a concentrated suspension of solid spheres. Chem Eng Sci 22(6):847–853
Gagn R, Boisvert A, Pigeon M (1996) Effect of superplasticizer dosage on mechanical properties, permeability, and freeze-thaw durability of high-strength concretes with and without silica fume. ACI Mater J 93(2):111–120
Gao JM, Qian CX, Wang B et al (2002) Experimental study on properties of polymer-modified cement mortars with silica fume. Cem Concr Res 32(1):41–45
Gao PW, Deng M, Feng NQ (2001) The influence of superplasticizer and superfine mineral powder on the flexibility, strength and durability of HPC. Cem Concr Res 31(5):703–706
Giraudeau C, D'Espinose De Lacaillerie JB, Souguir Z et al (2009) Surface and intercalation chemistry of polycarboxylate copolymers in cementitious systems. J Am Ceram Soc 92 (11):2471–2488
Golaszewski J, Szwabowski J (2004) Influence of superplasticizers on rheological behavior of fresh cement mortars. Cem Concr Res 34(2):235–248
Goowin JW (1975) The rheology of dispersion. Colloid Sci 2:246–293
Grasley ZC, Lange DA (2007) Constitutive modeling of the aging viscoelastic properties of portland cement paste. Mech Time Depend Mater 11(3–4):175–198
Griesser A (2002) Cement-superplasticizer interactions at ambient temperatures. Swiss Federal Institute of Technology, Zürich
Gu P, Xie P, Beaudoin JJ et al (1994) Investigation of the retarding effect of superplasticizers on cement hydration by impedance spectroscopy and other methods. Cem Concr Res 24(3):433–442
Gu PY, Pan QM (1994) Study on rheological properties of viscoelastic fluids. J Zhejiang Univ (Eng Sci) 28(1):88–93 (in Chinese)
Håkansson U, Hässler L, Stille H (1992) Rheological properties of microfine cement grouts with additives. In: Grouting, soil improvement and geosynthetics, ASCE, pp 551–563
Han S (2012) The influencing mechanism of gypsum and alkali sulfate on the compatibility of cement with superplasticizers. Tsinghua University, Beijing (in Chinese)
Heywood NI, Cheng DCH (1984) Comparison of methods for predicting head loss in turbulent pipe flow of non-Newtonian fluids. Trans Inst Meas Control 6(1):33–45
Houst YF, Bowen P, Perche F (2005) Towards tailored superplasticizers. In: Global construction: ultimate concrete opportunities: proceedings of the international conference, Scotland, UK
Houst YF, Bowen P, Perche F et al (2008) Design and function of novel superplasticizers for more durable high performance concrete (superplastic project). Cem Concr Res 38(10):1197–1209
Houst YF, Flatt R J, Bowen P et al (1999) New superplasticizers: from research to application. In: Proceedings of international conference on modern concrete materials: binders, additions and admixtures, London, UK, pp 445–456
Hsu KC, Chiu JJ, Chen SD et al (1999) Effect of addition time of a superplasticizer on cement adsorption and on concrete workability. Cem Concr Compos 21(5):425–430
Hu C, de Larrard F (1996) The rheology of fresh high-performance concrete. Cem Concr Res 26 (2):283–294
Hu SG, Zhang YH, Wang FZ (2012) Effect of temperature and pressure on the degradation of cement asphalt mortar exposed to water. Constr Build Mater 34:570–574
Huang DN (1980) Rheology and application science of cement. J Chin Ceram Soc 3:1–10 (in Chinese)

Huang DN, Xie YS (1984) Rheological concepts of fresh concrete. J Chin Ceram Soc 3:35–39 (in Chinese)
Huang Z, Thiagarajan VS, Lyngberg OK et al (1999) Microstructure evolution in polymer latex coatings for whole-cell biocatalyst application. J Colloid Interface Sci 215(2):226–243
Jiang TQ (2004) Rheology of chemical engineering. East China University of Science and Technology Press, Shanghai (in Chinese)
Jin RG, Hua YQ (1991) Polymer physics, 1st edn. Chemical Industry Press, Beijing (in Chinese)
Jolicoeur C, Simard MA (1998) Chemical admixture-cement interactions: phenomenology and physico-chemical concepts. Cem Concr Compos 20(2):87–101
Kauppi A, Banfill PFG, Bowen P et al (2003) Improved superplasticizers for high performance concrete. In: Proceedings of the 11th international congress on the chemistry of cement, New Delhi, India, 2(LTP-CONF-2003-001), p 8
Kapur PC, Scales PJ, Boger DV et al (1997) Yield stress of suspensions loaded with size distributed particles. AIChE J 43(5):1171–1179
Kasami H, Ikeda T, Yamane S (1979) On workability and pumpability of superplasticized concrete-experience in Japan. ACI Spec Publ 62:67–86
Khatib JM, Mangat PS (1999) Influence of superplasticizer and curing on porosity and pore structure of cement paste. Cem Concr Compos 21(5):431–437
Kim BG, Jiang S, Jolicoeur C et al (2000) The adsorption behavior of PNS superplasticizer and its relation to fluidity of cement paste. Cem Concr Res 30(6):887–893
Knapen E, Van Gemert D (2009) Cement hydration and microstructure formation in the presence of water-soluble polymers. Cem Concr Res 39(1):6–13
Kodama K, Okazawa S (1992) Development of a superplasticizer for high strength concrete. Semento Konkurito 546:24–32
Kong XM, Cao EX, Hou SS (2010a) Research progress of polycarboxylate superplasticizer. China Concr 5:28–37 (in Chinese)
Kong XM, Liu YL, Yan PY (2010b) Temperature sensitivity of mechanical properties of cement asphalt mortars. J Chin Ceram Soc 4:553–558 (in Chinese)
Kong XM, Wu CC, Zhang YR et al (2013a) Polymer-modified mortar with a gradient polymer distribution: preparation, permeability, and mechanical behaviour. Constr Build Mater 38:195–203
Kong XM, Zhang YR, Hou SS (2013b) Study on the rheological properties of Portland cement pastes with polycarboxylate superplasticizers. Rheol Acta 52(7):707–718
Kong XM, Zhang YR, Zhang JY et al (2011) Investigation on flowability and microstructure of fresh cement asphalt binder. J Build Mater 14(4):569–575 (in Chinese)
Krieger IM, Dougherty TJ (1959) A mechanism for non-Newtonian flow in suspensions of rigid spheres. Trans Soc Rheol (1957–1977) 3(1):137–152
Krstulović R, Žmikić A, Dabić P (1994) Examination of reaction between the NSF superplasticizer and cement. Cem Concr Res 24(5):948–958
Labouret S, Looten-Baquet I, Bruneel C et al (1998) Ultrasound method for monitoring rheology properties evolution of cement. Ultrasonics 36(1):205–208
Li QH, Kong XM (2009) Properties and microstructure of polymer modified mortar based on different acrylate latexes. J Chin Ceram Soc 1:107–114
Liu CC (2005) Copolymerization of polycarboxylic superplasticizer. Green Build 21(4):41–42 (in Chinese)
Liu YL, Kong XM, Yan PY (2011) Investigation on dynamical mechanical behaviours of cement-asphalt binders. Eng Mech 28(7):53–58 (in Chinese)
Liu YL, Kong XM, Zhang JY et al (2012a) Effect of curing temperature on strength development of cement asphalt mortars. J Build Mater 15(2):211–217 (in Chinese)
Liu YL, Kong XM, Zhang YR et al (2012b) Static and dynamic mechanical properties of cement-asphalt composites. J Mater Civ Eng 25(10):1489–1497
Liu YL, Kong XM, Zou Y et al (2009) Static and dynamic mechanical behaviour of cement asphalt mortars. J Railw Sci Eng 6(3):1–7 (in Chinese)

Malhotra VM (1989) Superplasticizers: a global review with emphasis on durability and innovative concretes. ACI Spec Publ 119:1–18
Malhotra VM (1999) Innovative applications of superplasticizers in concrete: a review. Roles Admix High Perform Concr 5:421–460
Martini SA, Nehdi M (2009) Coupled effects of time and high temperature on rheological properties of cement pastes incorporating various superplasticizers. J Mater Civ Eng 21 (8):392–401
Mewis J, Wagner NJ (2009) Current trends in suspension rheology. J Nonnewton Fluid Mech 157 (3):147–150
Miao CW, Ran QP, Hong JX et al (2009) Present situation and development trends of polycar-boxylate-type superplasticizers. Mater China 28(11):36–45 (in Chinese)
Mollah MYA, Adams WJ, Schennach R et al (2000) A review of cement-superplasticizer interactions and their models. Adv Cem Res 12(4):153–161
Morris JF (2009) A review of microstructure in concentrated suspensions and its implications for rheology and bulk flow. Rheol Acta 48(8):909–923
Murray BS (2011) Rheological properties of protein films. Curr Opin Colloid Interface Sci 16 (1):27–35
Nachbaur L, Mutin JC, Nonat A et al (2001) Dynamic mode rheology of cement and tricalcium silicate pastes from mixing to setting. Cem Concr Res 31(2):183–192
Nehdi M, Al Martini S (2009) Estimating time and temperature dependent yield stress of cement paste using oscillatory rheology and genetic algorithms. Cem Concr Res 39(11):1007–1016
Nehdi M, Mindess S, Aïtcin PC (1997) Statistical modelling of the microfiller effect on the rheology of composite cement pastes. Adv Cem Res 9(33):37–46
Nguyen QD, Boger DV (1992) Measuring the flow properties of yield stress fluids. Annu Rev Fluid Mech 24(1):47–88
Ohama Y (1987) Principle of latex modification and some typical properties of latex-modified mortars and concretes adhesion; binders (materials); bond (paste to aggregate); carbonation; chlorides; curing; diffusion. ACI Mater J 84(6):511–518
Ohama Y (1997) Recent progress in concrete-polymer composites. Adv Cem Based Mater 5 (2):31–40
Ohama Y, Demura K, Kobayashi K et al (1991) Pore size distribution and oxygen diffusion resistance of polymer-modified mortars. Cem Concr Res 21(2):309–315
Ohta A, Sugiyama T, Uomoto T (2000) Study of dispersing effects of polycarboxylate-based dispersant on fine particles. ACI Spec Publ 195:211–228
Papo A (1988) Rheological models for cement pastes. Mater Struct 21(1):41–46
Papo A, Piani L (2004a) Effect of various superplasticizers on the rheological properties of Portland cement pastes. Cem Concr Res 34(11):2097–2101
Papo A, Piani L (2004b) Flow behavior of fresh Portland cement pastes. Part Sci Technol 22 (2):201–212
Peng J, Qu J, Zhang J et al (2005) Adsorption characteristics of water-reducing agents on gypsum surface and its effect on the rheology of gypsum plaster. Cem Concr Res 35(3):527–531
Petit JY, Khayat KH, Wirquin E (2006) Coupled effect of time and temperature on variations of yield value of highly flowable mortar. Cem Concr Res 36(5):832–841
Petit JY, Khayat KH, Wirquin E (2009) Coupled effect of time and temperature on variations of plastic viscosity of highly flowable mortar. Cem Concr Res 39(3):165–170
Petit JY, Wirquin E, Duthoit B (2005) Influence of temperature on yield value of highly flowable micromortars made with sulfonate-based superplasticizers. Cem Concr Res 35(2):256–266
Petit JY, Wirquin E, Khayat KH (2010) Effect of temperature on the rheology of flowable mortars. Cem Concr Compos 32(1):43–53
Petit JY, Wirquin E, Vanhove Y et al (2007) Yield stress and viscosity equations for mortars and self-consolidating concrete. Cem Concr Res 37(5):655–670
Plank J, Dai Z, Andres PR (2006) Preparation and characterization of new Ca–Al–polycarboxylate layered double hydroxides. Mater Lett 60(29):3614–3617

Plank J, Gretz M (2008) Study on the interaction between anionic and cationic latex particles and Portland cement. Colloids Surf A 330(2):227–233

Plank J, Hirsch C (2007) Impact of zeta potential of early cement hydration phases on superplasticizer adsorption. Cem Concr Res 37(4):537–542

Plank J, Sachsenhauser B (2006) Impact of molecular structure on zeta potential and adsorbed conformation of α-allyl-ω-methoxypolyethylene glycol-maleic anhydride superplasticizers. J Adv Concr Technol 4(2):233–239

Plank J, Sachsenhauser B (2009) Experimental determination of the effective anionic charge density of polycarboxylate superplasticizers in cement pore solution. Cem Concr Res 39(1):1–5

Pourchet S, Comparet C, Nicoleau L et al (2007) Influence of PC superplasticizers on tricalcium silicate hydration. In: Proceedings of the 12th international congress on the chemistry of cement-ICCC

Pourchet S, Comparet C, Nonat A et al (2006) Influence of three types of superplasticizers on tricalciumaluminate hydration in presence of gypsum. In: Proceedings of the 8th CANMET/ACI international conference on superplasticizers and other chemical admixtures in concrete, Sorrento, October 20–23, 2006, pp 151–158

Pourchet S, Liautaud S, Rinaldi D et al (2012) Effect of the repartition of the PEG side chains on the adsorption and dispersion behaviors of PCP in presence of sulfate. Cem Concr Res 42 (2):431–439

Probstein RF, Sengun MZ, Tseng TC (1994) Bimodal model of concentrated suspension viscosity for distributed particle sizes. J Rheol (1978-Present) 38(4):811–829

Puertas F, Santos H, Palacios M et al (2005) Polycarboxylate superplasticiser admixtures: effect on hydration, microstructure and rheological behaviour in cement pastes. Adv Cem Res 17(2):77–89

Qian XL, Zhao SL, Zhang XB et al (2002) The working mechanisms and property of high range water-reducers. J Nanjing Tech Univ 24(2):61–64 (in Chinese)

Rahman MK, Baluch MH, Malik MA (2014) Thixotropic behavior of self-compacting concrete with different mineral admixtures. Constr Build Mater 50:710–717

Ran QP (2007) Structure, adsorption, dispersion and mechanism of comb-shaped copolymers. Nanjing University, Jiangsu (in Chinese)

Ran QP, Miao CW, Liu JP et al (2009a) Mechanism and effects of side chain length of comb-like copolymer dispersant on the dispersion of cement paste. J Chin Ceram Soc 37(7):1153–1159 (in Chinese)

Ran Q, Somasundaran P, Miao C et al (2009b) Effect of the length of the side chains of comb-like copolymer dispersants on dispersion and rheological properties of concentrated cement suspensions. J Colloid Interface Sci 336(2):624–633

Ran Q, Somasundaran P, Miao C et al (2010) Adsorption mechanism of comb polymer dispersants at the cement/water interface. J Dispers Sci Technol 31(6):790–798

Rao MA (2014) Flow and functional models for rheological properties of fluid foods. In: Rheology of fluid, semisolid, and solid foods. Springer US, pp 27–61

Ravi KM, Sutton DL (1990) New rheological correlation for cement slurries as a function of temperature. In: SPE annual technical conference and exhibition, society of petroleum engineers

Rößler C, Eberhardt A, Kučerová H et al (2008) Influence of hydration on the fluidity of normal Portland cement pastes. Cem Concr Res 38(7):897–906

Romano RCDO, Pileggi RG (2012) Temperature's role in the rheological behaviour of cementitious pastes prepared with air-entraining admixtures. Appl Rheol 22:24333–24338

Roussel N (2006) A thixotropy model for fresh fluid concretes: theory, validation and applications. Cem Concr Res 36(10):1797–1806

Roussel N (2007) Rheology of fresh concrete: from measurements to predictions of casting processes. Mater Struct 40(10):1001–1012

Roussel N, Geiker MR, Dufour F et al (2007) Computational modeling of concrete flow: general overview. Cem Concr Res 37(9):1298–1307

Roussel N, Stefani C, Leroy R (2005) From mini-cone test to Abrams cone test: measurement of cement-based materials yield stress using slump tests. Cem Concr Res 35(5):817–822
Rubio-Hernández FJ, Velázquez-Navarro JF, Ordóñez-Belloc LM (2013) Rheology of concrete: a study case based upon the use of the concrete equivalent mortar. Mater Struct 46(4):587–605
Rumpf H (1962) The strength of granules and agglomerates. Interscience, New York
Saija LM (1995) Waterproofing of portland cement mortars with a specially designed polyacrylic latex. Cem Concr Res 25(3):503–509
Sakai E, Kasuga T, Sugiyama T et al (2006) Influence of superplasticizers on the hydration of cement and the pore structure of hardened cement. Cem Concr Res 36(11):2049–2053
Sarkar SL, Aimin X (1992) Preliminary study of very early hydration of superplasticized C3A+ gypsum by environmental SEM. Cem Concr Res 22(4):605–608
Scales PJ, Johnson SB, Healy TW et al (1998) Shear yield stress of partially flocculated colloidal suspensions. AIChE J 44(3):538–544
Schmidt W, Brouwers HJH, Kühne HC et al (2014) Influences of superplasticizer modification and mixture composition on the performance of self-compacting concrete at varied ambient temperatures. Cem Concr Compos 49:111–126
Schultz MA, Struble LJ (1993) Use of oscillatory shear to study flow behavior of fresh cement paste. Cem Concr Res 23(2):273–282
Schwartzentruber LDA, Le Roy R, Cordin J (2006) Rheological behaviour of fresh cement pastes formulated from a Self-Compacting Concrete (SCC). Cem Concr Res 36(7):1203–1213
Shen Z, Wang GT (1991) Colloid and surface chemistry. Chemical Industry Press, Beijing (in Chinese)
Sheinn AMM, Ho DWS, Tam CT (2002) Rheological model for self-compacting concrete-paste rheology. In: Proceedings of the 27th conference on our world in concrete and structures, Singapore, pp 28–29
Shi TJ, Wu DF (2009) Foundation of polymer rheology. Chemical Industry Press, Beijing (in Chinese)
Shin JY, Hong JS, Suh JK et al (2008) Effects of polycarboxylate-type superplasticizer on fluidity and hydration behavior of cement paste. Korean J Chem Eng 25(6):1553–1561
Shroff AV, Joshi NH, Shah DL (1996) Rheological properties of micro fine cement dust grouts. Grouting and Deep Mixing Balkema
Song H, Do J, Soh Y (2006) Feasibility study of asphalt-modified mortars using asphalt emulsion. Constr Build Mater 20(5):332–337
Struble LJ, Lei WG (1995) Rheological changes associated with setting of cement paste. Adv Cem Based Mater 2(6):224–230
Struble L, Sun GK (1995) Viscosity of Portland cement paste as a function of concentration. Adv Cem Based Mater 2(2):62–69
Struble L, Szecsy R, Lei WG et al (1998) Rheology of cement paste and concrete. Cem Concr Aggreg 20(2):269–277
Su Z (1995) Microstructure of polymer cement concrete. Ph.D. thesis, Material Sciences Group, Delft University of Technology, Delft, Netherlands
Su Z, Sujata K, Bijen JM et al (1996) The evolution of the microstrcture styrene acrylate polymer-modified cement pastes at the early stage of cement hydration. Adv Cem Base Mater 3:87–93
Subramaniam KV, Lee J, Christensen BJ (2005) Monitoring the setting behavior of cementitious materials using one-sided ultrasonic measurements. Cem Concr Res 35(5):850–857
Subramaniam KV, Wang X (2010) An investigation of microstructure evolution in cement paste through setting using ultrasonic and rheological measurements. Cem Concr Res 40(1):33–44
Sun Z, Voigt T, Shah SP (2006) Rheometric and ultrasonic investigations of viscoelastic properties of fresh Portland cement pastes. Cem Concr Res 36(2):278–287
Swamy RN (1989) Superplasticizers and concrete durability. ACI Special Publication, vol 119
Thomas DG (1965) Transport characteristics of suspension: VIII. A note on the viscosity of Newtonian suspensions of uniform spherical particles. J Colloid Sci 20(3):267–277

Uchikawa H, Hanehara S, Shirasaka T et al (1992) Effect of admixture on hydration of cement, adsorptive behavior of admixture and fluidity and setting of fresh cement paste. Cem Concr Res 22(6):1115–1129

Umlauf R (1993) Rheological characterization of microfine cement suspension-examination with a shear stress controller rheometer Grouting in Rock and Concrete. Balkenra 91–95

Valič MI (2000) Hydration of cementitious materials by pulse echo USWR: method, apparatus and application examples. Cem Concr Res 30(10):1633–1640

Vand V (1948) Viscosity of solutions and suspensions. II. Experimental determination of the viscosity–concentration function of spherical suspensions. J Phys Chem 52(2):300–314

Wallevik JE (2006) Relationship between the Bingham parameters and slump. Cem Concr Res 36 (7):1214–1221

Wang DM, Zhang LR, Zhang WL et al (2013) Effects of superplasticizers on multi-level flocculation structure of fresh cement paste. J Build Mater 15(6):755–759 (in Chinese)

Wang F, Liu Z, Wang T et al (2008a) A novel method to evaluate the setting process of cement and asphalt emulsion in CA mortar. Mater Struct 41(4):643–647

Wang FZ, Wang T, Hu SG et al (2008b) Rheological behavior of cement asphalt mortar. Eng J Wuhan Univ 41(4):69–72 (in Chinese)

Wang LJ, Huang FY, Ma XC (2008c) Experimental research on the saturation point of superplasticizers in cement based on fractal dimension. J Wuhan Univ Technol 30(2):28–31 (in Chinese)

Wang LJ, Tan XQ, Cao ML (2008d) Study on flocculated cement based on fractal theory. J Shenyang Jianzhu Univ (Nat Sci) 23(1):82–84 (in Chinese)

Wang Q, Yan PY, Ruhan A et al (2011) Strength mechanism of cement-asphalt mortar. J Mater Civil Eng 23(9):1353–1359

Wang R, Wang PM (2008) Application of polyacrylic ester latex to cement mortar. J Chin Ceram Soc 36(7):946–949

Wang R, Wang PM, Li XG (2005) Physical and mechanical properties of styrene-butadiene rubber emulsion modified cement mortars. Cem Concr Res 35(5):900–906

Wang T (2008) Research and application on CA mortar in Ballastless slab track of high speed railway. Wuhan University of Technology, Wuhan (in Chinese)

Wang X, Subramaniam KV, Lin FB (2010) Ultrasonic measurement of viscoelastic shear modulus development in hydrating cement paste. Ultrasonics 50(7):726–738

Wang ZM (2006) The interface chemistry phenomena and rheological properties of "cement-water-superplasticizer" system. Beijing University of Technology, Beijing (in Chinese)

Winnefeld F, Becker S, Pakusch J et al (2007) Effects of the molecular architecture of comb-shaped superplasticizers on their performance in cementitious systems. Cem Concr Compos 29(4):251–262

Wu ZW, Lian HZ (1999) High performance concrete. China Railway Publishing Press, Beijing (in Chinese)

Xu G, Beaudoin JJ, Jolicoeur C et al (2000) Interfacial transition zone characterization of Portland cement mortars containing relatively high dosages of polynaphthalene sulfonate superplasticizers. Concr Sci Eng (Fr) 2(7):150–157

Xu YM (1989) A unified rheological model for non-dilatancy viscoplastic fluids. J Wuhan Univ Technol 11(4):431–436 (in Chinese)

Yahia A, Khayat KH (2001) Analytical models for estimating yield stress of high performance pseudoplastic grout. Cem Concr Res 31(5):731–738

Yamada K, Takahashi T, Hanehara S et al (2000) Effects of the chemical structure on the properties of polycarboxylate-type superplasticizer. Cem Concr Res 30(2):197–207

Yamada K, Yanagisawa T, Hanehara S (1999) Influence of temperature on the dispersibility of polycarboxylate type superplasticizer for highly fluid concrete. In: International RILEM symposium on self-compacting concrete, pp 437–448

Yang JB, Yan PY, Kong XM et al (2010) Study on the hardening mechanism of cement asphalt binder. Sci China Technol Sci 53(5):1406–1412

Yang Z, Shi X, Creighton AT et al (2009) Effect of styrene–butadiene rubber latex on the chloride permeability and microstructure of Portland cement mortar. Constr Build Mater 23(6):2283–2290

Ye DM, Sun ZP, Zhen BC et al (2012) Current research status and development of polymer modified cementitious repair material. Mater Rev 7:028 (in Chinese)

Yoshioka K, Sakai E, Daimon M et al (1997) Role of steric hindrance in the performance of superplasticizers for concrete. J Am Ceram Soc 80(10):2667–2671

Yoshioka K, Tazawa E, Kawai K et al (2002) Adsorption characteristics of superplasticizers on cement component minerals. Cem Concr Res 32(10):1507–1513

Zhang DY (2001) Study on the preparation of architectural latex coatings and its dispersion, rheology mechanism. South China University of Technology, Guangzhou (in Chinese)

Zhang LR, Wang DM, Zhang WL et al (2013) Observation of multi-level flocculation structure of fresh paste using laser scanning confocal microscopy. J Chin Electron Microsc Soc 32(3):231–236 (in Chinese)

Zhang YR, Kong XM, Cao EX (2010) Influence of temperature on flowability and hydration rate of fresh cement asphalt binder. J Chin Ceram Soc 38(11):156–161 (in Chinese)

Zhang YR, Kong XM, Hou SS et al (2012) Study on the rheological properties of fresh cement asphalt paste. Constr Build Mater 27(1):534–544

Zhang YR, Kong XM, Zhang ZL et al (2011) Impermeability of polymer modified mortar with different acrylate latexes. Science and Technology of Commercial Mortar (in Chinese)

Zhong S, Chen Z (2002) Properties of latex blends and its modified cement mortars. Cem Concr Res 32(10):1515–1524

Zhou Z, Solomon MJ, Scales PJ et al (1999) The yield stress of concentrated flocculated suspensions of size distributed particles. J Rheol (1978-Present) 43(3):651–671

Zingg A, Holzer L, Kaech A et al (2008) The microstructure of dispersed and non-dispersed fresh cement pastes-new insight by cryo-microscopy. Cem Concr Res 38(4):522–529

Chapter 2
Methodology

In this chapter, the raw materials, the preparation of specimens, the testing methods and the equipments used in this research are introduced in detail. On the basis of the following measurements, the obtained experimental data are discussed in the following chapters.

2.1 Raw Materials

2.1.1 Cement

Three batches of commercial cement were employed in this research, respectively corresponding to Cement I, Cement II and Cement III. Cement I and II were provided by China Building Materials Academy and Cement III was from Lafarge Shui On Cement Co. Ltd. All the three batches of cement comply with the Chinese standard GB8076-2008, whose chemical and mineralogical compositions are listed in Table 2.1.

2.1.2 Superplasticizers

Two types of superplasticizers were used in this research including a self-synthesized polycarboxylate (PCE) type superplasticizer and a commercial polycondensate type superplasticizer of β-naphthalene sulfonate formaldehyde (NSF). Their molecular structures are shown in Fig. 2.1.

The PCE superplasticizer was a comb-shaped co-polymer of acrylic acid (AA), methyl polyethylene glycol methacrylate (MPEGMA) and 2-acrylamido-2-methylpropane sulfonic acid (AMPS) with a monomer molar ratio of

Y. Zhang, *Study on Microstructure and Rheological Properties of Cement-Chemical Admixtures-Water Dispersion System at Early Stage*, Springer Theses, DOI 10.1007/978-981-10-4570-7_2

Table 2.1 Chemical and mineral compositions of cement

Cement	Chemical composition (mass %)								Mineral composition (mass %)			
	SiO_2	Al_2O_3	Fe_2O_3	CaO	MgO	SO_3	Na_2Oeq	f–CaO	C_3S	C_2S	C_3A	C_4AF
I	22.10	4.04	3.38	61.91	2.66	2.87	0.56	0.79	57.34	18.90	6.47	11.25
II	21.56	4.06	3.43	61.51	2.63	2.89	0.53	0.66	57.40	20.30	6.32	11.19
III	21.56	4.44	2.78	62.38	2.32	3.14	0.6	0.79	46.00	27.14	7.05	8.45

Note The composition was obtained according to EN 196-2:2005 and Chinese Standard GB/T176-2008 “chemical analysis of cement”

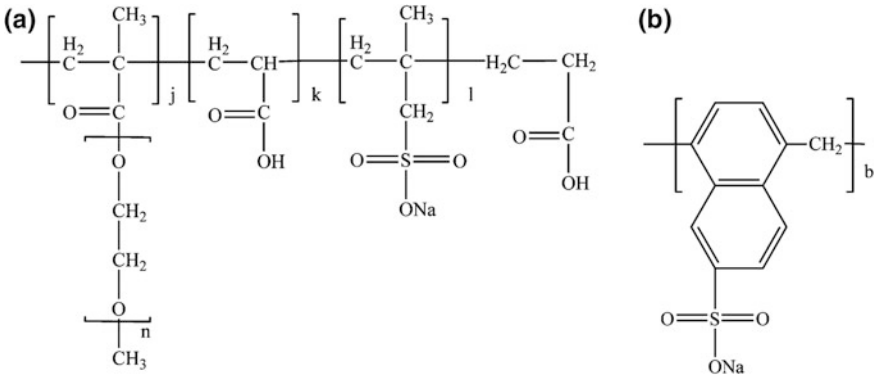

Fig. 2.1 Schematic drawing of chemical structure of superplasticizers. **a** PCE; **b** NSF

2.12:1.00:0.29 prepared via free radical polymerization by using ammonium persulfate (APS) as initiator at 80 °C. The weight average molecular weight (Mw) of MPEGMA was about 1300 and the average polymerization degree of the poly (ethylene oxide) was about 28. A general description of the preparation procedure of the PCE superplasticizer is summarized as follows. (1) 70.0 g of water was pre-charged into a flask vessel equipped with two feeding pipes. (2) The flask was firstly washed by using nitrogen gas for 3 times and heated up to 80 °C in an oil bath. (3) 196.0 g of the mixture of monomers, together with 1.3 g of the chain transfer agent, was dissolved in 170.0 g of deionized water. (4) Initiator solution was prepared by dissolving 1.0 g of APS in 40.0 g of deionized water. (5) Then the initiator solution and the monomer solution were separately fed into the vessel dropwise over 2.5 and 2.0 h respectively. (6) The inside temperature was kept constant at 80 ± 2 °C during polymerization. After completion of dosing, the whole reactant mixture was kept at 80 °C for an additional post-polymerization time of 30 min under stirring to complete the polymerization and then was allowed to cool down to a room temperature at 25 °C. An aqueous solution of PCE superplasticizer with a solid content of ca. 40 wt% was obtained. The number average molecular weight (Mn) of the synthesized PCE was 3.66×10^4 and the polydispersity index (Mw/Mn) was 2.48.

The commercial NSF superplasticizer was provided by Huadi Synthetic Material Co. Ltd.

2.1.3 Polymer Latexes

Two styrene-acrylate copolymer latexes with different particle sizes and T_g produced by BASF (China) Co. Ltd, latex L1 and latex L2, were used, whose properties are listed in Table 2.2.

Table 2.2 Properties of acrylate latexes

Polyacrylate latexes	Solid content (%)	Particle size (nm)	T_g (°C)	Viscosity (mPa.s)	pH	MFFT[a] (°C)	Density (g/cm^3)
L1	50	200	10	500–2000	7.0–9.0	12	1.03
L2	57	300	−6	140–200	7.0–8.5	<1	1.04

[a]Minimum film formation temperature

Table 2.3 Properties of asphalt emulsions

Type of asphalt emulsions	Solid content (%)	Particle size (μm)	Storage stability 1 day (%)	Residue on 1.18 mm sieve (%)	Penetration depth at 25 °C (0.1 mm)	Density (g/cm^3)
Anionic	61.16	2.9	0.30	0.02	73	1.02
Cationic	59.29	3.1	0.31	0.02	98	1.02

Note These properties were measured according to Chinese Industry Standard JTJ 052-2000

2.1.4 Asphalt Emulsions

Two types of anionic and cationic asphalt emulsions were provided by China Petrochemical Corporation, whose properties are shown in Table 2.3.

2.1.5 Organic Monomers, Homo-polymers and Co-polymers

To disclose the influences of the charge feature of molecules on the adsorption and the retardation effects in cement pastes, organic monomers possessing different charges in aqueous solution, and their corresponding linear homo-polymers were chosen. Moreover, two series of comb-shaped co-polymers with varied molar ratios of functional groups in backbones were synthesized without changing the charge density.

2.1.5.1 Organic Monomers and Their Corresponding Homo-polymers

Analytical grade of chemicals, acrylic acid (AA), sodium p-styrene sulfonate (SSS), [3-(methacryloylamino) propyl] trimethyl ammonium chloride (MAPTAC) were used as received (all >98% purity). Poly(acrylic acid) (PAA) with weight average molecular weight (Mw) of ca. 5000 was provided by Beijing Chengzhi Yongchang Chemicals Co. Ltd. Analytical grade of poly(sodium-p-styrene sulfonate) (PSSS) with Mw of 70,000 was purchased from Acros Organics. Cationic polymer, poly ([3-(methacryloylamino) propyl] trimethyl ammonium chloride) (PMAPTAC) was synthesized via semi-batch radial polymerization by using ammonium persulfate

(APS) as initiator at 80 °C. 45.0 g of water was pre-charged into a flask vessel equipped with two feeding pipes. The flask was firstly washed by using nitrogen gas for 3 times and then the mixture was heated up to 80 °C in oil bath. 335.0 g of MAPTAC solution with mass concentration of 32.8% and 65.0 g of APS solution with mass concentration of 1.7% were then separately fed into the vessel dropwise in 2.5 and 3.0 h respectively. After completion of both feedings, the reactant mixture was kept at 80 °C under stirring for another 2.0 h to complete the polymerization. An aqueous solution of PMAPTAC with solid content of ca. 25.0% was obtained. The synthesized PMAPTAC sample was purified via dialysis and then analyzed by size exclusion chromatography (SEC) to measure the molecular weight distribution (described in Sects. 2.2.1 and 2.2.2).

2.1.5.2 Comb-Shaped Co-polymers

The comb-shaped co-polymers were prepared via semi-batch free radical polymerization at 80 °C by co-polymerizing the monomers of AA, MPEGMA and sodium methyl acryl sulfonate (SMAS) with monomer molar ratio of 1.0:0.47:0.13, based on the basic recipe PAS100-0, given in Table 2.4. The initiator for polymerization was ammonium persulfate (APS) and 3-mercaptopropionic acid (MPA) was used as chain transfer agent to control the molecular weight. By partly replacing the monomer AA with AMPS in the polymerization recipes, the ratio of $–COO^-$ groups to $–SO_3^-$ groups can be adjusted without changing the charge density in the synthesized polymer molecules. Thus, the effects of $–COO^-$ and $–SO_3^-$ groups in co-polymer molecules on their behaviors in cementitious system can be studied. The synthesis formula of the comb-shaped co-polymers is presented in Fig. 2.2.

Amphoteric co-polymers were synthesized based on the basic recipe PAM100-0 (Table 2.4), in which the molar ratio of monomer AA to MPEGMA was fixed at 1.0:0.25. Cationic charges can be introduced into the molecules by simply replacing the monomer AA with MAPTAC in a certain ratio and the synthesized molecules

Table 2.4 Monomer combination in synthesis of the co-polymers

No.	AA	MPEGMA1300	SMAS	AMPS	MAPTAC
PAM100-0	1	0.25	–	–	0
PAM88-12	0.88	0.25	–	–	0.12
PAM75-25	0.75	0.25	–	–	0.25
PAM50-50	0.5	0.25	–	–	0.5
PAM0-100	0	0.25	–	–	1
PAS100-0	1	0.47	0.13	0	–
PAS70-30	0.7	0.47	0.13	0.3	–
PAS50-50	0.5	0.47	0.13	0.5	–
PAS0-100	0	0.47	0.13	1	–

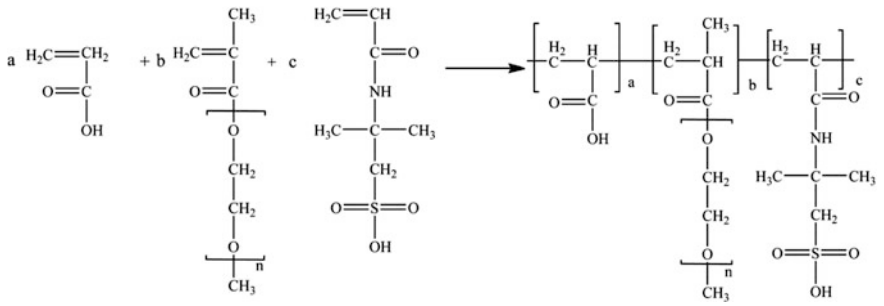

Fig. 2.2 Synthesis formula of the co-polymers containing both carboxyl and sulfonic groups

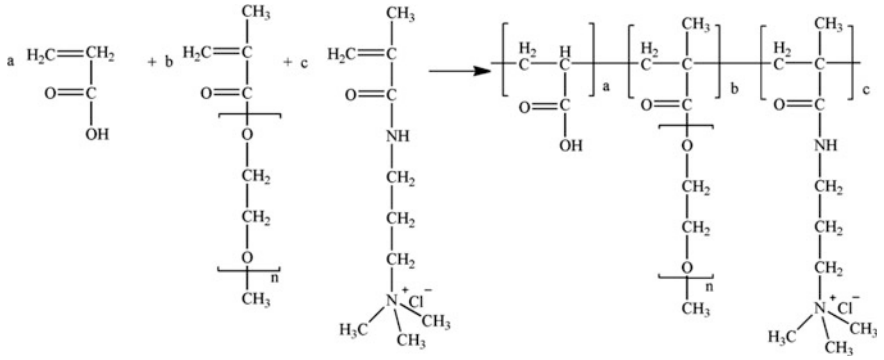

Fig. 2.3 Synthesis formula of the amphoteric co-polymers containing the cationic group $\equiv N^{+}-$

become amphoteric. Complete replacement of AA with MAPTAC makes the produced molecule turn to cationic one (PAM0-100). The synthesis formula of the amphoteric co-polymers is presented in Fig. 2.3.

Detailed description of the preparation procedure of the above mentioned co-polymers (PAM and PAS series) is summarized as follows. Monomers with mix proportion as described in Table 2.4, together with the chain transfer agent, were dissolved in deionized water and an aqueous solution with mass concentration of 55.0% was prepared. Initiator solution with mass concentration of 2.0% was prepared by dissolving APS in deionized water. In the polymerization process, 350.0 g of monomer solution was used and the molar ratio of initiator to total monomers was fixed at 1.0%. A flask vessel filled with 35.0 g of water and 35.0 g of monomer solution as pre-charge and equipped with two feeding pipes, was firstly washed by using nitrogen gas for 3 times and heated up to 80 °C in oil bath. Then the initiator solution and the rest of the monomer solution were separately fed into the vessel dropwise over 2.5 and 2.0 h respectively. The inside temperature was kept constant at 80 ± 2 °C during polymerization. After complete dosing, the whole reactant mixture was kept at 80 °C for additional post-polymerization time of 30 min under

stirring to complete polymerization and then was allowed to cool down to room temperature of 25 °C. The obtained products appeared yellowish transparent solutions with solid contents in a range of 36.0–38.0 wt%.

2.1.6 Antifoaming Agent

RHODOLINE DF 642, antifoaming agent, was provided by Rhodia (China) Co. Ltd.

2.1.7 Sand

Both standard sand (complying with GB178) and 40–70 mesh quartz sand were used for the preparation of mortar specimens.

2.1.8 Deionized Water

Deionized water was used in all experiments in this research including the synthesis of polymers and the preparation of cement pastes and mortars.

2.2 Characterization of the Synthesized Polymers

2.2.1 Size Exclusion Chromatography (SEC)

SEC has been a standard method for polymer fractionation and analysis of molecular weight distribution of polymers based on separation of polymer fractions with different molecular size, i.e. hydrodynamic volume. Integration of a light scattering instrument in the SEC system allows obtaining absolute molecular weights that do not rely on calibration with standards of known molecular mass. In this research, SEC equipped with a multi-angle laser light scattering (LS) detector (DAWN HELEOS II, Wyatt Technology, USA) and a refractive index (RI) detector (Optilab rEX, Wyatt Technology, USA) was used to determine the Mw, number average molecular weight (Mn) and the polydispersity (PDI) of the prepared polymers. Meanwhile, polymer content in the prepared polymer solution can be estimated by separation of polymers and oligomers with relatively high molecular weight from the synthesized product, which contains polymers, oligomers, macro-monomers (Mw of ca. 1300) and probably residual monomers with lower

molecular weight than 1000. For all polymers, 0.1 mol/L $NaNO_3$ solution at pH of 7 was used as the eluent in SEC measurement. The synthesized polymers were diluted to concentration of 5 mg/mL (10 mg/L for samples of PAM0-100, PAS0-100, PMAPTAC) and directly injected into a 0.2 mL loop with a spectra system auto sampler. Temperature during measurement was kept constant at 25 °C and the flow rate was adjusted to 0.5 mL/min. SEC columns of SB-804 HQ connected with SB-802.5 HQ (OHpak, Shodex, USA) were used for SEC measurement of all polymers.

2.2.2 *Purification of the Synthesized Polymers*

As well understood that the synthesis of co-polymers cannot reach conversion of 100% and known from the result of SEC measurements, the obtained samples from the synthesis of the co-polymers contain fractions of polymers, oligomers, un-reacted macro-monomer and those monomers with smaller molecular weight, and a tiny amount of salts from decomposition of initiator. In this research, dialysis technique was adopted to remove un-reacted monomers, salts and a part of oligomers with small molecular weights from the samples and to obtain purified co-polymer solutions, as shown in Fig. 2.4. A cellulose ester semipermeable membrane MD44-7 with nominal molecular weight cut-off of 7000 Da provided by Beijing Ruida Henghui Science and Technology Development Co. Ltd was used, which allows globulin with molecular weight of 7000 and smaller molecules to pass through. The synthesized product was firstly diluted to 10.0 wt% and then 40 mL of the diluted polymer solution was introduced into a dialysis bag with diameter of 25 mm and length of 300 mm, which is made of the semipermeable membrane.

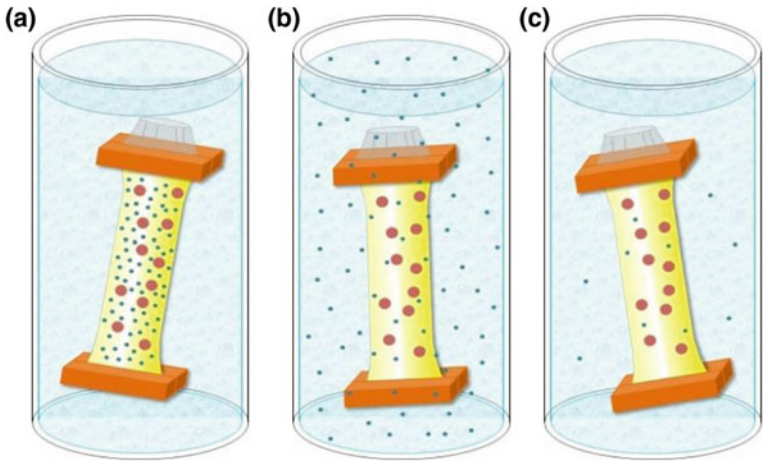

Fig. 2.4 Purification of the synthesized polymers

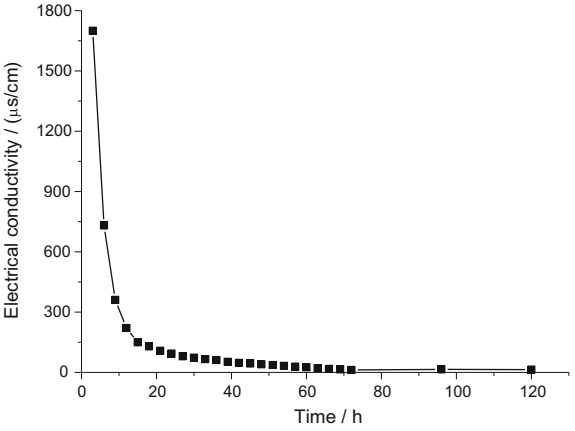

Fig. 2.5 Development of electrical conductivity of the dialysate during dialysis of the synthesized samples

Subsequently, 10 completely sealed dialysis bags filled with the polymer solutions were placed into a container filled with 5000 mL deionized water as dialysate. In order to accelerate the diffusion process of the monomers and salts across the semipermeable membrane, the water bath was kept at 40 °C under stirring and renewed every 3 h. The electrical conductivity of the dialysate was measured by using a conductivity meter (FE30, Mettler Toledo, Switzerland) every 3 h before the dialysate was renewed. It is noticed from Fig. 2.5 that the electrical conductivity of the dialysate sharply decreased at the beginning of the dialysis (first 24 h), which indicated a fast diffusion of the salts and monomers from the sample inside the dialysis bag to the water bath. With continuous dialysis for 4 days, the electrical conductivity of dialysate kept slowly decreasing. Knowing that the electrical conductivity of deionized water was about 10 μS/cm, we ended the dialysis process when the electrical conductivity of dialysate dropped below 30 μS/cm. Thus, most of salts, residual monomers and oligomers that are able to pass across the semipermeable membrane were effectively removed from the sample. After purification by dialysis, the solid content of the obtained solution was measured. From this value, information about the polymer content in the original synthesized product can be calculated. In this manner, the synthesized products, including PMAPTAC homo-polymer, PAM and PAS co-polymers were purified for Fourier transform infrared spectrum (FTIR) analysis and for all the following investigations on their behaviors in cementitious system.

2.2.3 Fourier Transform Infrared Spectrum (FTIR)

The chemical structures of the purified co-polymers were characterized by FTIR (Nicolet 6700 FTIR, Thermo Fisher Scientific, USA) instrument with a resolution of 4 cm^{-1}. The purified co-polymer solution was homogeneously mixed with KBr

salt and completely dried in a vacuum oven at 80 °C. The mixture was pressed into a tablet and then scanned in the transmission mode from 400 to 4000 cm^{-1} at room temperature of 25 °C.

2.3 Specimens Preparation

2.3.1 Fresh Cement Pastes with the Three Types of Chemical Admixtures

Fresh cement pastes (FCPs) with different W/Cs and varied dosages of superplasticizers, latexes and asphalt emulsions at different temperatures were prepared, which respectively correspond to the Cement-Superplasticizer-Water system, Cement-Latex-Water system and Cement-Asphalt-Water system according to the admixture contained in the FCPs. The formulations of the FCPs are shown in Table 2.5. P/C is defined as the mass solid/solid ratio of polymer to cement. Sp/C, L/C and A/C respectively refer to the mass solid/solid ratios of superplasticizer to cement, latex to cement and asphalt emulsion to cement. W/C is the water to cement ratio. The amount of water in the chemical admixtures was incorporated into the calculation of W/C ratio. A/P denotes the antifoaming agent to polymer ratio in all specimens. Cement I was adopted in the preparation of Cement-Superplasticizer-Water system and Cement-Latex-Water system while Cement III was used in the Cement-Asphalt-Water system.

Before preparing the FCPs, all the raw materials and the mixing bowl as well as the mixer rotor were stored in an environmental chamber with temperature of 0, 20 and 40 °C for 24 h. Then, the raw materials were mixed in accordance with the Chinese standard GB/T8077 and the detailed mixing procedure is described as follows. (1) Water, chemical admixtures and antifoaming agent were firstly added into a mixer and mixed well. (2) Cement was gradually introduced over a time span of 2 min into the mixer at 62 rpm. After a 10 s interval, mixing was resumed for an additional 2 min at 125 rpm. The whole mixing process took about 5 min in total. (3) After being mixed, the freshly mixed paste was kept in a mixing bowl covered with a soaked towel to avoid water evaporation and was then stored at constant environmental temperatures equal to the targeted test temperatures for 0, 25, 55, 85 and 115 min. Thus, counting from the time point of water-cement contact, each paste was actually tested at 5, 30, 60, 90 and 120 min after the contact of cement with water.

Table 2.5 Formulations of fresh cement pastes

Chemical admixtures	P/C[a] (%)	W/C	A/P	0 °C	20 °C	40 °C
PCE superplasticizer	0.00	0.25, 0.29, 0.35, 0.4	0	√	√	√
	0.05	0.25, 0.29, 0.35, 0.4	0	√	√	√
	0.10	0.25, 0.29, 0.35, 0.4	0	√	√	√
	0.15	0.25, 0.29, 0.35, 0.4	0	√	√	√
	0.20	0.25, 0.29, 0.35, 0.4	0	√	√	√
	0.30	0.25, 0.29, 0.35, 0.4	0	√	√	√
	0.40	0.25, 0.29, 0.35, 0.4	0	√	√	√
	0.50	0.25, 0.29, 0.35, 0.4	0	√	√	√
	0.60	0.25, 0.29, 0.35, 0.4	0	√	√	√
	0.70	0.25, 0.29, 0.35, 0.4	0	√	√	√
	0.80	0.25, 0.29, 0.35, 0.4	0	√	√	√
	0.90	0.25, 0.29, 0.35, 0.4	0		√	
	1.00	0.25, 0.29, 0.35, 0.4	0		√	
	1.50	0.25, 0.29, 0.35, 0.4	0		√	
	2.00	0.25, 0.29, 0.35, 0.4	0		√	
	0.00	0.14, 0.15, 0.2, 0.33	0		√	
	0.10	0.14, 0.15, 0.2, 0.33	0		√	
	0.20	0.14, 0.15, 0.2, 0.33	0		√	
	0.30	0.14, 0.15, 0.2, 0.33	0		√	
	0.40	0.14, 0.15, 0.2, 0.33	0		√	
	0.50	0.14, 0.15, 0.2, 0.33	0		√	
	0.60	0.14, 0.15, 0.2, 0.33	0		√	
	0.70	0.14, 0.15, 0.2, 0.33	0		√	
	0.80	0.14, 0.15, 0.2, 0.33	0		√	
	0.90	0.14, 0.15, 0.2, 0.33	0		√	
	1.00	0.14, 0.15, 0.2, 0.33	0		√	
	1.50	0.14, 0.15, 0.2, 0.33	0		√	
	2.00	0.14, 0.15, 0.2, 0.33	0		√	
	0.00	0.5	0	√	√	√
	0.05	0.5	0		√	
	0.10	0.5	0		√	
	0.15	0.5	0		√	
	0.20	0.5	0		√	
	0.30	0.5	0		√	
	0.40	0.5	0		√	
	0.50	0.5	0		√	
	0.00	0.6	0	√	√	√
	0.00	0.7	0	√	√	√
	0.00	0.8	0	√	√	√

(continued)

Table 2.5 (continued)

Chemical admixtures	P/C[a] (%)	W/C	A/P	0 °C	20 °C	40 °C
	0.00	1.0	0		√	
	0.00	1.4	0		√	
	0.00	1.6	0		√	
	0.00	2.0	0		√	
	0.00	3.0	0		√	
NSF superplasticizer	0.1	0.29, 0.4	0		√	
	0.3	0.29, 0.4	0		√	
	0.5	0.29, 0.4	0		√	
	0.8	0.29, 0.4	0		√	
	1.0	0.29, 0.4	0		√	
Polymer latexes L1 and L2	0	0.5	0.02%	√	√	√
	1	0.5	0.02%	√	√	√
	3	0.5	0.02%	√	√	√
	6	0.5	0.02%	√	√	√
	9	0.5	0.02%	√	√	√
	12	0.5	0.02%	√	√	√
	20	0.5	0.02%		√	
	35	0.5	0.02%		√	
	60	0.5	0.02%		√	
Anionic asphalt emulsion	0	0.4	0.02%	√	√	√
	1	0.4	0.02%		√	
	3	0.4	0.02%		√	
	6	0.4	0.02%		√	
	9	0.4	0.02%		√	
	10	0.4	0.02%	√	√	√
	20	0.4	0.02%		√	
	35	0.4	0.02%	√	√	√
	50	0.4	0.02%	√	√	√
	60	0.4	0.02%		√	
Cationic asphalt emulsion	10	0.4	0.02%	√	√	√
	20	0.4	0.02%		√	
	35	0.4	0.02%	√	√	√
	50	0.4	0.02%	√	√	√
	60	0.4	0.02%		√	

[a]Mass solid/solid ratios of superplasticizer to cement, latex to cement and asphalt emulsion to cement are respectively denoted as Sp/C, L/C and A/C

Table 2.6 Initially added amount of monomers and their homo-polymers in the pastes

Item	AA	SSS	MAPTAC	PAA	PSSS	PMAPTAC	MPEGMA
(g/g cement) (%)	0.12	0.34	0.36	0.12	0.34	0.36	2.15
(μmol/g cement)	16.5	16.5	16.5	16.5	16.5	16.5	16.5

2.3.2 *Fresh Cement Pastes with the Organic Monomers and the Polymers*

To investigate the effects of $-COO^-$, $-SO_3^-$ and $\equiv N^+-$ on the adsorption and cement hydration, FCPs containing the organic monomers AA, SSS, MAPTAC and the corresponding homo-polymers were prepared at the temperature of 20 °C. Cement I was used. The W/C of the pastes was set to 0.4 and the addition of the monomers and polymers was 16.5 μmol/g cement with identical molar quantity of the functional groups. The quantity of the monomers was counted by mole of the substance and the quantity of the homo-polymers was measured by mole of the repeating units. Their mass ratios to cement are listed in Table 2.6. The same mixing procedure described in Sect. 2.3.1 was applied.

Similarly, FCPs containing the purified comb-shaped co-polymers were prepared at the temperature of 20 °C. Cement II was used and the W/C of the pastes was set to 0.35. The addition of the purified co-polymers in cement pastes was varied as 0.1, 0.2 and 0.4% by weight of cement (bwoc), respectively. The same mixing procedure described in Sect. 2.3.1 was applied.

2.3.3 *Hardened Cement Pastes and Mortars with the Three Types of Chemical Admixtures*

Cement pastes and mortars were prepared according to the formulations presented in Table 2.7. P/C is defined as the mass solid/solid ratio of polymer to cement. W/C is the water to cement ratio. Sp/C, L/C and A/C respectively refer to the mass solid/solid ratios of superplasticizer to cement, latex to cement and asphalt emulsion to cement. In the formulations of cement mortars, the mass ratio of sand to the sum of cement and polymer is expressed as S/(C + P). The antifoaming agent to polymer ratio in all specimens was set at 0.0005. All specimens were prepared in a mixer equipped with paddles rotating helicoidally at successive speeds. The mixing procedure of cement pastes and mortars followed the Chinese standards GB/T8077 and GB/T17671-1999, respectively. Three different curing conditions were used: the standard curing condition [moist curing at 20 °C and 95% relative humidity (R.H.)], the dry curing condition (1-day moist curing and 27-day curing at 20 °C and 65% R. H.) and the mix curing condition (21-day moist curing and 7-day dry curing).

Table 2.7 Mix proportions of hardened cement pastes and mortars

Polymers	Specimen no.	W/C	P/C[a] (%)	S/(C + P)	A/P (%)
PCE superplasticizer	PC-1-1-(S1)-B	0.29	0	1.33	0.05
	PC-1-2-(S1)-B	0.29	0.1	1.33	0.05
	PC-1-3-(S1)-B	0.29	0.3	1.33	0.05
	PC-1-4-(S1)-B	0.29	0.5	1.33	0.05
	PC-2-1-(S1)-B	0.29	0	1.33	0.05
	PC-2-2-(S1)-B	0.29	0.1	1.33	0.05
	PC-2-3-(S1)-B	0.29	0.3	1.33	0.05
	PC-2-4-(S1)-B	0.29	0.5	1.33	0.05
Polymer latexes	L1-1-(S1)-M	0.50	0	3.00	0.05
	L1-2-(S1)-M	0.50	1	3.00	0.05
	L1-3-(S1)-M	0.50	3	3.00	0.05
	L1-4-(S1)-M	0.50	6	3.00	0.05
	L1-5-(S1)-M	0.50	12	3.00	0.05
	L2-1-(S1)-M	0.50	0	3.00	0.05
	L2-2-(S1)-M	0.50	1	3.00	0.05
	L2-3-(S1)-M	0.50	3	3.00	0.05
	L2-4-(S1)-M	0.50	6	3.00	0.05
	L2-5-(S1)-M	0.50	12	3.00	0.05
Asphalt emulsions	AAE-1-(S2)-G	0.50	0	3.00	0.05
	AAE-2-(S2)-G	0.50	20	3.00	0.05
	AAE-3-(S2)-G	0.50	40	3.00	0.05
	AAE-4-(S2)-G	0.50	60	3.00	0.05
	AAE-5-(S2)-G	0.72	80	3.00	0.05
	CAE-1-(S2)-G	0.50	0	3.00	0.05
	CAE-2-(S2)-G	0.50	20	3.00	0.05
	CAE-3-(S2)-G	0.50	40	3.00	0.05
	CAE-4-(S2)-G	0.50	60	3.00	0.05
	CAE-5-(S2)-G	0.72	80	3.00	0.05

PC-series, L1-series, L2-series, AAE-series and CAE-series refer to the specimens with PCE superplasticizer, latex L1, latex L2, anionic asphalt emulsion and cationic asphalt emulsion respectively; S1 and S2 represent the standard sand and quartz sand, respectively; B-series, M-series and G-series respectively refer to the specimens cured under standard curing, mix curing and dry curing conditions

[a]Mass solid/solid ratios of superplasticizer to cement, latex to cement and asphalt emulsion to cement are respectively denoted as Sp/C, L/C and A/C

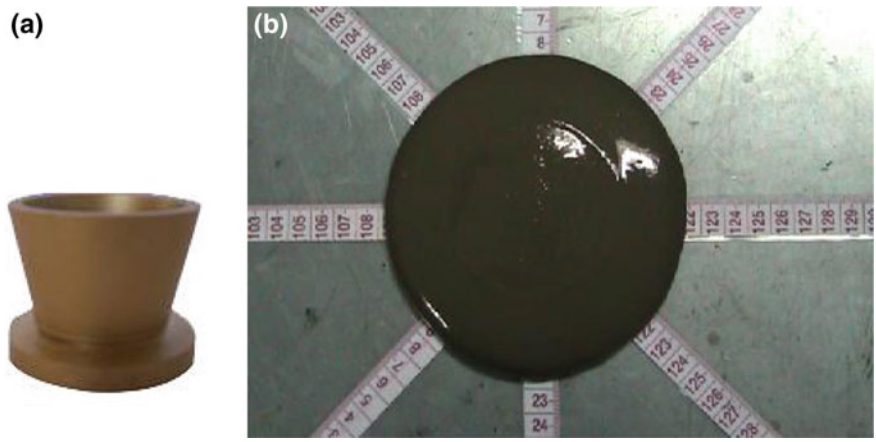

Fig. 2.6 Mini-cone test method: **a** cone and **b** spread diameter

2.4 Testing Methods

2.4.1 Fluidity Measurement

Mini-cone test is a simple and effective method to get a rough view on the fluidity of cementitious materials, which is represented by spread diameter as shown in Fig. 2.6. The spread diameter has been proved to be able to classify different materials in terms of their ability to fill a formwork. A larger spread diameter indicates superior fluidity of the pastes.

In this research, a copper cone with top diameter of 36 mm, bottom diameter of 60 mm and height of 60 mm was used (Fig. 2.6a). Before testing, all the instruments (the cone and glass plate) were stored at the targeted temperature of 0, 20 and 40 °C. The measurement was performed at 5, 30, 60, 90 and 120 min after the contact of cement with water. At every predetermined interval, a portion of the FCP was extracted and remixed at a speed of 125 rpm for 30 s to ensure the homogeneity. After that, the fresh paste was poured into the cone right away and then, the cone was quickly lifted up. After the paste stopped flowing, the average value of four perpendicularly crossing spread diameters of the cement paste was recorded. The fluidity tested at 5 min was defined as the initial fluidity and the spread diameters tested at different measuring time were defined as D_5, D_{30}, D_{60}, D_{90} and D_{120} respectively. The whole measuring process lasted for less than 2 min and the portion of the tested FCP was abandoned as waste disposal after each test to ensure the temperature of the remaining paste unaffected.

2.4.2 Rheological Properties

The rheological properties of FCPs can be roughly described by Bingham model, in which two intrinsic rheological parameters, yield stress τ_0 and plastic viscosity μ_p are involved (Aiad 2003; Axelsson and Gustafson 2006; Roussel et al. 2007; Wallevik 2006). In this research, the two rheological parameters at different temperatures were tested by using a rheometer (Brookfield RV-III, USA). The preparing method, storing time and the measuring temperatures of the FCPs are consistent with those described in Sect. 2.4.1. The yield stress and plastic viscosity values tested at 5 min were defined as initial ones while the ones at measuring time (t) were defined as $\tau_0(t)$ and $\mu_p(t)$.

Four-bladed vane spindle V-71, V-72 and V-73 with different measuring ranges were applied during the measurement of yield stress to accommodate the varied yield stress for all the pastes, as shown Fig. 2.7b. The yield stress was measured along a cylindrical surface defined by the outer tips of the vane blades, which effectively eliminated slippage phenomenon. Before testing, the fresh paste was well mixed with a rotator mixer at a rotation speed of 125 rpm for 30 s to break the particle agglomerates in the suspension. After a pause of 10 s, a stress-strain curve of the fresh cement paste under shear stress was recorded at a rotation speed of 2 rpm by the rheometer. Yield stress was finally obtained when the fresh paste started to yield.

Regarding the measurement of plastic viscosity, standard disc spindle RV2 and RV3 were applied for the FCPs with low viscosity whilst RV4 and RV5 were used for the measurements of high viscosity paste. The same procedure of pre-shearing was performed on the FCPs before testing. Plastic viscosity of the FCPs was measured at different rotation speeds, which involved a stepwise ramp up from 5 to 150 rpm (5, 10, 15, 20, 40, 60, …, 150 rpm). At each rotation speed, viscosity was recorded after the equilibrium was reached. Take the torque-rotation speed curve presented in Fig. 2.8 as an illustrative example, and it is seen that the FCP fairly behaves like a Bingham fluid, whose viscosity keeps almost constant after yield with the change of shear rate. As the disc spindles were used for measuring viscosity, the slippage was inevitable due to the formation of water film between the

Fig. 2.7 Brookfield RV-III rheometer (**a**), vane spindles (**b**) and disc spindles (**c**)

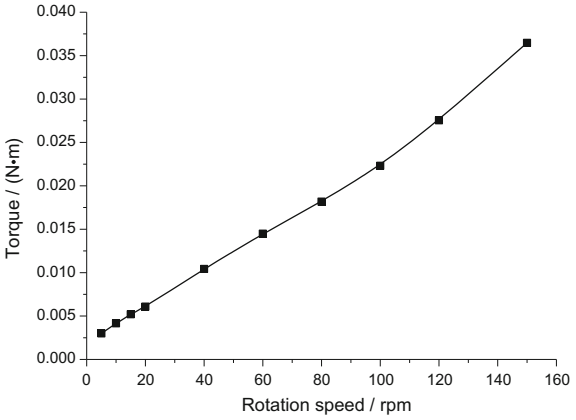

Fig. 2.8 Plot of torque versus rotation speed for the cement paste (W/C: 0.35, P/C: 0.5%, 5 min, 0 °C)

cement paste and the rotating spindle. However, if the slippage effect was strong, the slope of the curve of torque vs. rotation speed will noticeably decrease with the increase in rotation speed. This was not the case in our measurements as seen in Fig. 2.8. This suggests that the slippage effect induced by disc spindles in our tests was thought to be negligible in the testing rotation range. In this research, the viscosity at rotation speed of 100 rpm was chosen as the representative plastic viscosity.

2.4.3 Viscoelastic Properties

Fresh cement paste is considered as a viscoelastic material, because it responds to external forces in a manner intermediately between an elastic solid and a viscous fluid. Viscoelastic properties play important roles in affecting the fluidity, consistence and workability of FCPs (Bellotto 2013; Ferrandis and Leveque 2003; Grasley and Lange 2007; Nachbaur et al. 2001; Subramaniam et al. 2005; Subramaniam and Wang 2010; Wang et al. 2010).

In this research, a microrheology analyzer (Rheolaser LAB6™) was adapted to in situ follow the development of the viscoelastic properties of FCPs in the presence of PCE superplasticizer during the early hours after mixing, as presented in Fig. 2.9. This method measures the mean square displacement (MSD) of cement grains based on diffusing wave spectroscopy (DWS) and gives an insight into the elastic and viscous properties of the suspension system from a microstructural point of view. Before tests, the analyzer was equilibrated at 20 °C for 30 min. After that, the well mixed FCP was poured into a cylindrical glass cell of 20 mL with a 25 mm diameter and then placed into the channels. A fixed coherent laser beam (wavelength 658 nm) is incident upon the sample which contains scaterrers (cement grains here). The MSD curves of cement grains in the FCP were continuously recorded at a constant temperature of 20 °C for 4 h. From the curves, seven

Fig. 2.9 Microrheology analyzer (Rheolaser LAB6™)

parameters including elastic index (EI), macroscopic viscosity index (MVI), storage modulus G', loss modulus G'', and Maxwell parameters, the viscosity of dashpot η and the elastic modulus of spring G, were extracted to quantitatively analyze the viscoelastic properties of FCPs.

2.4.4 Microstructure Examination

The rheological properties of FCPs are primarily determined by the microstructure of the paste (Barnes and Hutton 1989; Xu 1989). The observation for FCPs at a mesoscopic scale is one of the most direct way to analyze the microstructure of the FCPs and further understand the variations of the rheological properties.

2.4.4.1 Optical Microscope

A high sensitivity and high resolution analytical tool Morphologi G3 (Malvern Instruments Limited, Malvern, UK) was employed to characterize the structural organization of cement grains in different dispersion media like air, deionized water, ethanol and an aqueous solution of ethanol, superplasticizer solutions, latexes, asphalt emulsions, as shown in Fig. 2.10. The instrument captures the image of each particle by scanning the sample underneath the microscope optics, while keeping the particles in focus. Advanced graphing and data classification

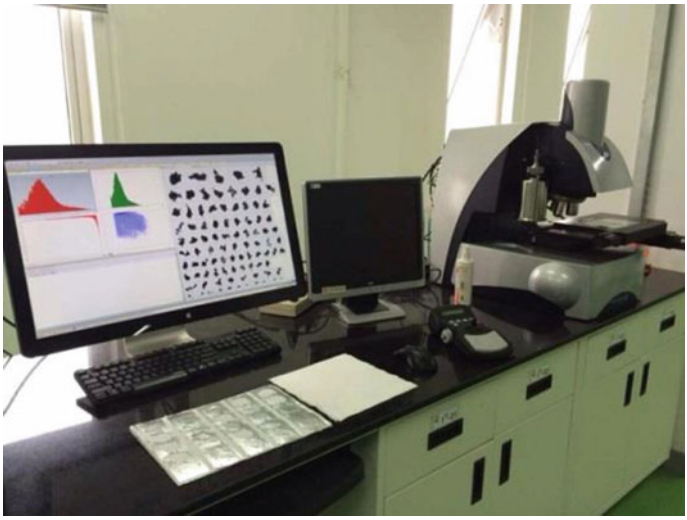

Fig. 2.10 Morphologi G3 optical microscope

options in the software ensure that the extracted relevant data concerning the morphological properties for each particle from the measurement are as straightforward as possible, via an intuitive visual interface.

The cement suspension samples with different dispersion media were prepared as follows.

(1) C-A system: a small amount of cement powder was dispersed on a stage using an integrated dry powder disperser with an air pressure of 200 and 500 kPa.
(2) C-E system or C-W system: cement powder was introduced into deionized water or ethanol with the mass ratio of 1:200, and then was mixed at a speed of 125 rpm for 2 min. After a 10 s interval, mixing was resumed for an additional 2 min at 125 rpm.
(3) C-EW system: an aqueous solution of ethanol was prepared with mass ratio of ethanol to water of 1:1 and then cement powder was introduced into the solution with mass ratio of 1:200. They were mixed according to the above procedure.
(4) C-E + C-W system: equal mass of C-E mixture and C-W mixture were taken and mixed well.
(5) C-W-P system: three aqueous solutions with PCE mass concentration of 0.1, 0.3 and 0.5% were prepared, and then cement powder was introduced to the solutions with mass ratio of 1:200 and mixed well, respectively corresponding to C-W-P0.1, C-W-P0.3 and C-W-P0.5 system.
(6) C-W-N0.5 system: an aqueous solution with NSF mass concentration of 0.5% was prepared, and then cement powder was introduced to it with mass ratio of 1:200 and mixed well.

(7) C-W-L system: two aqueous solutions with latex mass concentration of 3% were prepared, and then cement powder was introduced to the solutions with mass ratio of 1:200 and mixed well.
(8) C-W-A system: an aqueous solution with anionic asphalt mass concentration of 10% was prepared, and then cement powder was introduced to the solutions with mass ratio of 1:200 and mixed well.

The well-mixed cement suspension of 2 mL was taken and injected into a wet cell. The dispersed cement powder on the stage as well as the suspension in the wet cell were instantly subjected to the observation by Morphologi G3. In the meantime of scanning the particles, the high-quality image of each particle was captured and a 2-dimensional projection using geometrical calculations was performed on these collected images. Finally, apart from a global picture containing all the scanned particles, some structural parameters such as particle size, shape and so on, were constructed on the basis of tens to hundreds of thousands of particles. The whole process including sample preparation and analysis by Morphologi G3 lasted for 15 min. That is to say, the effects of cement hydration within such a short period can be neglected in the case of cement and water mixtures.

Moreover, a phase contrast microscope (OLYMPUS BH-2) was employed to observe the microstructure evolution of C-W-A system during the early stage of cement hydration. To clearly observe the cement grains and asphalt particles, the fresh cement paste with 20% asphalt at W/C of 0.5 was diluted 10 times to ensure that the particles in the suspension were well dispersed.

2.4.4.2 SEM

Environmental scanning electron microscope (ESEM) (FEI, Quanta 200FEG, USA) and SEM (CSM-950) were used to observe the microscopic morphology of FCPs and HCPs respectively. After well-mixing, blank FCPs, the FCPs with 0.1% PCE superplasticizer at W/C of 0.29, the FCPs with 3 and 9% latexes at W/C of 0.5, and the FCPs with 10, 35 and 60% anionic asphalt emulsion at W/C of 0.4 were observed in a low vacuum mode (300–500 Pa). Some internal parts of HCPs with 12% latexes at W/C of 0.5 cured for 28 days were taken and dried at 60 $\pm$ 2 °C for 24 h. The parts were processed by carbon-plating before being observed by SEM.

2.4.4.3 3-D Laser Scanning Microscope

In order to clearly observe the microstructure of FCPs with asphalt emulsion, a 3-D laser scanning microscope (OLYMPUS LEXT OLS4100) was employed to capture the global 2-D morphology images, 3-D morphology images and 3-D topographic maps at mass ratios of asphalt to cement of 0, 0.35, 0.6 and 1.0 and W/C of 0.4. All the observations were initiated right after the pastes were well prepared.

2.4.5 Adsorption Amount

The adsorption amounts of superplasticizers, organic monomers and polymers on cement grains were determined by total organic carbon (TOC) measurement using TOC analyzer (Shimadzu, TOC-VCPH, Japan), the measurement range of which is from 4 ppb to 4000 ppm. After well mixed, the fresh cement paste was immediately centrifuged at 3000 rpm for 10 min. A clear supernatant solution was then collected by using a membrane filter with pore diameter of 0.22 μm. Subsequently, the supernatant solution was diluted with deionized water to a suitable concentration for TOC measurement, which should be located in the range of 20–60 mg/L in order to match the 100 mg/L standard curve used in the TOC analyzer. 100 mL diluted solution was used for the measurement of concentration of carbon element. Finally, the adsorption amount on cement of per unit mass could be calculated by subtracting the amount of carbon element remaining in the aqueous solution from the amount initially added in cement paste. It should be mentioned that a tiny amount of carbon (ca. 0.014 mg/g cement) can be detected in the blank cement paste and it should be subtracted in the calculation of their adsorption amounts on cement grains. Given that the different molecular weights for AAA, SSS, MAPTAC and the corresponding homo-polymers, their adsorption amounts in cement pastes were expressed in the form of molar amount of the functional groups (μmol/g cement) for the purpose of comparing the effects of charge properties on the adsorption behaviors. For the comb-shaped co-polymers, PCE and NSF superplasticizers, their adsorption mass on cement of per unit mass (mg/g cement) were discussed.

2.4.6 Precipitation Measurement

It has been well established that $–COO^-$ groups may chelate Ca^{2+} ions in solution (Li and Kong 2009; Pourchet et al. 2007; Yamada et al. 2000). Consequently, when AA or PAA is added into fresh cement paste, complexes, which are either water soluble or water insoluble may be formed due to the reaction between $–COO^-$ and Ca^{2+} in aqueous phase of the FCPs. If water insoluble products are formed, which are then precipitated from the solution phase, the adsorption measurement as described in Sect. 2.4.5 may give wrong results because the carbon contained in the precipitates is falsely considered as the adsorbed carbon on cement surface. Thus, the adsorption amounts of chemicals on cement surface will be overestimated. In order to confirm whether precipitates were formed when the chemicals were added into cement pastes, precipitation experiments were conducted by mixing cement pore solution with AA, SSS, MAPTAC, PAA, PSSS and PMAPTAC respectively. The measuring procedure is summarized as follows. (1) A blank cement paste with W/C of 0.4 was prepared with the same mixing procedure as described in Sect. 2.3.2. (2) After mixing for 4.25 min, a supernatant pore solution of the blank cement paste was

obtained by centrifuge in accordance with the method described in Sect. 2.4.5. (3) Subsequently, 100 mL pore solution was taken and a selected chemical was added into the pore solution. (4) According to the mixing proportions shown in Table 2.6, the dosages of AA, SSS, MAPTAC, PAA, PSSS and PMAPTAC in the pore solution of 100 mL were 0.297, 0.850, 0.908, 0.297, 0.850 and 0.908 g, respectively and the mixtures were kept stirring for 2 h. (5) The mixtures were then quietly stored for 4 h for observation of precipitation. (6) If a mixture became turbid, it was then centrifuged and filtrated to obtain the supernatant solution. (7) The concentration of the remaining chemical in solution was measured again by TOC analyzer as described in Sect. 2.4.5. This way, the precipitation ratio R of the chemical could be calculated by the formula: $R = (1 - C_1/C_2) \times 100\%$, where C_1 is the concentration of carbon element remaining in the supernatant solution after centrifuge separation and C_2 stands for the initial concentration of carbon element when the chemical was added in the pore solution. (8) By deduction of the amount of the precipitated chemical from the amount of the adsorbed chemical that was measured in Sect. 2.4.5, the overestimated adsorption amount could be corrected.

2.4.7 Particle Size and Zeta Potential

To recognize the changes in the microstructure of FCPs caused by adding PCE and NSF superplasticizers, particle size distribution and zeta potential of the cement pastes at different Sp/Cs were measured by using an acoustic and electroacoustic spectrometer (Dispersion Technology, DT 1201, USA). The measuring range of zeta potential is from –3000 to +3000 mV and the measuring error is in the vicinity of $\pm$ 2 mV.

The FCP was poured into a sample chamber right after mixing and was subjected to the measurement of particle size. Raw data of ultrasound attenuation within a frequency range of 3–35 MHz reflecting the microstructure of sample could provide direct information on the particle size distribution of the FCPs. Prior to measuring zeta potential, a zeta probe was calibrated by using the pore solution of cement paste as ionic background for the zeta potential measurement of the corresponding cement paste. After a mixing time of 4 min, 40 mL fresh paste was immediately transferred into a 50 mL sample cell equipped in DT1201. Afterwards, the probe was dipped into the well mixed FCP and the zeta potential was measured. The value of zeta potential was calculated from the colloidal vibration current which was determined by the measurement. During the measurement, the FCP was kept stirring by using a magnetic mixer at 200 rpm in order to keep the mixture homogeneous. The measurement of zeta potential was repeated 7 times over 10 min for each sample and an average of these zeta values was recorded.

Similarly, the effects of the organic monomers and their corresponding homo-polymers as well as the comb-shaped co-polymers on the zeta potential of FCPs were also investigated. Because of the poor fluidity of FCPs containing organic

monomers at W/C of 0.4, some of which showed spread diameters as small as 60 mm, the W/C in all the cement pastes with these chemicals was heightened to 0.5 in order to ensure the operability and the accuracy of the zeta potential measurement.

2.4.8 Cement Hydration

Heat evolution during cement hydration was monitored to reveal the influences of different chemical admixtures, organic monomers and polymers on the hydration dynamics. Two types of calorimeter were used in this research.

2.4.8.1 Iso-Thermal Calorimetry

Isothermal calorimetry was adopted to monitor the heat evolution during cement hydration at 0, 20 and 40 °C by using a TAM-air micro-calorimeter (Thermometric AB, Sweden). Before tests, the calorimeter was regulated at targeted temperatures and then equilibrated for 24 h. Thereafter, the freshly mixed pastes were promptly decanted to an ampoule of 20 mL and then placed into the channels. The heat evolution of cement hydration at the targeted temperature was recorded after an auto-equilibrium of 45 min. With respect to the heat evolution within 45 min, a syringe method was used where a 20 mL ampoule and a lid with two syringes, a stirrer and a motor were equipped. A power supply was enclosed. According to the mix proportion, cement powder and liquid were respectively placed into an ampoule cup and the syringes. Then, the ampoule was covered by the lid and placed into the channels. Subsequently, the calorimeter with the ampoule in the channel was regulated at targeted temperatures and then equilibrated for 24 h. Afterwards, the liquid was promptly injected into the ampoule and the cement powder with the liquid were mixed using the stirrer for 1 min. The heat evolution was recorded since the contact of cement with water and the record lasted for 2 h.

2.4.8.2 Semi-adiabatic Temperature Test

A self-regulated semi-adiabatic calorimeter was employed to measure the internal temperature of the paste that was kept in a well-insulated cabinet. The environmental temperature was kept constant during the entire testing period. Because of the exothermic feature of cement hydration, monitoring temperature development was a useful method for obtaining information on the hydration kinetics of cement (Li and Kong 2009; Zhang et al. 2012). The insulating cabinet was pre-calibrated to obtain its heat loss coefficient. Heat of hydration Q, expressed in joules per gram of cement (J/g), can be obtained by adding up lost heat flux over time Q_{los} and heat Q_{tc} used for changing the paste temperature. The isolated cell heat loss coefficient α_{hl}, the mixture composition and thermal capacity of each component are necessary for

calculating the Q_{los} and Q_{tc}. The hydration heat can be calculated by the following formula,

$$dQ = dQ_{los} + dQ_{tc} = \frac{\alpha_{hl}(T_t - T_{en})dt}{m_c} + \frac{m_i c_i dT}{m_c} \tag{2.1}$$

where m_{i} is the mass of each component of the paste (g), m_{c} is the mass of the cement (g), c_{i} denotes the thermal capacity of each component of the paste (J/(g K)), T_t represents the internal temperature of the FCP at moment t, and T_{en} is the target environmental temperature.

$$\begin{aligned} Q &= \int_0^t dQ = \frac{\alpha_{hl}}{m_c}\int_0^t (T_t - T_{en})dt + \frac{m_i c_i}{m_c}\int_0^t dT \\ &= \frac{\alpha_{hl}}{m_c}\int_0^t (T_t - T_{en})dt + \frac{m_i c_i}{m_c}(T_t - T_0) \end{aligned} \tag{2.2}$$

where T_0 is the inner temperature of the FCP at the initial moment. As mentioned above, the raw materials and samples were kept at the target environmental temperatures; thus, T_0 is equal to T_{en}. Equation (2.2) can then be rewritten as

$$Q = \frac{1}{m_c}\left\{\alpha_{hl}\int_0^t (T_t - T_{en})dt + m_i c_i (T_t - T_{en})\right\} \tag{2.3}$$

2.4.9 Mercury Intrusion Porosimetry (MIP)

MIP has been a standard method to determine pore structure in cementitious materials (Diamond 2000). Although it is often criticized that the pore size distribution calculated from the MIP is not the actual pore size distribution in the paste, it is still a valuable technique in making comparative assessment of the pore structure in the given system which does not require the absolute pore size (Wild 2001). Moreover, the threshold diameter and the pore volume are effective indices to reflect the variations of the connectivity and the capacity of the pore in cement pastes (Diamond 2000). Therefore, in this research, the shifts of pore size distribution, the threshold diameter and the total pore volume were respectively compared and discussed for the pastes at different W/Cs and P/Cs. After cured for 7 days and 28 days respectively, the HCPs were cut into small cylinders with diameter of 10 mm and thickness of 5 mm and placed into alcohol bath for 24 h. After 3 days storage in an oven with an ambient temperature of 60 ± 2 °C, three specimens were randomly selected and subjected to MIP tests for pore structure characterization by using Hg-porosimetry (Autopore, IV 9510, USA). Differences in mercury volume can be

found by re-intruding the pastes after the first intrusion-extrusion cycle was completed (Kaufmann et al. 2009; Moro and Böhni 2002). It is considered that a part of the mercury is entrapped in the pores of certain geometric shape in HCPs which is usually called inkbottle pores (Aligizaki 2005; Willis et al. 1998). As well known, the addition of superplasticizers brings significant effects on the rheological properties of FCPs through modifying the microstructure of the FCPs. The entrapped mercury volume may indirectly provide extra information on the structure and morphology of pores in the HCPs. Therefore, two cycles of intrusion-extrusion were performed. Entrapped mercury volume and retention factor Rf were obtained as follows (Sakai et al. 2006). $Rf = V_{en}/V_1 = (V_1 - V_2) \times 100\%/V_1$, where V_{en} is the entrapped mercury volume, V_1 and V_2 are the volume of mercury intruded during the first and the second cycle respectively.

2.4.10 Alternating Current (AC) Impedance

AC impedance spectroscopy technique has been widely used to investigate the microstructure and the permeability of hardened cementitious materials based on the relationships between the parameters of AC impedance and the structure of porous cementitious systems (Cabeza et al. 2002, 2003, 2006; Gu et al. 1994; McCarter and Brousseau 1990). AC impedance concerns the application of a low-amplitude AC excitation by surface electrodes over a range of frequencies. The current response (i.e., gain and phase angle) could be measured by the impedance analyzer.

Cubic mortar specimens with size 40 × 40 × 40 mm were fabricated. Similar to the chloride permeability measurement according to ASTM C1202, after being cured, all mortars were vacuum-saturated for 2 h prior to being soaked in a saturated $Ca(OH)_2$ aqueous solution for 18 h. Then, the mortars were ready for the AC impedance measurements which were performed using an impedance gain/phase analyser (Agilent 4294A, Palo Alto, CA, USA) in high-frequency range from 40 kHz to 100 MHz and a potentiostat/galvanostat (PARSTAT 2263, Amtek, USA) in low-frequency range from 0.1 Hz to 100 kHz (Zhang et al. 2011).

References

Aiad I (2003) Influence of time addition of superplasticizers on the rheological properties of fresh cement pastes. Cem Concr Res 33(8):1229–1234

Aligizaki KK (2005) Pore structure of cement-based materials: testing, interpretation and requirements. CRC Press, Boca Raton

Axelsson M, Gustafson G (2006) A robust method to determine the shear strength of cement-based injection grouts in the field. Tunn Undergr Space Technol 21(5):499–503

Barnes HA, Hutton JF (1989) An introduction to rheology. Elsevier, Amsterdam

Bellotto M (2013) Cement paste prior to setting: a rheological approach. Cem Concr Res 52: 161–168

Cabeza M, Keddam M, Nóvoa XR et al (2006) Impedance spectroscopy to characterize the pore structure during the hardening process of Portland cement paste. Electrochim Acta 51(8): 1831–1841
Cabeza M, Merino P, Miranda A et al (2002) Impedance spectroscopy study of hardened Portland cement paste. Cem Concr Res 32(6):881–891
Cabeza M, Merino P, Nóvoa XR et al (2003) Electrical effects generated by mechanical loading of hardened Portland cement paste. Cement Concr Compos 25(3):351–356
Diamond S (2000) Mercury porosimetry: an inappropriate method for the measurement of pore size distributions in cement-based materials. Cem Concr Res 30(10):1517–1525
Ferrandis JY, Leveque G (2003) In situ measurement of elastic properties of cement by an ultrasonic resonant sensor. Cem Concr Res 33(8):1183–1187
Grasley ZC, Lange DA (2007) Constitutive modeling of the aging viscoelastic properties of Portland cement paste. Mech Time Depend Mater 11(3–4):175–198
Gu P, Xie P, Fu Y et al (1994) AC impedance phenomena in hydrating cement systems: frequency dispersion angle and pore size distribution. Cem Concr Res 24(1):86–88
Kaufmann J, Loser R, Leemann A (2009) Analysis of cement-bonded materials by multi-cycle mercury intrusion and nitrogen sorption. J Colloid Interface Sci 336(2):730–737
Li QH, Kong XM (2009) Properties and microstructure of polymer modified mortar based on different acrylate latexes. J Chin Ceram Soc 37(1):107–114
McCarter WJ, Brousseau R (1990) The AC response of hardened cement paste. Cem Concr Res 20(6):891–900
Moro F, Böhni H (2002) Ink-bottle effect in mercury intrusion porosimetry of cement-based materials. J Colloid Interface Sci 246(1):135–149
Nachbaur L, Mutin JC, Nonat A et al (2001) Dynamic mode rheology of cement and tricalcium silicate pastes from mixing to setting. Cem Concr Res 31(2):183–192
Pourchet S, Comparet C, Nicoleau L et al (2007) Influence of PC superplasticizers on tricalcium silicate hydration. In: Proceedings of the 12th international congress on the chemistry of cement-ICCC
Roussel N, Geiker MR, Dufour F et al (2007) Computational modeling of concrete flow: general overview. Cem Concr Res 37(9):1298–1307
Sakai E, Kasuga T, Sugiyama T et al (2006) Influence of superplasticizers on the hydration of cement and the pore structure of hardened cement. Cem Concr Res 36(11):2049–2053
Subramaniam KV, Lee J, Christensen BJ (2005) Monitoring the setting behavior of cementitious materials using one-sided ultrasonic measurements. Cem Concr Res 35(5):850–857
Subramaniam KV, Wang X (2010) An investigation of microstructure evolution in cement paste through setting using ultrasonic and rheological measurements. Cem Concr Res 40(1):33–44
Wallevik JE (2006) Relationship between the Bingham parameters and slump. Cem Concr Res 36(7):1214–1221
Wang X, Subramaniam KV, Lin FB (2010) Ultrasonic measurement of viscoelastic shear modulus development in hydrating cement paste. Ultrasonics 50(7):726–738
Wild S (2001) A discussion of the paper "Mercury porosimetry-an inappropriate method for the measurement of pore size distributions in cement-based materials" by S. Diamond. Cem Concr Res 31(11):1653–1654
Willis KL, Abell AB, Lange DA (1998) Image-based characterization of cement pore structure using wood's metal intrusion. Cem Concr Res 28(12):1695–1705
Xu YM (1989) A unified rheological model for non-dilatancy viscoplastic fluids. J Wuhan Univ Technol 11(4):431–436 (in Chinese)
Yamada K, Takahashi T, Hanehara S et al (2000) Effects of the chemical structure on the properties of polycarboxylate-type superplasticizer. Cem Concr Res 30(2):197–207
Zhang YR, Kong XM, Hou SS et al (2012) Study on the rheological properties of fresh cement asphalt paste. Constr Build Mater 27(1):534–544
Zhang YR, Kong XM, Zhang ZL et al (2011) Impermeability of polymer modified mortar with different acrylate latexes. Science and technology of commercial mortar (in Chinese)

Chapter 3
Rheological Properties of Fresh Cement Pastes

Rheological properties of fresh cement pastes (FCPs) play essential roles in determining the workability of fresh mortars or concrete during the construction process and even affecting the mechanical properties and durability of hardened concrete to some extents (Huang 2000; Pu 2004). In modern mortars and concrete, various chemical admixtures are incorporated to improve the rheological properties of FCPs. Much research has been dedicated to correlating the rheological properties of cementitious systems with their mixture compositions and the environmental factors like temperature. However, there is little research regarding the combined effects of various influencing factors from the microstructure point of view and as a result, some controversial phenomena have not been well explained so far.

In this chapter, the rheological properties of FCPs in the presence of superplasticizers, latexes and asphalt emulsions were systematically investigated. Influencing factors including chemical admixtures to cement ratio, water to cement ratio (W/C), temperature and elapsed time were considered. Fluidity and rheological tests were conducted at 0, 20 and 40 °C to characterize the development of the rheological behaviors of FCPs over elapsed time. Specific effects of superplasticizers, latexes, asphalt emulsions, W/C, temperature and elapsed time were discussed in detail. Moreover, on the basis of the experimental results, the working mechanisms of these admixtures in FCPs were proposed.

3.1 Cement-Superplasticizer-Water System

As one of the most important chemical admixtures, superplasticizers are introduced into FCPs to achieve a high fluidity. By changing the superplasticizer dosage (Sp/C), W/C, temperature and time, the fluidity, yield stress and plastic viscosity, viscoelastic properties of the Cement-Superplasticizer-Water system were investigated systematically and working mechanism of superplasticizers were proposed.

Y. Zhang, *Study on Microstructure and Rheological Properties of Cement-Chemical Admixtures-Water Dispersion System at Early Stage*, Springer Theses, DOI 10.1007/978-981-10-4570-7_3

Moreover, the effects of two typical superplasticizers, NSF superplasticizer and PCE superplasticizer, on the fluidity of FCPs were compared.

3.1.1 Fluidity

3.1.1.1 Effects of Mix Proportion on the Initial Fluidity

Figure 3.1 presents the initial fluidity of FCPs with varied W/Cs and superplasticizer dosages at 20 °C. It is easily found that: (1) a larger W/C leads to higher initial fluidity. At W/C lower than 0.15 (W/C < 0.15), the FCPs hardly flow regardless of Sp/C, and the spread diameters are lower than 80 mm. As W/C is between 0.15 and 0.33 (0.15 < W/C < 0.33), only when a certain dosage of superplasticizers is added can the FCPs flow. If W/C is larger than 0.33 (W/C > 0.33), the pastes could flow freely in the absence of superplasticizers. (2) By adding superplasticizers in the FCPs with W/C > 0.33, the initial fluidity presents a linear increase at low dosages, and then reaches a maximum value at a certain dosage, which is defined as the critical dosage. Beyond the critical dosage, the fluidity of the FCPs is scarcely changed by further addition of superplasticizers. (3) The maximum fluidity of FCPs ascends with increase of W/C and reaches a maximum value at W/C of 0.40, while the critical dosage descends at a higher W/C. (4) In addition, at the same Sp/C, the initial fluidity of the FCPs with PCE superplasticizer is higher than that with NSF superplasticizer. And at the same W/C, the maximum fluidity of FCPs with PCE is obviously larger than that with NSF superplasticizer.

It is well known that, in a fresh cement paste, cement usually presents majorly flocculation of cement grains under electrostatic interactions that entraps a large quantities of mixing water (Wang 2006). Together with a few individual cement grains, these flocculated structures of cement grains constitute the dispersion phase of the FCPs, as schematically shown in Fig. 3.2a. On the other hand, the mixing

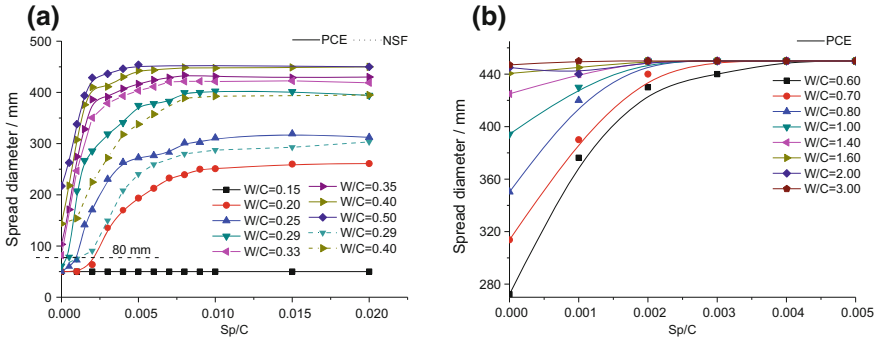

Fig. 3.1 Initial fluidity of FCPs with varied W/Cs and Sp/Cs at 20 °C. **a** W/C = 0.15–0.5; **b** W/C = 0.6–1.0

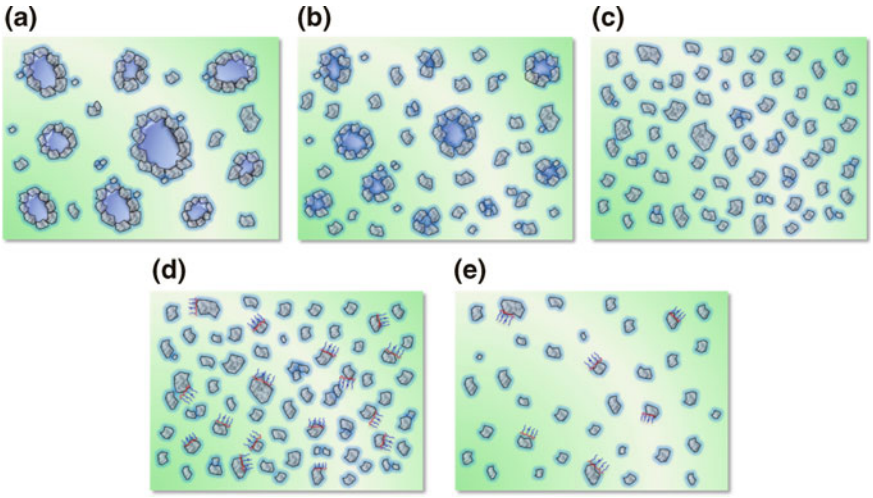

Fig. 3.2 Schematic illustration of the effects of PCE superplasticizer on the microstructure of FCPs. **a** Blank FCP; **b** FCP with moderate PCE; **c** FCP with adequate PCE; **d** FCP at low W/C; **e** FCP at high W/C (Cement grain; Flocculated structure; Free water; Entrapped water; PCE)

water in FCPs can be sorted into four categories: chemically bonded water in the form of hydrates and hydroxides as hydration products (HW), adsorbed water (AW), i.e., physically bonded water on cement surface, entrapped water (EW) in the flocculated cement structure and free water (FW). As a solid-liquid dispersion system, it is understood that the rheological behavior of a fresh cementitious mixture is mainly dependent on the content of FW in the system, because the other three types of water function as solid phase (Cao et al. 2012). Obviously, a higher W/C results in an increment of the content of FW in the pastes. Therefore, the initial fluidity of FCPs boosts significantly with the increase of W/C.

With regard to the variation of the initial fluidity in the presence of superplasticizers, it could be well interpreted on the basis of the working mechanism of superplasticizers. Specifically, a higher superplasticizer dosage brings about higher fluidity because more flocculated structures are disassembled and hence more entrapped water is released (as shown in Fig. 3.2b). When the flocculated cement grains are almost fully disassembled or stop changing with the addition of superplasticizers, the initial fluidity reaches to a maximum value and remains stable irrespective of further addition of superplasticizers.

With the increase of W/C, the maximum fluidity certainly ascends due to the increased content of free water. On the assumption that the amounts of flocculated structures in the blank FCPs with different W/Cs are the same, the distance amongst flocculated structures of cement grains is definitely closer at lower W/C, as schematically shown in Fig. 3.2d, e. Such way, more superplasticizer is needed for

the FCPs at low W/C to achieve the complete disassembly of the flocculated structures. As a consequence, the critical dosage at low W/C is larger than that at high W/C.

Furthermore, NSF enhances the dispersion of cement grains only by electrostatic repulsion, whereas PCE favors the dispersion by the coupled effects of electrostatic repulsion and steric repulsion. At the same Sp/C and W/C, PCE with stronger dispersing capability disassembles more flocculated structures and releases more entrapped water in comparison to NSF, thereby more significantly increasing the initial fluidity of FCPs and the maximum fluidity.

3.1.1.2 Effects of Temperature on the Initial Fluidity

As well known, FCP is a reactive solid-liquid dispersion system (Schmidt et al. 2014). After the contact of cement with water, dissolution of several mineral phases takes place immediately and various ions diffuse from the mineral phases of cement grains into the aqueous phase, accompanied by the production of hydrates such as Aft. A high temperature will accelerate the ion diffusion and the production of Aft, and further cause the variation of the fluidity of FCPs.

The initial fluidity of FCPs at three different temperatures of 0, 20, and 40 °C is shown in Fig. 3.3. It is clearly seen that a higher temperature tend to depress the initial fluidity for each FCP. Similar results were reported by Kong et al. (2013) and he proposed that the flocculated structures were decisive factor for the initial rheological behaviors of cement pastes. As temperature increases, more flocculated structures are formed because of the faster dissolution as well as early hydration, and therefore more free water is entrapped into these flocculated structures. Consequently, a higher temperature leads to a decrease in the initial fluidity of FCPs.

For FCPs with higher W/C, the impacts of the volume fraction of solid phase on the fluidity are considered to be less sensitive (Zhou et al. 1999). Therefore, the impacts of temperature on the initial fluidity of FCPs with a high W/C are not remarkable (Fig. 3.3). On the other hand, the effects of temperature on initial fluidity are also obviously weakened as superplasticizer is added in the paste, as shown in Fig. 3.3. We know that the function of superplasticizer in heightening initial fluidity is achieved through the adsorption on the cement surface (Ran 2007). At an elevated temperature, more charges are produced due to the accelerated dissolution and hydration at early stage. For blank FCPs, these charges lead to the formation of more flocculated structures and the decrease of initial fluidity, while for the pastes with superplasticizers, the charges provide more adsorption sites for superplasticizers. In the case of a high superplasticizer dosage, ample PCE molecules in FCPs ensure sufficient adsorption on the surface of cement grains, which facilitates the superior dispersion state of cement grains even at elevated temperatures. As a result, the impacts of temperature on the initial fluidity are weakened as superplasticizer dosage is high. In other words, the initial fluidity of FCPs with higher Sp/C exhibits lower temperature sensitivity. The schematic illustration of the

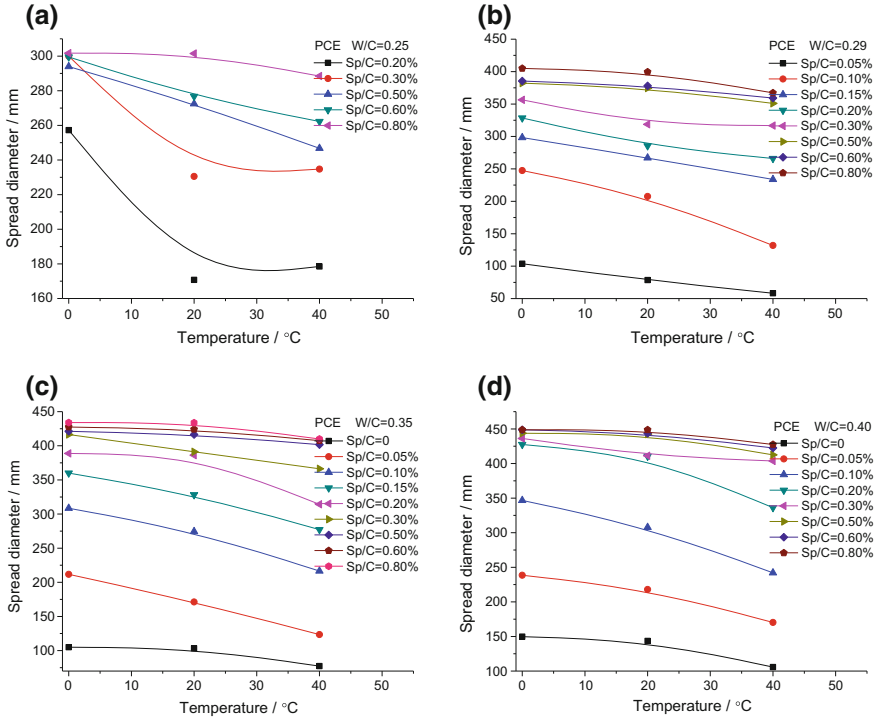

Fig. 3.3 Variation of initial fluidity of FCPs with temperature at varied Sp/Cs. **a** W/C = 0.25; **b** W/C = 0.29; **c** W/C = 0.35; **d** W/C = 0.40

adsorption of superplasticizer onto the surface of cement grains for the FCPs with different dosages at 0, 20 and 40 °C is shown in Fig. 3.4. The real adsorption behaviour of superplasticizers on the cement surface at different temperatures will be discussed later in Chap. 5.

3.1.1.3 Effects of Mix Proportion on the Fluidity Retention

As previously mentioned, the development of the fluidity of FCPs over elapsed time, which is the so-called fluidity retention, is crucial to guarantee appropriate on-site workability. The fluidity usually descends over elapsed time before setting due to the continuously progressing cement hydration, which consumes the free water and facilitates the construction of the flocculated structures. The fluidity of FCPs prepared with varied W/Cs and Sp/Cs was tested over elapsed time at 20 °C, as presented in Figs. 3.5 and 3.6. The fluidity continues decreasing over elapsed time for all the tested FCPs and the decline rate diminishes in the case of high superplasticizer dosages. That is to say, the fluidity retention is enhanced by the incorporation of superplasticizer. This phenomenon is consistent with the early

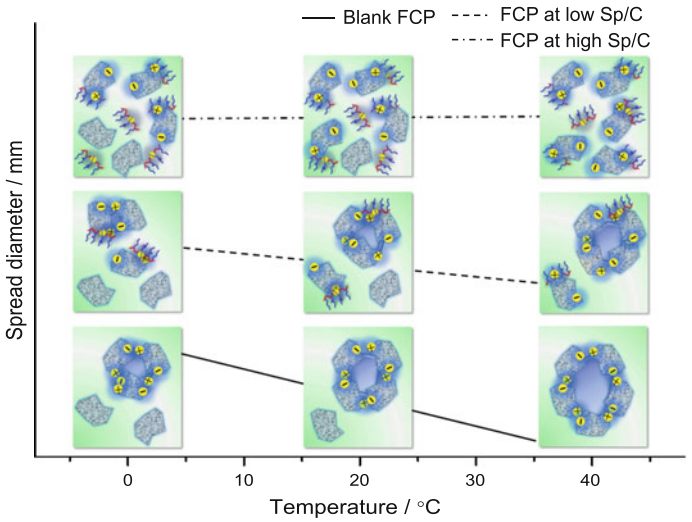

Fig. 3.4 Schematic illustration of adsorption of superplasticizer on cement surface

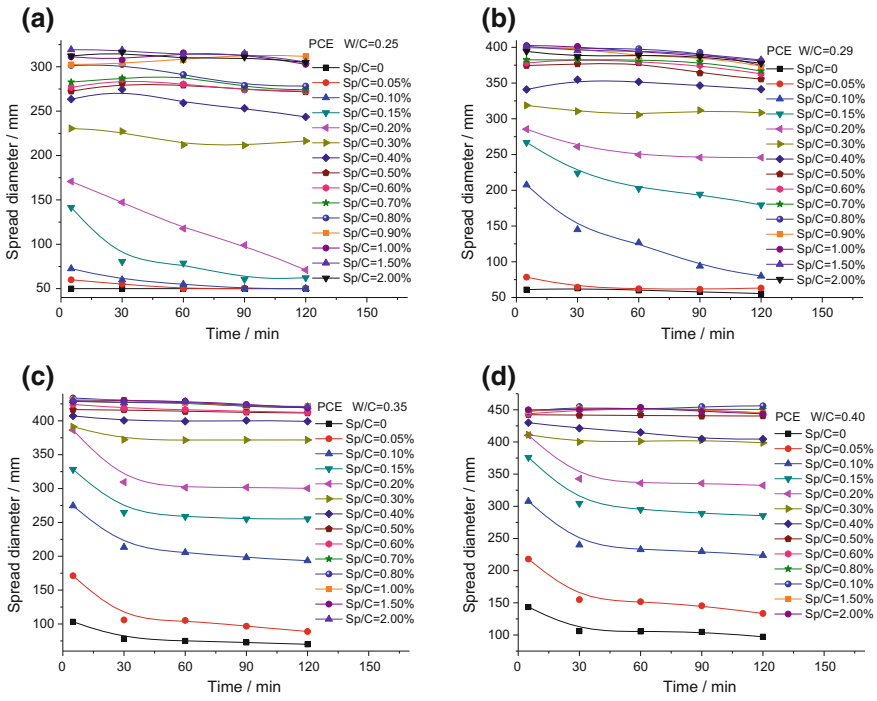

Fig. 3.5 Fluidity retention of FCPs with varied dosages of PCE superplasticizer at 20 °C. **a** W/C = 0.25; **b** W/C = 0.29; **c** W/C = 0.35; **d** W/C = 0.4

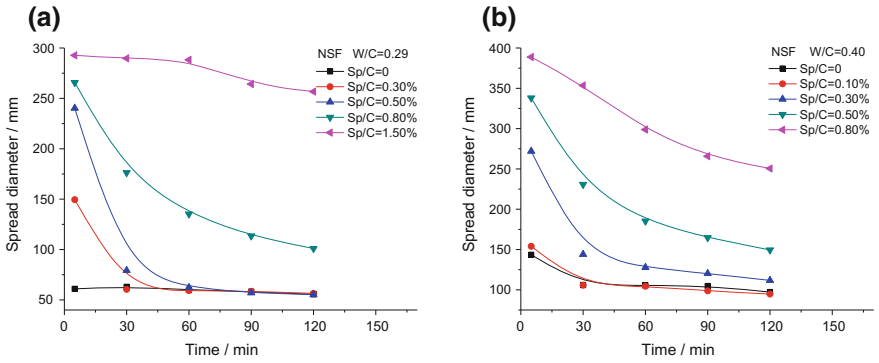

Fig. 3.6 Fluidity retention of FCPs with varied dosages of NSF superplasticizer at 20 °C. **a** W/C = 0.29; **b** W/C = 0.4

findings from other authors and they found that the addition of the superplasticizers usually retarded cement hydration to different extents (Cheung et al. 2011; Pourchet et al. 2006, 2007). Moreover, as cement hydration proceeds, part of the adsorbed superplasticizers may be consumed by being embedded or integrated into hydration products (Flatt and Houst 2001; Plank et al. 2010). More addition of superplasticizers will compensate the consumption of superplasticizers during the cement hydration. As a result, a higher dosage of superplasticizers enhances the fluidity retention of FCPs.

Compared to NSF superplasticizer, PCE superplasticizer more significantly enhances the fluidity retention of FCPs. This may be related to the stronger retardation effects of PCE superplasticizer on cement hydration as well as its superior dispersion effects on cement grains because of its long side chains, which will be discussed in detail in Chap. 5.

3.1.1.4 Effects of Temperature on the Fluidity Retention

High temperatures accelerate cement hydration, which undoubtedly consume more superplasticizers by being adsorbed on the surface of the newly formed hydration products and by being embedded or integrated into hydration products. Along with progressing cement hydration, more hydrates are produced at higher temperatures. Meanwhile, the superplasticizers gradually lose the effectiveness due to the consumption and further flocculated structures may be re-built in FCPs more quickly at a higher temperature. Consequently, the fluidity of FCPs will decrease with time more obviously.

The fluidity retention for FCPs with varied W/Cs under various temperatures was measured, as shown in Figs. 3.7, 3.8 and 3.9. At 0 and 20 °C, for FCPs with lower Sp/C, obvious decreases in the fluidity during the first 30 min are found, whilst the fluidity slightly decreases over elapsed time at higher Sp/C. This is

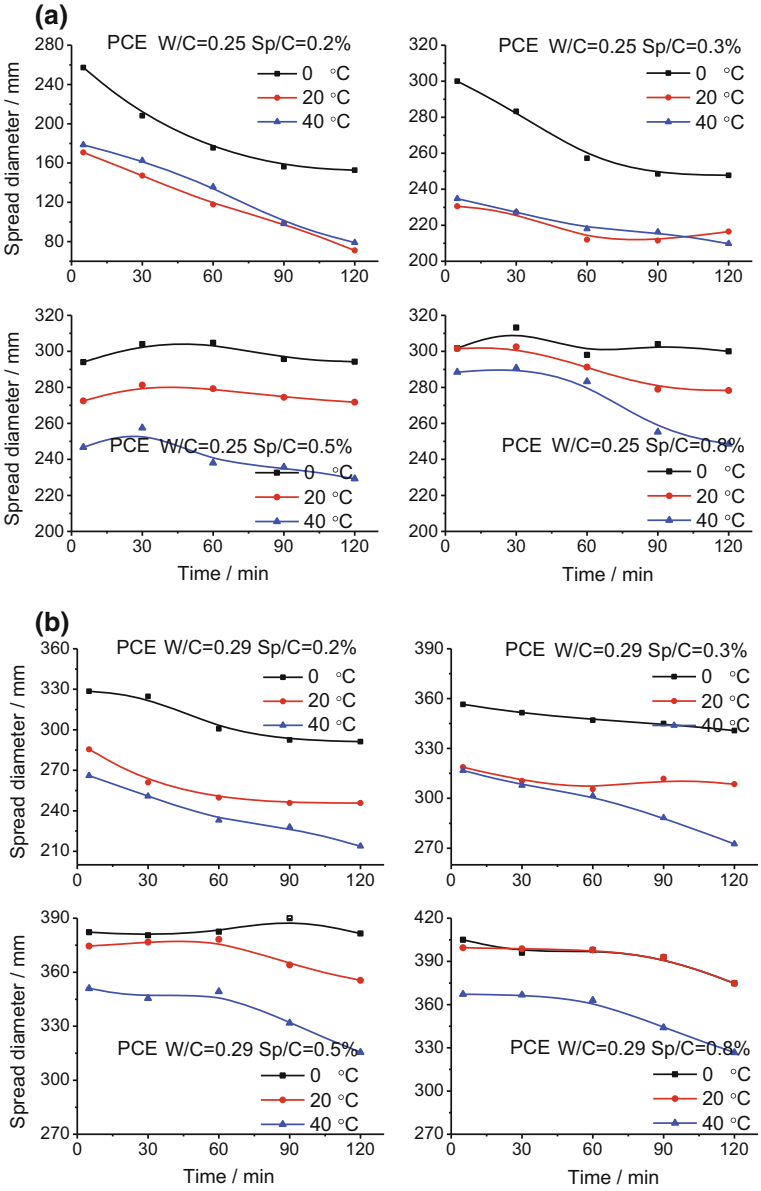

Fig. 3.7 Variation of fluidity retention of FCPs with temperature at varied Sp/Cs. **a** W/C of 0.25; **b** W/C of 0.29

because the inclusion of a small amount of superplasticizers could obviously heighten the initial fluidity of FCPs at 0 and 20 °C. However, along with progressing cement hydration, this small dosage of superplasticizer is quickly

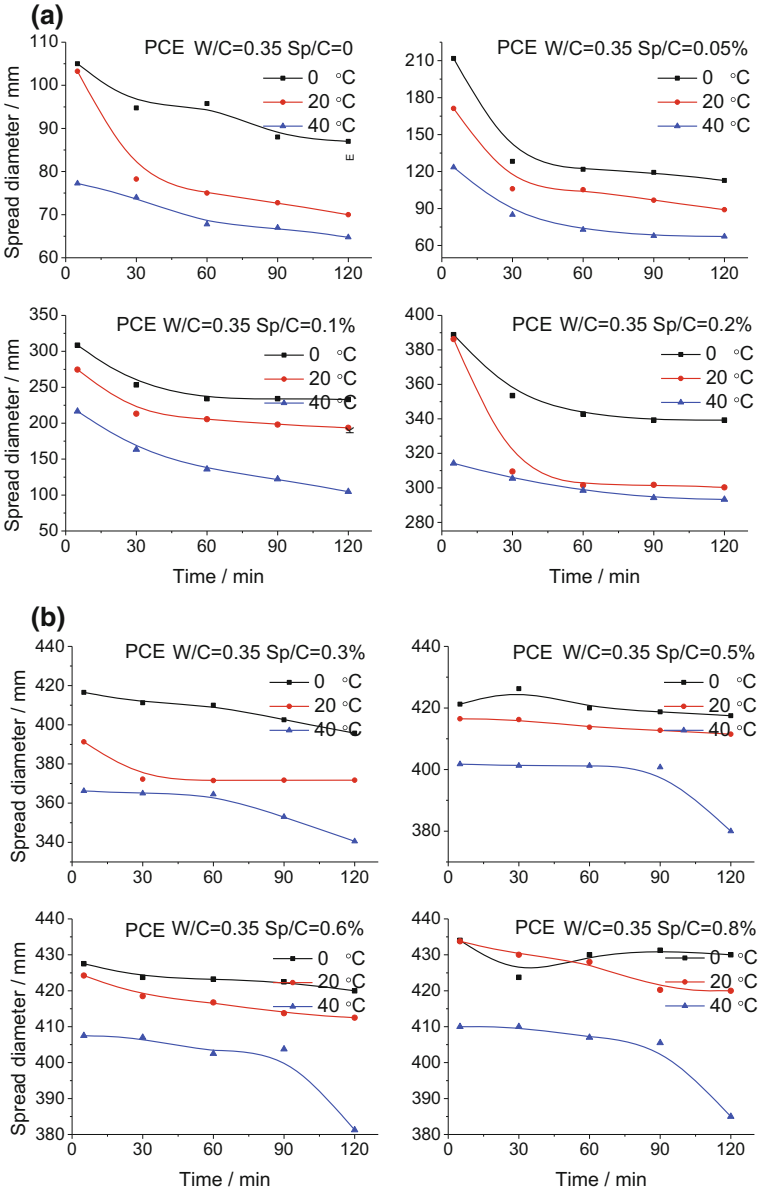

Fig. 3.8 Variation of fluidity retention of FCPs with temperature at W/C of 0.35. **a** Sp/C = 0–0.2%; **b** Sp/C = 0.3–0.8%

consumed and flocculated structures are re-built in FCPs. Therefore, significant decreases in the fluidity are observed in the first 30 min. At higher Sp/C, sufficient adsorption of superplasticizers on cement grains and strong retardation effects of

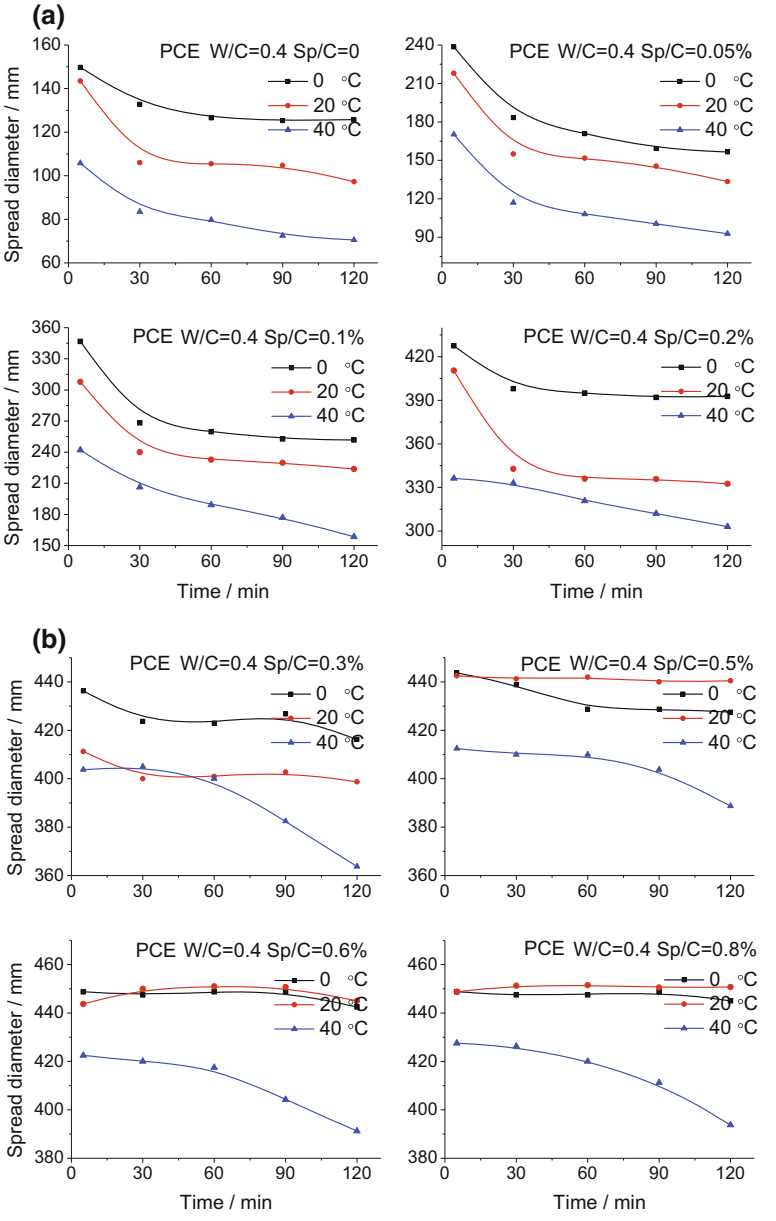

Fig. 3.9 Variation of fluidity retention of FCPs with temperature at W/C of 0.4. **a** Sp/C = 0–0.2%; **b** Sp/C = 0.3–0.8%

superplasticizers on cement hydration lead to the stronger fluidity retention of FCPs.

At 40 °C, FCPs with lower Sp/C present weaker fluidity retention and at higher Sp/C, FCPs have stronger fluidity retention in the first 90 min. A sudden decline in the fluidity at 120 min under 40 °C is supposed to stem from the insufficiency of superplasticizer caused by the accelerated cement hydration at elevated temperatures.

Overall, from the results in Figs. 3.7, 3.8 and 3.9, it is noted that in most cases, a high temperature leads to a sharp drop in the fluidity over elapsed time. A larger dosage of superplasticizer in FCPs definitely brings about lower temperature dependence of the fluidity retention, i.e., lower temperature sensitivity.

3.1.2 Yield Stress and Plastic Viscosity

Fluidity represents the workability of FCPs in practical project. From the rheological point of view, FCPs have been considered as a high concentration suspension system with elasticity, viscosity and plasticity. It is well documented that the rheological behaviors of cement mixtures could be described by many different mathematical models (Aiad 2003; Axelsson and Gustafson 2006; Roussel et al. 2007; Wallevik 2006) in which the Bingham model is the simplest and the most commonly used one for rheological investigation on cement paste. In this study, the rheological behavior of FCPs is relatively simple on the basis of the torque versus rotation speed curve of the FCP presented in Fig. 2.8, so that it is reasonable to describe the rheological properties of FCPs by using the Bingham model. The two intrinsic rheological parameters of yield stress and plastic viscosity in the model are measured to investigate the rheological properties of FCPs.

3.1.2.1 Initial Yield Stress and Plastic Viscosity

The measured initial yield stress and plastic viscosity of the FCPs at 20 °C are presented in Fig. 3.10. Clearly, the curves in Fig. 3.10 behave in much the inverted way as the initial fluidity curves in Fig. 3.1. A reduction of W/C from 0.5 to 0.25 leads to an increase in the yield stress and the plastic viscosity. With the inclusion of PCE, the yield stress and the plastic viscosity decrease considerably at first and then remain stable irrespective of further addition of PCE.

Usually, the rheological properties of cement mixtures with superplasticizers are strongly influenced by the mixture temperature. As shown in Fig. 3.11, a high temperature leads to an increase in the initial yield stress, which should be ascribed to the faster dissolution and early hydration at elevated temperatures. In Fig. 3.12, remarkable drops in the initial plastic viscosity with temperature are observed in the

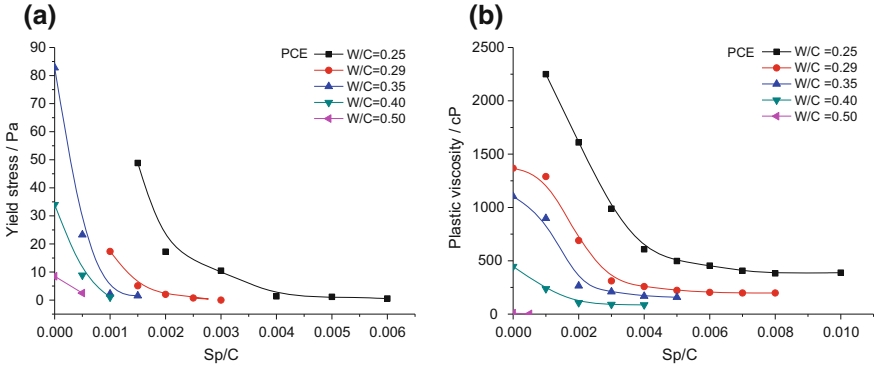

Fig. 3.10 Initial rheological parameters of FCPs with varied W/Cs and Sp/Cs at 20 °C. **a** Yield stress; **b** Plastic viscosity

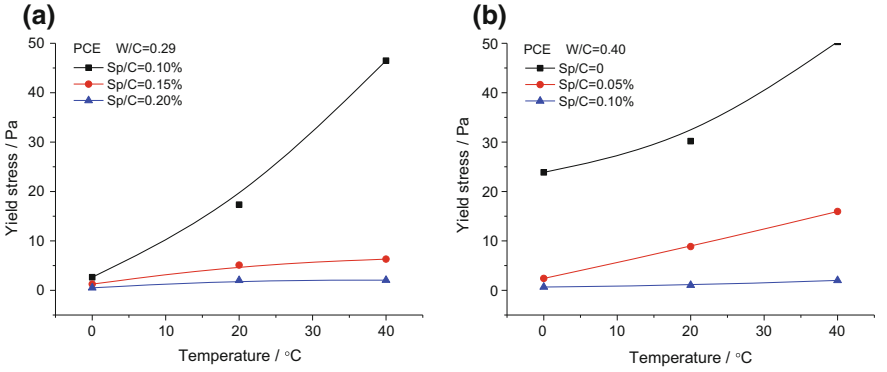

Fig. 3.11 Variation of initial yield stress of FCPs with temperature at varied Sp/Cs. **a** W/C = 0.29; **b** W/C = 0.4

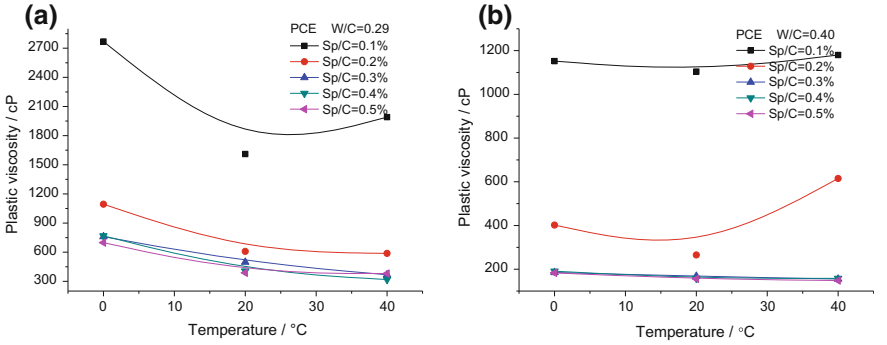

Fig. 3.12 Variation of initial plastic viscosity of FCPs with temperature at varied Sp/Cs. **a** W/C = 0.29; **b** W/C = 0.4

most case of FCPs, which was also reported by Petit et al. (2005, 2006, 2007, 2009, 2010) and Golaszewski and Szwabowski (2004). We suppose this phenomenon is associated with the reduced interactions among cement grains caused by the enhanced thermal motion and low medium viscosity under elevated temperatures. Additionally, high Sp/C and W/C in the FCPs reduce the temperature effects on initial rheological parameters, which is fully compatible with the fluidity results shown in Figs. 3.3 and 3.4.

3.1.2.2 Development of Yield Stress and Plastic Viscosity Over Time

The rheological parameters over elapsed time for FCPs at 20 °C are exhibited in Figs. 3.13 and 3.14. It is clearly noted that the yield stress and the plastic viscosity

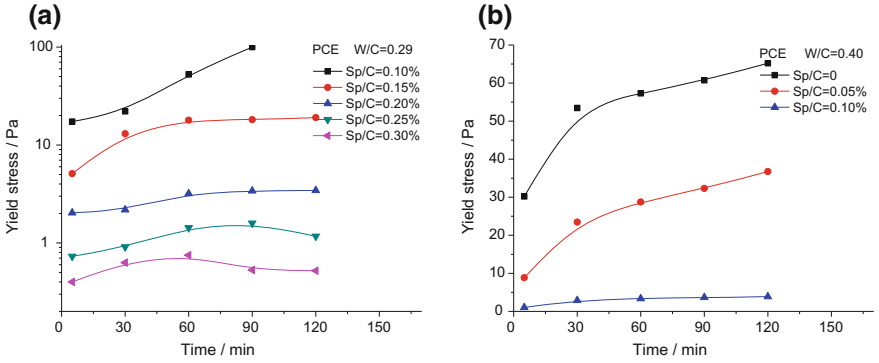

Fig. 3.13 Yield stress over elapsed time for FCPs with varied Sp/Cs at 20 °C. **a** W/C = 0.29; **b** W/C = 0.4

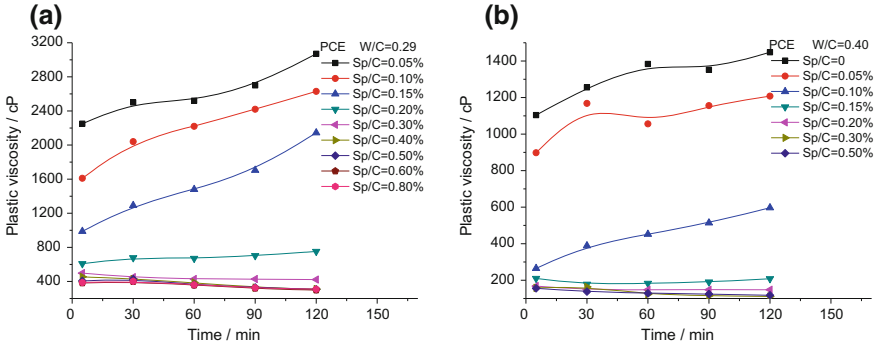

Fig. 3.14 Plastic viscosity over elapsed time for FCPs with varied Sp/Cs at 20 °C. **a** W/C = 0.29; **b** W/C = 0.4

increase over time at low Sp/C, and their growth rates descend with the increased superplasticizer dosage in the FCPs. These phenomena are consistent with the results of the fluidity. When the superplasticizer dosage increases to a certain dosage (Sp/C = 0.2%, 0.3%), the yield stress and the plastic viscosity start to decline over elapsed time, which may correlate with the adsorption rate, disassembly of flocculated structures as well as the retardation effect at high dosages of superplasticizer.

Similarly, the development of rheological parameters over elapsed time is affected by temperature, as shown in Figs. 3.15 and 3.16. It demonstrates that an elevated temperature leads to the increased growth rate of the yield stress over elapsed time due to the accelerated cement hydration. With regard to the plastic viscosity, the temperature effects are dependent on the superplasticizer dosage. Specifically, at low dosages, the plastic viscosity ascends over elapsed time and the growth rate boosts at elevated temperatures. By contrast, in the case of FCPs with high Sp/C, the plastic viscosity declines over elapsed time and the decreasing rate drops at elevated temperatures. In addition, the temperature effects on the change rates of the yield stress and the plastic viscosity are weakened at high dosages, which is also related to the adsorption of PCE on cement grains and its retardation effects.

3.1.3 Viscoelastic Properties

It is reported that viscoelastic properties of FCPs not only play important roles in affecting the fluidity, consistence and workability of FCPs, but also affect the volume stability of hardened cement pastes (HCPs) (Bellotto 2013; Ferrandis and Leveque 2003; Grasley and Lange 2007; Nachbaur et al. 2001; Subramaniam et al. 2005; Subramaniam and Wang 2010; Wang et al. 2010). Currently, various techniques have been employed to investigate the viscoelastic properties of FCPs, such as dynamic rheometer, electrical or ultrasonic reflection. Using these techniques, the elastic and viscous behaviors of FCPs can be characterized by directly measuring the loss and storage moduli. In this study, a microrheology analyzer (Rheolaser LAB6™) was adopted to in situ follow the development of the viscoelastic properties of FCPs in the presence of PCE superplasticizer during the early hours after mixing.

3.1.3.1 Theory Background

(1) Microrheology

Microrheology is a new domain of rheology to study the viscoelastic behavior of a multi-phase system such as emulsions, suspensions, gels or colloidal dispersions at

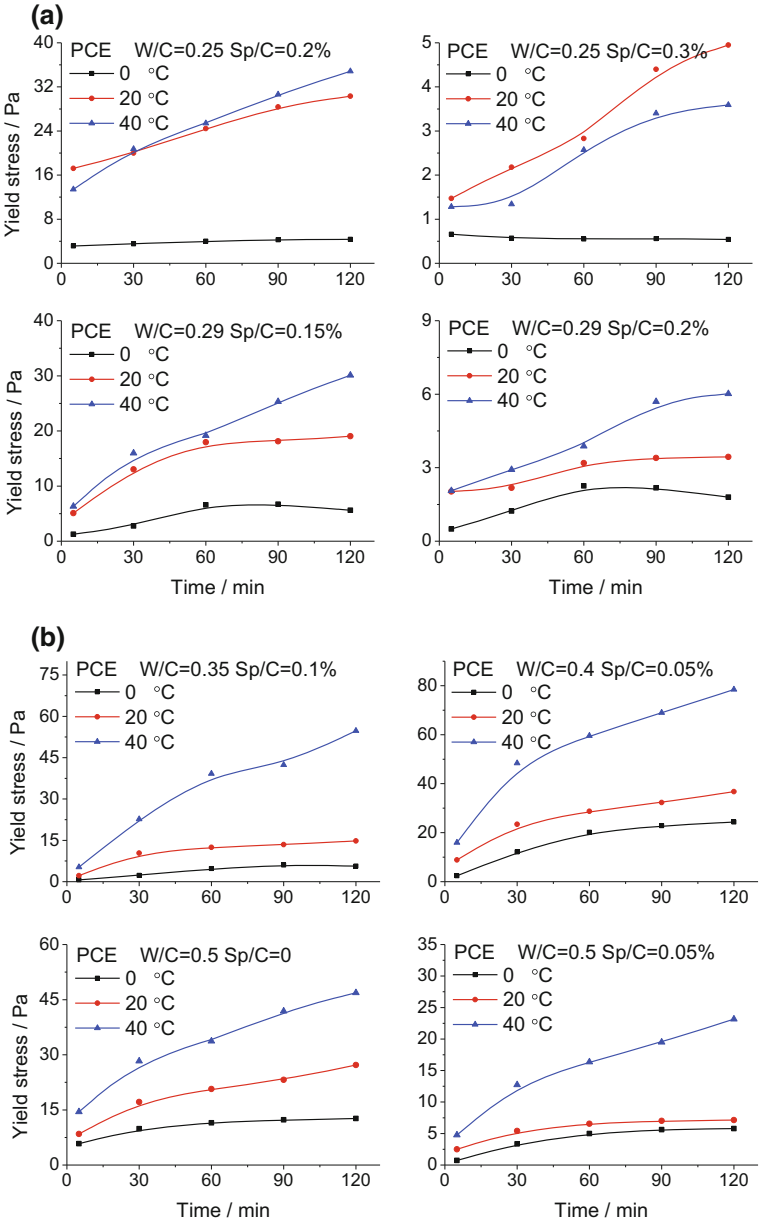

Fig. 3.15 Yield stress over elapsed time for FCPs at varied temperatures and Sp/Cs. **a** W/C = 0.25 and 0.29; **b** W/C = 0.35, 0.4 and 0.5

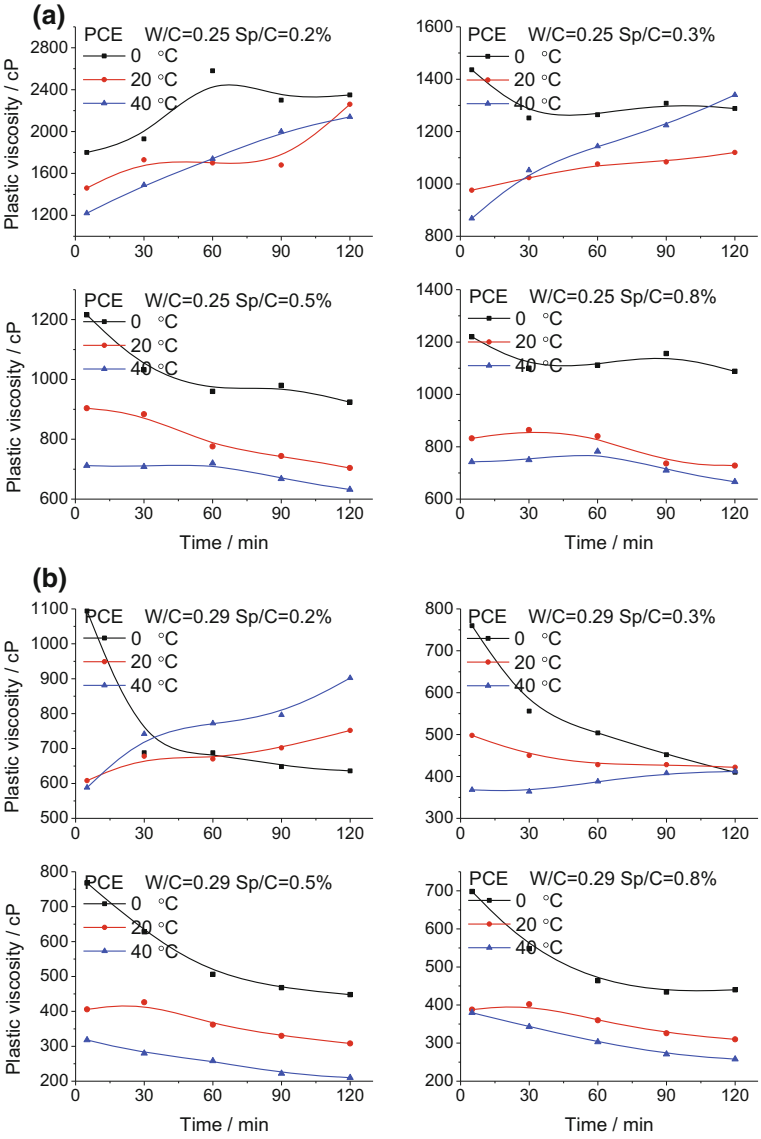

Fig. 3.16 Plastic viscosity over elapsed time for FCPs at varied temperatures and Sp/Cs. **a** W/C = 0.25; **b** W/C = 0.29; **c** W/C = 0.35; **d** W/C = 0.4

a micron length scale (Gardel et al. 2005a, b). It refers to measure the local deformation of a sample originated from an applied stress or thermal energy, which is directly correlated to the elastic and viscous properties of the system (Gardel et al. 2005a, b). In this study, the measurement of FCPs was performed using a microrheology analyzer. This technology uses a multi-speckle diffusing wave

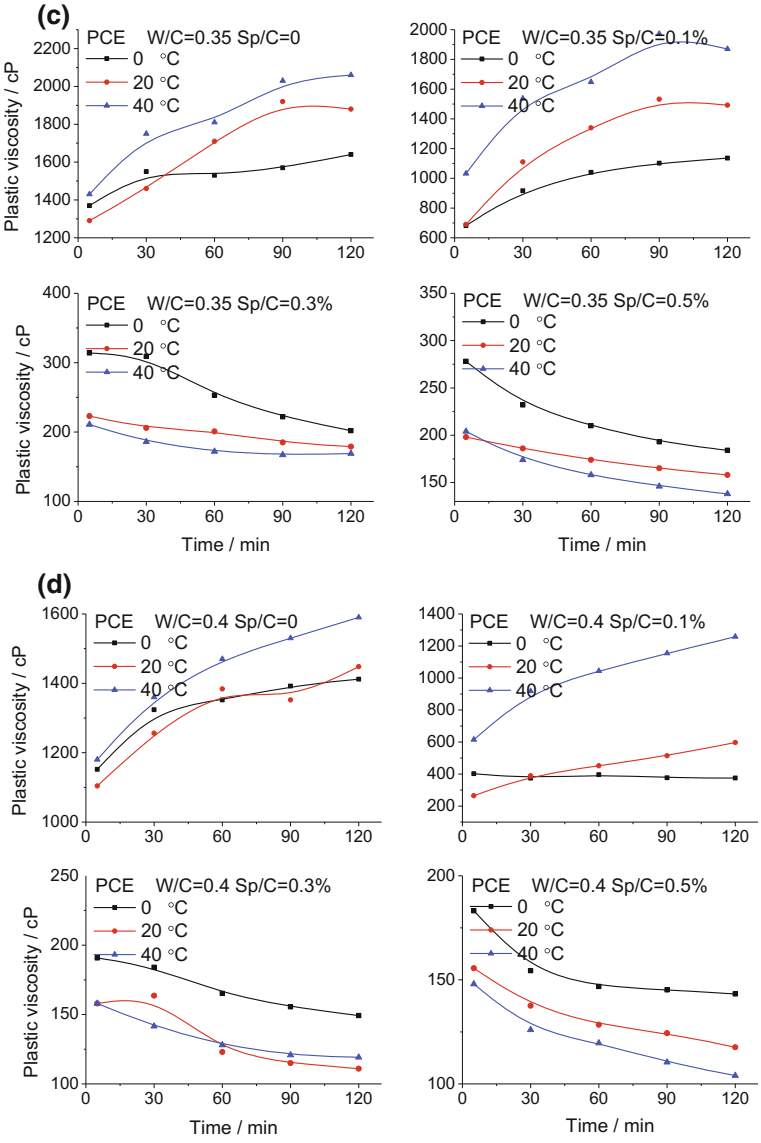

Fig. 3.16 (continued)

spectroscopy (MS-DWS) set-up in a backscattering configuration with a video camera detection, to measure the displacement of particles (Bellour et al. 2002). The scheme of this apparatus is depicted in Fig. 3.17 and the principle of DWS measurement is shown in Fig. 3.18. Unlike traditional rheology test methods where a shear force and shear strain are usually involved, this method enables a

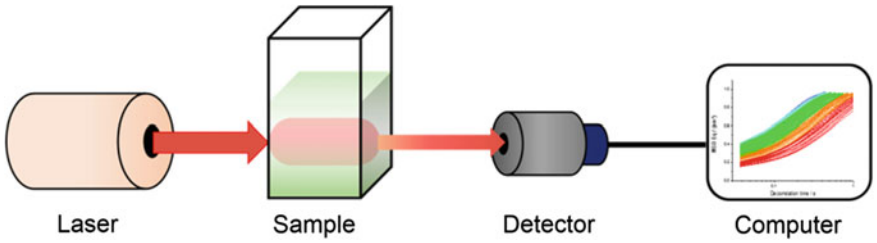

Fig. 3.17 Schematic representation of the experimental microrheometer

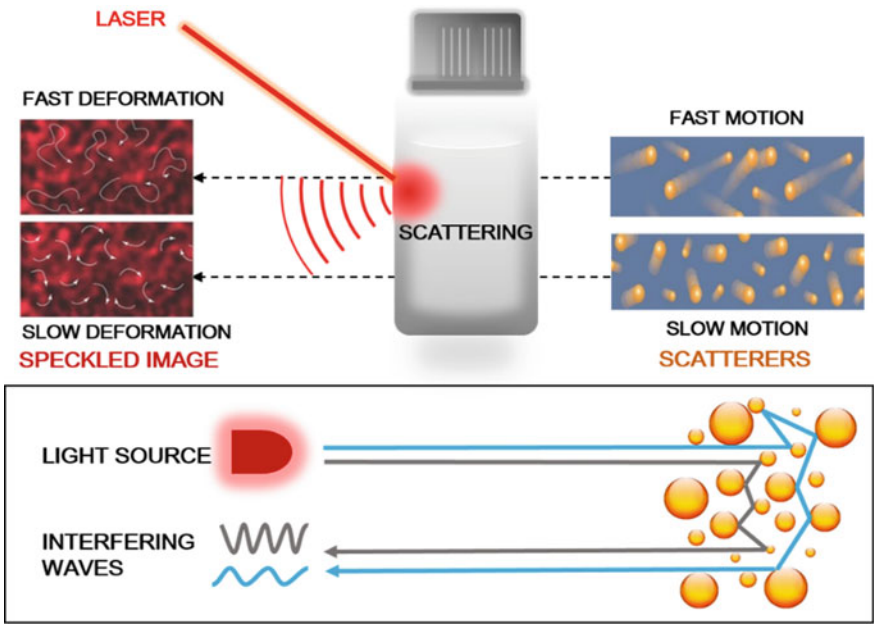

Fig. 3.18 The principle of the multi speckle diffusing wave spectroscopy (MS-DWS) measurement and the relationship between the motion rate and the deformation rate (Tisserand et al. 2012)

non-disturbing measurement without any disturbance to the sample, and the same sample can be continuously monitored versus elapsed time. After the sample is placed in a cell, a fixed coherent laser beam (wavelength 658 nm) is incident upon the sample which contains scaterrers (cement grains here). The laser is multiply scattered many times by the particles into the sample, which leads to the interfering back scattering waves. An interference image called a "speckle image" is detected by a multi-pixel detector. In dynamic mode, particle motion induces spot movements of the speckle image (Brunel and Snabre 2003). The particle mobility in terms of speed and displacement is closely related with the viscoelastic properties of the whole system, so is the deformation of the speckle image (Fig. 3.18). Fast

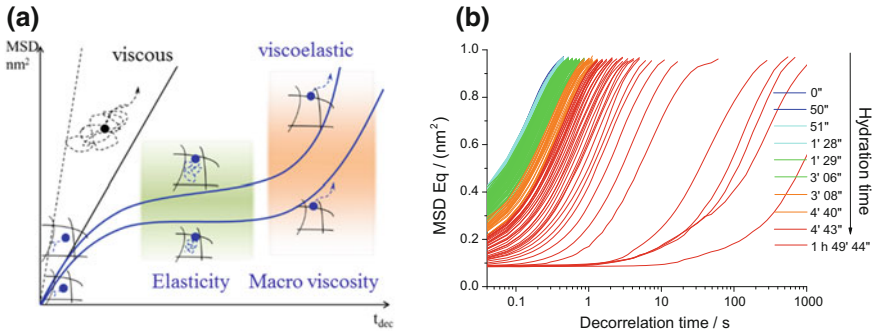

Fig. 3.19 MSD curves of purely viscous and viscoelastic samples **a** and a blank FCP during cement hydration **b**

motion of particles results in fast deformation of speckle image and slow motion of the particles leads to a slow deformation of the speckle image. Based on the speckle image, a patented algorithm was used to quantitatively characterize the deformation rate of the speckle image and further plot the curve of the mean square displacement (MSD) of the scatterers versus decorrelation time t_{dec} (Brunel 2009).

For a single measurement of a stable colloid system, the decorrelation time t_{dec} is the measurement time, which is used to follow the change of the speckle image (Brunel 2009). From the MSD curve with respect to the decorrelation time, the two viscoelastic moduli, G' and G'', can be calculated using the generalized Stokes-Einstein relation (Mason 2000):

$$\tilde{G}(s) = \frac{k_B T}{\pi a s \langle \Delta \tilde{r}^2(s) \rangle} = G' + iG'' \tag{3.1}$$

where k_B is Boltzmann constant, T is temperature in kelvins, s is the Laplace frequency, which is proportional to $1/t_{dec}$, a represents the radius of the tracer, and $\langle \Delta \tilde{r}^2(s) \rangle$ denotes the Laplace transform of the MSD.

Samples with different microstructures possess different viscoelastic properties, thereby producing varied MSD curves. From the shape of MSD curves as shown in Fig. 3.19a, viscoelastic properties of samples could be analyzed qualitatively (Tisserand et al. 2012). In the case of a purely viscous sample, the MSD grows linearly with the decorrelation time as the particles are completely free to move in the sample and the slope of the MSD curve is associated with the viscosity of the sample. With respect to a viscoelastic sample, particles in the sample are not free to move but constrained in a "cage" or "network structure" formed by the neighboring particles. Smaller size of "cage" or "network structure" brings about a stronger constraining effect, which is indicated by the more pronounced elasticity of the sample. Overall, the MSD curve of a viscoelastic sample could be divided into three periods with respect to the decorrelation time. At the very initial decorrelation time, the particles are free to move in the continuous medium phase, so the MSD curve

develops linearly and the slope is mostly related to the viscosity of the dispersant medium. Then, they are blocked by their neighbors, and the slope of MSD curve decreases and finally the MSD reaches a plateau. This is a characteristic of the elasticity of the sample. A lower plateau means a "cage" with smaller size and stronger elasticity. Thus, the height of the plateau characterizes the elastic modulus of the sample. At longer decorrelation time, the particles are able to find a way to escape from the "cage" and the MSD grows linearly again, which is a characteristic of the macroscopic viscosity as it corresponds to the moving speed of the particles in the sample. The longer time needed by the particles to finish a displacement implies the lower particle mobility and the higher macroscopic viscosity. The following parameters extracted from MSD curves enable to characterize the viscoelastic properties of samples (Tisserand et al. 2012).

- Elasticity index (EI) is computed from the elastic plateau value, which corresponds to the inverse of the height of the MSD plateau.
- Macroscopic viscosity index (MVI) is a global computation and corresponds to a viscosity index at zero shear rate, which is the inverse of the slope of MSD curve in later linear scale.
- The storage modulus G', which represents the elastic behavior or the elastic energy storage of the material, and the loss modulus G'', which signifies the viscous behavior or energy dissipation of the material, can be calculated using the generalized Stokes-Einstein relation (Mason 2000). For an elastic solid, the storage modulus dominates in the material and the loss modulus is low. For a viscous liquid, the loss modulus dominates. Thus, a material can be readily identified as an elastic solid or a viscous liquid by comparing the values of G' and G''.
- When the viscoelastic properties of the sample are described by the Maxwell model, the elastic modulus of a Hookean spring G and the viscosity of a Newtonian dashpot η could be obtained.

(2) Application of microrheology analyzer in FCPs

As discussed above, the principle of the microrheology analyzer is based on the measurement of the Brownian motion of particles. As a typical solid-liquid suspension system (Roussel et al. 2010), a FCP can be a suitable object to be measured by the microrheology analyzer. This method may provide abundant information about the rheological properties as well as the viscoelastic properties of the FCP samples. Information of cement hydration and setting of FCPs could also be obtained by following the evolution of those parameters provided by the microrheology analyzer. In addition, the impacts of chemical admixtures, including viscosity modifier and superplasticizer on properties of FCPs could be easily investigated by this method. The test results of MSD curves of a FCP captured by the microrheology analyzer are shown in Fig. 3.19b. The MSD curves emerge in blue at first and then in green, and lastly in red with the progressing cement hydration. As cement hydration proceeds, the movement of MSD curves from top to bottom and from left to right suggests an increasing elasticity of the FCP with the

elapsed time. This conclusion is fully consistent with the results of oscillatory rheometer and ultrasonic reflection measurements reported by other researchers (Chung et al. 2009; Wang et al. 2010). As a consequence, it is confirmed that the microrheology analyzer could be a good tool used to follow the development of the viscoelastic properties of FCPs. The corresponding parameters extracted from the MSD curves could also be applied in the quantitative analysis of their viscoelastic properties.

3.1.3.2 EI and MVI

The development of EI and MVI of FCPs with different W/Cs and Sp/Cs during the first 2 h is plotted in Fig. 3.20. In most cases, both EI and MVI gradually increase with elapsed time and finally reach a plateau, which means the elasticity and macroscopic viscosity increase over time. The reason is majorly connected to the continuous cement hydration after contact of cement with water. Along with the progressing cement hydration, a portion of free water is consumed and hydration products are formed. The newly formed hydrates, by creating new links among cement grains, would increase the inter-particle crosslinking and thus lead to a

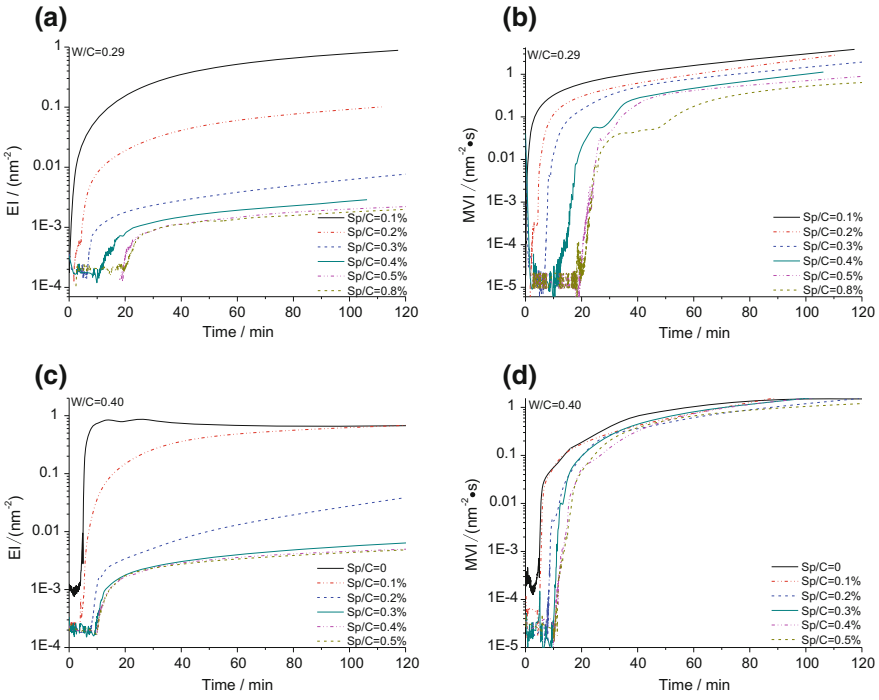

Fig. 3.20 Variations of EI and MVI of FCPs with different Sp/Cs with elapsed time. **a**, **b** W/C = 0.29; **c**, **d** W/C = 0.4

stronger "network structure". Correspondingly, the elasticity and macroscopic viscosity of FCPs become more pronounced. After a rapid initial burst of dissolution and early formation of hydration products, the cement hydration steps into the induction period in which the hydration reaction is proceeding at a relatively low rate. During this period, the microstructure of FCPs slowly develops and the parameters, EI and MVI slowly grow over the elapsed time.

In the case of FCPs with high Sp/C, EI and MVI evolution curves start with a flat part at a very low value, followed by a sharp increasing part. It is interestingly noted that the length of the flat part is extended by the increase of superplasticizer dosages and then almost keeps constant when Sp/C is beyond the critical dosage. The delayed fast increase of EI and MVI by the addition of PCE must be related to the abovementioned dispersing effects and early retarding effects of PCE. The addition of PCE in FCPs leads to an increased dispersion degree of cement grains and depresses the early formation of ettringite crystals. It has been realized that in the very early hydration period (<20 min), PCE clearly retards the formation of ettringite and reduces the size of ettringite crystals (Cheung et al. 2011). In this way, PCE disassembles the flocculated structures in FCPs, thereby lessening the inter-particle crosslinking, and delays the establishment of the "network structure". These two effects of PCE, the dispersing effects and the early retarding effects lead to the flat parts of the EI and MVI curves.

When the dosage of superplasticizer is beyond the critical dosage, the dispersion degree of particles reaches maximum and hence the length of the flat part keeps almost constant. On the other hand, the macroscopic viscosity of FCPs is also related to the dispersion of cement grains and the content of free water, so MVI behaves in a similar way to EI.

Moreover, the values of EI and MVI as well as their growth rates over time are clearly reduced by the addition of superplasticizer as seen in Fig. 3.20, which also originates from the effects of superplasticizer in terms of improving the dispersion state of cement grains and retarding the early cement hydration.

Compared to the case of FCPs at W/C of 0.29, EI and MVI of FCPs at W/C of 0.4 are lower and the effects of superplasticizer are less remarkable. This is a result of the larger distance among the cement grains at higher W/C. In that case, the size of "cage" is so large that it is less sensitive to the addition of superplasticizer although the distance can be further enlarged by the superplasticizer. Similarly, the impact of volume fraction of solid phase on the viscosity of FCPs at higher W/C is considered to be weaker (Cheung et al. 2011). Hence, the variations of EI and MVI with Sp/C at W/C of 0.4 are not as significant as the FCPs with W/C of 0.29.

3.1.3.3 G' and G''

In order to have a better insight of the viscoelastic properties of FCPs, G' and G'' over a range of frequencies during the first few hours were obtained. The variations of G' and G'' versus frequency at a given elapsed time are reported in Fig. 3.21. With increasing frequency, moduli generally present increasing trends with slight

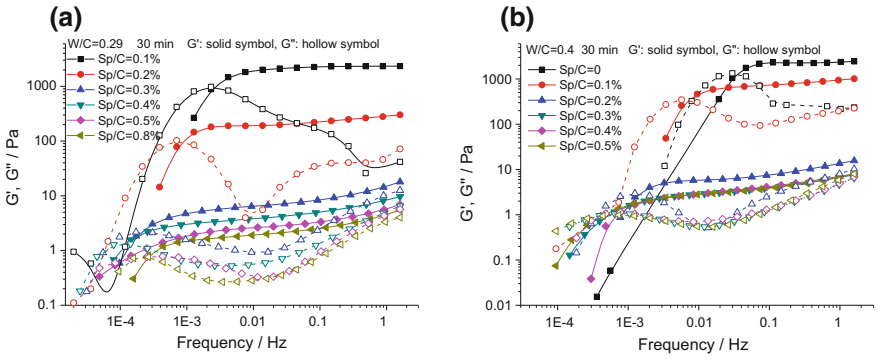

Fig. 3.21 Variations of G' and G'' of FCPs with different Sp/Cs versus frequency. **a** W/C = 0.29; **b** W/C = 0.4

fluctuations. An increase of both G' and G'' up to a nearly constant value is noticed with increasing frequency at high superplasticizer dosages, which is fully compatible with the earlier findings reported in reference (Papo and Piani 2004). In addition, $G' < G''$ is observed in the range of lower frequency, suggesting that the viscous behavior is pronounced in this range of frequency. Oppositely, G' exceeds G'' in the higher frequency, indicating that the elastic behavior is becoming the dominant feature. Furthermore, with the increase of Sp/C, the intersection point of G' curve and G'' curve gradually shifts towards left and the moduli exhibit less frequency dependence. These phenomena reflect the paste is undergoing a significant structural change when superplasticizer is introduced into the cement paste.

Another interesting observation from the plot of G'' against frequency in Fig. 3.21 is that along with the general growth of G'' with frequency, a peak of G'' appears at a certain frequency for all samples. It has been well understood (Liu et al. 2013; Menard 2008) that when a dynamic load is exerted to a viscoelastic material, the strain does not simultaneously develop with the stress and a delayed strain response is usually observed. Lag angle is used to describe such delayed strain-stress response. The bigger lag angle indicates the more pronounced viscoelastic feature of the material and leads to the larger loss modulus G''. On the other hand, the viscoelasticity of materials is highly dependent on the frequency of the dynamic load. At a certain frequency, the material exhibits the most significant viscoelastic feature, which is called the characteristic frequency of the material. That is to say, the lag angle of a viscoelastic material is dependent on the loading frequency. From the location of the maximum peak of the lag angle or the peak of the loss dynamic modulus G'', the characteristic frequency of the material can be determined. Thus, the characteristic frequency of the fresh cement pastes can be obtained as listed in Table 3.1. A general observation from Table 3.1 is that the characteristic frequency of the sample decreases with the increase of the Sp/C in cement pastes. This suggests that the addition of superplasticizer certainly changes the viscoelastic behavior of the fresh cement pastes.

Table 3.1 The characteristic frequency of cement pastes at varied W/Cs and Sp/Cs

W/C	0.29						0.40				
Sp/C (%)	0.1	0.2	0.3	0.4	0.5	0.8	0	0.1	0.2	0.3	0.5
Frequency/10^{-4} Hz	2.1	0.6	0.17	0.13	0.2	0.21	20	4.0	1.02	0.60	0.60

At one certain frequency, the variation trends of G' and G'' with the elapsed time shown in Fig. 3.22 behave in much the same way as the curves in Fig. 3.20. Initially, G' as well as G'' present a linear increase over time and then reach a plateau. This demonstrates that the main evolution of the "network structure" in FCPs occurs within a few minutes after the mixing process due to the fast dissolution of clinker phases and the initial formation of hydrates, whereas the structure changes less drastically in the next hours before setting. Due to the abovementioned dispersing effects and the early retarding effects of PCE superplasticizer, the moduli of FCPs keep stable initially and then start to rise over the elapsed time at high superplasticizer dosages. Moreover, higher Sp/C brings about lower moduli as well as lower growth rates.

When G' and G'' are compared in Fig. 3.22, it is not hard to find that G' is always higher than G'' for the FCPs with low Sp/C at W/C of 0.29, which means an elastic feature or solid-like behavior prevails, corresponding to the well-known gel state of cement pastes (Zhou et al. 1999). Nevertheless, in the case of high Sp/C or high W/C, G' is lower than G'' at the beginning but it grows beyond G'' at the end. The junction between G' and G'' curves within the first few minutes suggests that the rheological behavior of FCPs transforms from a slightly liquid-like behavior to a strongly solid-like behavior. Obviously, this phenomenon is consistent with the fact that the microstructure of FCPs is undergoing a substantial change from a rather dispersed fluid state to a highly structured solid state resulting from the

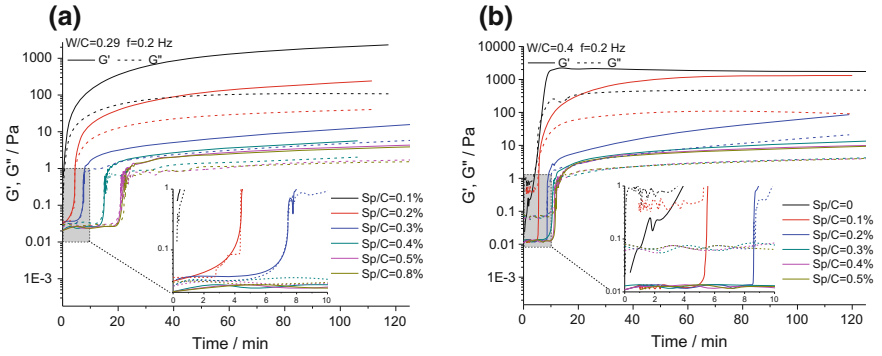

Fig. 3.22 Variations of G' and G'' of FCPs with different Sp/Cs versus elapsed time. **a** W/C = 0.29; **b** W/C = 0.4

establishment of the "network structure" due to the electrostatic interactions between cement grains and the bridging effects of the newly formed hydrates. On the other hand, at the plateau part of the curve, G' is about 20 times higher than G'' at low dosages of superplasticizer whereas G' is only twice as much as G'' at high Sp/C, suggesting that the elastic characteristic of the FCPs is weakened by the incorporation of superplasticizer in cement pastes.

3.1.3.4 Maxwell Model Parameters

When the viscoelastic properties of FCPs are described by Maxwell model, the parameters including the elastic modulus of spring G and the viscosity of dashpot η could be acquired. Their variation trends with elapsed time (Fig. 3.23) are in good agreement with those of EI and MVI, i.e., initially G and η present a linear increase over time and then reach a plateau, and the inclusion of superplasticizer significantly reduces the elasticity and viscosity of the FCPs. At lower W/C, the effects of superplasticizer on the Maxwell parameters are more remarkable.

The ratio of η to G, η/G is an indicator to determine which feature is dominant in a material, either elasticity or viscosity. It is shown in Fig. 3.23c, f, there are some fluctuations of η/G at the beginning, which is caused by the unstableness of G and η right after mixing. Namely, the fresh cement paste needs some minutes to establish a relatively stable structure without agitation. After that, η/G of FCPs increases over elapsed time. That is to say, although η and G both rise due to the cement hydration, η seems to grow more rapidly than G. Meanwhile, η/G also presents an increasing trend with increasing Sp/C. This demonstrates that the addition of superplasticizer reduces G more significantly than η. As mentioned previously, the elasticity is directly related to the "network structure" of FCPs. The main effect of superplasticizer is to release the entrapped water and to increase the dispersion degree of cement grains in FCPs. As a result, the "network structure" could be strongly weakened and subsequently the elasticity of FCPs sharply drops. However, the viscosity of FCPs is majorly determined by other factors such as the volume fraction of solid phase in the solid-liquid system, interactions between particles, the frictions between particles and the viscosity of the medium etc., besides the dispersion degree of cement grains (Chougnet et al. 2007). From the results above, it could be concluded that superplasticizer has more significant effects on the elastic modulus G than the viscosity η. This is in agreement with the previous finding that the addition of superplasticizer could decrease the yield stress more obviously than the viscosity (Flatt 2004; Golaszewski and Szwabowski 2004; Petit et al. 2007).

From Figs. 3.22 and 3.23a, b, d, e, it is also noted that the parameters of fresh cement pastes, G', G'', G and η start with a flat period and then sharply grow during cement hydration. It is noticed that the duration of the flat period is in the range of 0–20 min and is dependent on the dosage of PCE in the cement pastes. The more dosage of PCE leads to the longer flat period and the maximum flat period is

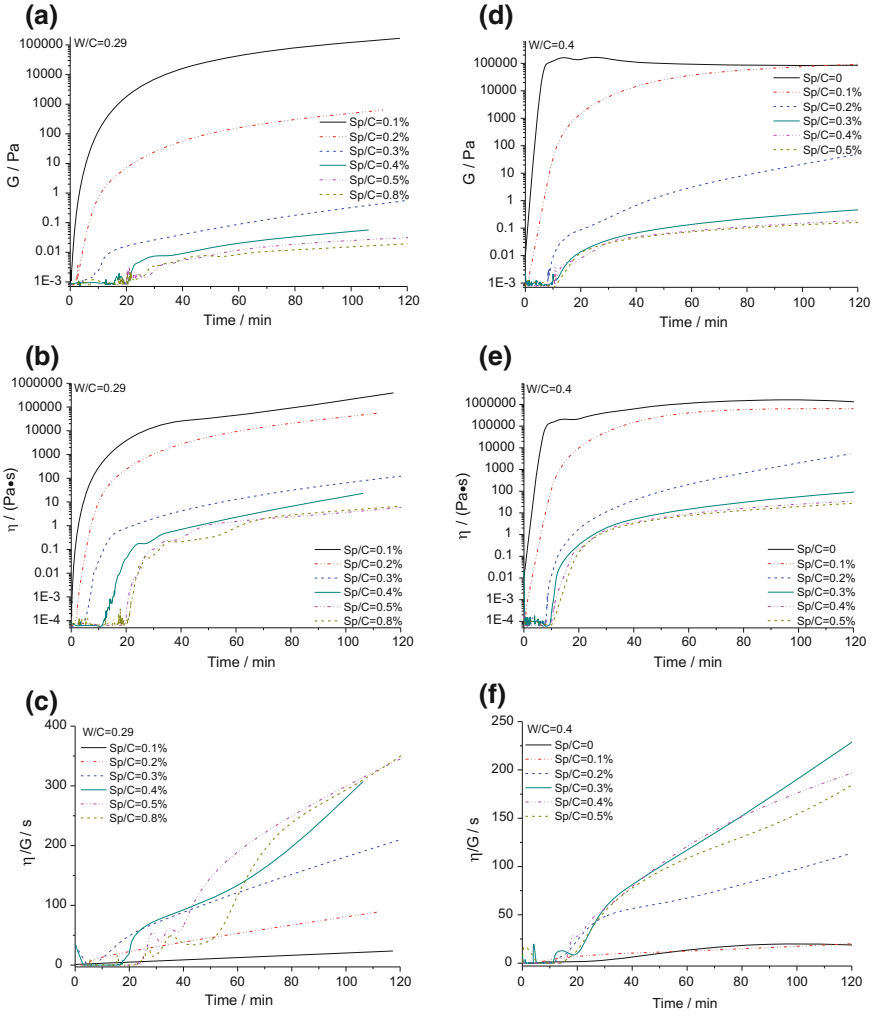

Fig. 3.23 Variations of Maxwell model parameters of FCPs with different Sp/Cs versus elapsed time. **a**, **b**, **c** W/C = 0.29; **d**, **e**, **f** W/C = 0.4

reached at the critical dosage. It is believed that this must be again related to the dispersing effects as well as the retarding effects on early hydration. It has been well understood that in such a short period (within 20 min) after mixing, dissolution of various phases such as C_3S, C_3A and sulfate carriers and the early formation of ettringite crystals are the main processes involved in cement hydration. The adsorbed PCE on surface of cement grains may retard the initial dissolution of various clinker phases and early precipitation of ettringite, and hence change the electrostatic interactions among the dispersed particles in cement pastes.

3.2 Cement-Latex-Water System

Polymer latexes are often used in cement mortars and concrete as modifiers to improve their properties such as adhesion, fracture toughness, flexural strength, cracking resistance and waterproof. It has been often reported that polymer latexes also influence the fluidity of fresh cementitious mixtures. A few of latexes could increase the fluidity of FCPs while some significantly reduce the fluidity. The relevant working mechanism has not been elucidated so far. In this section, two types of polyacrylate latexes L1 and L2 with negative charges were used to investigate the effects of latexes on the fluidity of FCPs at different dosages, temperature and elapsed time, aimed at revealing their working mechanism. Considering that the variation trends of rheological parameters are fully compatible with the fluidity of FCPs, only the results of their fluidity are presented here.

3.2.1 Initial Fluidity

3.2.1.1 Effects of Mix Proportion

As seen from Fig. 3.24, the incorporation of both polymer latexes L1 and L2 has significant influences on the fluidity of the FCPs at 20 °C. For latex L1, the fluidity is slightly lowered at L/C of 1% and then increased markedly to a maximum value when the L/C is in the vicinity of 9%. In the presence of latex L2, the fluidity declines dramatically at first (L/C < 3%) and then increases to a maximum at the L/C of 12%. With further addition of polymer latexes, the fluidity begins to decrease.

Basically speaking, it is the changes in the microstructure of FCPs caused by the incorporation of chemical admixtures that are responsible for the variations of the fluidity. Similar to superplasticizers, the latexes with negative charges could be

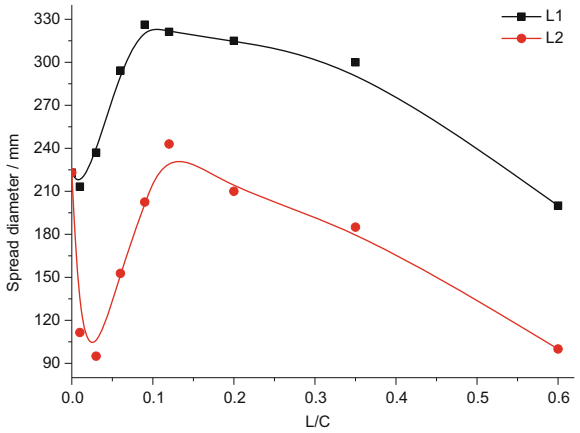

Fig. 3.24 Variation of initial fluidity of FCPs with the addition of polymer latexes

adsorbed on positively charged cement surface under the electrostatic attractive forces. The adsorption will induce electrostatic and/or steric effects and even stereo effects between the cement grains (Pacheco-Torgal et al. 2016), thereby disassembling the flocculated structures of cement grains and increasing the fluidity of the paste, which is called the plasticizing effects of latexes. When the flocculated structures are almost fully disassembled or stop changing with the addition of latexes, the fluidity will reach to maximum at the critical dosage. However, different from superplasticizers, the polymer particles in latex exist in a condensed state with size of 300 nm. At low dosages (L/C < 3%), the adsorption of polymer particles on cement surface may lead to a transformation of zeta potential of the FCPs from a positive value to a negative one. It has been widely accepted that a suspension dispersion system is most unstable if the $|\zeta|$ of the system is in the vicinity of 0 mV, in which the particles tend to form the largest flocculated structures (Fazullin et al. 2015; Li et al. 2016). In this case, a low dosage of latex, namely, a low coverage on the cement surface, facilitates the formation of flocculated structures, which is defined as the neutralizing effects of latexes, as illustrated in Fig. 3.25b. As a result, the fluidity of the FCPs decreases with the incremental latex dosage when L/C is lower than 3%. With further addition of latex, more coverage of latex particles on cement surface results in the decrease of zeta potential to a more negative value, which enhances the electrostatic repulsion between cement grains and thus the dispersion degree of cement grains (Fig. 3.25c). Therefore, the fluidity of FCPs starts to ascend with the growth of L/C. When the flocculated structures are almost fully disassembled or stop changing, the fluidity of FCPs reaches a maximum value at a critical dosage.

Beyond the critical dosage, the part of latex particles with submicron size remaining in the aqueous phase increases the contents of solid phase in the paste. This is defined as the filling effects of latexes and is unbeneficial to the fluidity (Zhang and Kong 2014). Accordingly, the addition of latexes reduces the fluidity of FCPs when the contents of L1 and L2 are respectively larger than 9 and 12%.

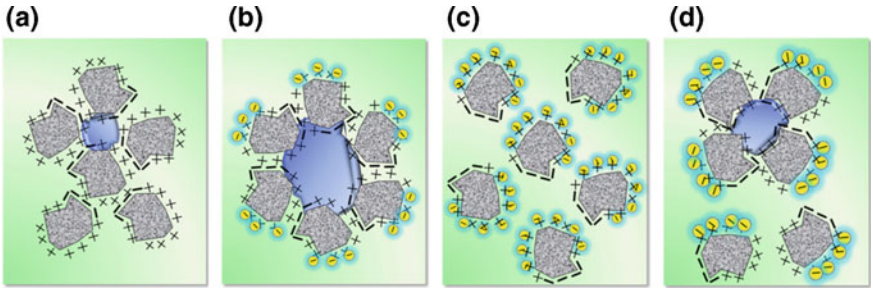

Fig. 3.25 Schematic illustration of the effects of latexes on the microstructure of FCPs. (Cement grain; Free water; Entrapped water; L1; L2)

Compared to L2, L1 enhances the fluidity of FCPs more significantly due to its smaller polymer particle size. Specifically, at the same L/C, the number of small polymer particles in L1 is much more than that in L2 and therefore, more L1 particles are adsorbed on cement grains to neutralize the charges on cement surface, as shown in Fig. 3.25c, d. Moreover, it is noted that the lowest fluidity of FCPs was obtained at 1% L1 and 3% L2, respectively, while the maximum fluidity was arrived at 9% L1 and 12% L2, which is also related to their different particle sizes. For example, it took 3% L2 with larger particle size to neutralize the charges on cement surface whereas only 1% L1 with smaller particle size enables the absolute zeta potential decrease to be lowest, and further leads to the formation of a greatest quantity of flocculated structures and the lowest fluidity.

Based on the above discussions, the working mechanism of polymer latexes on the initial fluidity of FCPs has been proposed. Further microstructural analysis will be conducted in the next chapter to validate it.

3.2.1.2 Effects of Temperature

Figure 3.26 shows the variation of initial fluidity of FCPs with temperature. Clearly, a higher temperature causes a decrease in the initial fluidity for all the FCPs except for the one with 12% L2. For the FCPs with L1, the impacts of temperature on initial fluidity are higher as the dosage of L1 is high, and at 40 °C, the fluidity of the FCPs almost keeps constant although different dosages of latexes are added. It is supposed that the initial fluidity of FCPs containing latexes is determined by the flocculated structures and the stability of latexes. At one certain dosage, as temperature rises, more charges are produced by the faster dissolution as well as early hydration, which leads to the formation of more flocculated structures and consequently to a decrease in the initial fluidity. In the case of high latex dosages, more charges should provide more adsorption sites for the latex, thereby disassembling

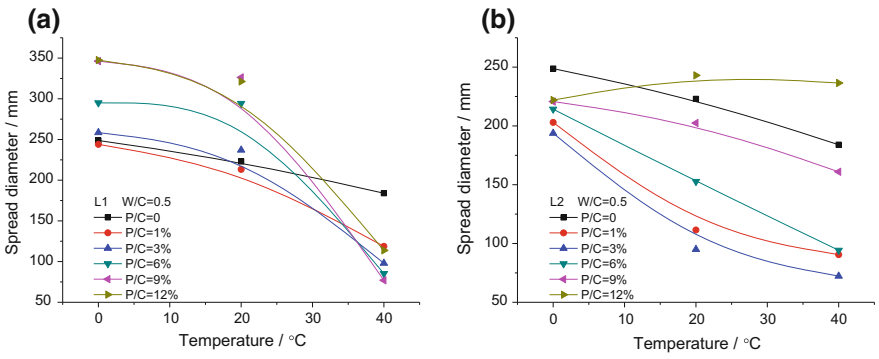

Fig. 3.26 Variation of initial fluidity of FCPs with temperature at varied L/Cs. **a** Latex L1; **b** Latex L2

the flocculated structures and increasing the fluidity, similar to the superplasticizers. However, the demulsification of latex may occur at an elevated temperature, particularly in the case of high latex dosages, which weakens the plasticizing effects of latexes at high temperatures. As a result, the initial fluidity of FCPs with higher L/C at an elevated temperature is lower, and the FCPs exhibit a strong temperature sensitivity as the dosage of L1 is high.

By contrast, for the FCPs with latex L2, the impacts of temperature on the initial fluidity are weakened at high dosage of L2. This may be related to the lower film formation temperature of L2, −5 °C. Specifically, the demulsification of latex L2 occurs at all the temperatures used here (0, 20 and 40 °C) and the plasticizing effects of latexes are not affected by the temperature any more. Thus, the initial fluidity of FCPs is only dependent on the flocculated structures, and the temperature sensitivity of initial fluidity is solely determined by the effects of temperature on these flocculated structures. Specifically, at an elevated temperature, the accelerated dissolution and early cement hydration produce more charges, which could induce the formation of more flocculated structures and could likewise consume more polymer particles by adsorption under high temperatures, and the FCPs with a high latex content have a low temperature sensitivity because of the sufficient number of polymer particles that reduce the flocculated structures. Particularly, at the L/C of 12%, the initial fluidity is slightly affected by the temperature because the flocculated structures at varied temperatures have been effectively disassembled.

3.2.2 Fluidity Retention

3.2.2.1 Effects of Mix Proportion

Similar to superplasticizers, the addition of polymer latexes could delay the cement hydration via depressing the dissolution of mineral phases and the diffusion (Li and Kong 2009). So, with the increase of latex dosage in FCPs, the fluidity retention of FCPs is enhanced, as shown in Fig. 3.27. In the presence of L1, the fluidity retention of FCPs is evidently heightened at high dosages, while the fluidity almost keeps constant within 2 h. At lower dosage of L2, the fluidity retention of FCPs is stronger due to the poorer initial fluidity. With the incorporation of L2, an enhancement of fluidity retention is also observed. Compared to latex L2, latex L1 could more significantly enhance the fluidity retention of FCPs. This may be related to the greater retardation effects of latex L1 on cement hydration, which will be discussed and confirmed in detail in the Chap. 5.

3.2.2.2 Effects of Temperature

A high temperature accelerates cement hydration and consequently, reduces the fluidity retention of FCPs. The effects of temperature on the fluidity retention of

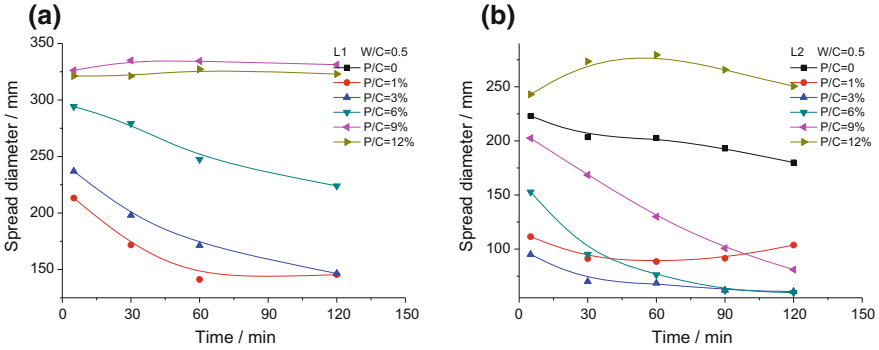

Fig. 3.27 Fluidity retention of FCPs with varied dosages of latexes at 20 °C. **a** Latex L1; **b** Latex L2

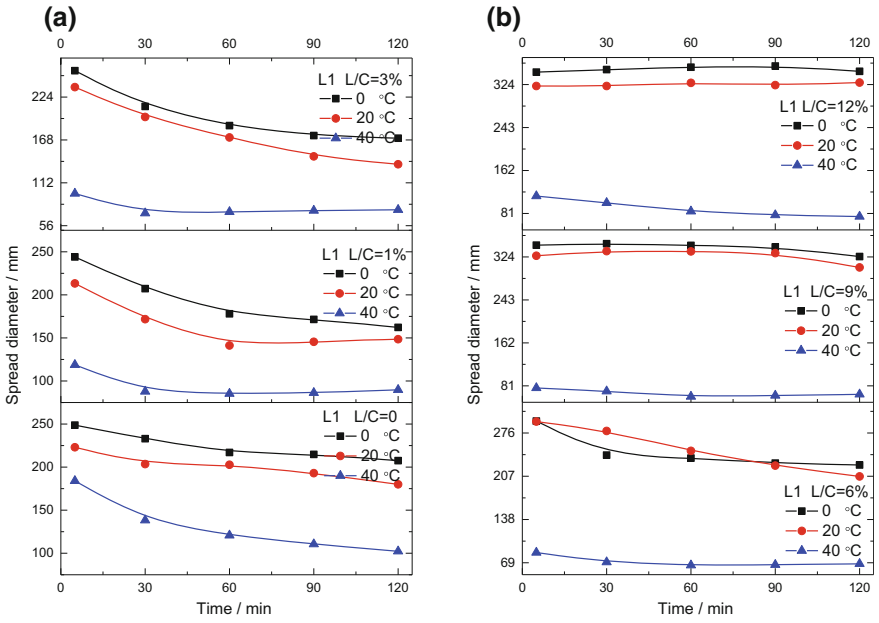

Fig. 3.28 Variation of fluidity retention of FCPs with temperature at varied dosages of L1. **a** L/C = 0–3%; **b** L/C = 6–12%

FCPs are shown in Figs. 3.28 and 3.29. At low dosages, an elevated temperature leads to a larger decreasing rate of fluidity with time, namely weaker fluidity retention. At high dosages, the fluidity retention is slightly affected by the temperature. This is believed to stem from the stronger retardation effects of latexes on cement hydration. That is to say, high dosages of latexes bring about so significant depression on cement hydration that the fluidity of FCPs fails to decrease with time

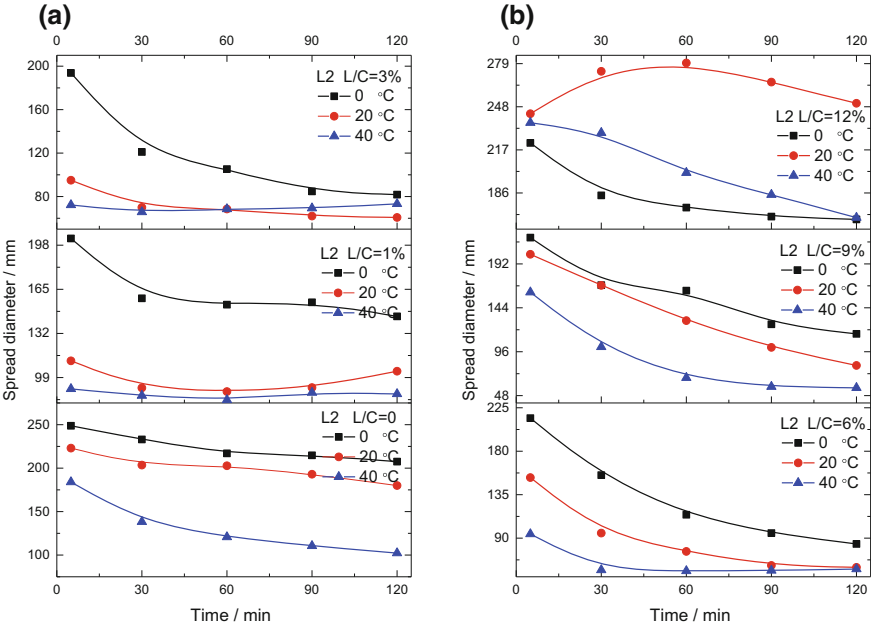

Fig. 3.29 Variation of fluidity retention of FCPs with temperature at varied dosages of L2. **a** L/C = 0–3%; **b** L/C = 6–12%

even at elevated temperatures. The sensitivity of the fluidity retention gradually descends with the growth of L/C, which is consistent with the results in Sect. 3.1.1.4 where superplasticizers are incorporated in FCPs.

3.3 Cement-Asphalt-Water System

Cement asphalt mortar (CAM) serves as a vibration-absorbing layer during operation in the slab track structure of high speed railways; its properties including workability are largely determined by the rheological properties of its binding material, cement asphalt paste (CA paste). In this section, the fluidity of fresh CA pastes was measured, and such influencing factors as type of asphalt emulsion, temperature, and elapsed time were considered. In addition, the yield stress of the CA pastes with different A/Cs was measured at three different temperatures.

3.3.1 *Fluidity*

3.3.1.1 Effects of Mix Proportion on Initial Fluidity

The initial fluidity of two series of fresh CA pastes with a range of A/Cs from 0 to 0.6 at 20 °C is shown in Fig. 3.30 (Kong et al. 2011). At an asphalt content of lower than 20%, the initial fluidity increases with the growth of A/C but begins to decrease at an A/C of 0.2. One should note that even at an A/C of 0.6, the initial fluidity of the CA paste is still larger than that of blank paste. That is to say, the addition of asphalt emulsions into the FCPs induces a plasticizing effect. This plasticizing effect in the system of FCPs caused by superplasticizers or latexes has been discussed in Sects. 3.1 and 3.2. After being mixed with water, cement grains begin to dissolve and hydrate, developing a heterogeneous charge distribution on the surface of hydrating cement grains (Plank and Gretz 2008). Silicate hydrates exhibit a negative surface charge, whereas aluminate hydrates possess a positively charged surface. This mosaic structure facilitates the formation of flocculated cement grains that entrap large quantities of mixing water, thereby decreasing the fluidity of cement paste. If chemical admixtures like superplasticizers or latexes are added into the FCPs, their adsorption on cement surface will prevent the flocculation. In this case, the fluidity of FCPs can be significantly improved. In such a way, for the FCPs containing asphalt emulsion with particle size in micron, the increase in fluidity could be explained by the adsorption of both anionic and cationic asphalt particles onto the cement surface due to electrostatic interaction, as shown in Figs. 3.31 and 3.32. Meanwhile, the inclusion of asphalt emulsion apparently increases the content of solid phase in the pastes due to the existence of asphalt particles of micron, which is defined as the filling effects of asphalt emulsions. The theoretical mixing water content decreases with the growth of asphalt content (Table 3.2). As the filling effects exceed the dispersing effects of asphalt emulsions at A/C > 20%, the initial fluidity begins to decrease with the growth of A/C.

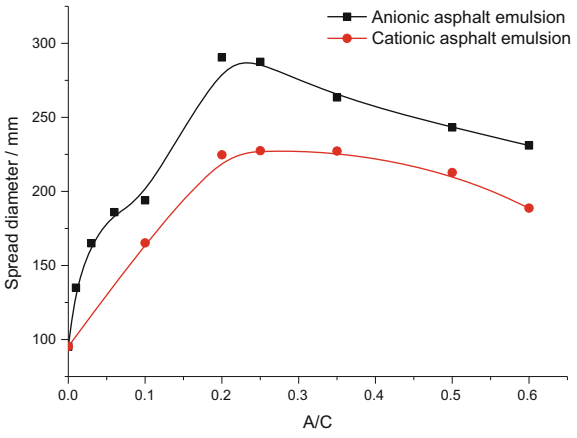

Fig. 3.30 Variation of initial fluidity of FCPs with the addition of asphalt emulsions

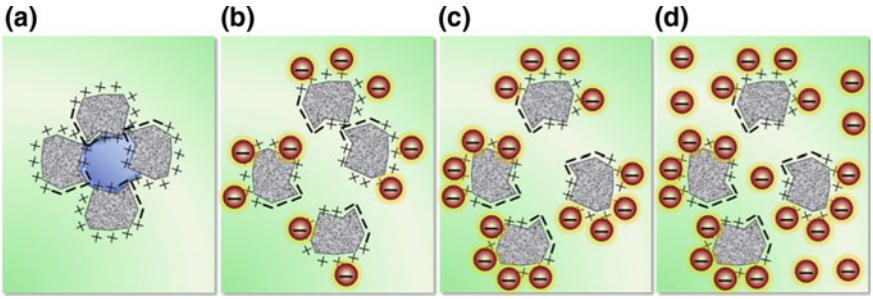

Fig. 3.31 Schematic illustration of the effects of anionic asphalt emulsion on the microstructure of FCPs. (Cement grain; Free water; Entrapped water; Anionic asphalt emulsion)

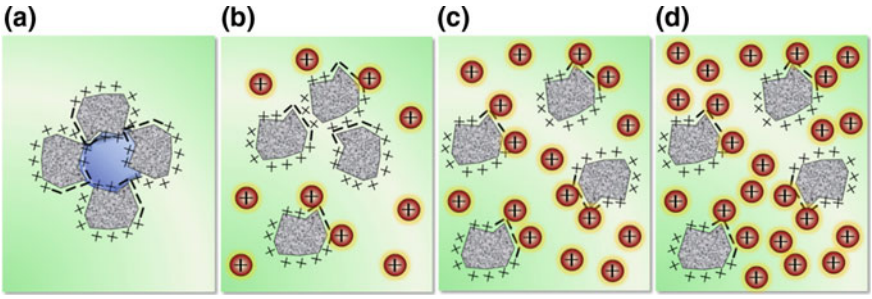

Fig. 3.32 Schematic illustration of the effects of cationic asphalt emulsion on the microstructure of FCPs

Table 3.2 Theoretical volume fraction of cement, asphalt and water in blank fresh cement paste and the pastes containing different dosages of asphalt (Zhang et al. 2010)

A/C (%)	ϕ_C	ϕ_A	ϕ_W
0	0.420	0	0.58
10	0.376	0.12	0.51
20	0.330	0.22	0.45
35	0.280	0.33	0.39
50	0.240	0.42	0.34
60	0.230	0.46	0.31

Moreover, the fluidity of CA pastes containing anionic asphalt emulsion is notably larger than those containing cationic one. On the surface of a hydrating cement grain, positively charged area covers a major part that is mainly contributed by aluminate hydrates. The hydration of silicate, on the other hand, generates a negatively charged area. Therefore, anionic asphalt emulsion is easier to be adsorbed on cement surface and more effective to disassemble flocculated cement

grains than cationic emulsion. Consequently, at the same asphalt content, anionic asphalt emulsion leads to a higher fluidity of CA pastes in most cases than cationic asphalt emulsion (Zhang et al. 2012). The schematic illustrations of the adsorption of anionic and cationic asphalt particles onto the surface of cement grains for the CA pastes with different asphalt contents at 20 °C are shown in Figs. 3.31 and 3.32.

In addition, it is noted that, compared to the submicronic latex particles, asphalt particles fail to cause a decrement of fluidity at low dosages (<3%). This phenomenon may be related to the stereo effects of asphalt particles, which was regarded as the third mechanism of additives (Pacheco-Torgal et al. 2016). More efforts to elucidate this mechanism are underway.

3.3.1.2 Effects of Temperature on Initial Fluidity

In practice, CAM is applied under construction temperatures ranging from 5 to 35 °C. Therefore, understanding the temperature effect on the rheological behavior of fresh CAMs is important. As shown in Fig. 3.33, a high temperature leads to a decrease in the initial fluidity of all the CA pastes. More asphalt content in the CA pastes reduces the temperature influence on initial fluidity. In addition, the CA pastes with cationic asphalt emulsion have comparatively stronger temperature dependence than the CA pastes with anionic asphalt emulsion (Zhang et al. 2010).

The test results listed in Table 3.3 show the decrease in the viscosity of both anionic and cationic asphalt emulsions with temperature. However, the initial fluidity of the fresh CA pastes decreases with temperature, seen in Fig. 3.33. The dominating factor leading to this result must lie in the cement aspect. On the basis of the discussion above, we conclude that both anionic and cationic asphalt emulsions can disassemble the flocculated cement grains by the electrostatic adsorption onto the part of the cement surface that bears counter ions.

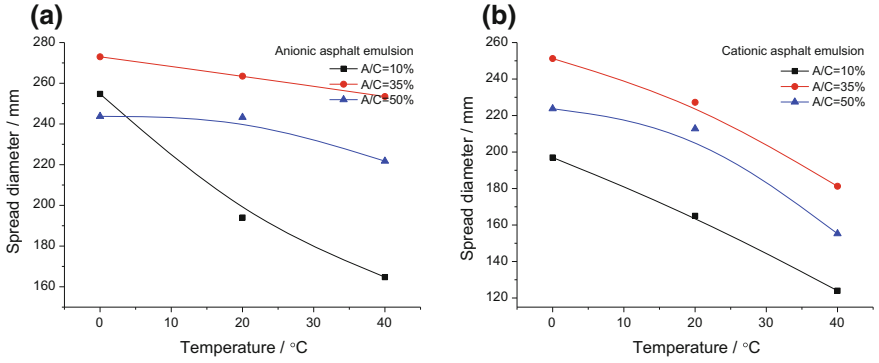

Fig. 3.33 Variation of initial fluidity of FCPs with temperature at varied A/Cs. **a** Anionic asphalt emulsion; **b** Cationic asphalt emulsion

Table 3.3 Viscosities of anionic and cationic asphalt emulsions at varied temperatures

Type of asphalt emulsion	Viscosity/cP		
	0 °C	20 °C	40 °C
Anionic	208.8	160.4	103.2
Cationic	119.2	90.0	50.4

Consequently, the rheological behavior is improved by the addition of the asphalt emulsion. At an elevated temperature, more charges are produced by the accelerated cement hydration in the fresh CA pastes, which could induce the formation of more flocculated structures and could likewise consume more asphalt particles by adsorption. As a result, the initial fluidity of the fresh CA pastes increases under high temperatures, and the CA pastes with high asphalt content have low temperature dependence because of the sufficient number of asphalt particles that reduce the flocculated structures. Anionic asphalt emulsion more effectively reduces flocculated structures than cationic asphalt emulsion. This can explain why the rheological behavior of the CA pastes containing cationic asphalt emulsion exhibits stronger temperature dependence than that with anionic asphalt emulsion.

The schematic illustration of the adsorption of anionic asphalt particles onto the surface of cement grains for the CA pastes with different asphalt contents at 0, 20 and 40 °C is compatible with the one with superplasticizers in Fig. 3.4.

3.3.1.3 Effects of Mix Proportion on Fluidity Retention

The development of fluidity over time of the FCPs with two types of asphalt emulsions was shown in Fig. 3.34. Clearly, the fluidity continues to increase over elapsed time for all the CA pastes. The growth of fluidity over time diminishes with the increase in asphalt content, i.e., the fluidity retention is enhanced by the addition

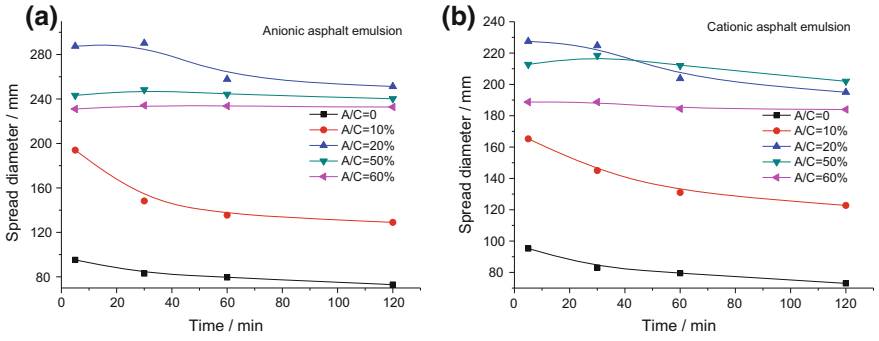

Fig. 3.34 Fluidity retention of FCPs with varied dosages of asphalt at 20 °C. **a** Anionic asphalt emulsion; **b** Cationic asphalt emulsion

of asphalt emulsion. Compared to cationic asphalt emulsion, anionic asphalt emulsion could more significantly heighten the fluidity retention of CA pastes.

For the fresh cement pastes, the changes in rheological properties with elapsed time are mainly ascribed to cement hydration, during which free water is consumed and hydrates are produced. The adsorption of asphalt particles on cement surface may lead to a strong retardation effect on cement hydration. The greater the amount of asphalt emulsion added is, the more noticeably the retardation effect could be observed. Consequently, for the CA pastes with high asphalt content, the decrease of the fluidity over time is low. Anionic asphalt emulsion exhibits a stronger retardation effect because it is easier to be adsorbed on cement surface, which causes better fluidity retention over time.

3.3.1.4 Effects of Temperature on Fluidity Retention

The development of the fluidity over time for the different CA pastes under various temperatures was measured (Fig. 3.35). It can be clearly found that a high temperature leads to a sharp decrease in the fluidity over elapsed time; this decrease may have resulted from the accelerated cement hydration under elevated temperatures. In the presence of asphalt emulsion at low dosages, the fluidity retention of

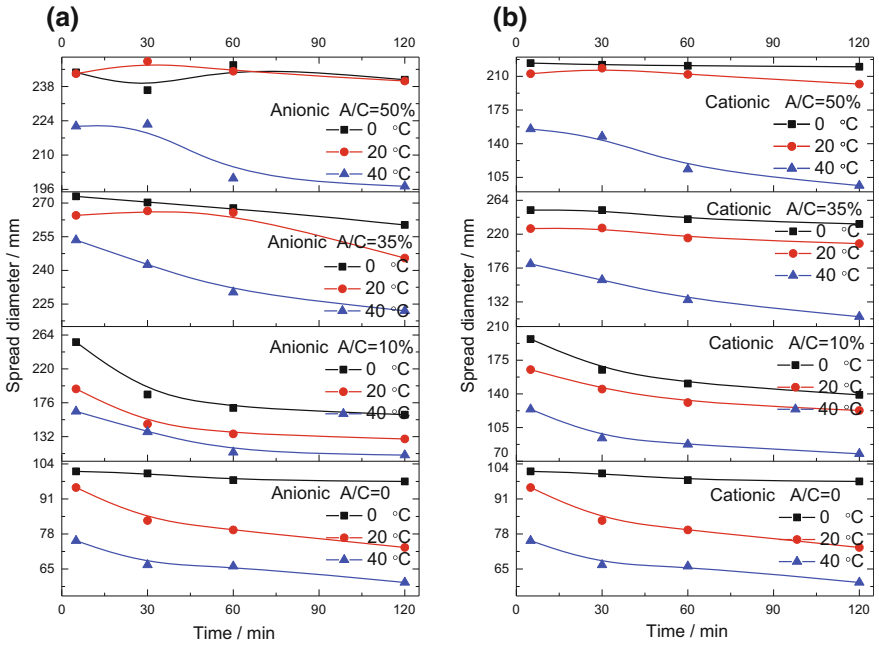

Fig. 3.35 Variation of fluidity retention of FCPs with temperature at varied A/Cs. **a** Anionic asphalt emulsion; **b** Cationic asphalt emulsion

FCPs is inferior and thus is slightly affected by temperature. At high dosages, the fluidity retention is enhanced at 0 and 20 °C but is decreased at 40 °C. It is supposed that asphalt emulsions could provide retardation effects on cement hydration as well, which is accordingly responsible for the enhanced fluidity retention with an increase of asphalt content at 0 and 20 °C. Consequently, some other factors should contribute to the decreased fluidity retention with an increase of asphalt content at 40 °C. We believe that this is most probably caused by the instability of the asphalt emulsion at high temperatures and the weak retardation effects on cement hydration.

For the CA pastes with the cationic asphalt emulsion, the fluidity retention is less affected by temperature, in comparison with the ones with anionic asphalt emulsion (Zhang et al. 2010). These phenomena can be explained by the stronger retardation effects of anionic asphalt emulsion on cement hydration and its better stability at elevated temperatures.

3.3.2 Yield Stress

3.3.2.1 Effects of Mix Proportion

The initial yield stress of fresh CA pastes and the development of the yield stress with time at 20 °C are shown in Figs. 3.36 and 3.37, respectively. It is clearly seen that the variation trends of the yield stress are compatible with the initial fluidity of FCPs. Specifically, with the addition of asphalt emulsion, the initial yield stress

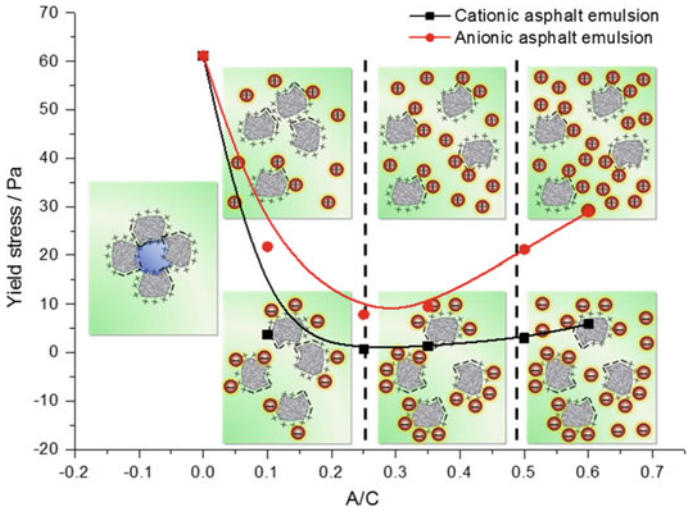

Fig. 3.36 Initial yield stress of FCPs with varied A/Cs at 20 °C

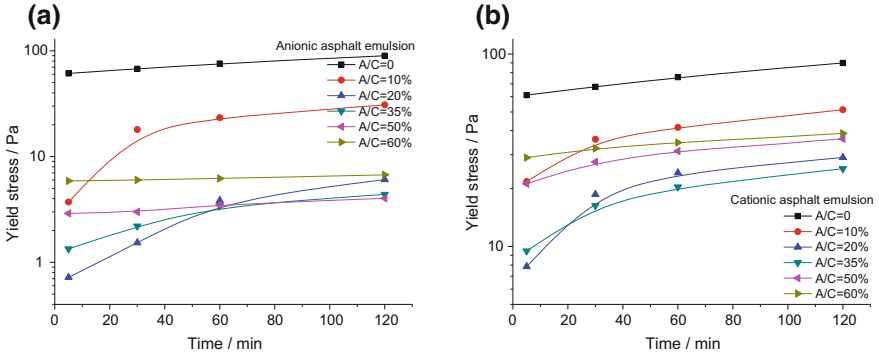

Fig. 3.37 Yield stress over elapsed time for FCPs with varied A/Cs at 20 °C. **a** Anionic asphalt emulsion; **b** Cationic asphalt emulsion

decreases at first and then begins to increase at the A/C of 0.2. The initial yield stress of FCPs with anionic asphalt emulsion is notably larger than that with cationic one. On the other hand, the yield stress gradually increases with time, and the increasing rate diminishes at high asphalt dosages. For the CA pastes with anionic asphalt emulsion, the growth rate of yield stress with time is lower than the ones with cationic asphalt emulsion.

3.3.2.2 Effects of Temperature

Similar to the Cement-Superplasticizer-Water system, an elevated temperature leads to an increment of the initial yield stress because of the faster dissolution of mineral phases and the early hydration, and the temperature sensitivity is reduced as the asphalt dosage is high, as shown in Fig. 3.38. Moreover, the CA pastes containing

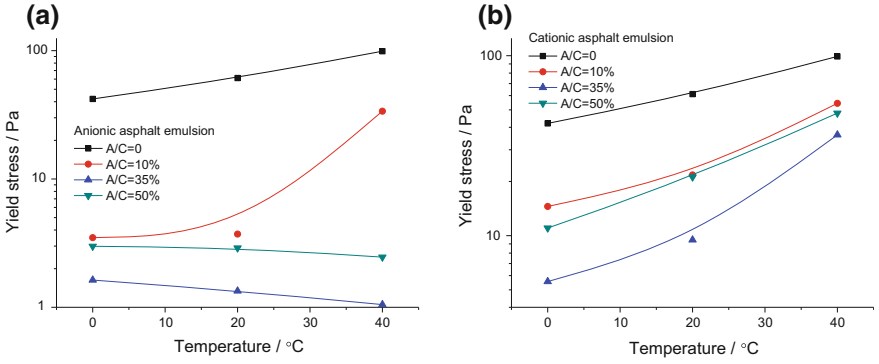

Fig. 3.38 Variation of initial yield stress of FCPs with temperature at varied A/Cs. **a** Anionic asphalt emulsion; **b** Cationic asphalt emulsion

anionic asphalt emulsion show comparatively weaker temperature sensitivity than those with cationic one.

At varied temperatures, the yield stress of CA pastes increases with elapsed time, and an elevated temperature leads to a sharp increase in the yield stress over time due to the accelerated cement hydration under elevated temperatures, as shown in Fig. 3.39. At 0 °C, the yield stress slightly increases during the first 120 min. As for the CA pastes with higher anionic asphalt content, the growth of the yield stress over time is lower than those with lower content at a certain temperature, and meanwhile they are less affected by the temperature change. This phenomenon can be explained by the stronger retardation effects on cement hydration when more asphalt emulsion is added to the CA pastes. For the CA pastes with cationic asphalt emulsion, the growth of the yield stress over time is less affected by temperature of 0 and 20 °C, but is largely increased at 40 °C with the increase in asphalt content, which is supposed to be caused by the instability of the cationic asphalt emulsion at high temperatures and the weak retardation effects on cement hydration. Similarly, for the CA pastes with higher cationic asphalt content, the growth of yield stress over time exhibits a stronger temperature sensitivity.

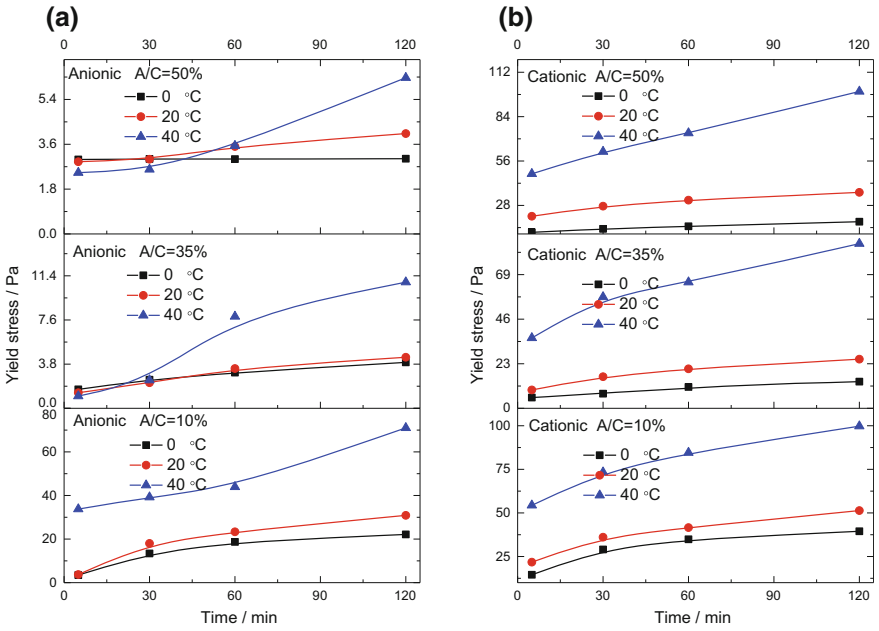

Fig. 3.39 Yield stress over elapsed time for FCPs at varied temperatures and A/Cs. **a** Anionic asphalt emulsion; **b** Cationic asphalt emulsion

3.4 Summary

The rheological behaviors of FCPs containing three types of chemical admixtures were systematically investigated and influencing factors including the dosage of chemical admixtures, W/C, temperature and elapsed time were discussed in detail. Based on experimental results, the synergistic mechanisms considering all the influencing factors were proposed from the microstructural point of view.

(1) Cement-Superplasticizer-Water system

The initial fluidity of the FCPs rises linearly with the addition of superplasticizers and reaches to a maximum value at a critical dosage. Beyond the critical dosage, the fluidity is little affected by the further addition of superplasticizers. It is supposed that a higher superplasticizer dosage produces an increased initial fluidity because more flocculated structures are disassembled and more entrapped water is released. At a dosage higher than the critical dosage, almost all the flocculated structures are disassembled and/or fail to change with the additional inclusion of superplasticizers, so the initial fluidity reaches a maximum and remains stable. The maximum initial fluidity increases as W/C increases and reaches a maximum value at the W/C of 0.35, whilst the critical dosage declines with the increased W/C. On the other hand, the fluidity retention over elapsed time is enhanced by adding superplasticizers due to their retardation effects on cement hydration. Compared to NSF superplasticizer, PCE superplasticizer more significantly enhances the initial fluidity and the fluidity retention of FCPs.

A higher temperature generally leads to a sharper drop in the initial fluidity and the fluidity retention, which stems from the acceleration in the dissolution of mineral phases and in the early cement hydration. However, for the FCPs with high superplasticizer dosages, the fluidity is slightly affected by temperature, which is supposed to be related to the sufficient adsorption of superplasticizers on cement grains and the retardation effects on cement hydration. Moreover, at higher W/C, the impacts of temperature on initial fluidity are less remarkable.

Yield stress and plastic viscosity, the two key parameters of the rheological properties of FCPs, show similar variation trends to the fluidity under influences of different influencing factors. Specifically, with the incorporation of PCE, the initial yield stress and the initial plastic viscosity decrease considerably at first and then remain stable beyond a certain dosage. Besides, the yield stress and the plastic viscosity increase over elapsed time at low Sp/C, and the growth rates significantly descend with the increased superplasticizer dosages in the FCPs. When the superplasticizer dosages increase to a certain dosage, the yield stress and plastic viscosity start to decline over elapsed time. At low Sp/C, an elevated temperature results in an increase in the initial yield stress, the initial plastic viscosity and their growth rates over elapsed time. By contrast, in the case of FCPs with high PCE dosages, the initial plastic viscosity obviously declines as temperature increases

while the decreasing rate of plastic viscosity over elapsed time descends at an elevated temperature. In addition, the rheological parameters show lower temperature dependence for the FCPs with higher Sp/C.

A microrheology analyzer was adapted to in situ follow the development of viscoelastic properties of FCPs for the first time. It enables a non-disturbing measurement on the FCPs through monitoring the mean square displacement of cement grains and gives an insight into the elastic and viscous properties of materials from a microstructural point of view. Various parameters including elastic index, macroscopic viscosity index, storage modulus, loss modulus and Maxwell parameters were obtained to analyze the viscoelastic properties of FCPs quantitatively. All these parameters show a progressive increase with time at first and then stay stable. The incorporation of PCE superplasticizer significantly decreases these parameters and their growth rates. Moreover, superplasticizer could evidently weaken the elastic feature of the FCPs due to its effects of improving the dispersion of cement grains and retarding cement hydration. The effects of superplasticizer are more pronounced at lower water to cement ratio.

(2) Cement-Latex-Water system

With the incorporation of polymer latexes with particle size of 200–300 nm, the initial fluidity of FCPs declines at first and then increases to the maximum at the critical dosage of polymer latexes. It is supposed that at low L/C (<3%), low coverage on the cement surface facilitates the formation of a large amount of flocculated structures. With further addition of latexes, more coverage of latex particles on cement surface brings about better dispersion of cement grains because of the neutralization of the heterogeneous charge distribution of original cement grains and hence an increment of the initial fluidity. The maximum initial fluidity is respectively achieved at 9% L1 and 12% L2. Beyond the critical dosages, the further addition of latex particles causes the decrease of the initial fluidity, which originates from the increased content of solid phase constituting both cement grains and polymer particles, namely the filling effects of polymer latexes. On the other hand, higher dosages of latexes are beneficial to the fluidity retention of FCPs. Compared to the FCPs with latex L2, the ones with latex L1 show stronger fluidity retention over elapsed time.

A higher temperature brings about a decrease in the initial fluidity for all the FCPs containing latexes in most cases, and the impacts of temperature are strengthened as the dosage of L1 increases due to its demulsification at elevated temperatures. By contrast, for the FCPs with latex L2, the impact of temperature on initial fluidity is weakened at high dosages, which may be related to its lower film formation temperature. The fluidity retention of FCPs obviously decreases at elevated temperatures, and the effects of temperature gradually descend with the growth of L/C because of the stronger retardation effects of latexes on cement hydration at higher dosages.

(3) Cement-Asphalt-Water system

In the case of the FCPs containing asphalt emulsion with particle size in microns, the initial fluidity grows with the increase of asphalt dosage at low A/C ($\leq 20\%$) due to the dispersing effects of asphalt particles. Meanwhile, the inclusion of asphalt emulsions notably increases the content of solid phase in the pastes due to the filling effects of asphalt particles. Therefore, the initial fluidity of CA pastes reaches maximum at the dosage of 20%. When A/C is larger than 20%, the filling effects exceed the dispersing effects, so that the initial fluidity of CA pastes begins to decrease. Moreover, the fluidity retention of the CA pastes over time is visibly improved with the increase in asphalt content. Compared with the cationic asphalt emulsion, anionic asphalt emulsion more strongly increases the initial fluidity and the fluidity retention of the CA pastes because of its favorable adsorption onto cement surface and greater retardation effects. The variation trends of yield stress are compatible with those of the fluidity of CA pastes.

The effects of temperature on the initial fluidity and the fluidity retention are dependent on the content and type of asphalt emulsions used in the CA pastes. A high asphalt content leads to a low temperature effect on the initial fluidity. For the CA pastes with anionic asphalt emulsion, a higher asphalt content causes a lower temperature effect on the fluidity retention. For the CA pastes containing cationic asphalt emulsion, an increase in asphalt content leads to a strong temperature sensitivity of fluidity retention because of the instability of cationic asphalt emulsion at high temperatures and its weak retardation effects on cement hydration.

References

Aiad I (2003) Influence of time addition of superplasticizers on the rheological properties of fresh cement pastes. Cem Concr Res 33(8):1229–1234

Axelsson M, Gustafson G (2006) A robust method to determine the shear strength of cement-based injection grouts in the field. Tunn Undergr Space Technol 21(5):499–503

Bellotto M (2013) Cement paste prior to setting: a rheological approach. Cem Concr Res 52 (10):161–168

Bellour M, Skouri M, Munch JP et al (2002) Brownian motion of particles embedded in a solution of giant micelles. Eur Phys J 8(4):431–436

Brunel L (2009) Formulaction. WO2010130766

Brunel L, Snabre P (2003) EP 1664744

Cao EX, Zhang YR, Kong XM (2012) Microstructure model of fresh cement paste with superplasticizer. Concrete 8:37–161 (in Chinese)

Cheung J, Jeknavorian A, Roberts L et al (2011) Impact of admixtures on the hydration kinetics of Portland cement. Cem Concr Res 41(12):1289–1309

Chougnet A, Audibert A, Moan M (2007) Linear and non-linear rheological behaviour of cement and silica suspensions. Effect of polymer addition. Rheol Acta 46(6):793–802

Chung C, Popovics JS, Struble LJ (2009) Early age stiffening of cement paste using ultrasonic wave reflection. In: Riding K (ed) Transition from liquid to solid: re-examining the behavior of concrete at early ages (ACI SP-259-1). American Concrete Institute, Farmington Hills, MI, pp 7–16

Fazullin DD, Mavrin GV, Shaikhiev IG (2015) Particle size and zeta potential changes in the disperse phase of water-emulsified waste waters in different treatment stages. Chem Technol Fuels Oils 51(5):501–505
Ferrandis JY, Leveque G (2003) In situ measurement of elastic properties of cement by an ultrasonic resonant sensor. Cem Concr Res 33(8):1183–1187
Flatt RJ (2004) Towards a prediction of superplasticized concrete rheology. Mater Struct 37 (5):289–300
Flatt RJ, Houst YF (2001) A simplified view on chemical effects perturbing the action of superplasticizers. Cem Concr Res 31(8):1169–1176
Gardel ML, Valentine MT, Weitz DA (2005a) Microrheology. Department of Physics and Division of Engineering and Applied Sciences, Harvard University, Cambridge
Gardel ML, Valentine MT, Weitz DA (2005b) Microrheology/Microscale diagnostic techniques. Springer, Berlin, pp 1–49
Golaszewski J, Szwabowski J (2004) Influence of superplasticizers on rheological behavior of fresh cement mortars. Cem Concr Res 34(2):235–248
Grasley ZC, Lange DA (2007) Constitutive modeling of the aging viscoelastic properties of Portland cement paste. Mech Time Depend Mater 11(3–4):175–198
Huang DN (2000) Additives, rheology and high performance concrete. China Concr Cem Prod (4):3–4 (in Chinese)
Kong XM, Zhang YR, Zhang JY et al (2011) Investigation on flowability and microstructure of fresh cement asphalt binder. J Build Mater 14(4):569–575 (in Chinese)
Kong XM, Zhang YR, Hou SS (2013) Study on the rheological properties of Portland cement pastes with polycarboxylate superplasticizers. Rheol Acta 52(7):707–718
Li QH, Kong XM (2009) Properties and microstructure of polymer modified mortar based on different acrylate latexes. J Chin Ceram Soc 37(1):107–114
Li Z, Lu P, Zhang D et al (2016) Population balance modeling of activated sludge flocculation: investigating the influence of extracellular polymeric substances (EPS) content and zeta potential on flocculation dynamics. Sep Purif Technol 162:91–100
Liu YL, Kong XM, Zhang YR et al (2013) Static and dynamic mechanical properties of cement-asphalt composites. J Mater Civ Eng 25(10):1489–1497
Mason TG (2000) Estimating the viscoelastic moduli of complex fluids using the generalized Stokes-Einstein equation. Rheol Acta 39(4):371–378
Menard KP (2008) Dynamic mechanical analysis: a practical introduction. CRC Press, Boca Raton
Nachbaur L, Mutin JC, Nonat A et al (2001) Dynamic mode rheology of cement and tricalcium silicate pastes from mixing to setting. Cem Concr Res 31(2):183–192
Pacheco-Torgal F, Ivanov V, Karak N et al (2016) Biopolymers and biotech admixtures for eco-efficient construction materials. Woodhead Publishing, Waltham
Papo A, Piani L (2004) Effect of various superplasticizers on the rheological properties of Portland cement pastes. Cem Concr Res 34(11):2097–2101
Petit JY, Wirquin E, Duthoit B (2005) Influence of temperature on yield value of highly flowable micromortars made with sulfonate-based superplasticizers. Cem Concr Res 35(2):256–266
Petit JY, Khayat KH, Wirquin E (2006) Coupled effect of time and temperature on variations of yield value of highly flowable mortar. Cem Concr Res 36(5):832–841
Petit JY, Wirquin E, Vanhove Y et al (2007) Yield stress and viscosity equations for mortars and self-consolidating concrete. Cem Concr Res 37(5):655–670
Petit JY, Khayat KH, Wirquin E (2009) Coupled effect of time and temperature on variations of plastic viscosity of highly flowable mortar. Cem Concr Res 39(3):165–170
Petit JY, Wirquin E, Khayat KH (2010) Effect of temperature on the rheology of flowable mortars. Cem Concr Compos 32(1):43–53
Plank J, Gretz M (2008) Study on the interaction between anionic and cationic latex particles and portland cement. Colloids Surf A Physicochem Eng Aspects 330(2):227–233
Plank J, Zhimin D, Keller H et al (2010) Fundamental mechanisms for polycarboxylate intercalation into C3A hydrate phases and the role of sulfate present in cement. Cem Concr Res 40(1):45–57

Pourchet S, Comparet C, Nonat A et al (2006) Influence of three types of superplasticizers on tricalciumaluminate hydration in presence of gypsum. In: Proceedings of the 8th CANMET/ACI international conference on superplasticizers and other chemical admixtures in concrete, Sorrento, 20–23 Oct 2006, pp 151–158

Pourchet S, Comparet C, Nicoleau L et al (2007) Influence of PC superplasticizers on tricalcium silicate hydration. In: Proceedings of the 12th international congress on the chemistry of cement-ICCC, 2007

Pu XC (2004) Super high strength high performance concrete. Chongqing University Press, Chongqing (in Chinese)

Ran QP (2007) Structure, adsorption, dispersion and mechanism of comb-shaped copolymers. Nanjing University, Jiangsu (in Chinese)

Roussel N, Geiker MR, Dufour F et al (2007) Computational modeling of concrete flow: general overview. Cem Concr Res 37(9):1298–1307

Roussel N, Lemaître A, Flatt RJ et al (2010) Steady flow of cement suspensions: a micromechanical state of the art. Cem Concr Res 40:77–84

Schmidt W, Brouwers HJH, Kühne HC et al (2014) Influences of superplasticizer modification and mixture composition on the performance of self-compacting concrete at varied ambient temperatures. Cem Concr Compos 49(5):111–126

Subramaniam KV, Wang X (2010) An investigation of microstructure evolution in cement paste through setting using ultrasonic and rheological measurements. Cem Concr Res 40(1):33–44

Subramaniam KV, Lee J, Christensen BJ (2005) Monitoring the setting behavior of cementitious materials using one-sided ultrasonic measurements. Cem Concr Res 35(5):850–857

Tisserand C, Fleury M, Brunel L et al (2012) Passive microrheology for measurement of the concentrated dispersions stability. Prog Colloid Polym Sci 139:101–105

Wallevik JE (2006) Relationship between the Bingham parameters and slump. Cem Concr Res 36 (7):1214–1221

Wang ZM (2006) The interface chemistry phenomena and rheological properties of "cement-water-superplasticizer" system. Beijing University of Technology, Beijing (in Chinese)

Wang X, Subramaniam KV, Lin FB (2010) Ultrasonic measurement of viscoelastic shear modulus development in hydrating cement paste. Ultrasonics 50(7):726–738

Zhang YR, Kong XM (2014) Influences of superplasticizer, polymer latexes and asphalt emulsions on the pore structure and impermeability of hardened cementitious materials. Constr Build Mater 53(28):392–402

Zhang YR, Kong XM, Cao EX (2010) Influence of temperature on flowability and hydration rate of fresh cement asphalt binder. J Chin Ceram Soc 38(11):156–161 (in Chinese)

Zhang YR, Kong XM, Hou SS et al (2012) Study on the rheological properties of fresh cement asphalt paste. Constr Build Mater 27(1):534–544

Zhou Z, Solomon MJ, Scales PJ et al (1999) The yield stress of concentrated flocculated suspensions of size distributed particles. J Rheol (1978–present) 43(3):651–671

Chapter 4
Mesostructure of Fresh Cement Pastes

From the microscopic point of view, the macroscopic properties of fresh cement pastes (FCPs), especially the rheological properties are primarily determined by their microscopic structure (Barnes and Hutton 1989; Xu 1989). In order to elucidate the working mechanisms of various chemical admixtures on the rheological properties of FCPs, special attention should be paid to the changes on the microstructure of pastes caused by the chemical admixtures. The observation of FCPs by microscopes is a direct way to analyze the microstructure of the FCPs. However, few literature concerning the microstructure of FCPs is found due to the lack of effective measuring and analytical methods. For example, the obtained images from a regular optical microscope are far from being satisfied due to its low resolution and the limited measuring area. SEM and TEM with high resolution are usually used to observe the local morphology of hydrates rather than the global microstructure of pastes. In addition, most research focuses on the qualitative characterization of the mesostructure of FCPs whilst the quantitative characterization remains a challenge. Accordingly, the clear correlation of mesostructure of FCPs with rheological behaviors has not been established so far.

In this chapter, Morphologi G3 with high sensitivity and resolution was employed to systematically explore the structural organization of cement suspensions in different dispersion media, namely water, ethanol or their mixtures. Based on analysis of tens to hundreds of thousands of particles in the suspensions, several structural parameters were obtained to quantitatively characterize the structural organization of cement grains in cement suspensions at a mesoscopic scale for establishing a correlation of mesostructure with macroscopic rheological properties of FCPs. Moreover, ESEM was adopted to qualitatively analyze the mesostructure of FCPs in the presence of superplasticizers, latexes and asphalt emulsions.

Y. Zhang, *Study on Microstructure and Rheological Properties of Cement-Chemical Admixtures-Water Dispersion System at Early Stage*, Springer Theses, DOI 10.1007/978-981-10-4570-7_4

4.1 Theoretical Background

Microfabric of rock and soil materials usually consists of morphological characteristics, geometric characteristics and energy characteristics, and could be described by some structural factors such as granular morphology, contact relation, orientation and porosity etc. (Cnudde et al. 2009; Dexter 1988; Yang 2005). Furthermore, a structural feature could be characterized quantitatively by one or several structural parameters. Fresh cement paste is generally considered as a concentrated suspension system and its mesostructure may also be characterized by this approach based on several structural parameters. In this research, special attentions were paid to the structural factors including granular morphology, granular agglomerates and the spatial distribution of particles. Three corresponding structural parameters, particle size, granular shape and fractal dimension of particle spatial distribution (Dpd), were extracted from the image analysis to quantitatively characterize the mesostructure of cement suspensions.

Cement grains are 3-dimensional objects with irregular shape, thus they cannot be fully described by a single dimension such as a radius or diameter. In order to simplify the measurement process, the particle size is defined by the diameter of an equivalent circle (CE diameter) having an area the same as the particle image, which is different from the volume diameter measured by a laser granulometry. The particle shape is described by circularity (C), which is the ratio of the circumference of a circle equal to the projected area to the perimeter of the particle, and is calculated as:

$$\mathrm{C} = \frac{2 \times \sqrt{\pi \times Area}}{\mathrm{Perimeter}} \tag{4.1}$$

where Area is the projected area of the particle and perimeter is the perimeter of the particle. Dpd provides necessary information about the distribution of particles in a 2-dimension image, i.e. the dispersion degree of particles, which is defined based on the statistical analysis theory about mesh simplification on a 2-dimension image.

$$\mathrm{D_{pd}} = -\lim_{\varepsilon \to 0} \frac{\ln N(\varepsilon)}{\ln \varepsilon} \tag{4.2}$$

in which, ε and $N(\varepsilon)$ are the side length of the mesh and the amount of mesh with side length of ε on the particle image respectively. In this case, higher Dpd reflects larger dispersion degree and vice versa.

4.2 Organization of Cement Grains in Various Dispersion Media

In this section, the structural organization of cement grains in different media including air, ethanol, deionized water and aqueous solution of ethanol were observed and the CE diameter, circularity and Dpd were calculated to quantitatively characterize the mesostructure of cement suspensions.

4.2.1 Cement-Air (C-A) System

The cement grains dispersed in air flow are observed by Morphologi G3 as shown in Fig. 4.1, in which it is seen that particle size of cement ranges from 0.3 to 100 μm (Fig. 4.2). We classify the particles as small particles (S), medium particles (M) and large particles (L) denoting the particles with size of 1–10 μm, 10–30 μm and larger than 30 μm respectively. Separated cement grains with spinous edges as well as a large quantity of loosely agglomerated cement grains are observed. The agglomerations of cement grains are presented in two modes: the association of small particles and the adhesion of small particles on large particles, as circled in Fig. 4.1a–c. We define the structures of the association of the small particles as S-S structures and the structures of the small particles sticking to the larger ones as L-S structures. It is believed that the intrinsic charges on cement surface originating from the fracture of valence bond during the grinding procedure of cement clinker are majorly responsible for the existence of these agglomerates (Muhua and Roy 1987). Moreover, small particles usually present strong adhesive forces (Van der Waals forces) because of their huge surface energy, and hence tend to form agglomerates more easily by associating with each other or adhering on the surface of large particles. If the dispersion pressure is increased to 500 kPa, the total amount of agglomerates significantly reduces as shown in Fig. 4.1d–f. The particle size distribution of cement grains in air fluid from 1 to 100 μm is exhibited in Fig. 4.2, with a mean size of 4.98 μm. The circularity and Dpd of C-A system are 0.91 and 1.84, respectively.

4.2.2 Cement-Ethanol (C-E) System and Cement-Water (C-W) System

When cement powder is dispersed in ethanol, it has been well-understood that neither dissolution of the mineral phases in cement nor any reaction between cement and ethanol takes place in a short time range (Autier et al. 2013). Thus, it can be assumed that the charges properties of cement grains presenting in ethanol should be similar to those of cement dispersed in air. The organization of cement

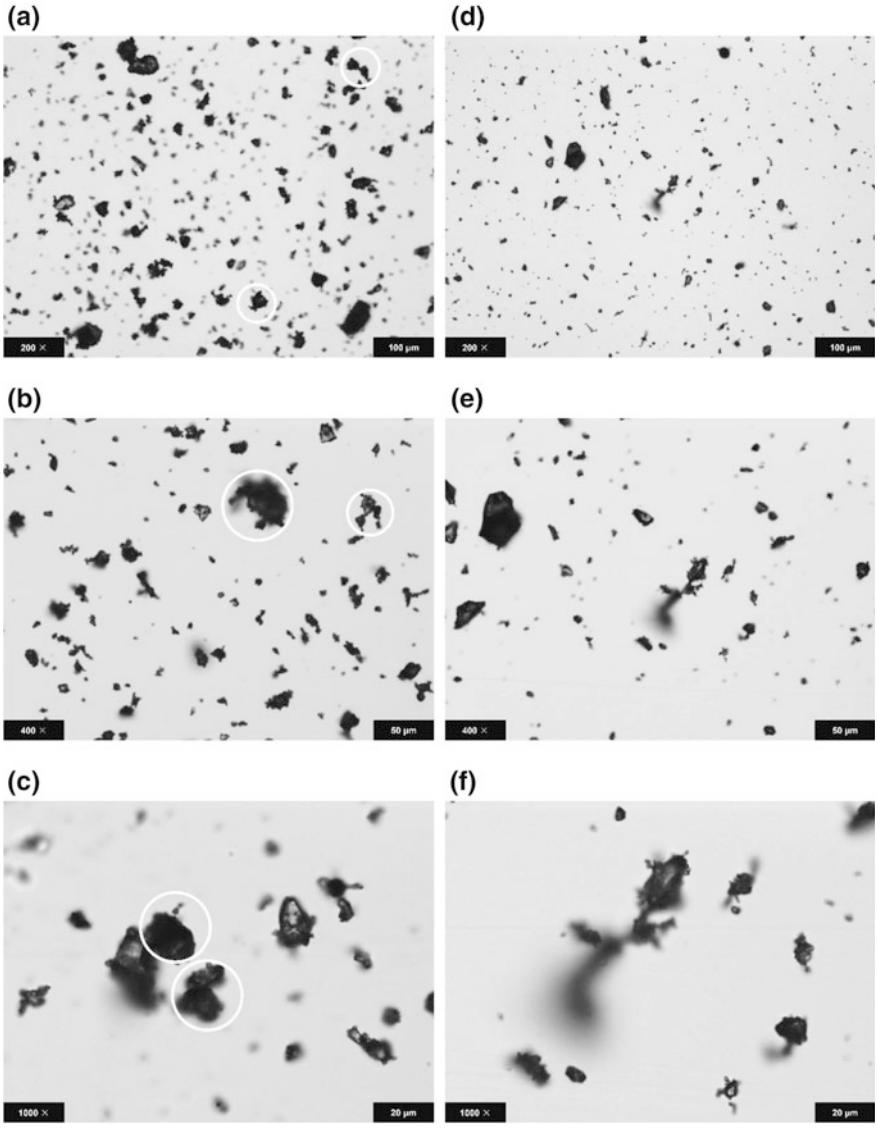

Fig. 4.1 Optical images of organization structure of cement grains in C-A system at different dispersed pressures. **a–c** 200 kPa; **d–f** 500 kPa

grains in C-E system should be similar to that of C-A system, i.e. the association of small particles (S-S structures) and the adhesion of small particles on large particles (L-S structures). Surprisingly, it is found from Fig. 4.3a–c that the cement grains present majorly individual particles, together with a small amount of association structure of L-S structures. That is to say, S-S structures, which abound in C-A

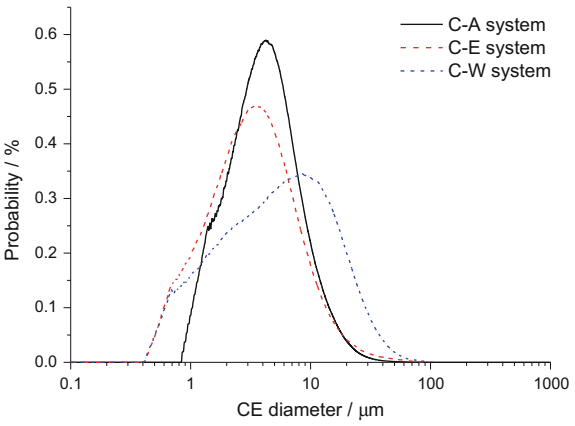

Fig. 4.2 Particle size distribution of C-A, C-E and C-W systems

system, are rarely observed in C-E system. From this finding, we may propose that the formation of S-S structures is mainly driven by the minimization of surface energy rather than by the electrostatic interaction among particles. This driving force in C-E system is weaker than that in C-A system because the interfacial energy between cement surface and ethanol is lower than that between cement surface and air (Adamson and Gast 1967). As a consequence, the cement grains exhibit better dispersion in ethanol medium than in air. The mean particle size of C-E system is 4.59 μm, which is slightly lower than that of C-A system due to the increased amount of small particles as seen in Fig. 4.2. The circularity and Dpd of C-E system are 0.83 and 1.87, respectively. These evidence the hypothesis that ethanol behaves as an inert and good dispersion medium for cement grains (Autier et al. 2013).

On the contrary, once cement comes into contact with water, quick dissolution of mineral phases as well as hydration starts immediately, which produces numerous positive and negative charges on cement surface and hence strong electrostatic interactions among cement grains that are believed to be much stronger than that in C-A or C-E system. The strong electrostatic interactions may cause more intensive association of cement grains. It is noted from Fig. 4.3d–f, cement grains of different sizes aggregate together and enwrap much water, as circled in Fig. 4.3d, e. The whole structure with blurry and spinous edge exhibits irregular shape of vesicle and is called flocculated structure, which contains the agglomeration of cement grains with full range of size. The association of large particles, L-L structures, which are absent in C-A and C-E systems, are produced mainly by the strong electrostatic interactions among cement grains. That is to say, the dispersion of cement grains in water is much worse than in the media of air and ethanol.

As seen from Fig. 4.2, the particle size distribution of C-W system evidently differs from those of C-A and C-E systems, in which the amount of the particles with size of larger than 20 μm sharply rises. As a result, the mean particle size of C-W system increases to 8.09 μm. In addition, the Dpd descends to 1.68, which demonstrates the dispersion degree of cement grains in deionized water is very low.

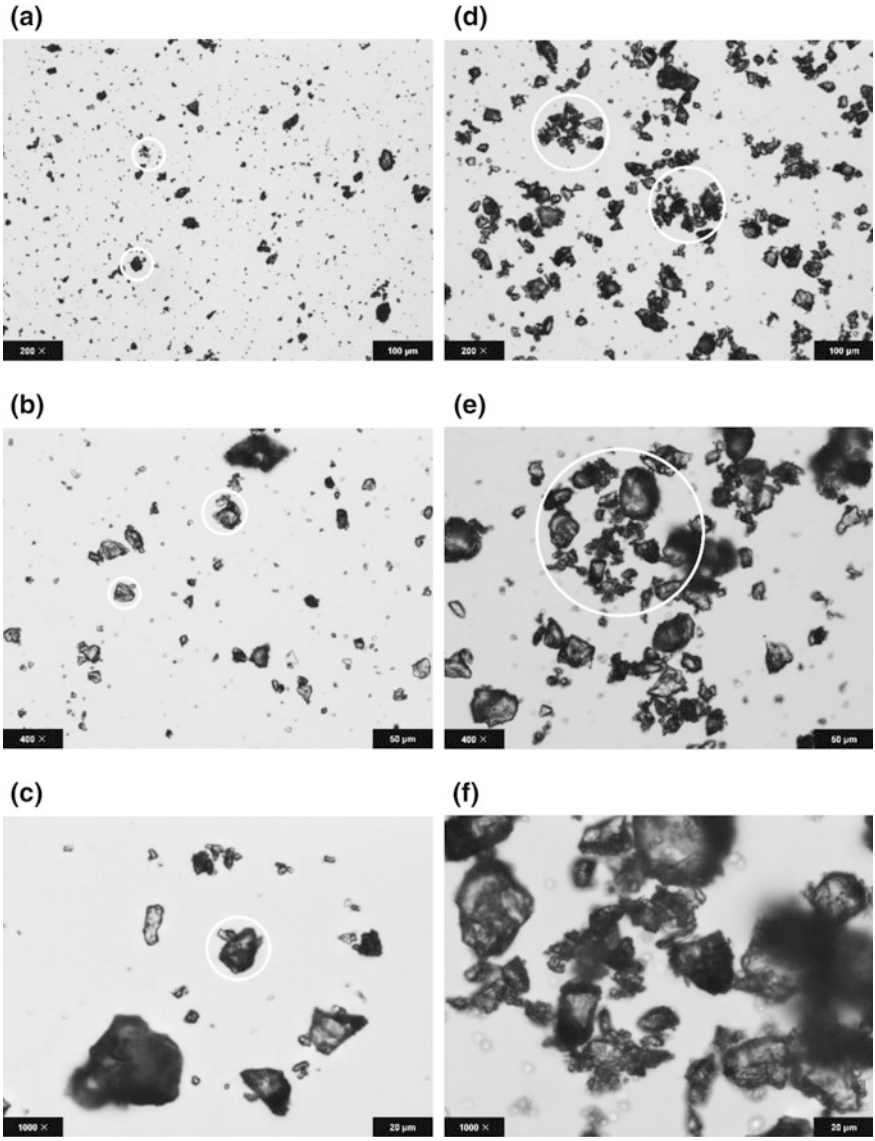

Fig. 4.3 Optical images of organization structure of cement grains in C-E system (**a**–**c**) and C-W system (**d**–**f**)

Typical images of large particles captured by Morphologi G3 are exhibited in Fig. 4.4. The abovementioned differences between C-E and C-W systems in term of granular morphology could be distinctly noticed.

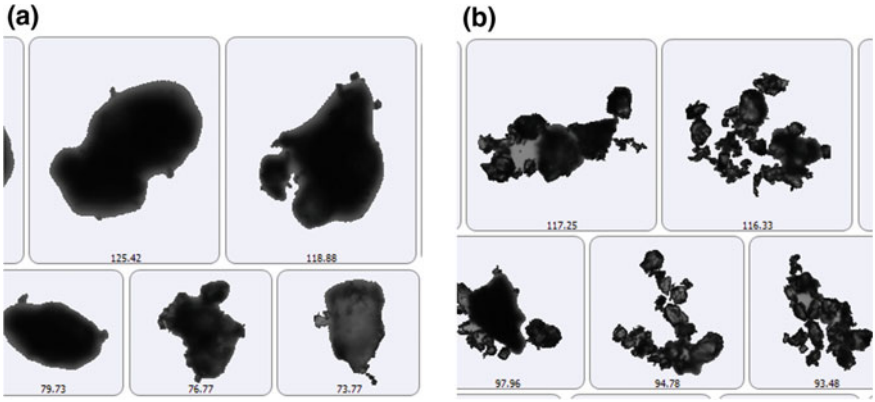

Fig. 4.4 Typical morphology and CE diameter of particles in C-E system (**a**) and C-W system (**b**) (μm)

4.2.3 C-EW System and C-E + C-W System

Compared to the case of ethanol as the dispersion medium, when the aqueous solution of ethanol is used as the dispersion medium for cement, it is expected that the water in solution may facilitate the dissolution of mineral phases and hydration of cement, and hence influences the agglomeration of cement grains. The structural organization of cement grains in C-EW system is presented in Fig. 4.5a–c. Flocculated structures with larger size than those in both C-W and C-E systems are observed in C-EW system. The severer flocculation in C-EW system than that in C-E system should be caused by the enhanced dissolution of mineral phases and the production of hydrates, which certainly creates more charges on surface of cement grains. On the other hand, when we compare the C-EW system with C-W system, the ion strength of the medium in C-EW system must be lower than that in C-W system, because of the less dissolution of mineral phases in C-EW system than in C-W system. We believe that the lowered ion strength of the medium in C-EW system should be responsible for the larger flocculated structures than those in C-W system. The mean particle size of C-EW system ascends to 9.40 μm from the 8.09 μm of C-W system and 4.59 μm of C-E system. Meantime, the decreases of circularity and Dpd to 0.80 and 1.51 indicate that the dispersion degree of particles is lowest in the mixture medium.

Different from being dispersed in the new type dispersion medium of ethanol solution (C-EW system), cement grains may form a distinctive structural organization if C-W system containing flocculated structures is mixed with C-E system with large amount of individual particles. By mixing the C-W system and C-E system with the mass ratio of 1:1, C-E + C-W system was obtained, whose mesostructure is displayed in Fig. 4.5d–f. A unique woolly cloudlike aggregation is observed in C-E + C-W system. Specifically, the aggregation structure contains

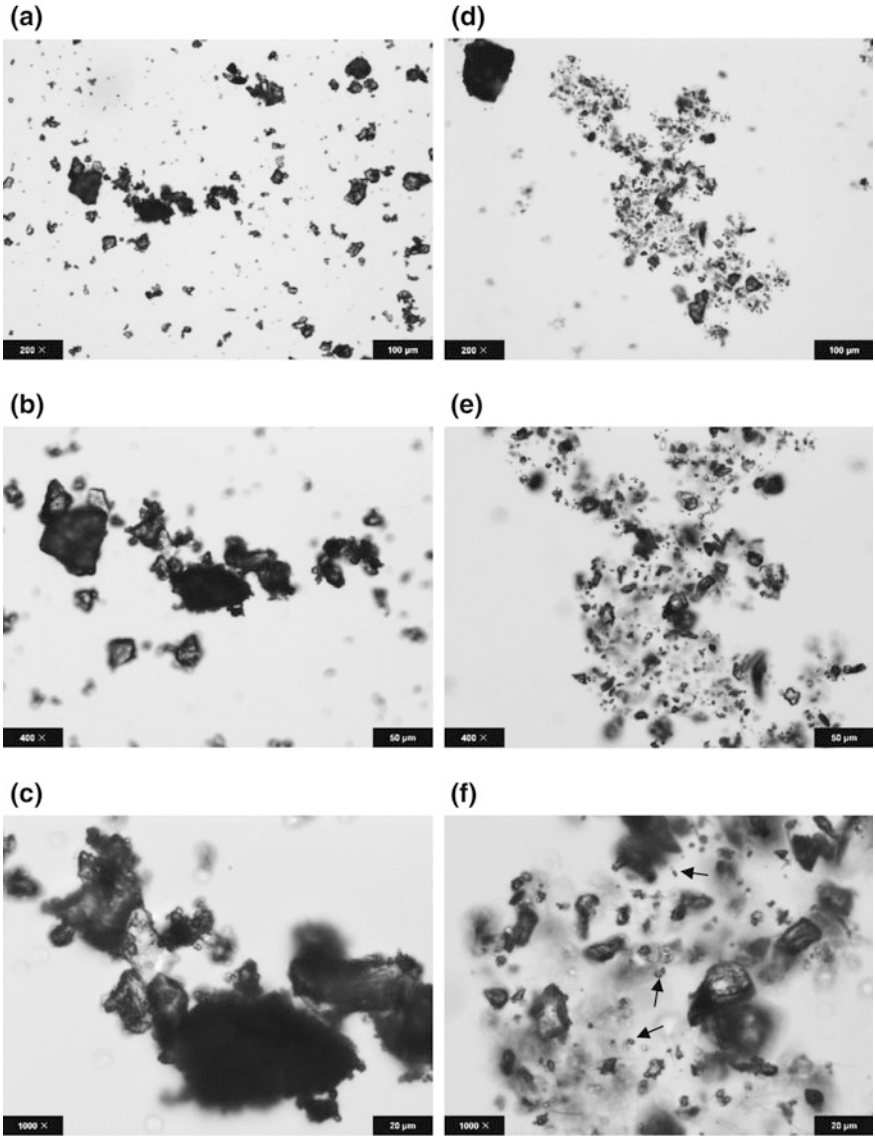

Fig. 4.5 Optical images of organization structure of cement grains in C-EW system (**a**–**c**) and C-E + C-W system (**d**–**f**)

two parts, the main body that is formed by a variety of flocculated particles and a covering layer of individual tiny particles, respectively corresponding to the typical structures in C-W system and C-E system. That is to say, the organization of cement grains in C-E + C-W system is simply a mixture of that in C-E system and C-W system whereas cement grains in ethanol solution (C-EW system) form flocculated

structures with larger size than that in both C-W and C-E systems. The difference between the morphologies of C-EW and C-E + C-W systems may be associated with the changes in the zeta potential of cement grains in different dispersion media.

In the particle size distribution curve of C-E + C-W system (Fig. 4.6), large particles with size of 30–300 μm are found. Consequently, the mean particle size increases to 10.12 μm and Dpd decreases to 1.51 due to the appearance of aggregations, indicating a bad dispersion state of cement grains in C-E + C-W system.

Figure 4.7 provides typical images of large particles in C-EW and C-E + C-W systems extracted by the image analytical software, in which the grey particles are supposed to be the adsorbed water and the entrapped water while the black ones are the cement grains. The significant variations on the granular morphology of the two systems could be clearly seen.

In summary, the results presented above indicate that this analytical approach using Morphologi G3 is a suitable technique to identify and differentiate the varied mesostructural organization of cement grains in different dispersion media in term of particle size, granular shape and fractal dimension of spatial distribution. It has been observed that S-S structures and L-S structures are the main dispersed phases in C-A system due to the huge surface energy of small particles and the existence of instinct charges on cement surface. Ethanol, an inert and good dispersion medium, enables cement grains to present majorly individual particles and a small amount of L-S structures. There is a large quantity of flocculated structures in C-W system caused by the strong electrostatic interactions among cement grains stemming from the dissolution of mineral phases and initial hydration of cement. Flocculated structures with larger size are observed in C-EW system, while in the case of C-E + C-W system, a unique woolly cloudlike agglomeration structure is observed. Based on the three structural parameters, it is found that the dispersion degree of cement grains in these media is in the order of C-E > C-A > C-W > C-EW > C-E + C-W.

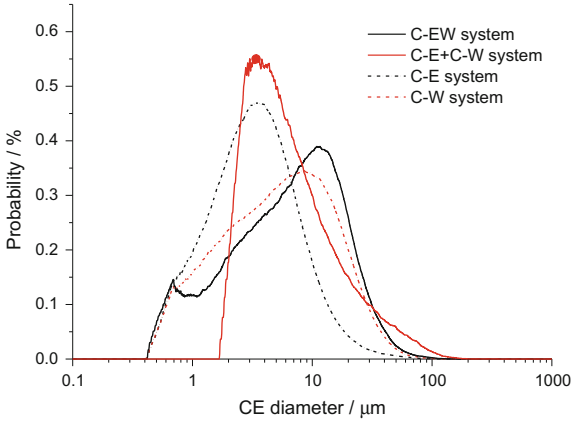

Fig. 4.6 Comparisons of particle size distribution of C-EW, C-E + C-W, C-E and C-W systems

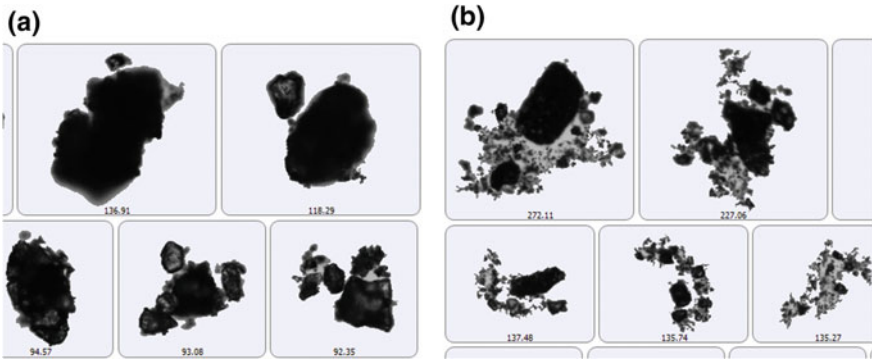

Fig. 4.7 Typical morphology and CE diameter of particles in C-EW system (**a**) and C-E + C-W system (**b**) (μm)

4.3 Influences of Superplasticizers on the Mesostructure of FCPs

It was deduced in Chap. 3 that the addition of superplasticizers in cement pastes increases the fluidity of FCPs through changing the mesostructure of the pastes. Specifically, superplasticizers destroy the flocculated structure of cement grains in cement pastes and thus lead to the enhanced dispersion degree of cement grains, due to the generation of electrostatic repulsion and/or steric hindrance between cement grains (Plank and Sachsenhauser 2009; Winnefeld et al. 2007). In order to validate this deduction, the influences of the PCE and NSF superplasticizers on the mesostructure of cement suspensions were quantitatively analyzed by the Morphologi G3 microscope in term of the granular images and the structural parameters of cement suspensions at varied dosages. In addition, ESEM was also adopted to qualitatively analyze the mesostructure of FCPs in the presence of PCE superplasticizer.

4.3.1 Morphologi G3 Optical Microscope

Indeed, the incorporation of superplasticizer causes a significant change on the granular morphology, agglomerates and the spatial distribution as shown in Figs. 4.8 and 4.9. Most of the cement grains with clear edges and hard corners, associated with some flocculated structures, are well dispersed under the influence of superplasticizers. The structural organization of cement grains depends on the superplasticizer amount and type. A higher superplasticizer dosage brings about flocculated structures with smaller size and evidently reduces their amounts in the meantime. In the dispersion medium of aqueous solution with PCE mass concentration of 0.5%, polygon crystals are present in greater numbers and small

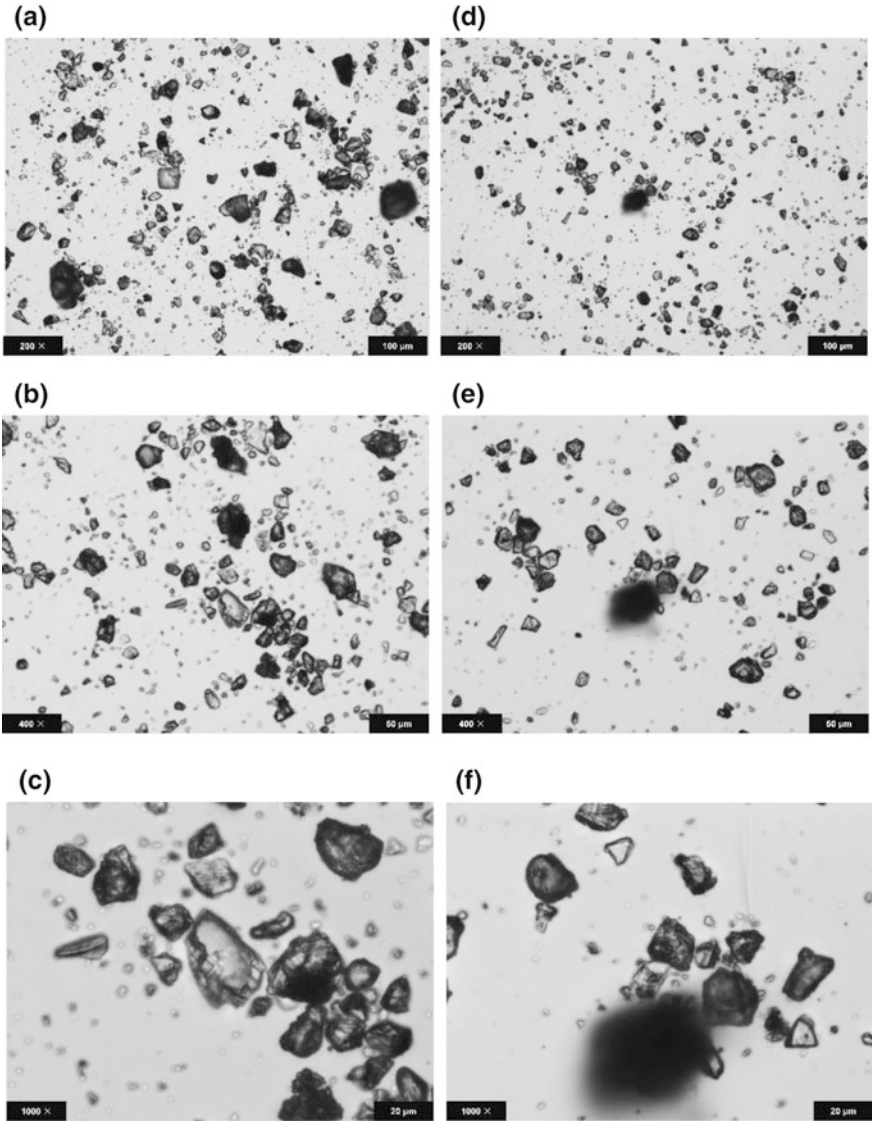

Fig. 4.8 Optical images of organization structure of cement grains in C-W-P0.1 system (**a–c**) and C-W-P0.3 system (**d–f**)

flocculated structures almost disappear, as shown in Fig. 4.9a–c. On the other hand, in the aqueous solution with NSF mass concentration of 0.5%, small flocculated structures are always visible regardless of the dosage of NSF, which may stem from the different dispersion capability of PCE and NSF. It has been well documented that the dispersing capability of PCE is stronger than that of NSF, and hence PCE

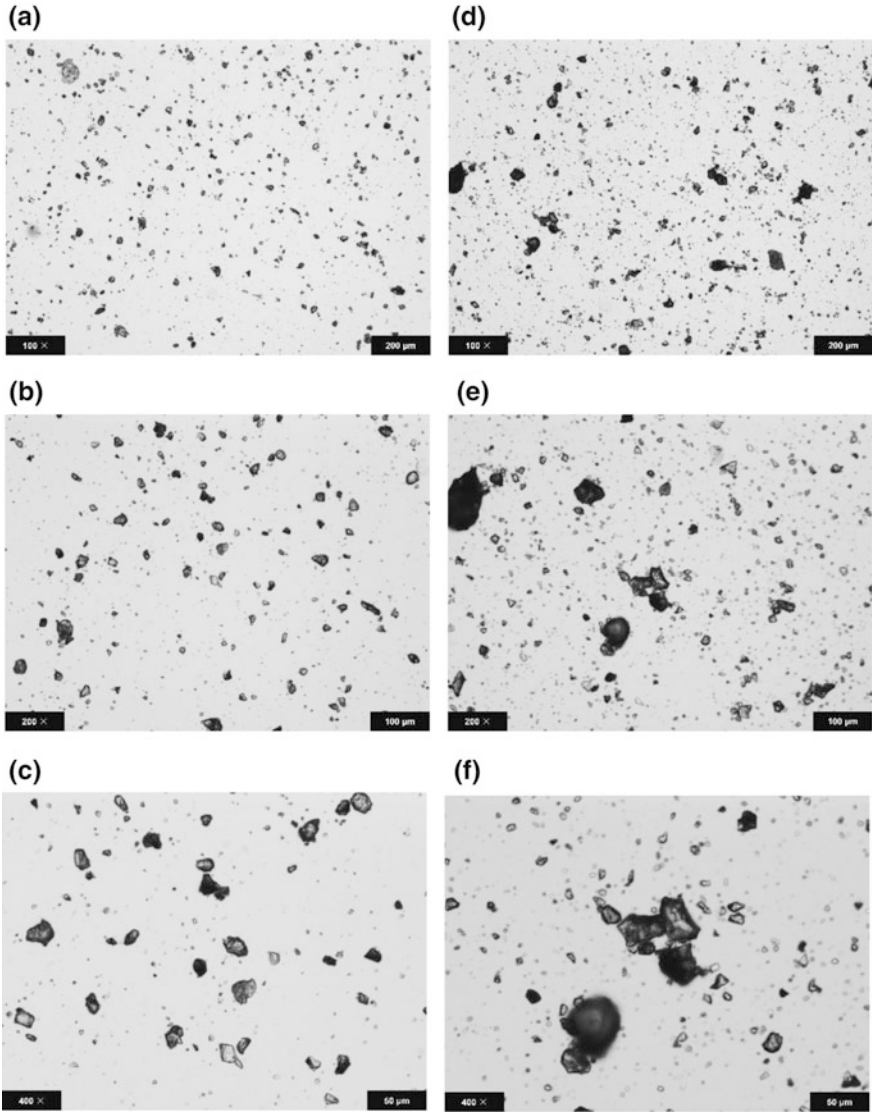

Fig. 4.9 Optical images of organization structure of cement grains in C-W-P0.5 system (**a–c**) and C-W-N0.5 system (**d–f**)

allows much better dispersion of cement grains in aqueous medium at the same dosage (Rubio-Hernández et al. 2013; Zhang and Kong 2015). Limited by the dispersion capability, NSF is less effective to disassemble the strongly bonded flocculated structures.

On the basis of the granular characteristics shown in Figs. 4.8 and 4.9, the flocculated structures could be roughly sorted into three groups (classes) according to the level of difficulty to be disassembled, which are denoted cluster I, II, and III from easy to difficult order. Factually, the division of the flocculated structures is closely dependent on the bonding forces between particles. It is seen from the micrograph that the cement grains are mainly composed by small particles of 1–10 μm (S), medium particles of 10–30 μm (M) and large particles of 30–100 μm (L), in which small particles tend to agglomerate together to form S-S structures due to their huge specific surface energy and could be broken apart easily in the presence of a low dosage of superplasticizer, namely cluster I structures. On the contrary, large particles with strong electrostatic interactions form L-L structures and are hard to be dispersed, i.e., cluster III structures. The rest of particles constitutes S-M-L structures corresponding to cluster II structures, as shown in Fig. 4.10. Obviously, the interaction forces between the particles are in the order of $F_{S\text{-}S} < F_{S\text{-}M\text{-}L} < F_{L\text{-}L}$. Thus, superplasticizers are able to disassemble different flocculated structures depending on their types and dosages, thereby presenting distinct plasticizing effects. Superplasticizers with stronger dispersing capability facilitate the disassembly of more strongly bonded flocculated structures (L-L structures), thereby increasing the fluidity of FCPs more significantly.

From a quantitative point of view, the variations of the three structural parameters reflect the influence of superplasticizers on the mesostructure of cement suspensions. The particle size distribution curves of the suspensions containing superplasticizers are presented in Fig. 4.11. It is noticed that the incorporation of superplasticizers leads to a notable left shifting of particle size distribution due to the decrease in the amount of large particles and the marked increase in small particles content. In such way, with the increase of superplasticizer concentration, the mean particle size decreases to 2.99 μm in C-W-P0.5 system from the 8.09 μm of C-W system while the circularity and Dpd rise to 0.89 and 1.94 from the original 0.83 and 1.68 in C-W system respectively, suggesting the superior dispersion state of cement grains in the aqueous medium with PCE superplasticizer. In comparison, C-W-N0.5 system displays a relatively inferior dispersion state indicated by the mean particle size of 3.71 μm and the Dpd of 1.86.

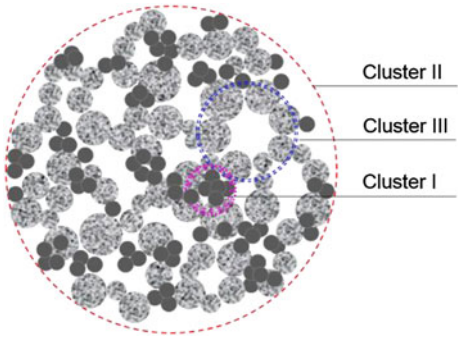

Fig. 4.10 Schematic illustration of flocculated structures of cement grains

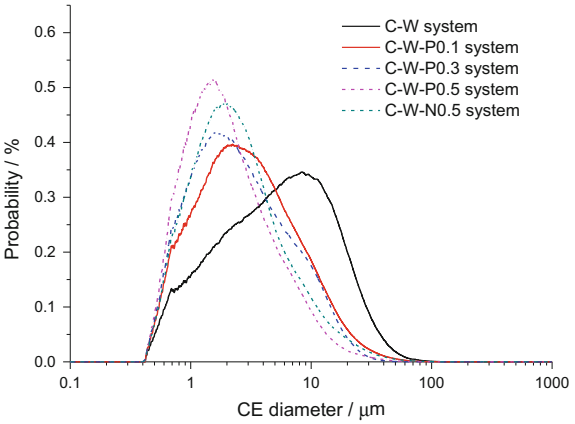

Fig. 4.11 Influences of superplasticizers on the particle size distribution of cement suspensions

Similarly, some typical images of large particles in C-W-P and C-W-N systems are presented in Fig. 4.12, where the significant variations of the structural organization depending on the types and concentrations of superplasticizers could be apparently observed. The high-quality images associated with the variations in particle size and shape as well as spatial distribution provide straightforward information on the mesostructure of cement suspensions, which is essential for understanding the working mechanism of superplasticizers.

4.3.2 ESEM

Figure 4.13 shows the ESEM images of the FCPs with and without PCE superplasticizer. For the blank FCP, as shown in Fig. 4.13a, many flocculated structures are formed in the fresh paste as marked by a red circle. For the FCP with superplasticizer, as shown in Fig. 4.13b, the cement grains are well dispersed. These are in good agreement with the results from Morphologi G3 optical microscope. Additionally, a few needle-like Aft crystals are clearly found in the blank FCP but not in the FCP with superplasticizer, as exhibited in Fig. 4.13c, d, which demonstrates that the addition of superplasticizer depresses the early hydration of cement grains to some extent.

4.3.3 Correlation of Mesostructure with Rheological Behaviors

The rheological behaviors of fresh cement pastes have been characterized by the spread diameter according to the fluidity test in Chap. 3 (Kong et al. 2013; Zhang

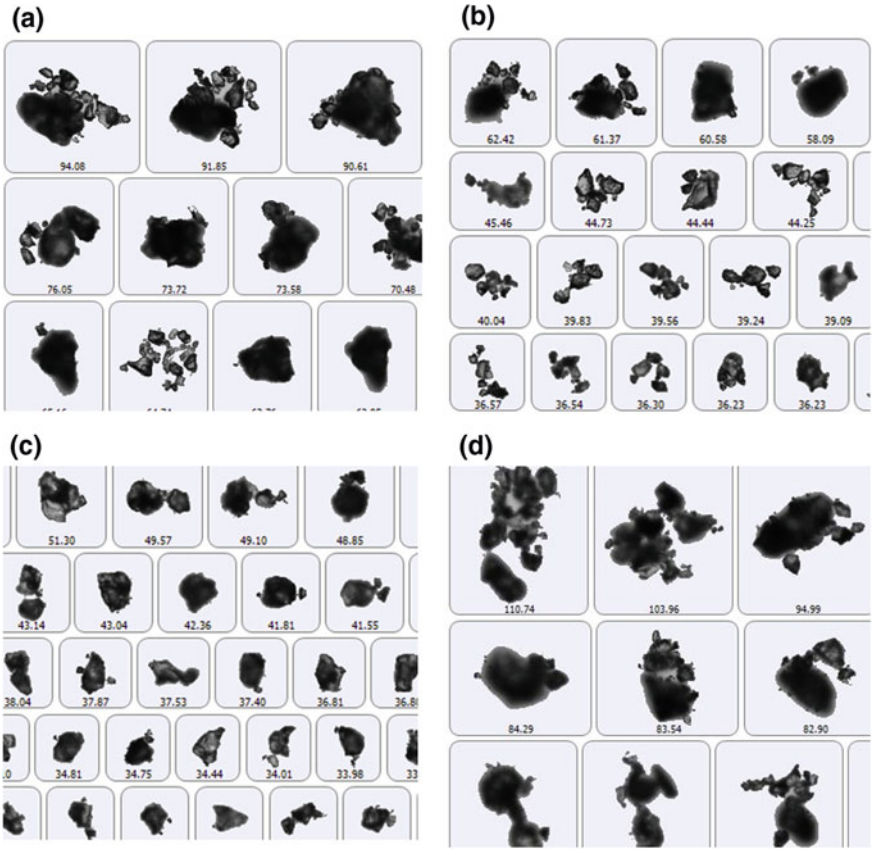

Fig. 4.12 Typical morphology and CE diameter of particles in C-W-P and C-W-N systems (μm). **a** C-W-P0.1 system; **b** C-W-P0.3 system; **c** C-W-P0.5 system; **d** C-W-N0.5 system

and Kong 2015). By comparing the initial fluidity curve of FCPs with the curves of the three structural parameters corresponding to different suspension systems (Fig. 4.14), it is interesting to see that the curves of Dpd and circularity behave in much the same way as the fluidity curve. Contrary to them, the mean particle size curve shows an inverted variation trend to the fluidity curve. That is to say, higher fluidity corresponds to larger Dpd and circularity as well as a lower mean particle size. Moreover, mean particle size and Dpd are more sensitive to indicate the change of the fluidity of FCPs.

The comparison between the structural parameters and the initial fluidity of the FCPs in varied media allows a better understanding on the real granular morphology in varied dispersion media, the influences of superplasticizers on the dispersion state of cement grains, and thus the mesostructural organization of cement

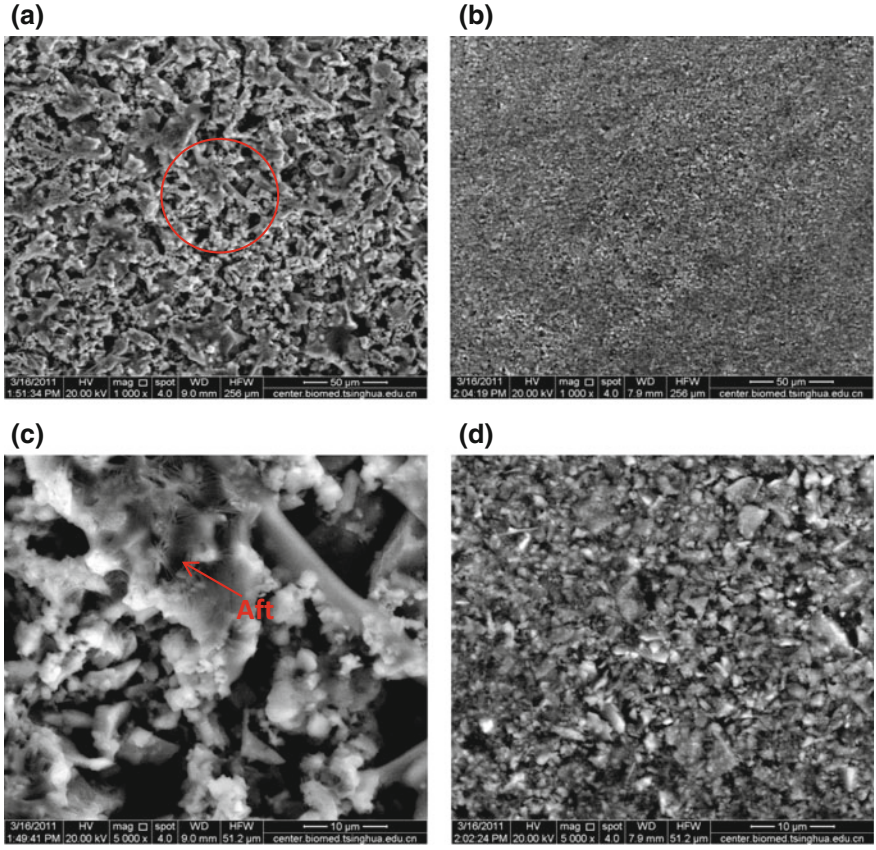

Fig. 4.13 ESEM images of fresh cement pastes in the absence and presence of superplasticizer at 5 min after mixing. **a** Sp/C = 0, 1000×; **b** Sp/C = 0.1%, 1000×; **c** Sp/C = 0, 5000×; **d** Sp/C = 0.1%, 5000×

grains in the suspensions. In this way, the connection between the mesostructure and the macroscopic rheological properties is established through these structural parameters.

4.4 Influences of Polyacrylate Latexes on the Mesostructure of FCPs

The incorporation of polyacrylate latexes enables to bring about the variations of rheological behaviors of FCPs, which is supposed to be caused by the changes of mesostructure of the pastes. However, different from superplasticizers with hydraulic radius of nanometer, the polymer particles in latexes exist in a condensed

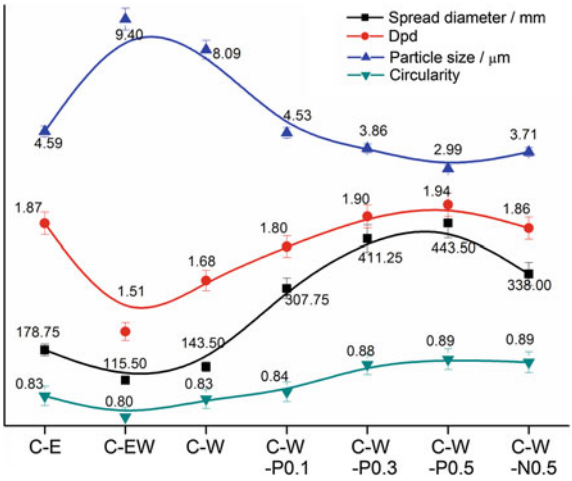

Fig. 4.14 Variations of fluidity and structural parameters of suspensions in different dispersion media

state with size of 200–300 nm. Therefore, for the FCPs containing latexes, in addition to the morphology, the agglomerates and the spatial distribution of cement grains, much attention are paid on the morphology of latex particles and their interaction modes with cement grains.

4.4.1 Morphologi G3 Optical Microscope

The mesostructure of cement suspensions with latexes is exhibited in Fig. 4.15. It is clearly noted that in the presence of 3% L1, separated cement grains with clear edges and hard corners, and a small amount of flocculated structures are found in Fig. 4.15a, b. By contrast, the addition of 3% L2 leads to the formation of a large amount of flocculated structures in the paste. From the curves of particle size distribution of C-W-L systems (Fig. 4.16), it is not hard to find that L1 reduces the content of particles of 10–100 μm whilst L2 results in a visible increment of the large particles of 50–100 μm. This phenomenon is consistent with the fluidity variation of FCPs that L1 enables to increase the initial fluidity whereas L2 decreases the initial fluidity of FCPs by inducing the flocculation of cement grains due to its neutralizing effect.

Additionally, a new peak appearing around 500 nm could be found in the curves of particle size distribution of C-W-L systems, which is a consequence of the existence of a large number of latex particles of submicron in the suspensions. Therefore, although there are a large number of flocculated structures in the FCP containing L2, the mean particle size of the system (7.25 μm) is still lower than that of the blank system (8.09 μm) and the dispersion index of 1.70 is slightly larger than 1.68 of C-W system as well.

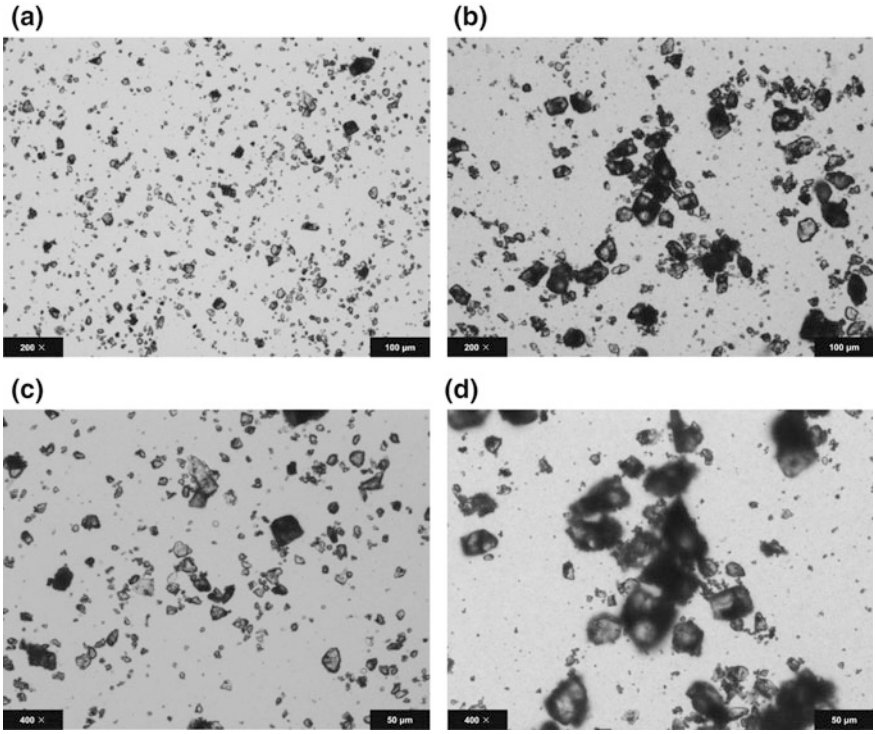

Fig. 4.15 Optical images of organization structure of cement grains in the C-W-L system. **a** 3% L1, 200×; **b** 3% L1, 400×; **c** 3% L2, 200×; **d** 3% L2, 400×

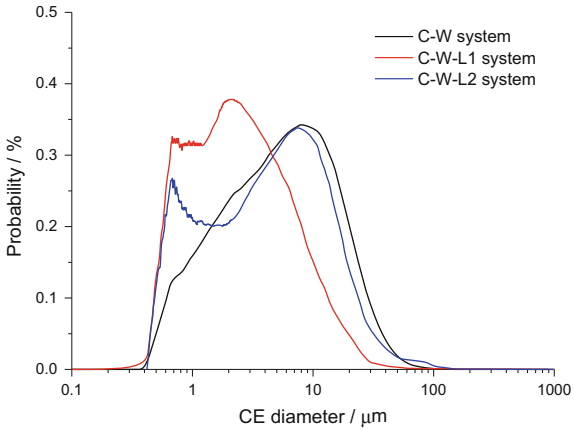

Fig. 4.16 Influences of polymer latexes on the particle size distribution of cement suspensions

4.4.2 ESEM

When polymer latexes were incorporated in the FCPs, the interaction modes of latex particles with cement grains were captured by ESEM, as shown in Fig. 4.17. The adsorption of spherical L1 particles and flattened L2 particles on cement surface is clearly presented in the Fig. 4.17a, b. The different morphologies of the polymer particles are caused by the rapider demulsification and film formation of latex L2 because it has lower Tg. With the growth of L/C, the latex particles fill in the pores between the cement grains besides being adsorbed on cement surface (Fig. 4.17c, d).

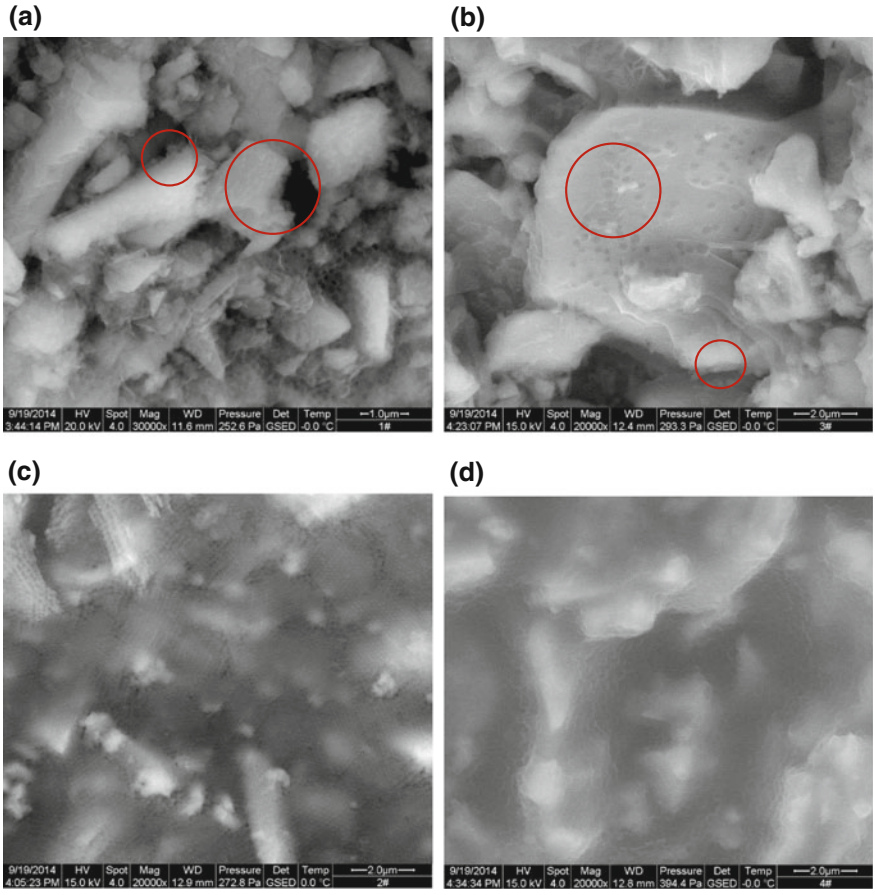

Fig. 4.17 ESEM images of the FCPs with latexes at 5 min after mixing. **a** FCP with 3% L1; **b** FCP with 3% L2; **c** FCP with 9% L1; **d** FCP with 9% L2

4.5 Influences of Asphalt Emulsion on the Mesostructure of FCPs

In this section, the mesostructure of FCPs containing anionic asphalt emulsion was analyzed by the Morphologi G3 and ESEM to reveal the working mechanism of asphalt emulsion with particle size of 3 μm on the rheological behavior of FCPs. In view of the large dosage of asphalt in the cement paste (A/C is ranging from 0.2 to 1.0 in a typical CA paste), a 3-D laser scanning microscope was adopted to observe the distribution of asphalt emulsion in the pastes at varied A/Cs.

4.5.1 Morphologi G3 Optical Microscope

Under the observation of Morphologi G3, some separated cement grains adsorbing asphalt particles, a few flocculated structures of small size and many spherical asphalt particles of microns are well dispersed in the system, as exhibited in Fig. 4.18. The microstructural evolution of C-W-A system is presented in Fig. 4.19. The agglomeration of an asphalt emulsion, including adsorption onto the cement surface, packing and condensation, and formation of a partly continuous asphalt membrane wrapping around the cement grains are clearly observed. The coverage of asphalt membrane on cement surface may lead to a strong retardation effect on cement hydration, which will be confirmed by measuring the semi-adiabatic temperature development of the CA paste during setting in next chapter.

Similar to the C-W-L system, due to the existence of many asphalt particles in the suspensions, the average particle size of C-W-A system is 3.44 μm and the Dpd is 1.99, which are respectively approximated to the size of asphalt particles of 3 μm and the Dpd of asphalt emulsion of 2.0. That is to say, the two structural parameters of C-W-A system mainly reflect the particles size of asphalt particles and their

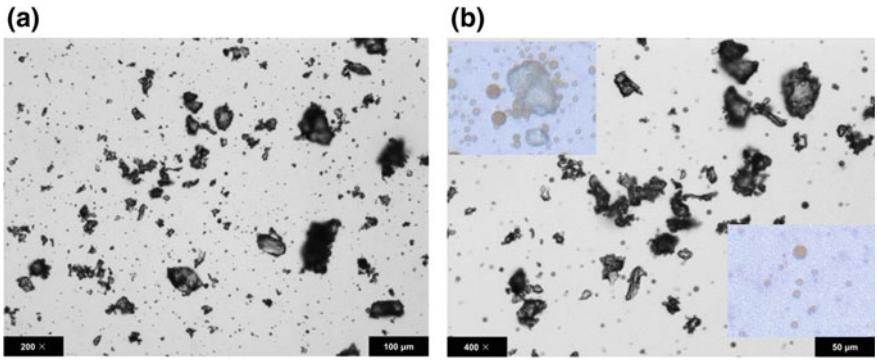

Fig. 4.18 Optical images of organization structure of cement grains and asphalt particles in C-W-A system at A/C of 0.1

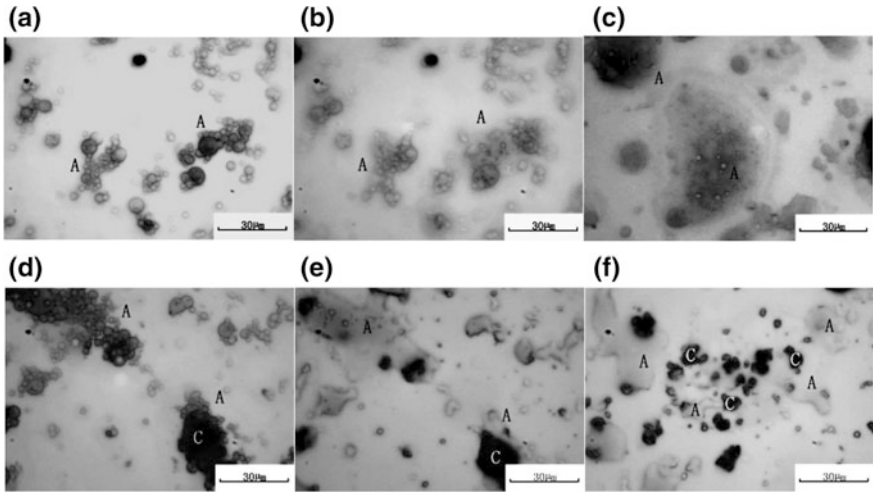

Fig. 4.19 Optical images of demulsification and film formation of asphalt emulsion. (**a**–**c**) Agglomerated asphalt particles at 30, 60 and 90 min; (**d**–**f**) Adsorbed asphalt particles on cement surface at 30, 60 and 90 min

dispersion state instead of cement grains. Thus, it is hard to establish a direct relationship between the fluidity and the microstructure of cement asphalt pastes based on the structural parameters.

4.5.2 ESEM

Figure 4.20 shows the ESEM images of fresh cement asphalt pastes. At A/C of 0.1, cement paste functions as a continuous phase and asphalt particles are well dispersed in the paste in term of being adsorbed on cement surface and filling in the pores between cement grains. With the increase in A/C from 0.35 to 0.6, the asphalt emulsion gradually transforms to be the continuous phase and enwraps the dispersion phase of cement grains.

4.5.3 3-D Laser Scanning Microscope

As shown in Fig. 4.21, the grey cement paste and the brown asphalt emulsion could be clearly distinguished by a 3-D laser scanning microscope when the two phases are mixed together. The 2-D morphology images, 3-D morphology images and 3-D topographic maps of FCPs at A/C of 0, 0.35, 0.6 and 1.0 are shown in Figs. 4.22 and 4.23. In the 3-D topographic maps, red, yellow, green, blue and purple colors

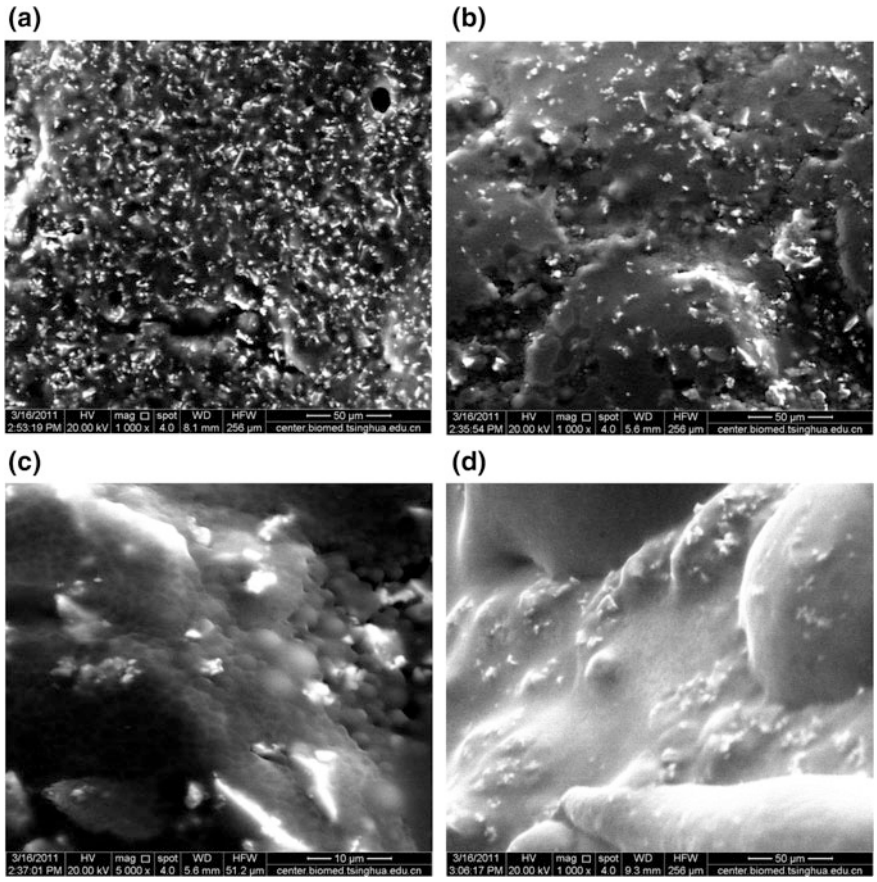

Fig. 4.20 ESEM images of the FCPs with asphalt emulsion at 5 min after mixing. **a** A/C of 0.1, 1000×; **b** A/C of 0.35, 1000×; **c** A/C of 0.35, 5000×; **d** A/C of 0.6, 1000×

are used to mark different heights of solid phases in the FCPs in the order of from high to low.

In the case of blank FCP, flocculated structures with large size are clearly observed and marked in the Fig. 4.22a–c. At A/C of 0.35, the flocculated structures of large size in the paste are broken into small pieces and the asphalt emulsion is uniformly distributed in the continuous cement paste, as shown in Fig. 4.22d–f, which means the dispersion state of cement grains in the paste has been effectively improved by the introduction of the asphalt emulsion. This phenomenon well corresponds to the changes of initial fluidity of FCPs containing anionic asphalt emulsion in Chap. 3.

With further addition of asphalt emulsion, an interpenetrating network is formed where brown area is supposed to be the asphalt and the grey one corresponds to the cement grains, as presented in Fig. 4.23a, b. There is no obvious flocculated

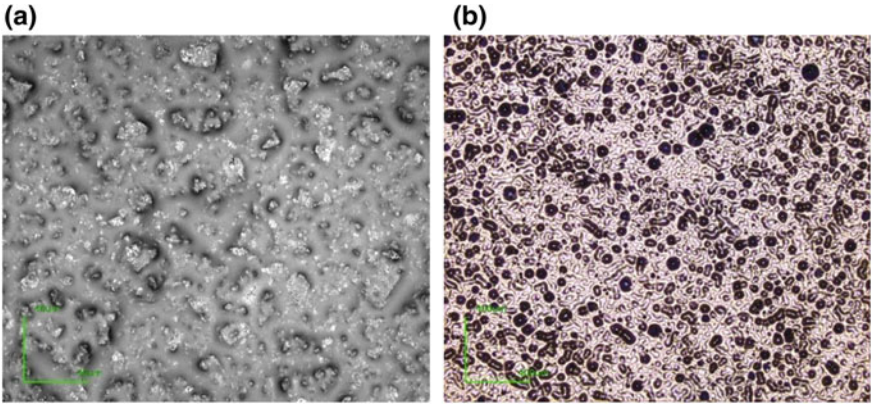

Fig. 4.21 2-D images of blank fresh cement paste (**a**) and asphalt emulsion (**b**)

structures and the green areas are well distributed in the image (Fig. 4.23c), which signifies the cement grains are well dispersed in the asphalt emulsion. As A/C is 1.0, asphalt emulsion behaves as the continuous phase and enwraps all the cement grains, so the dark global image is exhibited in Fig. 4.23d, e. The larger areas of blue and purple in Fig. 4.23f indicate the cement grains are well dispersed while the continuous green area may be related to the agglomerated asphalt particles.

All in all, the microstructure of FCPs in the presence of asphalt emulsion and its variations with varied A/Cs were characterized by using the combination of such methods for the first time, which directly validates the hypothesis of working mechanism of asphalt emulsion on changing fluidity in Sect. 4.3.3, namely the dispersing effects at low dosages and the filling effects at high dosages. Specifically, at low A/C, the amount of flocculated structures gradually reduces due to the adsorption of asphalt particles onto the cement surface and correspondingly the fluidity of FCPs rises. At high A/C, abundant asphalt particles in the paste definitely lead to a significant growth of friction forces between the dispersion phase including the cement grains adsorbing asphalt particles and the asphalt particles in the aqueous phase, thereby reducing the fluidity of FCPs.

4.6 Summary

In this chapter, the texture (organization structure) of cement grains in different dispersion media was analyzed with the aim of providing information on the association of cement grains in fresh cement pastes at a mesoscopic scale and establishing the correlation of mesostructure with macroscopic rheological properties. On the basis of the results above, the following points can be drawn:

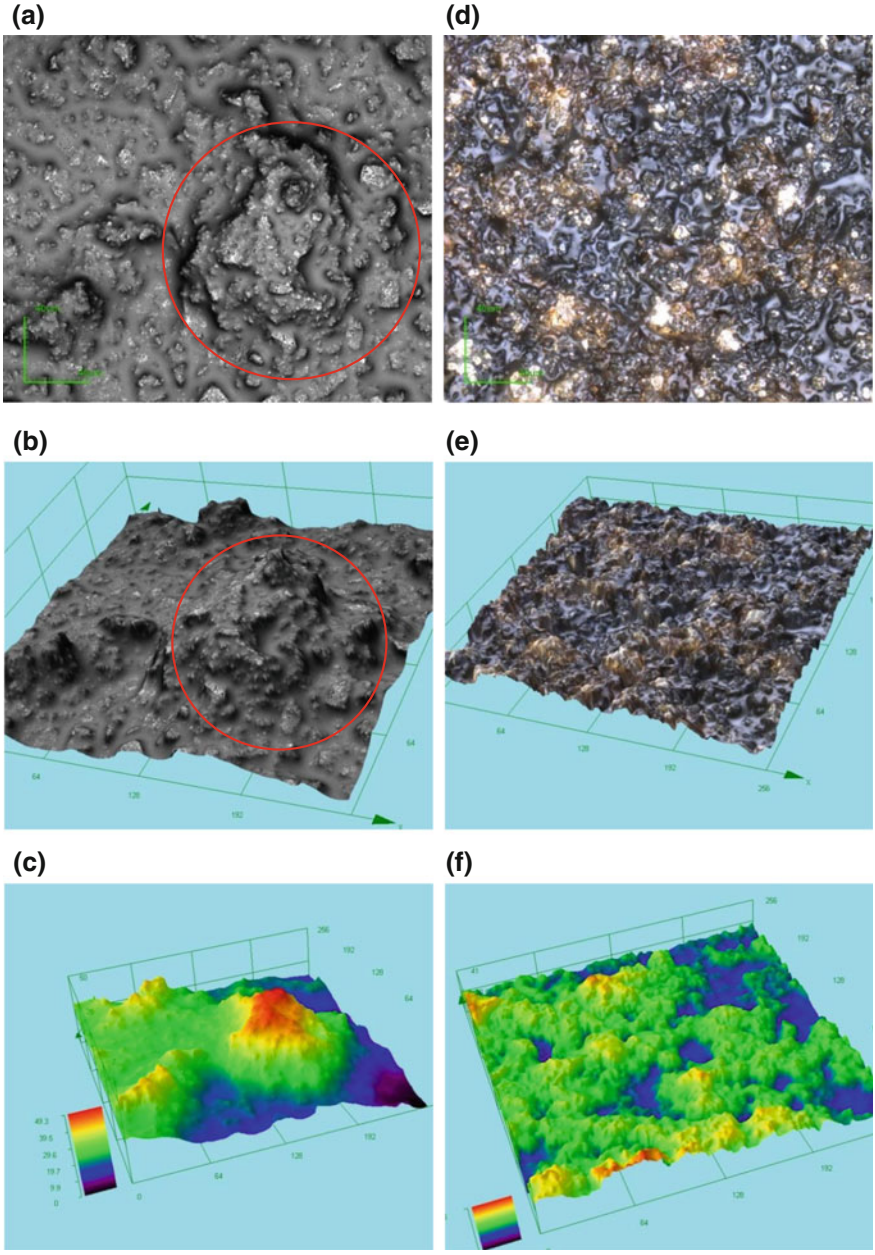

Fig. 4.22 Laser scanning images of blank FCP (**a–c**) and the pastes with anionic asphalt emulsion at A/C of 0.35 (**d–f**)

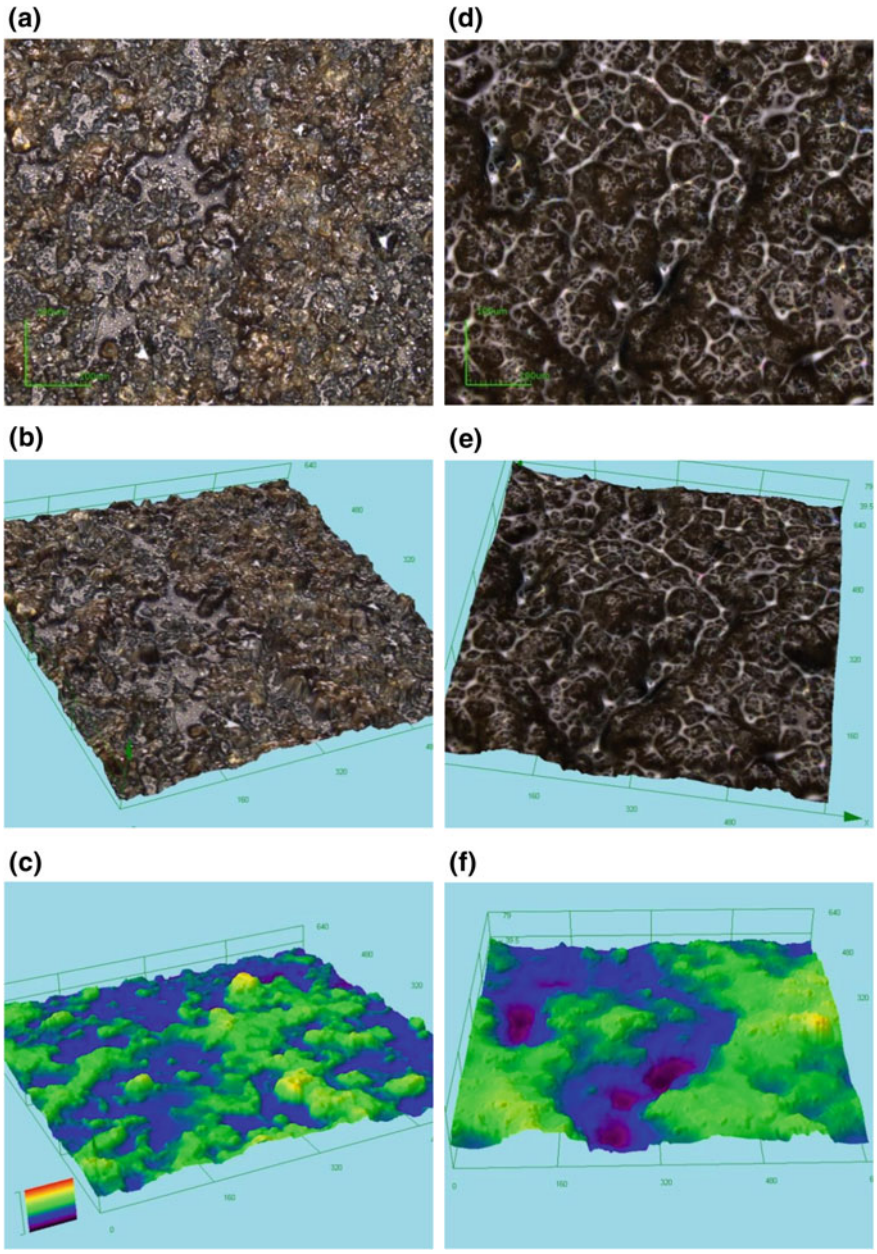

Fig. 4.23 Laser scanning images of FCPs with anionic asphalt emulsion at A/C of 0.6 (**a**–**c**) and A/C of 1.0 (**d**–**f**)

1. Morphologi G3 with high sensitivity and high resolution is a powerful tool to identify and differentiate the structural organization of cement grains dispersed in different media by providing high-quality images associated with structural parameters. Three structural parameters including particle size, granular shape and fractal dimension of particle spatial distribution (Dpd) allow to quantitatively characterize the organization of cement grains in varied media at a mesoscopic scale.
2. The association of the small particles (S-S structures) and the agglomeration of the small particles sticking to the larger ones (L-S structures) are the main dispersed phases in C-A system. Cement grains present majorly individual particles and a small amount of L-S structures in C-E system. There is a large quantity of flocculated structures in C-W system due to strong electrostatic interactions between cement grains which are produced by the quick dissolution of mineral phases as well as hydration at early stage. Flocculated structures with larger size are observed in C-EW system while in the case of C-E + C-W system, unique woolly cloudlike agglomeration structures are found. Based on the three structural parameters, it is found that the dispersion degree of cement grains in these media is in the order of C-E > C-A > C-W > C-EW > C-E + C-W.
3. When cement is dispersed in superplasticizer solutions, cement grains with clear edges and hard corners, are well dispersed due to the adsorption of superplasticizers on cement surface. With the increase of superplasticizer concentration, superior dispersion state is observed and the mean particle size decreases while both of the circularity and Dpd rise. According to the level of difficulty to be disassembled, the flocculated structures can be roughly sorted into three classes from easy to difficult order, i.e., cluster I, II, and III, corresponding to S-S structures, L-M-S structures and L-L structures respectively. Compared to NSF superplasticizer, PCE superplasticizer with stronger dispersing capability facilitates the disassembly of strongly bonded flocculated structures (L-L structures).
4. The relationship between the mesostructural organization of cement grains in suspensions and their rheological behaviors is established by employment of the three structural parameters. Higher fluidity corresponds to larger Dpd and circularity as well as a lower mean particle size. Moreover, the mean particle size and Dpd are more sensitive to indicate the change of the fluidity of FCPs.
5. With the incorporation of polymer latexes L1 and L2 with particle size of submicron, the adsorption of latexes on cement surface leads to the formation of a large amount of flocculated structures at low L/C (<3%). At high L/C, more adsorption of polymer particles brings about better dispersion state of cement grains because of the plasticizing effects of latexes. These phenomena are in line with the variations of FCPs that L1 enables to increase the initial fluidity of FCPs whereas L2 decreases it by inducing the flocculation of cement grains. Compared to L2, L1 more significantly strengthens the dispersion degree of cement grains and thus the fluidity of FCPs at the same dosage.

6. In the case of the FCPs containing asphalt particles of microns, the flocculated structures of cement grains are broken into small pieces and asphalt emulsion is uniformly distributed in the continuous cement paste at low A/C (<35%). With the increment of A/C, asphalt emulsion functions as the continuous phase and enwraps all the cement grains. This directly validates the hypothesis of the working mechanism of asphalt emulsion on changing rheological behaviors of FCPs in Chap. 3, namely the dispersing effects at low dosages and the filling effects at high dosages.

References

Adamson AW, Gast AP (1967) Physical chemistry of surfaces, 6th edn. Wiley, New York

Autier C, Azema N, Taulemesse JM et al (2013) Mesostructure evolution of cement pastes with addition of superplasticizers highlighted by dispersion indices. Powder Technol 249(11): 282–289

Barnes HA, Hutton JF (1989) An introduction to rheology. Elsevier, Amsterdam

Cnudde V, Cwirzen A, Masschaele B et al (2009) Porosity and microstructure characterization of building stones and concretes. Eng Geol 103(3):76–83

Dexter AR (1988) Advances in characterization of soil structure. Soil Tillage Res 11(3):199–238

Kong X, Zhang Y, Hou S (2013) Study on the rheological properties of Portland cement pastes with polycarboxylate superplasticizers. Rheol Acta 52(7):707–718

Muhua T, Roy DM (1987) An investigation of the effect of organic solvent on the rheological properties and hydration of cement paste. Cem Concr Res 17(6):983–994

Plank J, Sachsenhauser B (2009) Experimental determination of the effective anionic charge density of polycarboxylate superplasticizers in cement pore solution. Cem Concr Res 39(1): 1–5

Rubio-Hernández FJ, Velázquez-Navarro JF, Ordóñez-Belloc LM (2013) Rheology of concrete: a study case based upon the use of the concrete equivalent mortar. Mater Struct 46(4):587–605

Winnefeld F, Becker S, Pakusch J et al (2007) Effects of the molecular architecture of comb-shaped superplasticizers on their performance in cementitious systems. Cem Concr Compos 29(4):251–262

Xu YM (1989) A unified rheological model for non-dilatancy viscoplastic fluids. J Wuhan Univ Technol 11(4):431–436 (in Chinese)

Yang X (2005) Three-dimensional characterization of inherent and induced sand microstructure. Ph.D. dissertation. Georgia Institute of Technology

Zhang Y, Kong X (2015) Correlations of the dispersing capability of NSF and PCE types of superplasticizer and their impacts on cement hydration with the adsorption in fresh cement pastes. Cem Concr Res 69:1–9

Chapter 5
Mechanism of Chemical Admixtures: Adsorption, Hydration and Rheology

The understanding of the working mechanisms of chemical admixtures is essential for developing new types of admixtures with more efficient and robust performance and eventually adjusting the rheological properties of FCPs. Although much research has been dedicated to exploring the structure-property relationship of superplasticizers, there are still unsolved questions with regard to the specific mechanism through which various chemical admixtures affect the rheological properties of FCPs. Therefore, it is necessary, both practically and scientifically, to conduct in-depth investigation to elucidate the working mechanisms of different chemical admixtures in fresh cement pastes.

In the previous chapters, the working mechanisms of various chemical admixtures have been proposed according to their effects on the rheological properties of FCPs and mesostructure. Specifically, the chemical admixtures heighten the initial fluidity of FCPs by adsorbing on cement surface and disassembling the flocculated structures of cement grains, and meanwhile strengthen the fluidity retention of FCPs by retarding cement hydration. That is to say, it is the adsorption and retardation that play key roles in changing the rheological properties of FCPs. Hence, in this chapter, the working mechanisms of various chemical admixtures were disclosed from the viewpoints of adsorption behaviors and retardation effects.

Three organic monomers possessing different charging groups, including AA, SSS and MAPTAC, their corresponding homo-polymers and two series of self-synthesized co-polymers with varied charging groups in the backbone were chosen to investigate their adsorption behaviors and impacts on cement hydration in cement pastes by means of TOC tests and isothermal calorimeter respectively, with the aim of analyzing the essence of adsorption and retardation. Furthermore, the adsorption behaviors of superplasticizers, latexes and asphalt emulsions as well as their impacts on cement hydration were discussed and eventually the working mechanisms of chemical admixtures on rheological properties were revealed.

Y. Zhang, *Study on Microstructure and Rheological Properties of Cement-Chemical Admixtures-Water Dispersion System at Early Stage*, Springer Theses, DOI 10.1007/978-981-10-4570-7_5

5.1 Influences of Organic Monomers and Homo-polymers

As well known, the typical backbone of polycarboxylate molecules is mainly composed of AA repeating units. The existence of ample carboxylate groups in the backbone makes the polymer negatively charged in alkaline solution. By contrast, there are a large number of sulfonic groups in lignosulfonate and NSF superplasticizer that also present negative charges in aqueous phase. It is widely accepted that the adsorption of superplasticizers is driven by the electrostatic attraction forces between the PCE molecules and cement grains, which is believed to bring significant effects on cement hydration. In order to disclose the influences of the different functional groups on the adsorption and the retardation effects, organic monomers including AA, SSS, MAPTAC and their corresponding homo-polymers were chosen to investigate their adsorption behaviors and impacts on cement hydration in FCPs.

5.1.1 Adsorption Behavior

Previous research has pointed out that after being mixed with water, cement grains begin dissolving and hydrating, consequently developing a heterogeneous charge distribution on the surface of hydrating cement grains. Positively charged area covers a dominant part that is mainly contributed by aluminate hydrates. The dissolution and hydration of silicate, on the other hand, generates a negatively charged area. Therefore, the zeta potential of FCPs presents a positive value, as shown in Fig. 5.1. In addition, with the growth of W/C, the zeta potential of FCPs presents a linear decrement. This should be attributed to the intensified dissolution of mineral phases at high W/C and the lessened counter ions on aluminate hydrates (Plank and Gretz 2008).

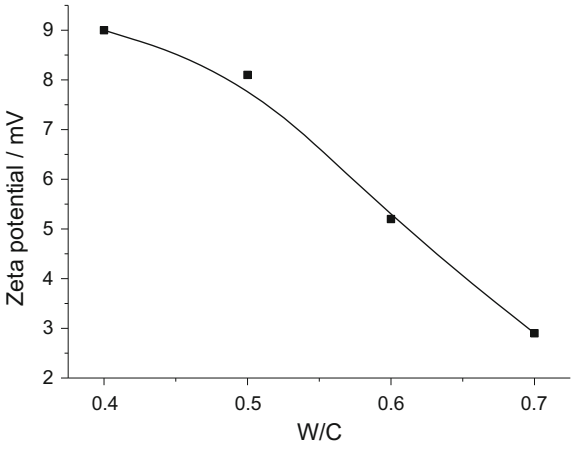

Fig. 5.1 Variation of zeta potential of fresh cement pastes at varied W/Cs

The organic monomers including AA, SSS as well as their corresponding homo-polymers PAA, PSSS possess negative charges in alkaline solution while MAPTAC and PMAPATC present positive charges. Theoretically speaking, all of them could be adsorbed on cement surface through electrostatic interactions. The adsorption amounts of the organic monomers including AA, SSS, MAPTAC as well as the corresponding homo-polymers on cement grains were measured by TOC measurements in combination with the precipitation experiments. As shown in Fig. 5.2, it is clearly seen that only the addition of PAA results in precipitation in the pore solution, while the pore solutions with the addition of other chemicals keep transparent. The precipitation ratio of PAA was measured as 15.0% in the pore solution and this portion of PAA should be deducted to obtain the real adsorption amount, marked as the corrected adsorption amount in Table 5.1. Table 5.1 presents the adsorption amount of each chemical as well as the variation of zeta potential of cement pastes. It is clearly seen that the monomers, AA, SSS and MAPTAC are hardly adsorbed on the surface of cement grains. Correspondingly, the zeta potential of cement paste is just slightly changed with the addition of these organic monomers within ± 3 mV, which is regarded as the measuring error. On the other hand, significant adsorption of PAA, PSSS and PMAPTAC on cement grains is found and their adsorption amounts vary in the circumstance of identical initial addition of molar amount. Specifically, large proportions of PAA and PSSS added in cement pastes are adsorbed on cement grains, while only a minor part of PMAPTAC is adsorbed. Meanwhile, the adsorption of these polymers leads to notable changes on the zeta potentials of the FCPs. PAA and PSSS remarkably decrease the zeta potential from +6.3 mV to large negative values, whereas higher positive zeta potential is observed in the presence of PMAPTAC in fresh cement

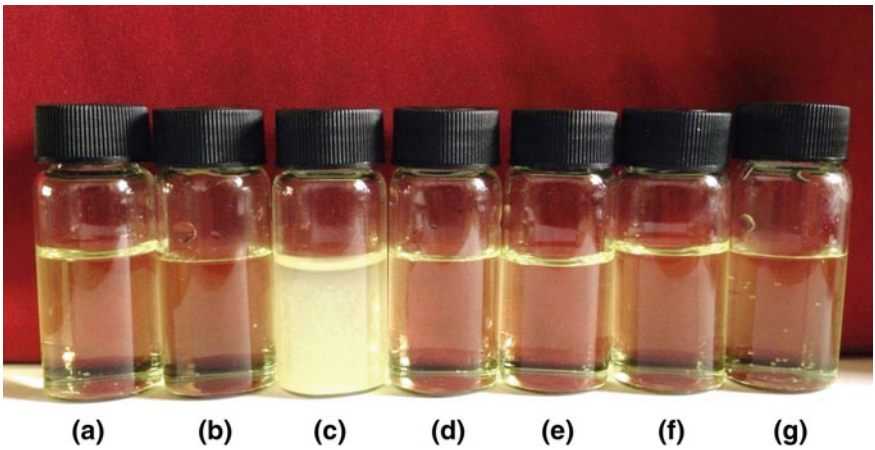

Fig. 5.2 Pore solutions of fresh cement pastes with addition of various organic monomers and homo-polymers. **a** Pore solution, **b** pore solution with AA, **c** pore solution with PAA, **d** pore solution with SSS, **e** pore solution with PSSS, **f** pore solution with MAPTAC, **g** pore solution with PMAPTAC

Table 5.1 The adsorption amounts of AA, SSS, MAPTAC and their corresponding homo-polymers as well as MPEGMA in cement pastes, and the zeta potential of the cement pastes in the presence of the monomers/polymers

Item		Blank	AA	SSS	MAPTAC	PAA	PSSS	PMAPTAC	MPEGMA
Initially added amount	(g/g cement) (%)	–	0.12	0.34	0.36	0.12	0.34	0.36	2.15
	(μmol/g cement)[a]	–	16.5	16.5	16.5	16.5	16.5	16.5	16.5
Adsorbed amount (μmol/g cement)[a]		–	0	0	0	14.0	10.8	2.2	2.86
Corrected adsorbed amount (μmol/g cement)[b]		–	0	0	0	11.5	10.8	2.2	2.86
Adsorption ratio (%)		–	0	0	0	69.8	65.5	13.3	17.3
Zeta potential (mV)		6.3	9.5	10.1	3.2	−24.0	−49.2	25.2	6.6

[a]For the organic monomers, it is measured by mole of the substances, while for their corresponding homo-polymers, it is measured by mole of the repeating unit

[b]The precipitated PAA in pore solution has been deducted from the adsorption amount indicated in the upper row

paste. Comparing the absorption behavior of PAA with that of PSSS, it is interesting to note that PSSS more significantly decreases the zeta potential than PAA although less PSSS is adsorbed on cement grains.

It has been well reported that the adsorption of chemical admixtures on cement grains is related to the charge types and the charge density in the molecules of the admixtures (Plank and Winter 2008). The higher charge density usually brings stronger interactions of admixtures with the mineral surfaces and consequently facilitates the adsorption on cement grains. However, when those organic monomers and the corresponding homo-polymers are compared, the monomers AA, SSS and MAPTAC fail to be adsorbed on cement grains although they possess the same charge density as their corresponding homo-polymers, which indicates that some another factors existing to influence the adsorption capability of the chemical admixtures on the surface of cement grains. Plank and Gretz (2008) stated that conformation of macromolecule, intermolecular forces and entropic effects also determined the adsorbed amount of chemical admixtures due to their contributions to the changes in free energy. The adsorption of chemicals on a solid surface is an entropy reduction process, which is unfavorable to the free energy reduction. Thus, the monomers are much more difficult to be adsorbed on cement surface than their corresponding homo-polymers due to their larger entropic loss upon the adsorption. In conclusion, the results in Table 5.1 confirm that the monomers are hardly adsorbed on cement surface while the adsorption of their corresponding homo-polymers is quite obvious, although the electrostatic interactions are quite similar in the two cases.

With regard to the different adsorption behaviors of PAA and PSSS from PMAPTAC, it should be attributed to the heterogeneous charge distribution on the surface of hydrating cement grains originating from different hydrating phases. As previously mentioned, the positively charged area covers a larger part in fresh cement paste due to the faster reaction of aluminate phases at early stage. As a consequence, the hydrating cement grains provide more adsorption sites for the negatively charged ions than the positively charged ones. This is the reason why the adsorption amounts of PAA and PSSS with anionic charges are prominently larger than that of PMAPTAC with cationic charges. Such way, the addition of PAA and PSSS decreases the zeta potential of the pastes to larger negative values whereas PMAPTAC increases the zeta potential from the initial value of +6.3 to +25.2 mV.

Aside from being adsorbed on the positively charged aluminate surface through electrostatic attraction forces, PAA is also able to be adsorbed on the negatively charged silicate surface through the bridging ions Ca^{2+} due to the complexation between $-COO^{-}$ groups and Ca^{2+} as illustrated in Fig. 5.3 (Plank and Gretz 2008). In contrast, PSSS does not have such effect with Ca^{2+}. Thus, the adsorbed amount of PAA is higher than that of PSSS as seen in Table 5.1. In the same way, the adsorption of PAA on the negatively charged mineral surfaces via Ca^{2+} bridging leads to less reduction of the zeta potential of cement paste due to the coverage on

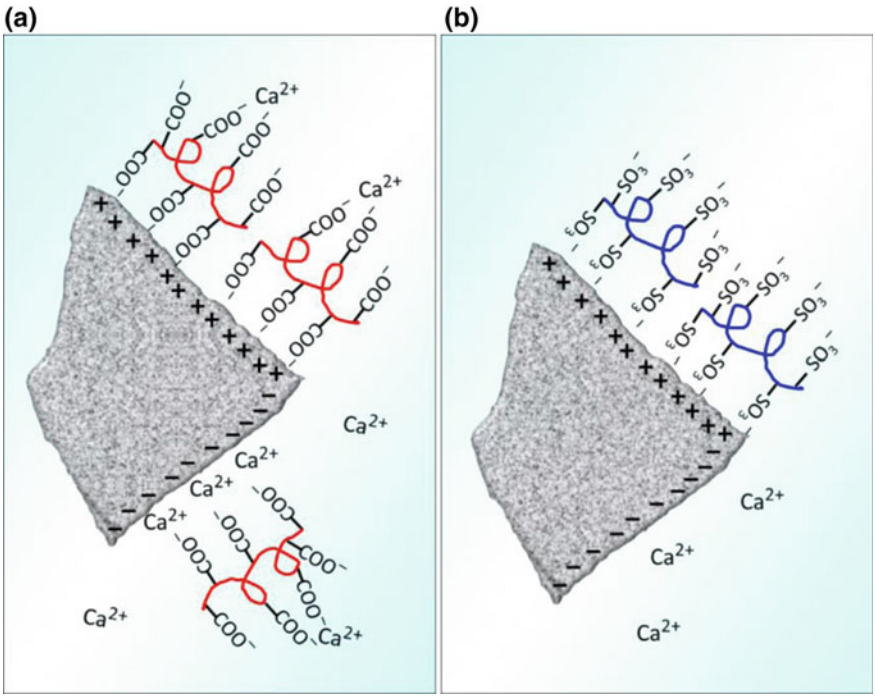

Fig. 5.3 Schematic diagrams of the adsorption of PAA and PSSS on the surface of cement grains

the anionic surface and the extension of the shear plane. In addition, the adsorbed PAA molecules may further catch Ca^{2+} in solution to form complexes (shown in Fig. 5.3), which may also weaken the capability of PAA to decline the zeta potential value of the cement paste to some extent. Similar phenomenon has been reported by Yoshioka et al. (2002). He proposed that the adsorption of anionic admixtures on the silicates through chelation effects had little influence on the zeta potential of cement paste. Thus, in the premise of owning the same charge density, PAA leads to less reduction of zeta potential of cement paste than PSSS does, although the adsorption ratio of PAA on cement surface is higher than that of PSSS.

5.1.2 *Effects on Cement Hydration*

The heat evolution of cement hydration can be divided into five stages according to the calorimetry curve of hydration rate versus time shown in Fig. 5.4: stages I initial period, stage II induction period; stage III acceleration period, stage IV deceleration period and stage V slow ongoing period (Scrivener and Nonat 2011). Usually, the adsorption of chemical admixtures on cement grains leads to visible changes in hydration kinetics of cement.

Figure 5.5 presents the exothermic heat flow of cement hydration in the cement pastes with incorporation of the monomers AA, SSS, MAPTAC and their corresponding homo-polymers. From Fig. 5.5a, it is noted that AA, SSS and MAPTAC have little influence on cement hydration, which is fully consistent with the adsorption results shown in Table 5.1 that no adsorption occurs as organic monomers are added in cement pastes. Figure 5.5b shows that the addition of the corresponding homo-polymers leads to a prolonged induction period, a delayed and lowered heat flow peak in the acceleration period of cement hydration, which is the so-called retardation effect on cement hydration. To analyze the influences of these

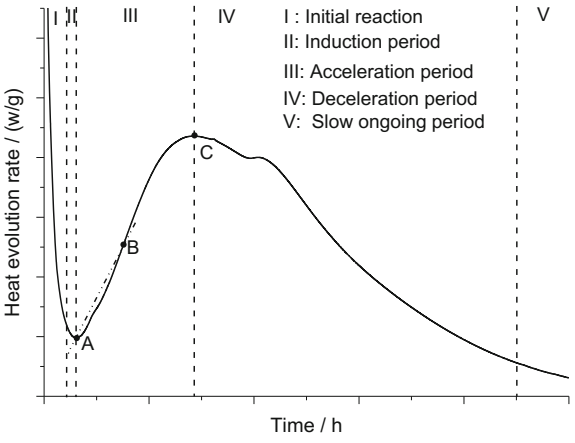

Fig. 5.4 A typical heat evolution curve of cement hydration

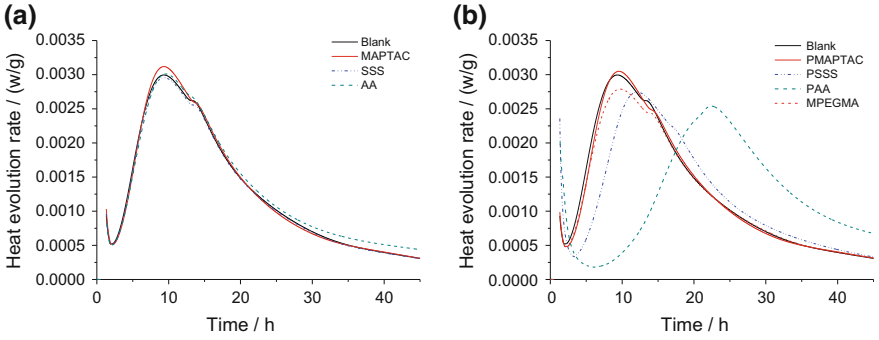

Fig. 5.5 Influences of monomers and homo-polymers on the hydration heat flow of cement paste. **a** Monomers, **b** homo-polymers and MPEGMA

polymers on the hydration kinetics in detail, six parameters are extracted from the heat evolution curves in Fig. 5.5 based on the illustration in Fig. 5.4. As shown in Fig. 5.4, t_A represents the ending time point of the induction period, t_C indicates the time point of the maximum heat generation rate and t_B, the inflection point between A and C on heat evolution curve, refers to the time point of the maximum acceleration rate. Correspondingly, the heat generation rate during the induction period $(dQ/dt)_A$, the cumulative heat flow at the beginning of the acceleration period Q_A, the maximum hydration rate $(dQ/dt)_C$ in the acceleration period and the cumulative heat flow during the acceleration period Q_{A-C} could be obtained. The secant slope on the heat evolution curve between A and B is defined as K_{A-B}, which represents the acceleration rate of hydration rate at the early stage of the acceleration period. The obtained hydration parameters are listed in Table 5.2.

Induction period is considered as a period during which cement hydration is proceeding at a very low rate and in the meantime, various ions slowly diffuse from the mineral phases of cement grains to the aqueous phase (Plank and Hirsch 2007). It is reported that the hydration rate in the induction period and the duration of the induction period t_A are related to the diffusion rate of various ions from the mineral phases to the aqueous phase. And the ion diffusion rate is mainly governed by the contact surface of the mineral phases with water (Pourchet et al. 2007). The adsorbed polymers undoubtedly hinder the exchange of water and ions between the hydrating cement grains and the aqueous phase due to their coverage on cement surface, thereby decreasing hydration rate and prolonging the induction period. It is noted in Table 5.2, slight influences on the heat evolution parameters of cement hydration are found when PMAPTAC is added, which is due to its low adsorption amount on cement surface. PAA and PSSS evidently prolong the induction period and depress the hydration rate $(dQ/dt)_A$ in the induction period, implying the decelerated ions diffusion caused by the prominent adsorption of PAA and PSSS on cement surface. In addition, PAA brings about more evident retardation on cement hydration than PSSS, which is in very good agreement with the fact that the adsorption amount of PAA is larger than that of PSSS.

Table 5.2 Parameters of cement hydration extracted from the calorimetry curves of blank cement paste and the cement pastes containing PAA, PSSS and PMAPTAC

Item	t_A (h)	$(dQ/dt)_A$ (mW/g)	Q_A (J/g)	K_{A-B} [mW/(g·h)]	$(dQ/dt)_C$ (mW/g)	Q_{A-C} (J/g)
Blank	1.94	0.52	1.51	0.364	2.95	49.71
PMAPTAC	2.21	0.47	1.85	0.382	3.03	50.11
PSSS	3.39	0.33	5.31	0.297	2.75	50.09
PAA	6.14	0.18	9.09	0.128	2.54	71.86

After the induction period, cement hydration steps into the acceleration period with rapid nucleation and growth of hydrates. On the assumption that the growth rate of C–S–H keeps constant, the hydration rate in the acceleration period is in proportion to the amount of growth active sites of C–S–H. Namely, the hydration rate at any time in the acceleration period is solely determined by the total amount of hydrates nuclei at that moment (Aligizaki 2005; Moro and Böhni 2002). Thus, K_{A-B} reflects the nucleation rate of C–S–H at the early stage of the acceleration period. From Table 5.2, it can be seen that K_{A-B} and $(dQ/dt)_C$ visibly drop with the incorporation of PAA whilst slight reduction is found when PSSS is added in cement paste, suggesting that PAA has marked impact on depressing the nucleation of hydrates during the acceleration period, which may be ascribed to the chelation effects of PAA with Ca^{2+} (Plank and Gretz 2008; Yoshioka et al. 2002).

With the growth of hydrates, a hydrates layer is gradually formed over the surface of cement grains, which further hinders the exchange of water and the ions and eventually brings about the deceleration period of cement hydration (diffusion controlled reaction) at time point t_C. The maximum hydration rate is mainly determined by the number of nuclei formed during the time period A to C (Kong et al. 2012). Lower hydration peak is related to fewer nuclei formed during A to C. Thus, from the lower hydration peak $(dQ/dt)_C$, it can be deducted that the total nuclei number is significantly reduced when PAA is added into cement paste.

Moreover, PAA obviously increases the cumulative heat flow Q_{A-C} during the acceleration period. This result again accords with the reduced nuclei number during A to C with addition of PAA, because thicker hydrates layer, namely higher hydration degree is required with fewer nuclei in order to reach full coverage of hydration products on cement surface and to switch the hydration into the deceleration period.

One may conclude that PAA prolongs the induction period, delays and depresses the hydration peak due to its higher adsorption amount on cement surface. The high adsorption amount of PAA reduces the diffusion rate of ions and water crossing the interface between cement and aqueous phase, and further depresses the nucleation process of cement hydration. Our results about the adsorption and retardation of AA and PAA in cement pastes indirectly confirm the results of Pourchet et al. (2006). They found that the interaction between Ca^{2+} and carboxyl groups depended on the distance separating the anionic groups. The isolated or diad carboxyl groups were

less efficient to drive the adsorption of polymer on cement and thus less effective for the retardation of cement hydration than triad, tetrad, pentad etc.

On the basis of the above results, it is not hard to found that polymer with positive charges (PMAPTAC) has slight influence on the hydration kinetics of cement whilst the polymers with negative charges (PSSS and PAA) retard cement hydration to different extents. In spite of the same negative charge density in the molecules, PAA with carboxyl groups exerts a stronger retardation effect than PSSS with sulfonic ones due to its larger adsorption amount and strong complexation effect with Ca^{2+} ions.

5.2 Influences of Comb-Shaped Co-polymers on Adsorption and Hydration

The different adsorption behaviors of PAA, PSSS and PMAPTAC linear homo-polymers without side chains and their impacts on cement hydration originating from the different functional groups $–COO^-$, $–SO_3^-$ and $\equiv N^+–$ have been elucidated in Sect. 5.1. As well known, the typical PCE superplasticizer is a comb-shaped polymer with polycarboxylate chain as backbone and poly (ethylene oxide) (PEO) as side chain. A large number of carboxyl groups ($–COO^-$) and sometimes a certain amount of sulfonic groups ($–SO_3^-$) are usually contained in the main chain, which makes the PCE molecules negatively charged in alkaline solution (Yamada et al. 2000; Yoshioka et al. 2002). By changing the molar ratio of monomer AA to AMPS during polymerization, the ratio of $–COO^-$ groups to $–SO_3^-$ groups can be adjusted without changing the charge density in the synthesized co-polymers. Thus, the effects of $–COO^-$ and $–SO_3^-$ groups in PCE superplasticizer on its performance in cementitious system can be studied. In the same way, cationic charges can be introduced into the PCE molecules by simply replacing the monomer AA with MAPTAC in a certain ratio and the synthesized co-polymers become amphoteric. Cationic co-polymers can be produced by complete replacement of AA with MAPTAC. In the following part, the effects of the various functional groups $–COO^-$, $–SO_3^-$ and $\equiv N^+–$ on the behaviors of model co-polymers were investigated.

5.2.1 Characterization of the Synthesized Co-polymers

5.2.1.1 SEC Measurement and Dialysis Results

SEC equipped with a laser light scattering (LS) detector and a refractive index (RI) detector was employed to determine the molecular weight of the prepared polymer and to roughly estimate the fraction of the desired polymer in the

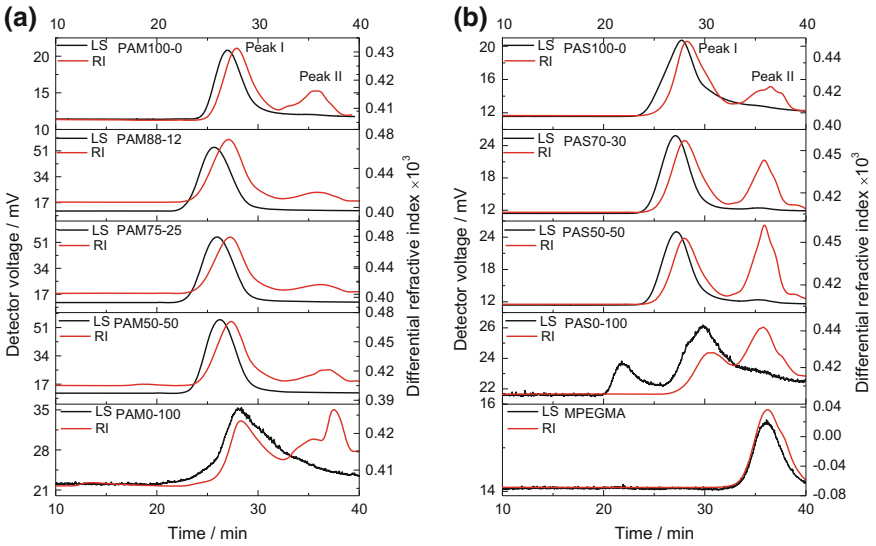

Fig. 5.6 SEC chromatograms of PAM co-polymers (**a**) and PAS co-polymers (**b**)

synthesized sample. SEC chromatograms of the samples of PAM series and PAS series before purification are given in Fig. 5.6. It is seen that the SEC chromatograms of the synthesized samples often exhibit multi-peaks. This indicates that rather than pure polymer, the synthesized products contain many components with different molar mass, which might be either the desired co-polymer, or the un-polymerized macro-monomer and even the residual monomers with smaller molar mass. In the SEC measurement, the combination of LS signals with RI signals allows a qualitative analysis for individual fraction in the synthesized samples. The LS signals are used for calculation of molecular weight, including Mw, Mn and molecular weight distribution Mw/Mn, and the RI signals can be used for the estimation of the concentration of each fraction in the sample by integration of the area for each peak. The analysis results of SEC for samples of both PAM series and PAS series are listed in Table 5.3. As shown in Fig. 5.6 and Table 5.3, it is seen that the synthesized PAM samples mainly contain two fractions, indicated as peak I and peak II. The fraction of peak I presents high molecular weight of Mw above 10,000 and peak II shows relatively lower Mw, which should be recognized as oligomers. It is noted that the molecular mass of the fraction II in the samples of PAM series, which is obtained from the LS signals, is not located around 1100, that is the average molecular weight of the macro-monomer MPEGMA (as given in Fig. 5.6a), and varies from samples, although the elution times of peak II are quite close. A single peak with molar mass of about 1100 is not observed. This implies that the fraction of peak II is not the unreacted macro-monomers, but would rather be oligomers that may be composed of several macro-monomer units linked by a few of monomer units. The absence of the macro-monomer peak indicates that the

Table 5.3 SEC analysis for the samples of PAM and PAS series and the polymer fraction in the solid part of the synthesized samples obtained from dialysis results

Samples	Polymer fraction			Oligomer fraction			Polymer (Mw > 7000) fraction in the solid part of the synthesized samples obtained from dialysis results (%)
	Mw	Mw/Mn	Mass fraction (%)	Mw	Mw/Mn	Mass fraction (%)	
MPEGMA				1093	1.071	95.1	–
PAM100-0	24,860	1.297	66.1	6729	1.132	31.5	78.0
PAM88-12	43,920	1.680	83.9	4496	1.189	13.6	53.2
PAM75-25	40,490	1.643	83.3	4769	1.218	13.9	51.3
PAM50-50	45,910	1.541	77.4	2726	1.304	19.6	75.9
PAM0-100	72,510	1.045	37.4	20,040	1.106	18.3	49.3
PAS100-0	15,840	1.232	60.6	5593	1.096	23.1	65.3
PAS70-30	19,060	1.496	55.7	2417	1.146	31.0	49.8
PAS50-50	20,580	1.358	43.7	1531	1.146	39.5	39.5
PAS0-100	21,680	1.190	30.7	5713	1.251	63.9	37.2

conversion of monomers is relatively high. Knowing that the polymerization rates for the monomers such like AA are much higher than that of the macro-monomer MPEGMA and the latter is hardly able to form homo-polymer (George 1991), we believe that the fraction of peak II in the samples might be produced after the main consumption of the monomers like AA and MAPTAC. The condition of relatively high concentration of macro-monomer and low concentration of monomers at late stage of the polymerization, i.e. after complete dosage of monomers, produces these oligomers with molecular weight of several thousands. In case of PAS series, two similar peaks (peak I and peak II) are found in the chromatograms as seen in Fig. 5.6b. Peak I represents the fraction of polymers in the samples with high molecular weight of 10,000–25,000 and peak II should be assigned to oligomers.

From SEC data presented in Table 5.3, it is found that the obtained products are not pure and the polymer contents in PAM and PAS samples present significant difference. Before we start to investigate the influences of these synthesized polymers on cement hydration, all the prepared samples were purified by dialysis technique. As described in Sect. 2.2.2, residual monomers, salts and oligomers with Mw < 7000 were removed from the samples by dialysis. After purification, the polymer (Mw > 7000) fraction in the solid part of the synthesized products can be calculated as listed in Table 5.3. It can be seen that the polymer fractions obtained from SEC analysis and from the dialysis experiment are quite comparable. Thus, in the following part of this chapter, the characterization of the obtained co-polymers by FTIR and the investigation of the co-polymers in cement pastes were carried out by using the purified co-polymers to avoid any disturbance from the remaining monomers, oligomers and salts.

5.2.1.2 FTIR Analysis

In order to confirm the co-polymerization of the various monomers in synthesis of the co-polymers (PAM and PAS series) as designed in Table 2.5, FTIR analysis was performed on the purified co-polymers and the spectra are given in Fig. 5.7. The broad peak around 3485 cm^{-1} and the sharp peak at 2873 cm^{-1} are respectively assigned to the O–H and C–H stretching bands. The absorption peak at 1652 cm^{-1} corresponds to the amino-carboxyl groups which derives from the monomer MAPTAC and AMPS. The peak of N–H amine band can be found at 1540 cm^{-1} for PAS series. The peak at 1726 cm^{-1} is assigned to the overlapping of C=O in AA repeating units and the macro-monomer MPEGMA units. Moreover, the characteristic band of MPEGMA also appears at 1109 cm^{-1} for C–O–C asymmetric stretching. The presence of these characteristic peaks in the FTIR spectra of the purified PAM and PAS samples demonstrates the successful co-polymerization of the involved monomers. On the other hand, with the increasing proportion of MAPTAC in the synthesis of PAM series, the peak of amino-carboxyl at 1652 cm^{-1} in the polymers becomes more intense while that of C=O at 1726 cm^{-1} from AA units gets lower when the height of peak at 1109 cm^{-1} for C–O–C is fixed constant, as seen from Fig. 5.7b. This indicates that the molar ratio of MAPTAC to AA in the PAM molecules increases as expected. Similar trend has been also found in PAS series (Fig. 5.7c). Thus, the ratio of repeating units of MAPTAC to AA in the PAM co-polymers (or AMPS to AA for the PAS co-polymers) can be semi-quantatively determined by comparing the heights of the characteristic peaks from both monomers. The peak at 1726 cm^{-1} is used as the characteristic peak of AA units and the peak at 1652 cm^{-1} is adopted to represent MAPTAC (or AMPS) units, when the peak at 1109 cm^{-1} assigned to MPEGMA is fixed. The variations of the two peaks in the PAM and PAS co-polymers are listed in Table 5.4, which provides clear evidence of the co-polymerization of various monomers and the variation trend of their corresponding repeating units in the obtained co-polymers, when monomer proportions are changed in synthesis.

5.2.2 Co-polymers with Positive Charges and Negative Charges (PAM)

Charge types of co-polymer could be adjusted from anionic to cationic by co-polymerization of AA, MAPTAC and MPEGMA with variations of molar ratio of AA to MAPTAC, as the samples of PAM series, which is confirmed by the FTIR analysis shown in Fig. 5.7b. Purified PAM co-polymers are used to investigate the effects of charge types in polymer chains on the adsorption behaviors of the co-polymers on cement surface. Figure 5.8 exhibits the adsorption behaviors of the co-polymers with varied ratios of AA repeating units to MAPTAC units and the zeta potential of cement pastes. It is clearly seen that at a fixed polymer to cement

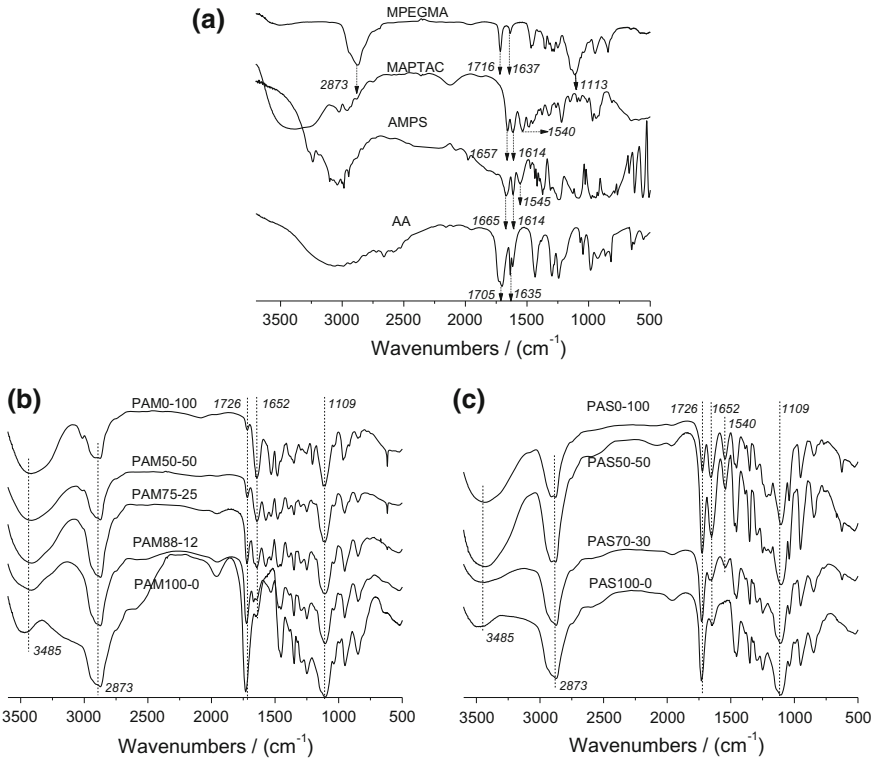

Fig. 5.7 FTIR spectra of monomers (**a**), PAM series (**b**) and PAS series (**c**)

Table 5.4 Intensity ratios of C=O peaks in the purified co-polymers obtained from the FTIR spectra

Peaks	PAM 100-0	PAM 88-12	PAM 75-25	PAM 50-50	PAM 0-100	PAS 100-0	PAS 70-30	PAS 50-50	PAS 0-100
Height (1726 cm^{-1})/ Height (1652 cm^{-1})	–	2.1	0.93	0.37	0.15	5.3	3.8	1.4	0.86

ratio, the adsorption amounts of the co-polymers dramatically decline as more cationic MAPTAC repeating units are incorporated in PCE molecules. The adsorption amount of the fully cationic PAM0-100 is far lower than that of the anionic co-polymer PAM100-0. This means that the adsorption capability of the negatively charged co-polymers is much higher than that of the positive ones, which is certainly attributed to the fact that the positively charged aluminate hydrates are dominant in an early hydrating cement paste. Besides, the chelating effect of $–COO^-$ with Ca^{2+} also contributes to the higher adsorption amount of the

PCE molecules containing more AA repeating units on cement grains (Plank and Gretz 2008; Yoshioka et al. 2002).

With the adsorption of co-polymers on the surface of cement grains, the zeta potential is bound to be changed, as indicated in Fig. 5.8. The addition of PAM100-0 bearing only anionic charges effectively decreases the zeta potential of cement pastes from +7.2 to −2 mV at dosage of 0.2%. With the increasing molar ratio of cationic charges to anionic charges in molecules, notable growth on zeta potential is observed in the presence of the co-polymers in cement pastes. When monomer AA is completely replaced by MAPTAC (PAM0-100), the inclusion of co-polymer in cement paste enables the zeta potential to increase to +23.8 mV, which is far higher than the value +7.2 mV for the blank cement paste.

The various purified PAM co-polymers are mixed into cement pastes to investigate the impacts of the charge types in co-polymers on cement hydration by calorimetry, as presented in Fig. 5.9a. It is seen that more polymer addition generally leads to stronger retardation effects on cement hydration. At a fixed polymer dosage, higher molar ratio of $\equiv N^+-$ groups to $-COO^-$ groups in molecules brings about lower retardation effects on cement hydration. PAM100-0 retards the cement hydration most significantly in terms of prolonging the induction period and reducing the maximum hydration rate. By contrast, the positively charged PAM0-100 has little influence on cement hydration compared to the blank cement paste. These phenomena could be fully interpreted from the viewpoint of their adsorption behaviors on cement grains. Figure 5.9b presents the variations of t_A and $(dQ/dt)_C$ with adsorption amount. It is evidently seen that a larger adsorption amount of polymers on cement surface leads to an increase of t_A and a decrease of $(dQ/dt)_C$ due to the hindrance to the diffusion of various ions across the adsorption layer during the cement hydration process. Additionally, the strong complexation effect of $-COO^-$ with Ca^{2+} is also responsible for the retardation because of the effect of depressing nucleation process (Scrivener and Nonat 2011).

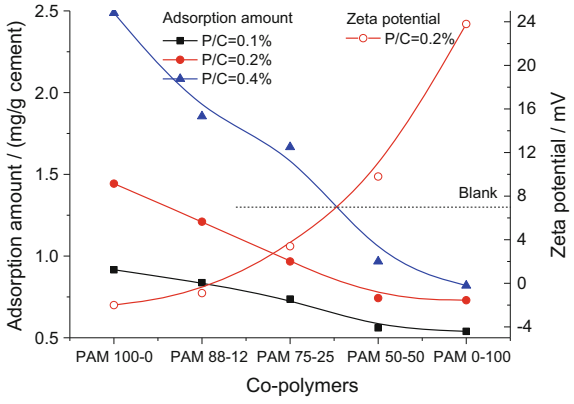

Fig. 5.8 Effects of the charge species of co-polymers on their adsorption behaviors in cement pastes at different dosages of polymer (P/C = 0.1, 0.2 and 0.4%)

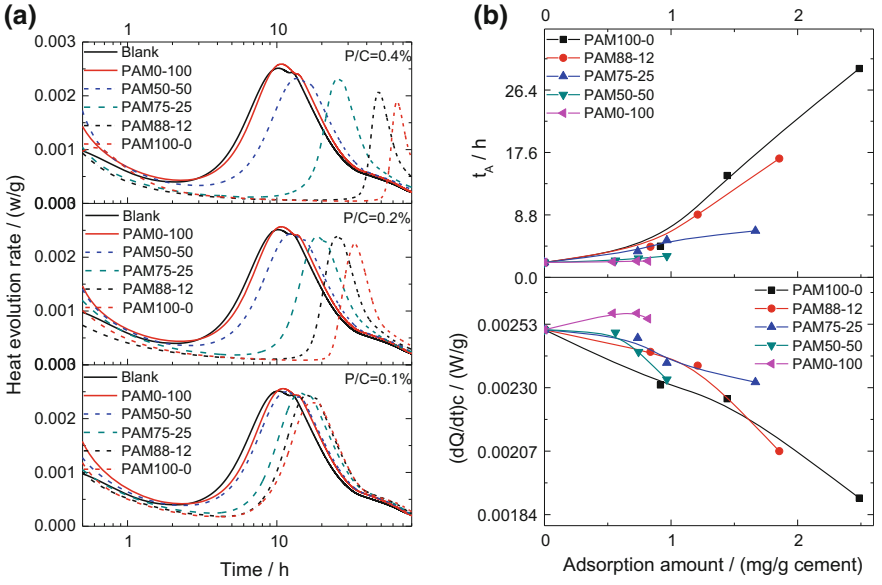

Fig. 5.9 Effects of the charge species of pure co-polymers on cement hydration. **a** Heat evolution rate of cement hydration at varied P/Cs, **b** variation of hydration parameters with adsorption amounts

5.2.3 Co-polymers with Carboxyl and Sulfonic Groups (PAS)

The effects of carboxyl and sulfonic groups in PCE molecules on their adsorption behaviors and on cement hydration are shown in Figs. 5.10 and 5.11 at varied dosages. It is found from Fig. 5.10 that a marked decrease in adsorption amount is recorded as more AA is replaced by AMPS in the preparation of co-polymers, implying that adsorption capability of carboxyl groups on cement surface is stronger than that of sulfonic groups, which is fully in agreement with the result shown in Table 5.1. As previously discussed in Sect. 5.1.1, the adsorption driving force of sulfonic groups on cement surface is only the electrostatic attraction, whereas carboxyl groups promote the adsorption of the co-polymers by the combined effects of electrostatic forces and more importantly the complexation with Ca^{2+} ions, as illustrated in Fig. 5.3. Thus, in the premise of the same negative charge density, the co-polymers with more carboxyl groups could be adsorbed in a more considerable amount on cement surface.

Based on the above mentioned adsorption behaviors, the finding that higher molar ratio of sulfonic groups to carboxyl groups in PCE molecules results in less prolongation of the induction period is in accordance with expectation, i.e., more replacement of AA units by AMPS units enhances the retardation effects on cement hydration, as presented in Fig. 5.11.

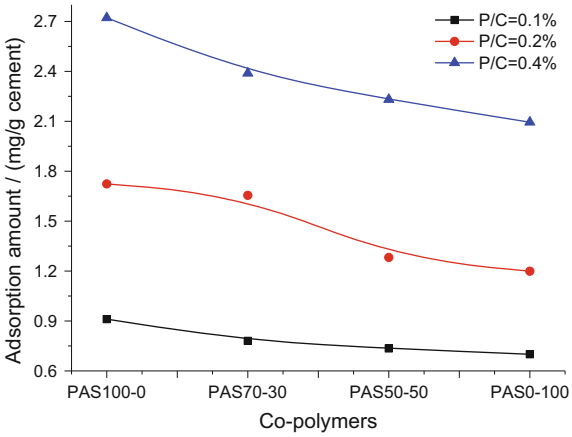

Fig. 5.10 Effects of carboxyl and sulfonic groups of pure co-polymers on their adsorption behaviors in cement pastes

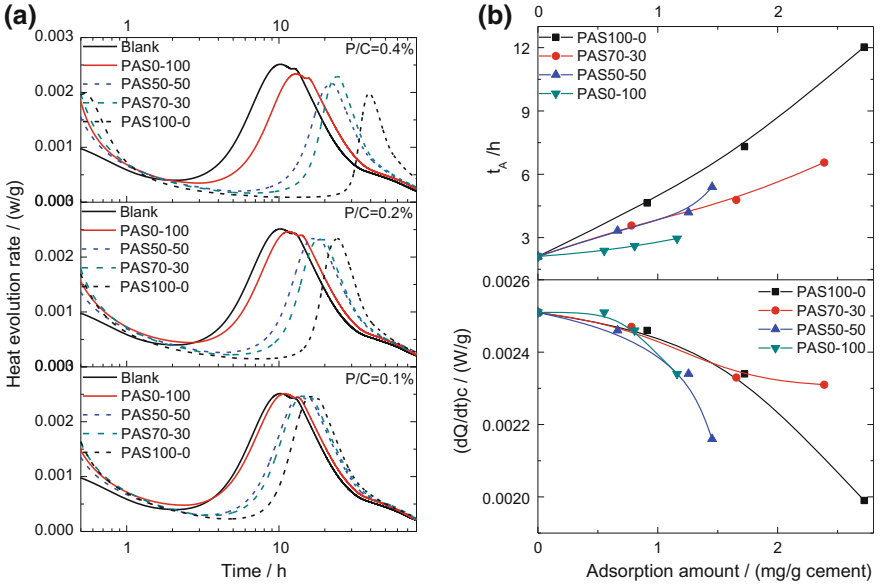

Fig. 5.11 Effects of carboxyl and sulfonic groups of pure co-polymers on cement hydration. **a** Heat evolution rate of cement hydration at varied P/Cs, **b** variation of hydration parameters with adsorption amounts

5.3 Cement-Superplasticizer-Water System

PCE superplasticizer and NSF superplasticizer are the two main types of superplasticizers popularly used in most of the cement-based materials nowadays. Based on the adsorption essence and retarding mechanism of the above model co-polymers stated in Sect. 5.2, the adsorption behaviors of NSF and PCE superplasticizers were comparatively investigated. The correlations of their adsorption on the surface of cement grains with the dispersing capability and the impacts on cement hydration were then ascertained. Finally, the working mechanism of different types of superplasticizers was disclosed from the two viewpoints of adsorption and retardation.

5.3.1 Adsorption Behavior

5.3.1.1 Adsorption Isotherm of Superplasticizers

With a positive zeta potential originating from C_3A phase as well as the Aft phase, cement grains can considerably adsorb negatively charged superplasticizer molecules because of the electrostatic attraction (Plank and Hirsch 2007; Yoshioka et al. 2002). Figure 5.12 shows the adsorption curves of both NSF and PCE superplasticizers on cement surface. The results in Fig. 5.12a indicate that the adsorption of NSF on cement grains follows a typical Langmuir monolayer adsorption model. Namely, the adsorption amount of NSF superplasticizer presents almost a linear increase at low dosages and then reaches a plateau that indicates adsorption

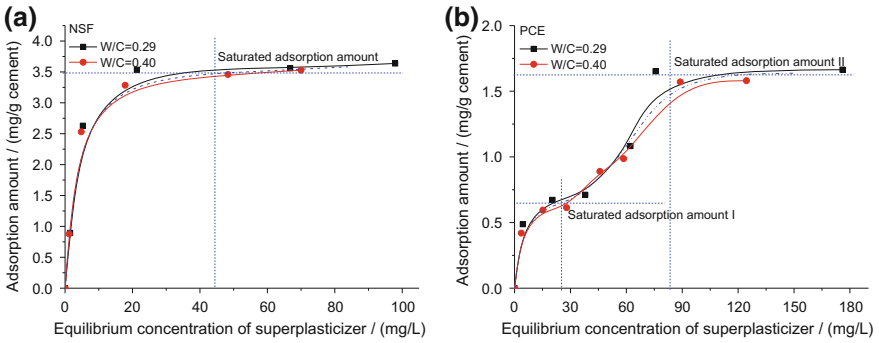

Fig. 5.12 Isothermal adsorption curves of superplasticizers on the surface of cement grains. **a** NSF, **b** PCE

saturation. This typical Langmuir monolayer adsorption behavior of NSF on cement grains has been reported frequently in the literatures (Hsu et al. 1999; Peng et al. 2005; Yoshioka et al. 2002).

On the other hand, the adsorption isotherm of PCE shown in Fig. 5.12b reaches a first plateau at a low concentration and then develops further to a second plateau at a higher concentration. This multi-step adsorption curve implies a multi-layer adsorption of PCE on the surface of cement grains, which is different from the previous findings reported by other researchers (Banfill et al. 2007; Hsu et al. 1999; Krstulovic et al. 1994; Plank and Sachsenhauser 2006; Yoshioka et al. 2002). This multi-layer adsorption of PCE was firstly mentioned by Yang and Hirsch (Dukhin and Goetz 2010; Hirsch 2005), who found that bilayer and even trilayer adsorption on cement grains occurred for some specific PCE superplasticizers at high dosages. According to the charge-controlled-reaction model proposed by Mollah et al. (2000), in which the charged surface of cement, ions especially the doubly charged ions such as Ca^{2+} and the electrostatic interaction were considered, the multi-layer adsorption of PCE on cement surface at high dosages observed in this research can be interpreted as follow.

Similar to the homo-polymers and co-polymers in Sects. 5.1 and 5.2, the existence of $–COO^-$ groups in PCE chains allows a strong complexation effect between $–COO^-$ and Ca^{2+}. In a hydrating cement paste, PCE molecules can be directly adsorbed on the positively charged mineral surfaces such as C_3A and Aft by electrostatic attractive forces. In the meanwhile, the abundant Ca^{2+} ions in the pore solution may neutralize the negatively charged surfaces such as C_3S and C–S–H, and provide additional adsorption sites for the adsorption of anionic polymer. Thus the adsorption of PCE on the negative surfaces of C_3S and C–S–H may also take place thanks to the bridging effect of Ca^{2+} ions. After the complete adsorption of the first-layer of PCE on cement surface, a steadily bound outer layer of Ca^{2+} ions facilitates the second adsorption layer of PCE due to the strong complexation effect of $–COO^-$ with Ca^{2+} ions, as shown in Fig. 5.13b. This way, the first plateau in the adsorption isotherm of PCE (Fig. 5.12b) represents the full coverage of cement surface by the first adsorbed PCE layer and the second plateau indicates the saturation of the second adsorption layer.

In the adsorption curves as seen in Fig. 5.14, the maximum adsorption amount is defined as the saturated adsorption amount and the dosage of superplasticizer at which the saturated adsorption is achieved can be correspondingly defined as the adsorption saturated dosage. The saturated adsorption amount of each superplasticizer is quite close at varied W/Cs, and the slightly larger adsorption amount at low W/C should be attributed to the higher zeta potential and consequently the more adsorption sites, as presented in Fig. 5.1. It is observed in Fig. 5.14 that the adsorption saturated dosage of NSF is 0.8% and the saturated adsorption amount is approximately 3.53 mg/g. For PCE, the first-layer saturated adsorption amount is 0.6 mg/g at dosage of 0.5% and the second layer saturated adsorption amount is 1.6 mg/g at dosage of 1.0 and 1.5% in the case of W/C of 0.29 and 0.4 respectively.

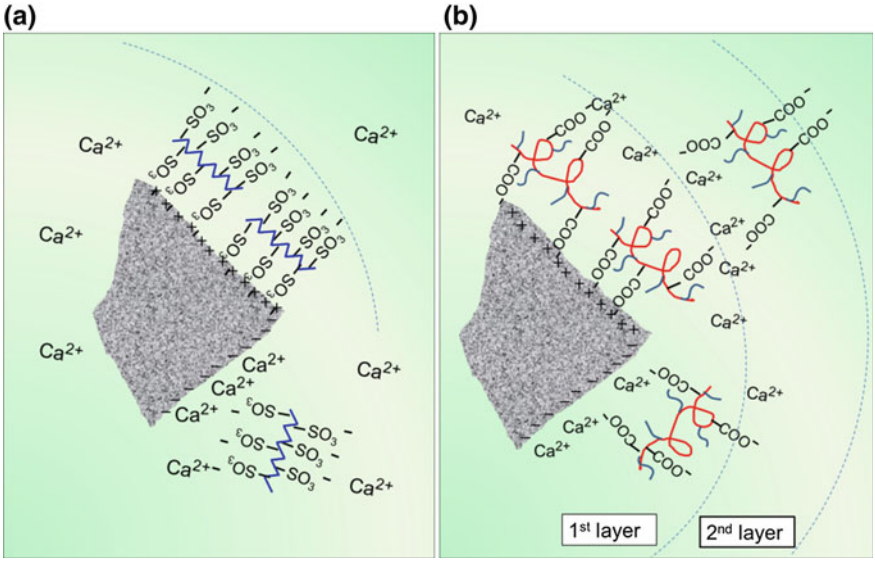

Fig. 5.13 Schematic drawings of the adsorbed superplasticizers on cement grains. **a** NSF, **b** PCE

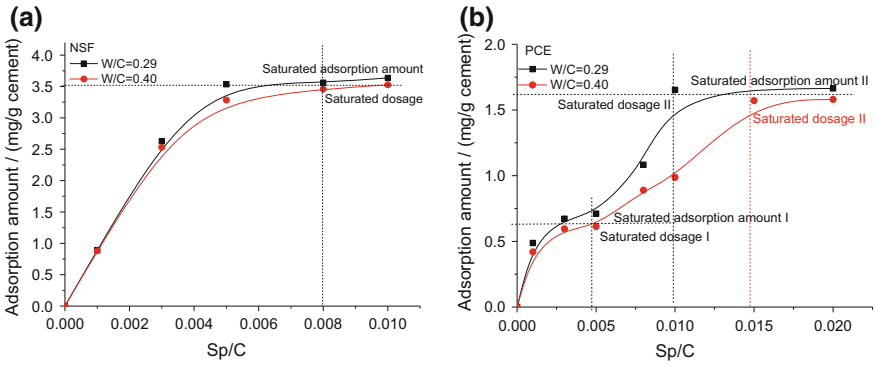

Fig. 5.14 Adsorption amount of superplasticizers on the surface of cement grains. **a** NSF, **b** PCE

The higher saturated adsorption amount of NSF than that of PCE is in good agreement with the earlier findings, suggesting that the adsorption layer of NSF on cement surface is more intensive and compacted due to its lower molecular weight and higher charge density (Burgos-Montes et al. 2012). For PCE, it is interestingly noted that more PCE is adsorbed in the second layer than in the first layer. This might be attributed to the more adsorption sites provided by the outer Ca^{2+} layer on the top of the first adsorption layer of PCE.

5.3.1.2 Zeta Potential of Fresh Cement Pastes with Superplasticizers

With the adsorption of superplasticizers on cement grains, the zeta potential of cement paste is bound to be changed, as shown in Fig. 5.15. The positive zeta potential of the cement paste definitely favors the adsorption of superplasticizers bearing anionic groups. The curves in Fig. 5.15 behave in much the inverted way as the adsorption curves in Fig. 5.14. Initially, the inclusion of superplasticizers leads to a sharp decrease in the zeta potential, from positive to negative values. At around the adsorption saturated dosage of NSF (P/C = 0.8%), the negative zeta potential stops changing, which is fully consistent with the phenomenon in Fig. 5.14 that no further adsorption of NSF occurs when Sp/C is beyond the adsorption saturated dosage. As for PCE, beyond the first-layer saturated dosage of 0.5%, zeta potential value is little affected by further adsorption of PCE. This demonstrates that the second layer adsorption of PCE on cement grains does not contribute to the drop of the zeta potential of cement paste, which is consistent with the conclusions that the adsorption through chelation effects had little influence on the zeta potential of cement paste (Yoshioka et al. 2002).

Furthermore, in comparison to PCE, NSF decreases the zeta potential of FCPs to a larger negative value as the saturated adsorption is achieved. Similar phenomena have been found in the work of other researchers (Ferrari et al. 2000; Plank and Sachsenhauser 2009). This should be attributed again to the higher negative charge density and larger adsorption amount of NSF. Moreover, two other factors may also be responsible for the less reduction of zeta potential of FCPs in the presence of PCE superplasticizer. One is that the long polyethylene oxide (PEO) side chains in the PCE molecule have a "shielding effect" on the negative charges provided by $-COO^-$ groups in the backbone and thus the shear plane of the cement grains shifts towards the aqueous phase. The other is the complexation effect between $-COO^-$ and Ca^{2+}, which lead to the formation of a Ca^{2+} rich layer outside the adsorbed PCE layer.

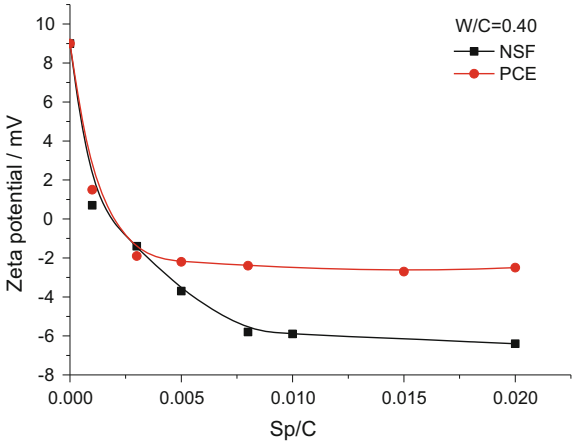

Fig. 5.15 Variation of zeta potential of FCPs with NSF and PCE at varied dosages

5.3.1.3 Effects of Temperature on the Adsorption and Zeta Potential

At an elevated temperature, more charges are produced due to the accelerated dissolution at early stage. As a consequence, the zeta potential of FCPs increases with the increase of temperature (Fig. 5.16). Meanwhile, the charges provide more adsorption sites for superplasticizers and thus, a larger adsorption amount of PCE superplasticizer is achieved at elevated temperatures. At higher dosage of superplasticizer, the increasing degree of adsorption amount with temperature is more remarkable, as presented in Fig. 5.16a.

More specifically in Fig. 5.16b, at 20 and 40 °C, a higher dosage of superplasticizers leads to a lower zeta potential of FCPs, which is due to the larger adsorption amount at higher Sp/C. On the contrary, at 0 °C, the growth of superplasticizer dosage causes an increment of the zeta potential from −11 to −4.2 mV in spite of larger adsorption amount of superplasticizer at higher superplasticizer dosages. These phenomena may be explained by the facts that cement grains are positively charged at 20 and 40 °C, while the adsorption of PCE neutralizes these positive charges and depresses the hydration of aluminates simultaneously. Hence, the zeta potential of FCPs descends with addition of superplasticizer. At 0 °C, the cement grains present negative charges (−12 mV) due to the weaker reaction of aluminate phases. Under such circumstances, the adsorption of superplasticizer is achieved mainly by chelating with Ca^{2+}, which may promote the dissolution of aluminate phases by disassembling the flocculated structures and subsequently increasing the contacting surface of mineral phases with water. Thus, the amount of positive charges increases with the inclusion of superplasticizer, and the zeta potential of FCPs presents an increasing trend with the growth of Sp/C.

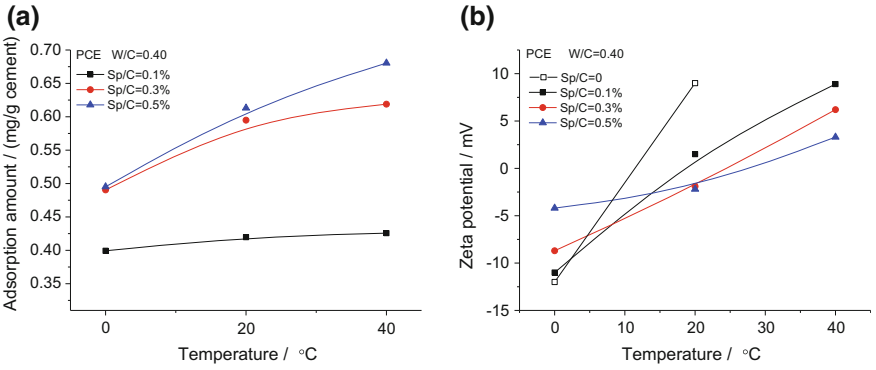

Fig. 5.16 Adsorption amount of PCE superplasticizer and zeta potential of FCPs at varied temperatures

5.3.1.4 Particle Size Distribution of Fresh Cement Pastes with Superplasticizers

The results of the ultrasound attenuation from DT-1201 acoustic & electroacoustic spectrometer reflect the particle size distribution of the FCPs, as shown in Fig. 5.17. The attenuation in low frequency corresponds to viscous absorption and that in high frequency refers to scattering losses. The total attenuation gradually decreases with the inclusion of superplasticizers, indicating that the content of large particles in the FCPs significantly declines (Dukhin and Goetz 2010). In Fig. 5.17, it is also noted that the attenuation curves stop changing at the critical dosages for both superplasticizers, which means that the particle size distribution in the cement pastes stays stable after the critical dosage of superplasticizer is reached. Looking back to the fluidity results that the initial fluidity of the FCPs reaches to a maximum value at the critical dosage and then remains constant, the working mechanism of superplasticizers on increasing fluidity proposed in Sect. 3.1 is confirmed. Specifically, a higher superplasticizer dosage leads to an increase of fluidity due to the more disassembled flocculated structures and the more release of the entrapped water. When the microstructure of FCPs stops changing with the addition of superplasticizers, especially the flocculated cement grains, the fluidity will remain stable irrespective of further addition of superplasticizers.

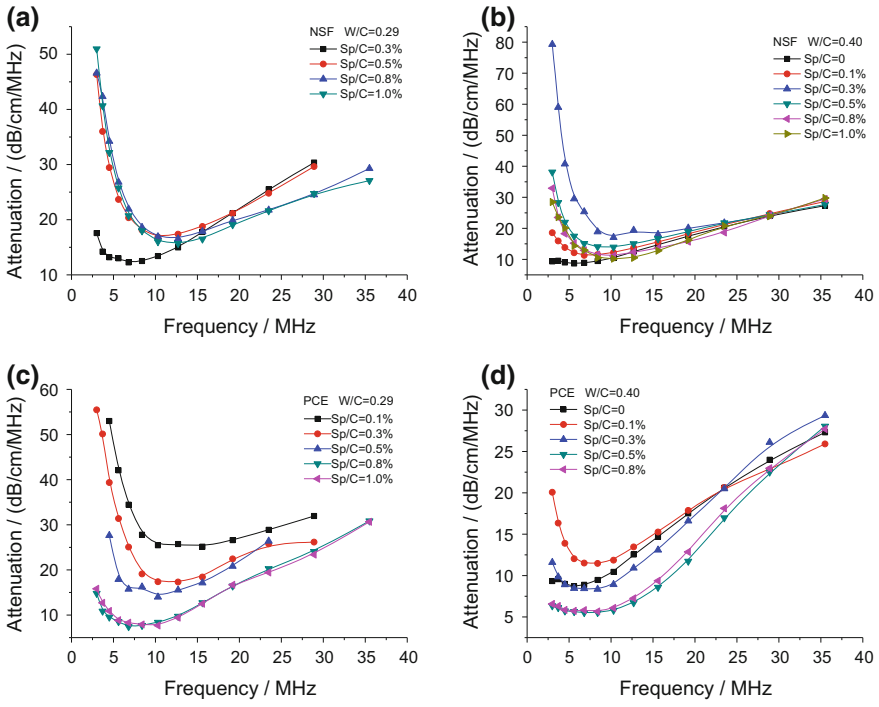

Fig. 5.17 Attenuation spectra of FCPs with superplasticizers at varied dosages

In addition, it is found that the attenuations in the low frequency range for the FCPs with PCE are generally lower than those for the FCPs with NSF, which reflects the better dispersing ability of PCE than that of NSF. The phenomena found above are also in good agreement with the conclusions of the initial fluidity and microstructure of FCPs.

5.3.2 *Correlation of Adsorption Behavior with Initial Fluidity*

By combining the fluidity curves (Fig. 3.1) with the adsorption curves (Fig. 5.14), it is interesting to see in Fig. 5.18 that the critical dosages of NSF are close to the adsorption saturated dosage of 0.8%. For PCE, the critical dosage at W/C of 0.4 is equal to the first-layer saturated dosage of 0.5% whilst at W/C of 0.29, the critical dosage of 0.8% is larger than the first-layer saturated dosage. These indicate that a larger adsorption amount of NSF on cement surface leads to higher initial fluidity of FCPs and the fluidity of FCPs reaches maximum when the adsorption of NSF on cement surface gets saturated, namely 100% surface coverage on cement grains. On the other hand, for PCE, the maximum fluidity of FCPs is achieved at the saturated

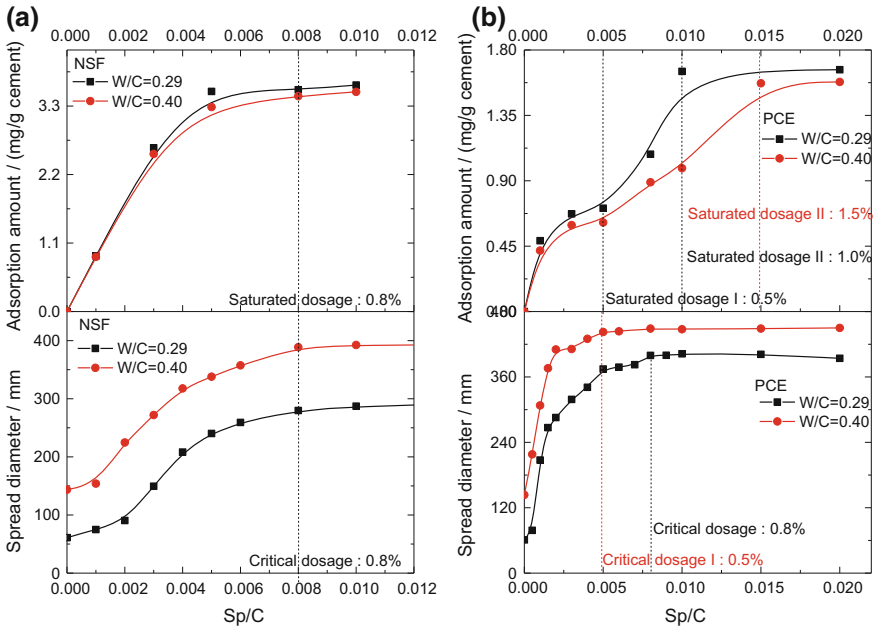

Fig. 5.18 Correlation of the fluidity of FCPs with the adsorption amount of superplasticizers on cement surface. **a** NSF, **b** PCE

dosage of the first-layer adsorption at high W/C, which implies that the second layer adsorption of PCE does not contribute to the growth of fluidity of FCPs. And at low W/C, the second layer adsorption of PCE is needed to achieve the maximum fluidity. This observation firmly validates the hypothesized mechanism of superplasticizers at varied W/Cs as shown in Fig. 3.2.

The adsorption curves of PCE and the initial fluidity curves of FCPs at varied temperatures are compared and shown in Fig. 5.19. Clearly, an elevated temperature results in a higher adsorption amount on cement surface. At low dosage of PCE, the effects of temperature on adsorption amount are weaker and thus the temperature sensitivity of initial fluidity is larger. At high dosages, adsorption amounts are visibly affected by the temperatures, which is contributed to the more adsorption sites and sufficient dosage of PCE. As a consequence, the temperature sensitivity of initial fluidity is reduced at high superplasticizer dosages. The above results well correspond to the schematic illustration of Fig. 3.4 in which the effects of temperature on the initial fluidity and adsorption amounts are presented.

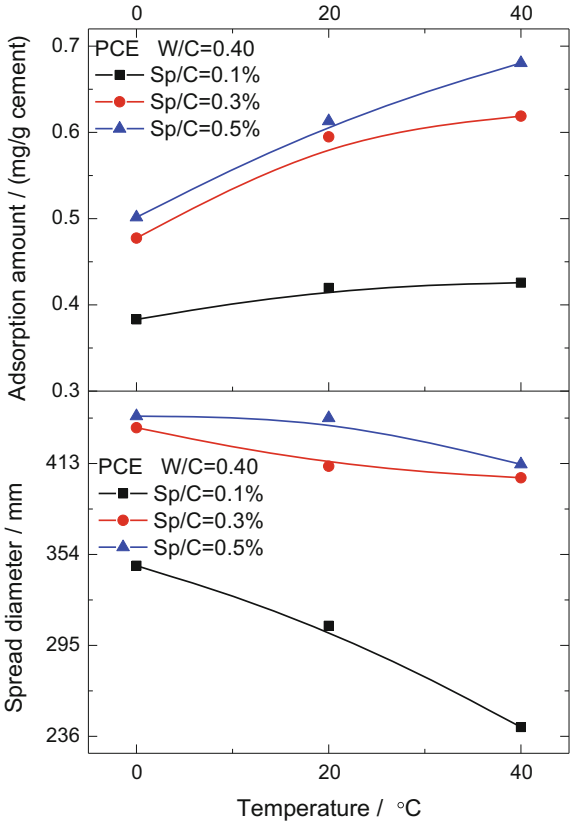

Fig. 5.19 Effects of temperature on the fluidity of FCPs and the adsorption amount of superplasticizers

5.3.3 *Effect on Cement Hydration*

5.3.3.1 Superplasticizers

Figure 5.20 presents the calorimetry results of the cement pastes with incorporation of the two types of superplasticizers. It is seen that the addition of superplasticizers leads to a prolonged induction period and a lowered maximum exothermic rate in the acceleration period of the cement hydration, which is the so-called retardation effects. Based on the previous findings in Sects. 5.1 and 5.2, it has been quite known that the retardation of cement hydration is predominantly due to the adsorption of superplasticizer molecules on the surface of hydrating cement grains as well as on some of the hydration products. The adsorbed superplasticizer molecule layers are thought to hinder the diffusion of water and ions at the cement-solution interface. In addition, the superplasticizers may form complexes with Ca^{2+} ions, which lead to both the reduction of Ca^{2+} ion concentration in solution and the inhibition of the nucleation and growth of Ca-containing hydration products. Therefore, the retardation effects of the two types of superplasticizer can be discussed from the abovementioned two aspects, i.e. the adsorption on cement surface and the complexation with Ca^{2+} ions. From the heat evolution curve in Fig. 5.4, parameters including the ending time point of the induction period t_A, the

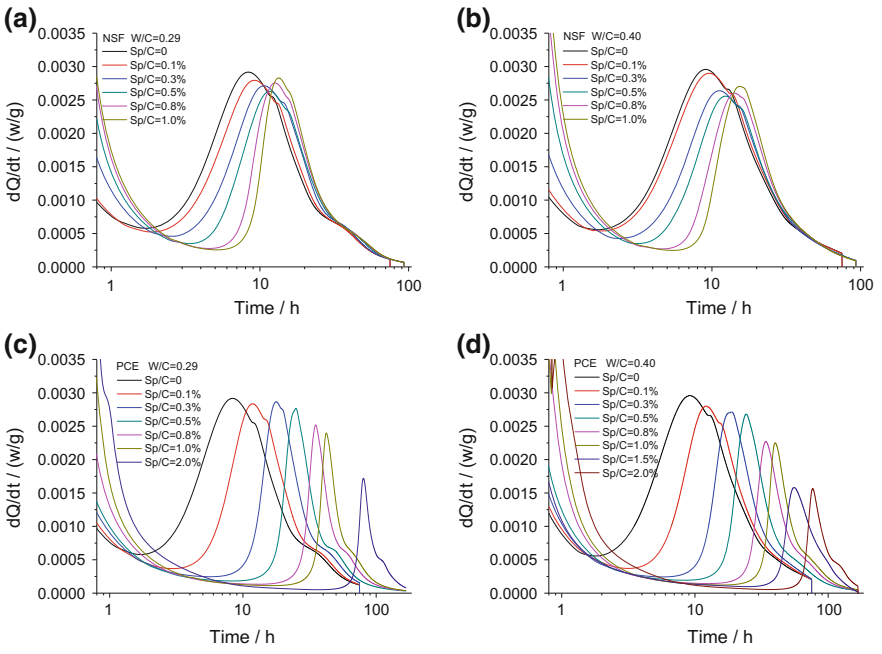

Fig. 5.20 Influences of superplasticizers on heat evolution of cement hydration. **a** NSF, W/C = 0.29, **b** NSF, W/C = 0.40, **c** PCE, W/C = 0.29, **d** PCE, W/C = 0.40

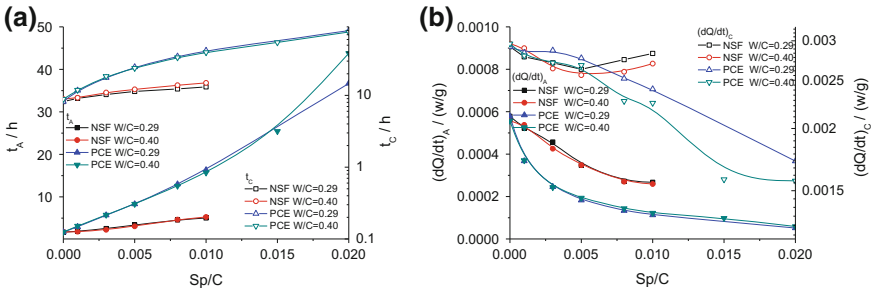

Fig. 5.21 Effects of superplasticizers on cement hydration at varied dosages. **a** Hydration time, **b** hydration rate

heat generation rate during the induction period $(dQ/dt)_A$, the time point of the maximum heat generation rate t_C and the maximum hydration rate $(dQ/dt)_C$ in the acceleration period were extracted and presented in Fig. 5.21, in order to analyze the influences of superplasticizers on the hydration kinetics.

It is noted that NSF and PCE evidently increase the t_A and t_C, and meanwhile reduce the hydration rate $(dQ/dt)_A$ and $(dQ/dt)_C$. Compared with NSF, PCE more significantly prolongs the induction period and depresses the maximum heat generation rate, suggesting that PCE has a marked retardation effect on cement hydration. This can also be explained by the complexation of $–COO^-$ in PCE with Ca^{2+} ions.

5.3.3.2 Temperature

Cement hydration is accelerated at elevated temperatures in term of shortening the induction period and increasing the maximum hydration rate, as exhibited in Fig. 5.22. The early hydration of cement during 2 h at varied temperatures and mixture proportions is presented in Figs. 5.23, 5.24, 5.25, 5.26, 5.27 and 5.28. It is noted that PCE superplasticizer plays an essential role in changing the exothermic rate within 5 min that is related to both hydration and dissolution rate. At a certain temperature, the addition of superplasticizer evidently depresses the exothermic rate in most case, and with the increment of Sp/C, the depression effects are enhanced. However, it is interesting to note that for the FCPs at low W/C, more PCE superplasticizer brings about a higher exothermic rate, which is believed to result from the fact that the better dispersion of cement grains in the aqueous phase provides a larger contact surface area of cement grains with water when PCE is added in the pastes at low W/C. In addition, the effects of temperature on cement hydration are weakened in the case of high superplasticizer dosages, as shown in Fig. 5.29.

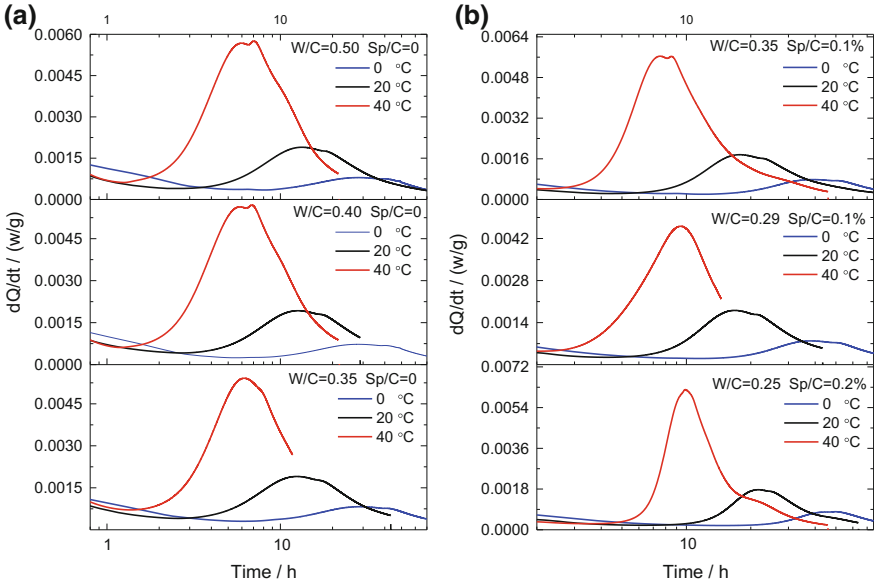

Fig. 5.22 Effects of temperature on cement hydration. **a** Blank FCPs, **b** FCPs with PCE superplasticizer

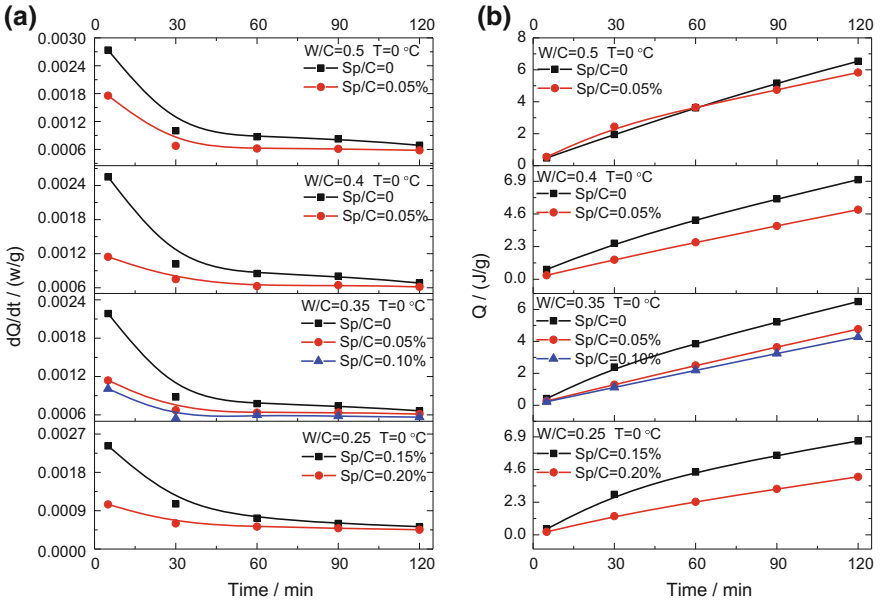

Fig. 5.23 Heat evolution of cement hydration in the FCPs with varied mix proportions at 0 °C. **a** Differential curves, **b** integral curves

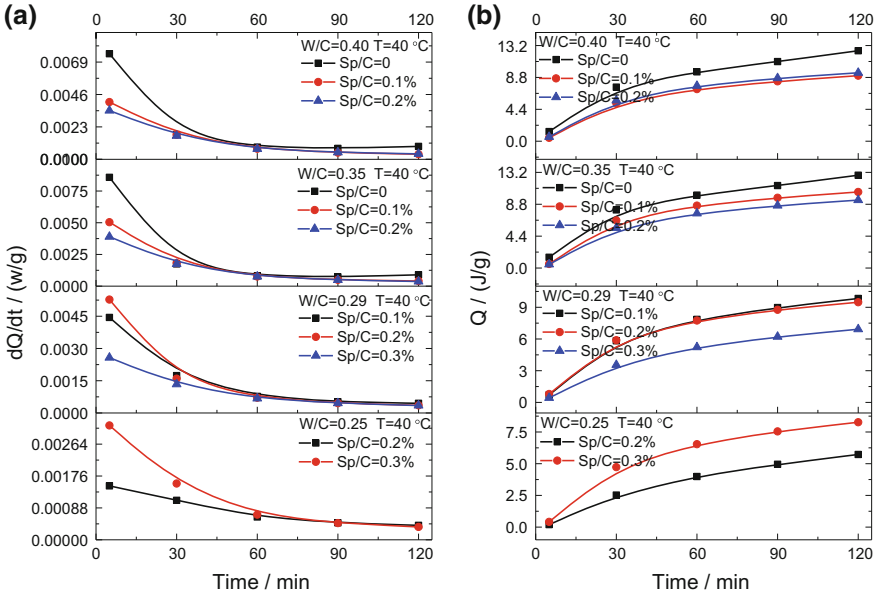

Fig. 5.24 Heat evolution of cement hydration in the FCPs with varied mix proportions at 40 °C. **a** Differential curves, **b** integral curves

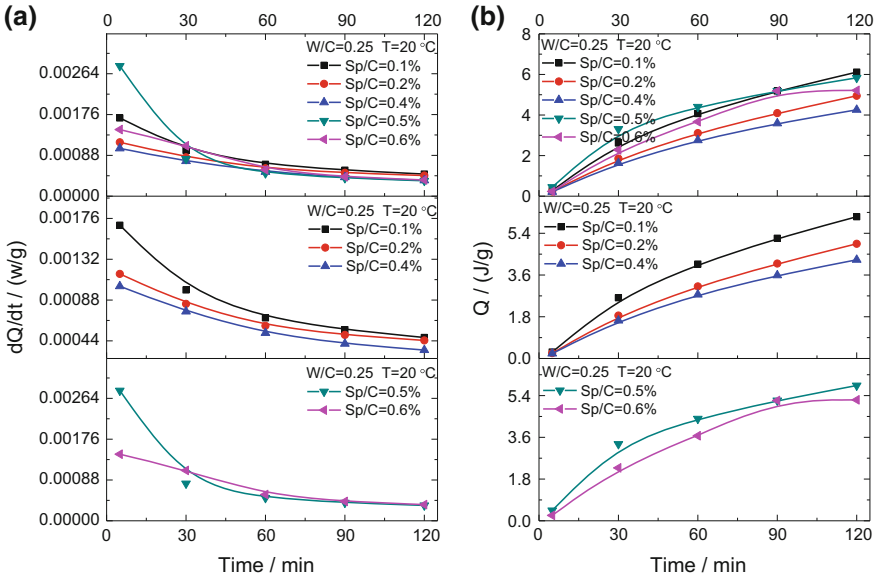

Fig. 5.25 Heat evolution of cement hydration in the FCPs with varied superplasticizer dosages at 20 °C (W/C = 0.25). **a** Differential curves, **b** integral curves

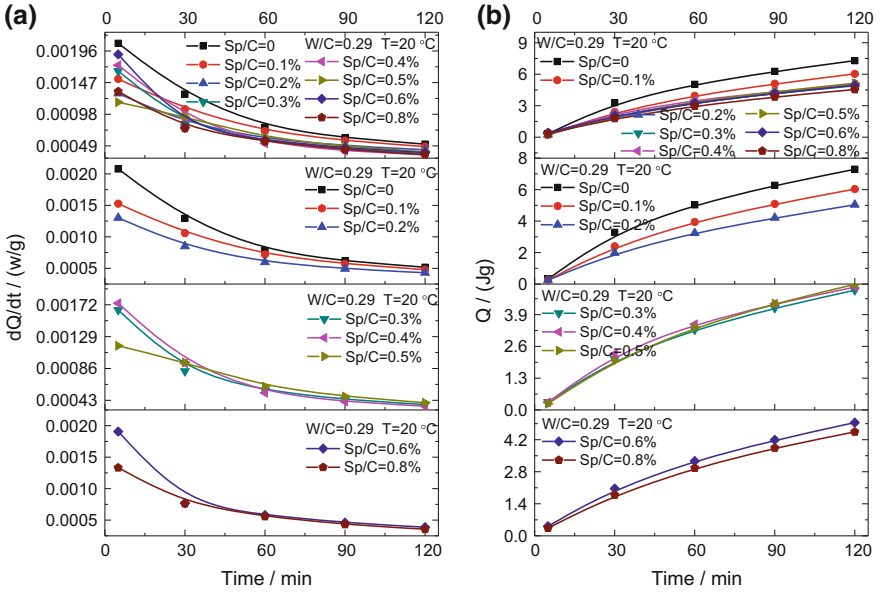

Fig. 5.26 Heat evolution of cement hydration in the FCPs with varied superplasticizer dosages at 20 °C (W/C = 0.29). **a** Differential curves, **b** integral curves

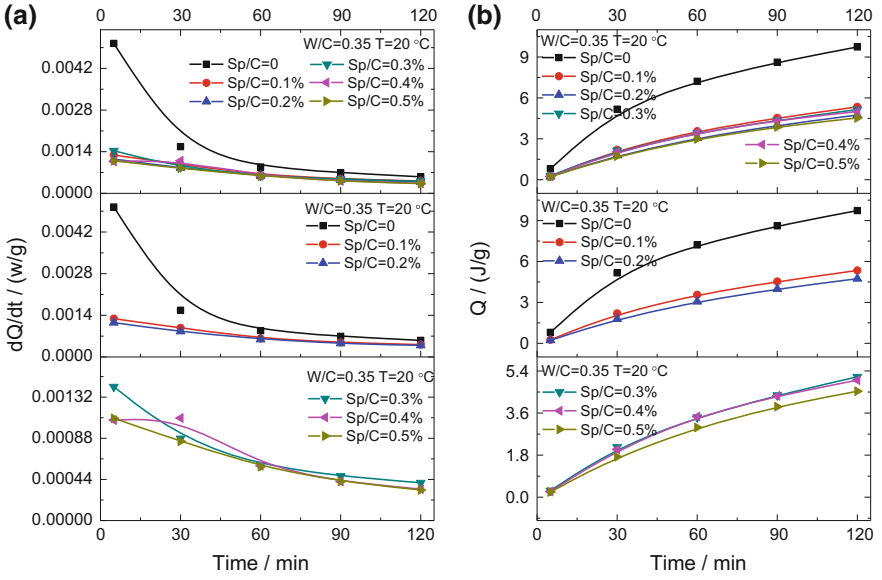

Fig. 5.27 Heat evolution of cement hydration in the FCPs with varied superplasticizer dosages at 20 °C (W/C = 0.35). **a** Differential curves, **b** integral curves

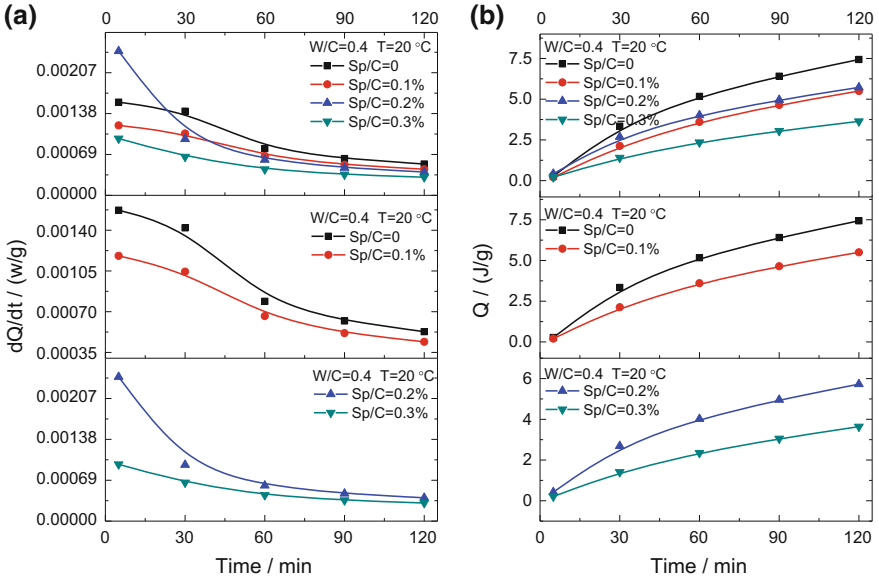

Fig. 5.28 Heat evolution of cement hydration in the FCPs with varied superplasticizer dosages at 20 °C (W/C = 0.40). **a** Differential curves, **b** integral curves

5.3.4 Correlation of Adsorption Behavior with Cement Hydration

By combining the cement hydration of FCPs with the adsorption amounts of superplasticizers, it is not hard to find that beyond the adsorption saturated dosage, cement hydration is little affected by more incorporation of NSF. Similar to the correlation of the adsorption behavior with the dispersing capability of NSF, it is supposed that the effects of NSF on cement hydration are majorly associated with the surface coverage ratio of NSF on cement grains. More specifically, a higher surface coverage ratio leads to a stronger retardation effect on cement hydration. By contrast, for the cement pastes with PCE, hydration is continuously affected by further addition of PCE even though the second adsorption layer has already been saturated. This suggests that besides the factor of the hindered diffusion rate caused by the adsorbed PCE molecule layers (the first and second adsorption layers) on cement grains, there must exist another factor leading to the continuously increasing retardation effect even after the cement surface is fully covered by PCE. As it is known from the adsorption curve in Fig. 5.12, with the growth of PCE dosage in cement paste, the adsorption amount of PCE increases together with the concentration of PCE remaining in the aqueous phase, until the adsorption reaches saturated. After the saturation of the second-layer adsorption, the further added PCE mostly remains in the aqueous phase, which still contributes to the retardation of

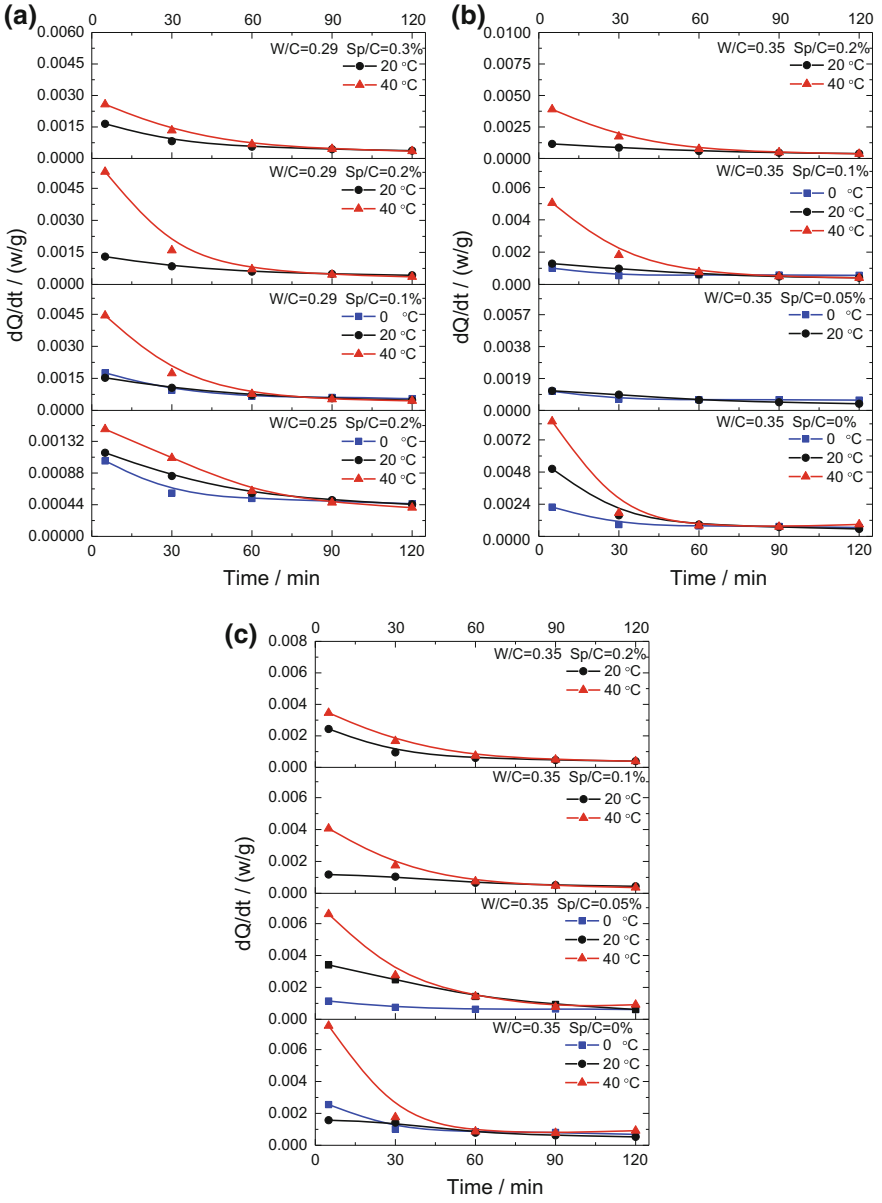

Fig. 5.29 Heat evolution of cement hydration in the FCPs with varied mix proportions and temperatures

cement hydration as seen in Fig. 5.20. This implies that together with the adsorbed PCE on cement surface, the part of PCE presenting in the aqueous phase also plays a very important role in retarding cement hydration. This should be attributed to the

strong complexation effects of $–COO^-$ groups in the PCE molecules with Ca^{2+} which is one of the key components determining the hydration kinetics. This phenomenon that polymers containing $–COO^-$ groups form complexes with Ca^{2+} ions has been experimentally verified in Sect. 5.1. The formation of the complexes of PCE molecules with Ca^{2+} in solution can be proposed as a possible reason to explain the fact that the PCE molecules remaining in the aqueous phase contribute to the retardation effect on cement hydration, which is in line with the literature (Ran et al. 2009), where it was reported that the retardation effect of PCE was proportional to the concentration of ionic functional groups remaining in the aqueous phase.

An elevated temperature leads to a higher hydration rate. In the presence of superplasticizers at low dosages, the effects of temperature on the hydration rate are significant due to the low adsorption amount. At high dosages, sufficient adsorption on cement surface effectively depresses the cement hydration even at elevated temperatures. Meanwhile, the ample PCE molecules remaining in the aqueous phase at high Sp/C inhibit the nucleation of hydrates to a large extent by chelating the Ca^{2+}. As a result, effects of temperature on the hydration rate are weakened, namely, weaker temperature sensitivity.

5.3.5 *Correlation of Cement Hydration with Fluidity Retention*

When we compare the cement hydration with the fluidity retention of FCPs at varied mixing proportions in Sect. 3.1, it is found that the fluidity retention is mainly dependent on cement hydration. Specifically, lower hydration rate corresponds to stronger fluidity retention while weaker temperature sensitivity of hydration rate results in slight temperature effects on the fluidity retention. Hence, the fluidity retention of FCPs could by enhanced from two aspects: decreasing temperature and increasing the superplasticizer dosage, both of which could affect the cement hydration to a certain extent. Compared to NSF, PCE superplasticizer presents stronger retardation effects on cement hydration and consequently, the FCPs with PCE have stronger fluidity retention capability than those with NSF at the same dosage.

5.4 Cement-Latex-Water System

The effects of polymer latexes with submicron size on the rheological properties are quite different from the superplasticizers of nanometer based on the previous results although they could also be adsorbed on the surface of cement grains. In this section, the adsorption behaviors of the two latexes L1 and L2 and their impacts on

cement hydration were comparatively investigated. Besides, the working mechanism of chemical admixtures with submicron size was then disclosed by establishing the correlation of fluidity of FCPs with their adsorption and retardation effects.

5.4.1 Correlation of Adsorption and Initial Fluidity

The adsorption of latexes bearing anionic groups on cement grains is bound to cause the reduction of the zeta potential of cement paste, as exhibited in Fig. 5.30. With the growth of latex dosage, the zeta potential of FCPs decreases initially and then begins to rise at the dosage of 1% for L1 and 3% for L2 respectively. Testing results show that the zeta potential of pure latex L1 and L2 at mass concentration of 24% in the aqueous phase (corresponding to L/C = 12%, W/C = 0.5) is −8.1 and −12.0 mV, and the zeta potential respectively drops to −16.9 and −23.1 mV at mass concentration of 6% in the aqueous phase (corresponding to L/C = 3%,

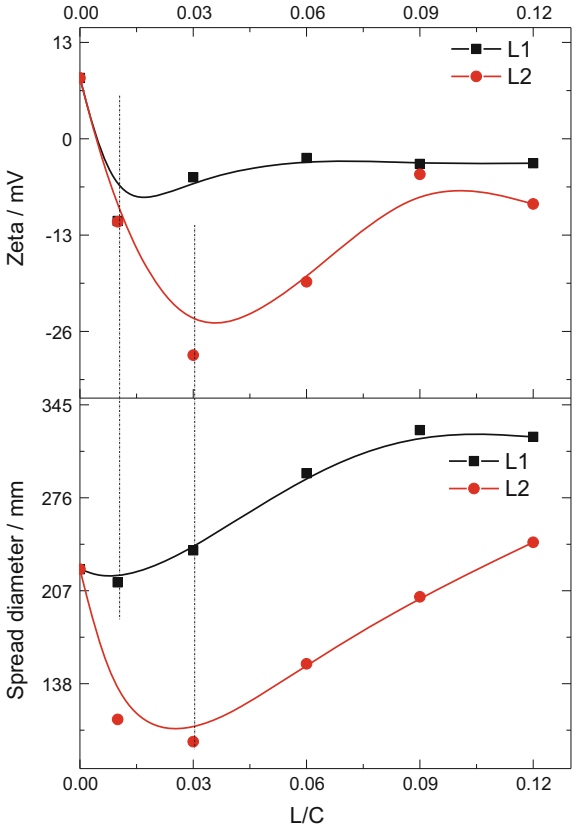

Fig. 5.30 Correlation of the fluidity of FCPs with the adsorption behaviors of polymer latexes on cement surface

W/C = 0.5). The zeta potential of blank FCP at W/C of 0.5 is +8.2 mV. For the FCPs containing latexes, the zeta potential is determined by both cement grains and polymer particles. At low L/C, the zeta potential of cement pastes is dominated by the cement grains. Hence the adsorption of latexes causes a decrement of zeta potential. At high L/C, the zeta potential of the pastes is mainly provided by the polymer latexes and then the zeta potential gradually increases with the increasing L/C.

By combining the zeta potential with the initial fluidity, it is interesting to note that the initial fluidity reaches the minimum values at the lowest zeta potential. Literatures indicate that particles tend to form the largest flocculated structures in the suspension dispersion system with zeta potential of 0 mV. In such way, the adsorption of polymer particles on cement surface at low dosages causes the decrease of zeta potential of the cement grains to 0 mV from the initial value of +8.2 mV, and further facilitates the formation of flocculated structures. In that case, the initial fluidity of the FCPs is lowest. At this moment, the very negative zeta potential of FCPs is provided by the latexes particles bearing anionic groups. Subsequently, the zeta potential increases with the further addition of latexes, which is dependent on the relationship between the latex concentration and zeta potential. The aforementioned working mechanism of latex provides a new sight into understanding the distinct impacts of various latexes on the rheological properties of fresh cement pastes.

5.4.2 *Correlation Between Cement Hydration and Fluidity Retention*

Similar to superplasticizers, the adsorbed polymer particles in latexes on the surface of cement grains could also hinder the diffusion of water and ions at the cement-solution interface and thereby retarding the cement hydration. As exhibited in Fig. 5.31, the addition of latexes induces a prolonged induction period and a lowered maximum exothermic rate in the acceleration period of the cement hydration. A higher latex dosage leads to a stronger retardation effect. As the dosage of L1 is up to 12%, the main exothermic peak is significantly delayed and decreased, the shoulder peak caused by the transformation of Aft to Afm seems to become the main peak. From the heat evolution curves in Fig. 5.31, various parameters were extracted and listed in Table 5.5. With the growth of latex dosage, the induction period t_A is gradually increased, and the heat generation rate $(dQ/dt)_A$ is visibly descended with a slight fluctuation of $(dQ/dt)_A$ at low dosages. Moreover, a sharply reduced K_{A-C} is found at high L/C, indicating that the presence of latex hinders the nucleation of C–S–H at early stage. Lower $(dQ/dt)_C$ and larger Q_{A-C} mean that the total nuclei number is significantly reduced by adding the latexes. Compared to the latex L2, L1 presents a stronger retardation effect on cement

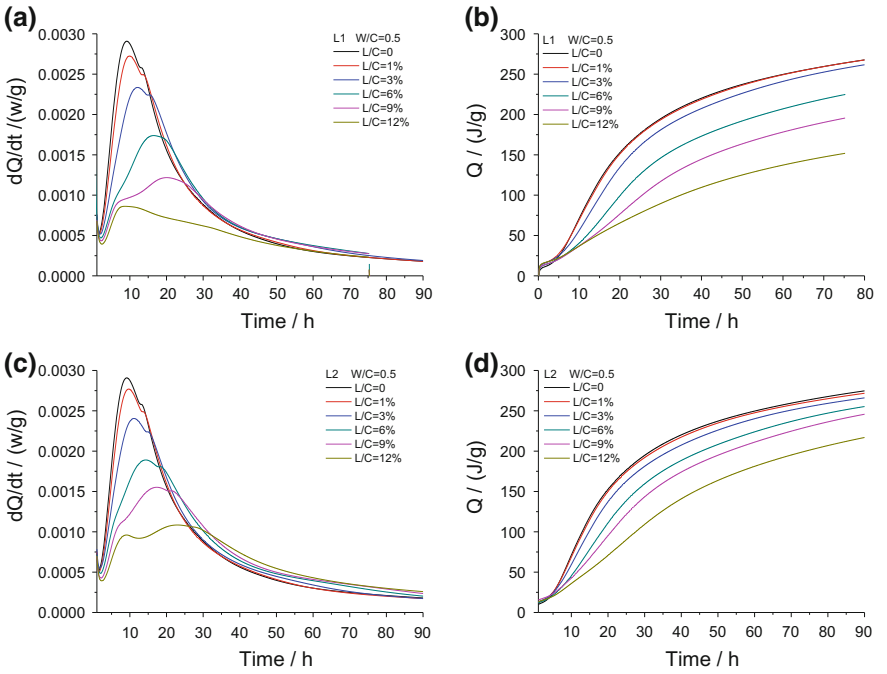

Fig. 5.31 Effects of polymer latexes on cement hydration. **a** Differential curves, L1, **b** integral curves, L1, **c** differential curves, L2, **d** integral curves, L2

Table 5.5 Parameters of cement hydration extracted from the calorimetry curves of blank cement paste and the cement pastes containing polymer latexes

Latex	L/C (%)	t_A/h	$(dQ/dt)_A$ (W/g)	Q_A (J/g)	K_{A-C} [W/(g·h)]	$(dQ/dt)_C$ (W/g)	Q_{A-C} (J/g)
L1	0	1.529	5.172E−04	11.158	3.662E−04	2.910E−03	48.618
	1	1.655	5.168E−04	16.196	3.097E−04	2.720E−03	47.862
	3	1.973	5.185E−04	16.659	2.186E−04	2.330E−03	51.643
	6	2.098	4.696E−04	14.582	1.147E−04	1.740E−03	59.114
	9	2.174	4.339E−04	14.813	6.200E−05	1.220E−03	58.891
	12	2.377	3.927E−04	17.581	5.903E−05	8.617E−04	15.309
L2	0	1.529	5.172E−04	11.158	3.662E−04	2.910E−03	48.618
	1	1.571	4.949E−04	13.680	3.247E−04	2.770E−03	48.679
	3	1.862	5.520E−04	14.874	2.467E−04	2.400E−03	49.038
	6	1.980	4.856E−04	13.768	1.600E−04	1.890E−03	55.591
	9	2.142	4.273E−04	17.380	1.010E−04	1.550E−03	57.709
	12	2.310	3.928E−04	15.403	9.738E−05	1.080E−03	59.371

hydration, which is related to its smaller particle size, higher adsorption amounts on cement surface and a larger number of carboxyl groups in the emulsifier.

The correlation of fluidity retention with cement hydration in the Cement-Latex-Water system is consistent with that in the Cement-Superplasticizer-Water system. Specifically, the addition of latexes retards cement hydration and thus enhances the fluidity retention. A higher dosage of latexes leads to a more significant retardation effect and eventually stronger fluidity retention of FCPs. At the same dosage, L1 has larger retardation effects than L2, so that the FCPs with L1 present stronger fluidity retention than those with L2.

5.5 Cement-Asphalt-Water System

The adsorption and coverage of asphalt particles on cement surface as well as the microstructural evolution of CA pastes have been observed under microscopes in Chap. 4. However, different from superplasticizers and latexes, particle size of microns in asphalt emulsions also plays an essential role in changing the rheological properties of FCPs, especially at high dosages.

5.5.1 Correlation Between Adsorption and Initial Fluidity

On the basis of the adsorption mechanism discussed in Sect. 5.1, it is known that either anionic asphalt or cationic asphalt emulsion can be selectively adsorbed on the surface of mineral phases and hydrates, and their adsorption amounts are proportional to their dosages in the CA pastes. Correspondingly, the initial fluidity increases with the addition of asphalt emulsions. As the dosage is larger than 35%, the initial fluidity begins to drop due to the increased volume fraction of solid phases. On the other hand, because of the predominant positive charges on cement surface, the adsorption amount of anionic asphalt particles is larger than that of the cationic ones. Thus, the CA pastes with anionic asphalt emulsion present visibly higher initial fluidity.

5.5.2 Correlation Between Cement Hydration and Fluidity Retention

5.5.2.1 Effects of Asphalt Emulsion on Cement Hydration

The coverage of asphalt membrane on cement surface may lead to a strong retardation effect on cement hydration. This effect was confirmed by measuring the semi-adiabatic temperature development of the CA paste during setting, as shown in Fig. 5.32. The temperature peak is markedly delayed with the increase in asphalt

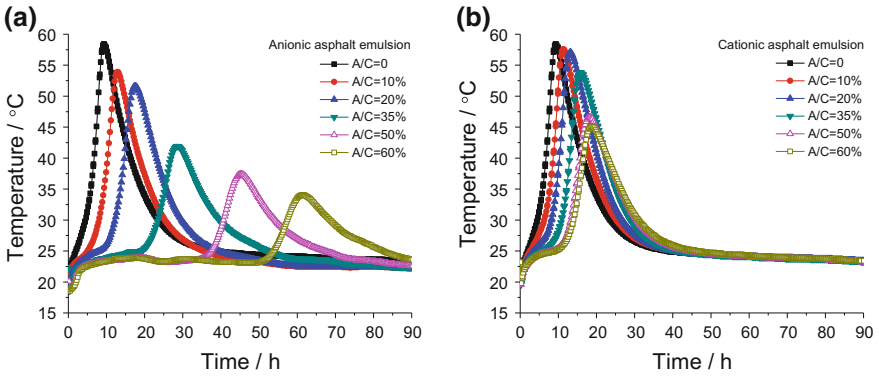

Fig. 5.32 Semi-adiabatic temperature development of CA pastes during setting at 20 °C. **a** CA pastes with anionic asphalt emulsion, **b** CA pastes with cationic asphalt emulsion

content for both CA pastes with anionic and cationic asphalt emulsions, indicating that the addition of the asphalt emulsion slows down cement hydration. The greater the amount of asphalt emulsion added, the more noticeable the retardation effects. Consequently, for the CA pastes with high asphalt contents, the growth of the yield stress over time is low. Figure 5.32 also shows that the addition of anionic asphalt emulsion leads to a more significant retardation effect than that observed in cationic asphalt emulsion in the fresh CA pastes. On the basis of the results presented in Sect. 5.1, we infer that the stronger retardation effects of anionic asphalt emulsion than cationic asphalt emulsion are closely related to the higher adsorption amount and the chelation of Ca^{2+} in solution with the anionic surfactant contained in an anionic asphalt emulsion.

5.5.2.2 Effects of Temperature on Cement Hydration

The semi-adiabatic temperature developments for the different CA pastes under varied environmental temperatures are shown in Fig. 5.33 to illustrate cement hydration behaviors under different environmental temperatures. At a fixed dosage, elevated temperatures lead to the shortened induction period and lower hydration rate. With the increments of A/C, the temperature sensitivity of hydration rate is reduced. For the CA pastes with anionic asphalt emulsion, the effects of temperature on hydration rate are lower, i.e., weaker temperature sensitivity (Zhang et al. 2010).

5.5.2.3 Correlation Between Cement Hydration and Fluidity Retention

Similar to the latexes, asphalt emulsions could significantly retard cement hydration and thus enhance the fluidity retention of FCPs. A higher dosage of asphalt

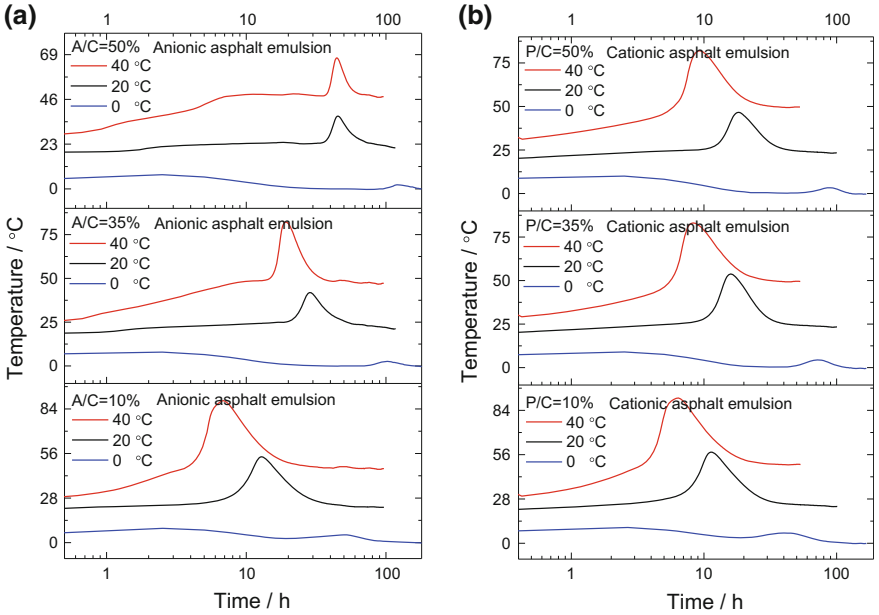

Fig. 5.33 Semi-adiabatic temperature development of CA pastes with different asphalt contents during setting at 0, 20 and 40 °C. **a** CA pastes with anionic asphalt emulsion, **b** CA pastes with cationic asphalt emulsion

emulsion leads to a more significant retardation effect and eventually stronger fluidity retention. At the same dosage, anionic asphalt emulsion has larger retardation effects than cationic one, so that the CA pastes with anionic asphalt emulsion present stronger fluidity retention than those with cationic one.

Different from the Cement-Superplasticizer-Water system, Cement-Asphalt-Water system presents obvious temperature sensitivity of fluidity retention at high asphalt dosages, which is due to the instability of asphalt emulsion at elevated temperatures. That is to say, the fluidity retention of CA pastes is determined mainly by two factors: cement hydration and the stability of asphalt emulsion. For the CA pastes with cationic asphalt emulsion, both the instability of the cationic asphalt emulsion at high temperatures and the weak retardation effects on cement hydration are responsible for the higher temperature sensitivity of fluidity retention.

5.6 Summary

In this chapter, three organic monomers possessing different charging groups and their corresponding homo-polymers as well as two series of self-synthesized comb-shaped co-polymers with varied charging groups in the backbone were

chosen to analyze the essence of adsorption and retardation of polymers. Furthermore, the working mechanisms of superplasticizers, latexes and asphalt emulsions on rheological properties of FCPs were disclosed fundamentally from the viewpoints of adsorption behaviors and retardation effects.

(1) The adsorption of organics on cement surface is closely related to both the charge density of the organics and the entropic loss upon adsorption. In the premise of the same dosage of charging groups, organic monomers AA, SSS and MAPTAC do not show visible adsorption on cement surface whilst the corresponding homo-polymers PAA, PSSS and PMAPTAC are able to be adsorbed on cement surface to different extents. The adsorption is driven mainly by the electrostatic attraction forces between the polymers and cement grains and the complexation effects of $–COO^-$ in polymers with Ca^{2+} ions. The adsorption ratios of anionic polymers are higher than 60% whilst only a minor part of cationic polymer is adsorbed, which is related to the fact that the positively charged aluminate hydrates are dominant in an early hydrating cement paste. The adsorption amount of PAA is higher than PSSS due to the complexation effects of $–COO^-$ with Ca^{2+}. On the other hand, the retardation effects of organics on cement hydration are determined by the adsorption on cement surface and the complexation effects. No retardation was observed for the monomers while for their corresponding homo-polymers, the retardation effects are in the order of PAA > PSSS > PMAPTAC.

(2) For the comb-shaped co-polymers, the charge characteristics of the main chain also strongly determine their adsorption behaviors and retardation effects, in the order of $–COO^- > –SO_3^- > \equiv N^+–$. Specifically, both the adsorption capacity and retarding effects of co-polymers with negative charges are stronger than those with positive charges. With the increasing molar ratio of cationic charges to anionic charges in the co-polymers, notable decreases in adsorption amounts and lower retardation effects are observed. On the other hand, in the premise of the same negative charge density, the co-polymers with more carboxyl groups show stronger impacts in term of adsorption on cement surface and retardation on cement hydration.

(3) NSF exhibits a typical mono-layer adsorption on cement surface. The enhancement of initial fluidity of FCPs and the retardation effects on cement hydration by the addition of NSF in cement pastes are directly related to its coverage on cement surface while the fluidity retention of FCPs is determined by the hydration rate. After full coverage, namely the saturation of the adsorption on cement grains, the initial fluidity of FCPs, the retardation effects and the fluidity retention reach maximum.

(4) PCE presents a multi-layer (double-layer) adsorption on cement surface. The increase of the fluidity of FCPs in the presence of PCE is proportional to the surface coverage of the first adsorption layer and the second layer does not contribute to the enhancement of the fluidity of FCPs especially at high W/C. Both the adsorbed PCE and the PCE remaining in the aqueous phase actively

participate in retarding cement hydration. A higher superplasticizer dosage leads to a lower hydration rate and thus stronger fluidity retention of FCPs.

(5) At low dosage of latexes (<3%), the adsorption of polymer particles on cement surface promotes the formation of a large amount of flocculated structures due to its neutralizing effects. Thus, the initial fluidity decreases at low L/C. With further addition of latexes, more coverage of latex particles on cement surface brings about better dispersion of cement grains and hence higher initial fluidity of FCPs. Moreover, the presence of latexes in the pastes brings about significant retardation on cement hydration and thereby stronger fluidity retention of FCPs. Compared to L2, L1 with smaller size could effectively increase the initial fluidity and the fluidity retention of FCPs due to its larger adsorption amount on cement surface.

(6) The adsorption and coverage of asphalt particles of microns on cement surface lead to an increment of initial fluidity at low dosages. However, the initial fluidity begins to decrease because of the increased volume fraction of the solid phases. The fluidity retention of the CA pastes over time is visibly improved by the increase of asphalt content due to its retardation effects on cement hydration. In comparison with cationic asphalt emulsion, anionic asphalt emulsion more strongly increases the fluidity of the CA pastes and retards cement hydration because of its favorable adsorption onto the surface of cement grains.

(7) The effects of temperature on the initial fluidity of FCPs are dependent on the adsorption amount of chemical admixtures on cement surface. Specifically, a larger adsorption amount at elevated temperatures corresponds to lower temperature sensitivity. For Cement-Superplasticizer-Water system, the temperature sensitivity of fluidity retention is only determined by the cement hydration. Namely, the accelerated hydration at elevated temperatures leads to weaker fluidity retention while the effects of temperature are reduced at high superplasticizer dosages due to the enhanced retardation effects. For the other systems, both the cement hydration and the stability of latexes or asphalt emulsions are responsible for temperature sensitivity of fluidity retention of FCPs.

References

Aligizaki KK (2005) Pore structure of cement-based materials: testing, interpretation and requirements. CRC Press, Boca Raton

Banfill PFG, Bowen P, Flatt RJ et al (2007) Improved superplasticisers for high performance concrete: the SUPERPLAST project. Abstract CD ROM of the 12th international congress on the chemistry of cement, Montreal, Canada, 8–13 July

Burgos-Montes O, Palacios M, Rivilla P et al (2012) Compatibility between superplasticizer admixtures and cements with mineral additions. Constr Build Mater 31(6):300–309

Dukhin AS, Goetz PJ (2010) Characterization of liquids, nano-and microparticulates, and porous bodies using ultrasound. Elsevier, Amsterdam

Ferrari G, Cerulli T, Clemente P et al (2000) Influence of carboxylic acid-carboxylic ester ratio of carboxylic acid ester superplasticizer on characteristics of cement mixtures. ACI Spec Publ 195:505–520

George O (1991) Principles of polymerization, 4th edn. Wiley, New York

Hirsch CM (2005) Untersuchung zur wechselwirkung zwischen polymeren fliessmitteln und zementen bzw. Mineralphasen der frühen zementhydratation. Technischen Universität München, München, p 3

Hsu KC, Chiu JJ, Chen SD et al (1999) Effect of addition time of a superplasticizer on cement adsorption and on concrete workability. Cement Concr Compos 21(5):425–430

Kong XM, Lu ZB, Shi J et al (2012) Impacts of phosphoric acid and phosphates on hydration kinetics of portland cement. J Chin Ceram Soc 40(11):1553–1558 (in Chinese)

Krstulović R, Žmikić A, Dabić P (1994) Examination of reaction between the NSF superplasticizer and cement. Cem Concr Res 24(5):948–958

Mollah MYA, Adams WJ, Schennach R et al (2000) A review of cement-superplasticizer interactions and their models. Adv Cem Res 12(4):153–161

Moro F, Böhni H (2002) Ink-bottle effect in mercury intrusion porosimetry of cement-based materials. J Colloid Interface Sci 246(1):135–149

Peng J, Qu J, Zhang J et al (2005) Adsorption characteristics of water-reducing agents on gypsum surface and its effect on the rheology of gypsum plaster. Cem Concr Res 35(3):527–531

Plank J, Gretz M (2008) Study on the interaction between anionic and cationic latex particles and Portland cement. Colloids Surf A 330(2):227–233

Plank J, Hirsch C (2007) Impact of zeta potential of early cement hydration phases on superplasticizer adsorption. Cem Concr Res 37(4):537–542

Plank J, Sachsenhauser B (2006) Impact of molecular structure on zeta potential and adsorbed conformation of Alpha-allyl-Omega-methoxypolyethylene glycol-maleic anhydride superplasticizers. J Adv Concr Technol 4(2):233–239

Plank J, Sachsenhauser B (2009) Experimental determination of the effective anionic charge density of polycarboxylate superplasticizers in cement pore solution. Cem Concr Res 39(1):1–5

Plank J, Winter C (2008) Competitive adsorption between superplasticizer and retarder molecules on mineral binder surface. Cem Concr Res 38(5):599–605

Pourchet S, Comparet C, Nicoleau L et al (2007) Influence of PC superplasticizers on tricalcium silicate hydration. In: Proceedings of the 12th international congress on the chemistry of cement, Montreal, Canada, 8–13 July

Pourchet S, Comparet C, Nonat A, et al (2006) Influence of three types of superplasticizers on tricalciumaluminate hydration in presence of gypsum. In: Proceedings of the 8th CANMET/ACI international conference on superplasticizers and other chemical admixtures in concrete, Sorrento, pp 151–158

Ran Q, Somasundaran P, Miao C et al (2009) Effect of the length of the side chains of comb-like copolymer dispersants on dispersion and rheological properties of concentrated cement suspensions. J Colloid Interface Sci 336(2):624–633

Scrivener KL, Nonat A (2011) Hydration of cementitious materials, present and future. Cem Concr Res 41(7):651–665

Yamada K, Takahashi T, Hanehara S et al (2000) Effects of the chemical structure on the properties of polycarboxylate-type superplasticizer. Cem Concr Res 30(2):197–207

Yoshioka K, Tazawa E, Kawai K et al (2002) Adsorption characteristics of superplasticizers on cement component minerals. Cem Concr Res 32(10):1507–1513

Zhang YR, Kong XM, Cao EX (2010) Influence of temperature on flowability and hydration rate of fresh cement asphalt binder. J Chin Ceram Soc 38(11):156–161 (in Chinese)

Chapter 6
Microstructure Model and Rheological Model of Fresh Cement Pastes

Various chemical admixtures are practically used to modify the rheological properties of FCPs through changing the microstructure of FCPs and impacting the interactions of cement grains (Banfill et al. 2007; Ferrari et al. 2010; Kauppi et al. 2003; Roncero et al. 2002). That is to say, it is the proper modification on the microstructure and interactions that are the key for achieving the desired rheological properties of FCPs. Although the variations of rheological properties of FCPs with varied mix proportions and environment factors have been well documented (Golaszewski and Szwabowski 2004; Kong et al. 2013; Sheinn et al. 2002), their corresponding microstructures are poorly investigated and only a few studies on FCPs without chemical admixtures are found in the literatures (Autier et al. 2013; Flatt and Bowen 2006; Wang et al. 2008a, b, 2013; Zhang et al. 2013).

In this chapter, based on the real microstructure of multi-sized particle suspensions observed in Chap. 4 and the working mechanism of chemical admixtures revealed in Chap. 5, a generic multi-scale microstructure model of FCPs in the presence of chemical admixtures at the initial time was established. Furthermore, taking into account the evolution essence of rheological properties, two models to describe the evolution of the rheological parameters were developed by introducing a relative hydration degree α', which integrated the effects of mix proportion, elapsed time and environmental temperature on the rheological properties. Finally, based on the above models, two equations to roughly predict the yield stress and the plastic viscosity of FCPs incorporating Sp/C, W/C, temperature and time as variables were deduced in order to quantitatively reflect the correlation of microstructure with the key rheological parameters of FCPs.

Y. Zhang, *Study on Microstructure and Rheological Properties of Cement-Chemical Admixtures-Water Dispersion System at Early Stage*, Springer Theses, DOI 10.1007/978-981-10-4570-7_6

6.1 Microstructure Model of Fresh Cement Pastes

Based on the real microstructure of multi-sized cement particle suspensions as well as the working mechanism of chemical admixtures, conceptual models of Cement-Superplasticizer-Water, Cement-Latex-Water and Cement-Asphalt-Water systems were proposed. In particular, for Cement-Superplasticizer-Water system, the volume of four types of water in the pastes and the volume fraction of solid phase at varied W/Cs and superplasticizer dosages were calculated and then a microstructure model of FCPs with superplasticizers at any mix proportion was established.

6.1.1 Cement-Water System

The organization structure of cement grains at varied dispersion media has been observed in previous chapters. Thus, the microstructure of blank FCPs at varied dispersion media could be schematically illustrated as in Fig. 6.1. In air, the association of small particles (S-S structures) and the agglomeration of small particles sticking to larger ones (L-S structures) are the main dispersed phases. In ethanol, there is no dissolution of the mineral phases or any reaction, and cement grains present majorly individual particles and a small amount of L-S structures, shown in Fig. 6.1b. In water, ample flocculated structures of different sizes that entrap a great deal of water (i.e., EW), together with few individual cement grains, are dispersed in the free water (FW). The edge of each cement grain is blurry and spinous due to the early hydration and the existence of adsorption water (AW). When cement powder is dispersed in the ethanol-water solution, flocculated structures with larger size than those in water are observed.

6.1.2 Cement-Superplasticizer-Water System

6.1.2.1 Hypothesis and Deduction

It has been proved by rheology theory that a suspension dispersion system fails to flow unless the volume fraction of solid phase ϕ is low than ϕ_M that denotes the volume fraction at geometrical maximum packing of solid phase (Frankel and Acrivos 1967; Flatt and Bowen 2006, 2007; Krieger and Dougherty 1959; Probstein et al. 1994). If the solid phase in a suspension system is mono-sized spherical particles, ϕ_M is 0.74. For poly-sized spherical particles, ϕ_M typically falls between 0.8 and 0.94, which is mainly determined by the particle size distribution of solid phase (Kapur et al. 1997; Krieger 1972). In the case of solid particles with irregular shape, ϕ_M is lowered due to the overlapped of particles as well as the

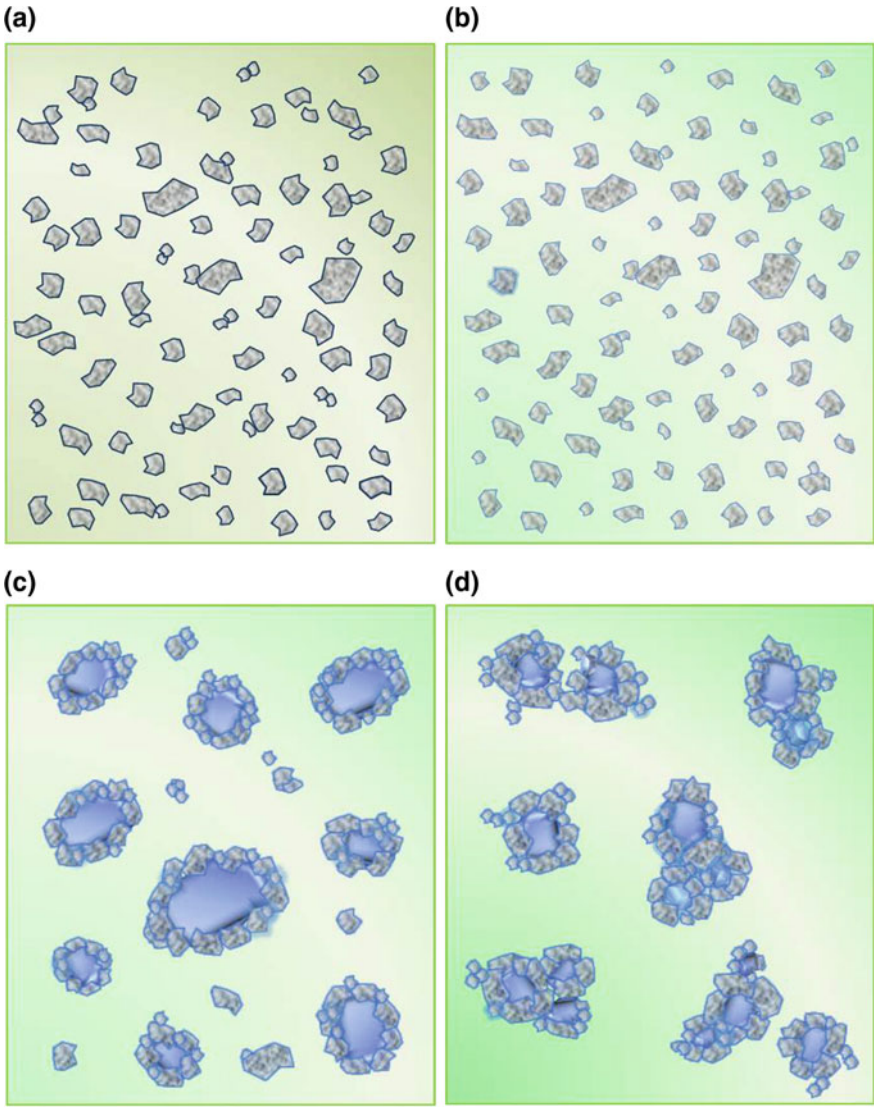

Fig. 6.1 Microstructure model of cement grains in varied dispersion media. **a** Air, **b** ethanol, **c** water, **d** ethanol and water

effects of long to diameter ratio of the particles (Zhou et al. 1995). Struble and Sun (1995) found ϕ_M was in the vicinity of 0.7 for the pastes with superplasticizers and was a little higher than that for the blank pastes. This indicates that the addition of superplasticizers does not cause any significant changes on the particle size distribution of solid phase despite that the flocculated structures have been broken into dispersed cement grains. This is consistent with the microstructure results of cement

suspensions provided by the morphologi G3 that the mean particle size of suspension decreases to 3.86 μm from the 8.09 μm of blank one whereas the standard deviations of particle size distribution for the suspensions without and with superplasticizers are quite close, varying from 1.05 to 1.09. Therefore, it is acceptable if we assume the ϕ_M of all the FCPs in this research was 0.7.

Based on the above assumptions, the microstructure of FCPs could be simplified as below:

(1) Since the hydration degree in the first few minutes is rather low, the content of HW could be neglected in the FCPs. Thus, the dispersion phase in the FCPs is composed of AW, EW, cement grains including the individual ones and those in the flocculated structures, while FW functions as the dispersion medium. The volumes of dispersion phase and dispersion medium are denoted as V_1 and V_{FW}, as shown in Fig. 6.2.

(2) When the dispersion phase is in the state of geometrical maximum packing, the pore volume among these packing particles V_{pore} could be obtained by the formula:

$$V_{pore} = V_1 \frac{1 - \phi_M}{\phi_M}. \tag{6.1}$$

(3) If $V_{FW} > V_{pore}$, free water could not only fill with the pore volume among the packing particles but also disperse these particles, which means the paste is able to flow.

Based on the discussions in Sect. 3.1, it is believed that FW plays a key role in affecting the rheological behavior of FCPs. According to the origins of these types of water, it is hypothesized that the water in FCPs appears in the chronological

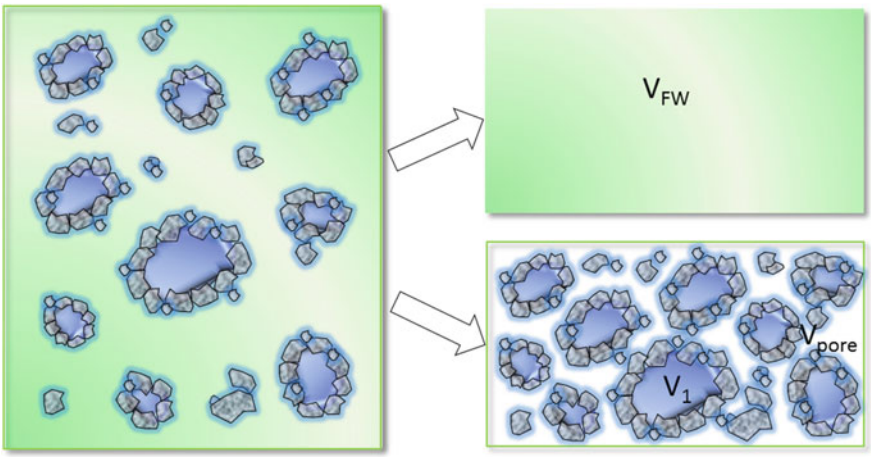

Fig. 6.2 Schematic drawing of fresh cement paste

order of AW > EW > FW when the W/C of the pastes gradually ascends. Specifically, with the increase of W/C, AW first appears and its content gradually grows. When the adsorption of water on the cement surface is saturated, the content of AW reaches to a maximum value. With the further increase of W/C, EW emerges in the pastes and its content gradually ascends to a maximum value. After that, FW could be found in the FCPs. Such way, the content of FW i.e., V_{FW} could be calculated on the basis of the following two critical phenomena found in the fluidity curves in Fig. 3.1.

(1) FCP-1 at W/C of 0.15 with overdosed PCE superplasticizer

In this case, the paste fails to flow, i.e., spread diameter is lower than 80 mm, but a slight increase in W/C enables the paste to flow. This indicates that V_{FW} in the FCP-1 is close to V_{pore}. Because almost all the flocculated structures have been completely disassembled in the presence of excessive superplasticizer expect for some strongly bonded ones, the dispersion phase in FCP-1 consists of all the cement grains, AW and remaining EW in the strongly bonded ones which is marked as REW. If the cement volume $V_C = m_C/\rho_C = 1$, then

$$\begin{cases} \frac{m_{FW}}{\rho_W} = V_{FW} \approx V_{pore} = \left(\frac{m_c}{\rho_c} + \frac{m_{AW+REW}}{\rho_w}\right) \cdot \frac{1-\phi_M}{\phi_M} \\ m_{FW} + m_{AW+REW} = m_W = \frac{W}{C} \cdot m_c = \frac{W}{C} \cdot \rho_c \end{cases} \tag{6.2}$$

where W/C = 0.15, ρ_c = 3.16 g/cm^3, ρ_w = 1.00 g/cm^3, so we get $m_{AW+REW} = V_{AW+REW} = 0.03$, $m_{FW} = V_{FW} = 0.44$. Here, it is needed to emphasize that AW reflects the adsorption capability of cement to water, which is related to cement type, so the maximum volume of AW is constant irrespective of W/C and Sp/C. On the other hand, the volume of REW is determined by the dispersion capability of superplasticizers. Superplasticizers with stronger dispersion capability lead to a lower volume of REW. In this research, only one type of superplasticizer was used, so the volume of REW is fixed. Therefore, the maximum value of V_{AW+REW} in any FCP will stay stable. Based on the assumptions on the appearance order of different types of water, it is believed that the existence of FW in the FCP-1 indicates the content of AW has already reached to the maximum value. Accordingly, it is concluded that the maximum value of V_{AW+REW} is 0.03.

Furthermore, if all mixing water is existing as adsorbed water, namely there is no EW and FW in the FCPs, we get,

$$\begin{cases} m_{AW} = m_W = \frac{W}{C} \cdot m_c = 3.16\frac{W}{C} \\ m_{AW} + m_{REW} = V_{AW} + V_{REW} \le 0.03 \end{cases} \tag{6.3}$$

It could be deduced that W/C $\le$ (0.03 − V_{REW})/3.16 = 0.01 − V_{REW}/3.16. That is to say, once W/C is larger than 0.01, EW could be found in the FCPs.

(2) FCP-2 at W/C of 0.33 without PCE superplasticizer

In this case, the blank paste fails to flow but a slight increase in Sp/C or W/C enables the paste to flow. This indicates that V_{FW} in FCP-2 is also close to V_{pore}. The dispersion phase in FCP-2 consists of all the cement grains including the individual ones and those in the flocculated structures, AW and EW. If the cement volume $V_C = m_C/\rho_C = 1$, then

$$\begin{cases} \frac{m_{FW}}{\rho_W} = V_{FW} \approx V_{pore} = \left(\frac{m_c}{\rho_c} + \frac{m_{AW+REW}}{\rho_w} + \frac{m_{EEW}}{\rho_w}\right) \cdot \frac{1-\phi_M}{\phi_M} \\ m_{FW} + m_{AW+REW} + m_{EEW} = m_W = \frac{W}{C} \cdot m_c = \frac{W}{C} \cdot \rho_c \end{cases} \tag{6.4}$$

where m_{EEW} denotes the content of the entrapped water that could be released by the superplasticizer used in this study. The EEW and the REW constitute the EW in the FCPs. It is known that W/C = 0.33 and $m_{AW+REW} = 0.03$, we get $m_{EEW} = V_{EEW} = 0.40$, $m_{FW} = V_{FW} = 0.61$ from Eq. (6.4).

Similarly, the existence of FW in the FCP-2 suggests the contents of EW and AW have already arrived at the maximum value and their total mass is $m_{AW+REW} + m_{EEW} = 0.43$. In the similar way, if all mixing water is existing as adsorbed water and entrapped water, namely there is no free water in the paste, we have

$$\begin{cases} m_{AW} + m_{EEW} + m_{REW} = m_W = \frac{W}{C} \cdot m_c = 3.16\frac{W}{C} \\ m_{AW+REW} + m_{EEW} \leq 0.43 \end{cases} \tag{6.5}$$

It is deduced that W/C $\leq$ 0.136. That is to say, the FW will not emerge in the FCPs until the W/C is larger than 0.136. At varied W/Cs, the FW content in the pastes could be obtained from Eq. (6.6).

$$m_{FW} = m_W - (m_{AW} + m_{EW}) = \frac{W}{C} \cdot m_c - 0.136 = 3.16\frac{W}{C} - 0.136 \tag{6.6}$$

Based on Eq. (6.5), the content of EEW at varied W/Cs could also be deduced as follows.

$$m_{EEW} = m_W - (m_{AW} + m_{REW)} = \frac{W}{C} \cdot m_c - 0.03 = 3.16\frac{W}{C} - 0.03 \tag{6.7}$$

On the basis of the Eqs. (6.3), (6.6) and (6.7), the contents of different types of water and the volume fraction of solid phase ϕ in the blank FCPs at varied W/Cs could be calculated and listed in Table 6.1.

Furthermore, the addition of PCE superplasticizer changes the microstructure of FCPs in the term of disassembling flocculated structures and transferring EW into FW. The released EW content by PCE of per unit mass could be defined as $\theta = \Delta_{EW}/ m_{sp}$. From Fig. 3.1, it is known that all the EEW is released at the critical dosage of superplasticizer (D_C), i.e., $\Delta_{EW} = V_{EEW}$. Thus, the θ at different W/Cs

Table 6.1 Volume of different types of water and the volume fraction of solid phase in the blank FCPs at varied W/Cs

W/C	0.13	0.15	0.2	0.25	0.29	0.35	0.4	0.5	0.6	0.7	0.8
V_C	1	1	1	1	1	1	1	1	1	1	1
V_T	0.41	0.47	0.63	0.79	0.92	1.11	1.26	1.58	1.90	2.21	2.53
V_{AW+REW}	0.03	0.03	0.03	0.03	0.03	0.03	0.03	0.03	0.03	0.03	0.03
V_{EEW}	0.38	0.40	0.40	0.40	0.40	0.40	0.40	0.40	0.40	0.40	0.40
V_{FW}	0.00	0.04	0.20	0.36	0.49	0.68	0.83	1.15	1.47	1.78	2.10
V_{HW}	0.00	0.00	0.00	0.00	0.00	0.00	0.00	0.00	0.00	0.00	0.00
ϕ	–	0.97	0.88	0.80	0.75	0.68	0.63	0.55	0.49	0.45	0.41

could be obtained, as shown in Table 6.2. Then, the contents of three types of water and volume fractions of solid phase ϕ in the FCPs at varied W/Cs and Sp/Cs could be calculated based on the Eq. (6.8), as listed in Table 6.3. It is noted that the volume fractions of solid phase ϕ decrease with the growths in W/C and Sp/C, and the paste could flow when ϕ is lower than 0.7. The variation trend of ϕ is in good agreement with the initial fluidity of the FCPs in Fig. 3.1.

$$\begin{cases} V_{\mathrm{AW+REW}} = 0.03 \\ V_{\mathrm{EEW}}\left(\frac{W}{C}, \frac{Sp}{C}\right) = 0.40 - 3.16 \cdot \frac{Sp}{C} \cdot \theta \\ V_{\mathrm{FW}}\left(\frac{W}{C}, \frac{Sp}{C}\right) = 3.16 \cdot \frac{W}{C} - 0.43 + 3.16 \cdot Sp/C \cdot \theta \\ \Phi\left(\frac{W}{C}, \frac{Sp}{C}\right) = \frac{1 + 0.03 + V_{\mathrm{EEW}}\left(\frac{W}{C}, \frac{Sp}{C}\right)}{1 + W/C} \end{cases} \tag{6.8}$$

6.1.2.2 Multi-scale Microstructure Model

Combined the data in Tables 6.1 and 6.3 with the fluidity curves in Fig. 3.1, a multi-scaled microstructure model of FCPs with varied W/Cs and Sp/Cs was established and schematically illustrated as follows.

For the FCPs at W/C $\leq$ 0.15, their microstructure models are shown in Fig. 6.3. In the blank FCP without PCE superplasticizer, most of the cement grains aggregate together and form flocculated structures of multi-scaled size and the rest

Table 6.2 The decreased EW content caused by the superplasticizer of per unit mass at varied W/Cs

W/C	0.2	0.25	0.29	0.35	0.4	0.5	0.6	0.7	0.8
Dc	1.20%	1.00%	0.80%	0.70%	0.50%	0.40%	0.35%	0.3%	0.2%
V_C	1	1	1	1	1	1	1	1	1
Δ_{EW}/g	0.40	0.40	0.40	0.40	0.40	0.40	0.40	0.40	0.40
m_{sp}/g	0.038	0.032	0.025	0.022	0.016	0.013	0.011	0.010	0.006
θ	10.51	12.60	15.80	18.02	25.20	31.60	35.87	41.92	66.37

Table 6.3 Volume of different types of water and the volume fraction of solid phase in the FCPs at varied Sp/Cs and W/Cs

W/C	0.05%	0.10%	0.20%	0.30%	0.40%	0.50%	0.60%	0.80%	1.00%	1.20%
0.2										
V_{EEW}	0.38	0.37	0.33	0.30	0.27	0.23	0.20	0.13	0.07	0.00
V_{FW}	0.22	0.24	0.27	0.30	0.33	0.37	0.40	0.47	0.53	0.60
ϕ	0.87	0.86	0.84	0.82	0.79	0.77	0.75	0.71	0.67	0.63
0.25										
V_{EEW}	0.38	0.36	0.32	0.28	0.24	0.20	0.16	0.08	0.00	0.00
V_{FW}	0.38	0.40	0.44	0.48	0.52	0.56	0.60	0.68	0.76	0.76
ϕ	0.79	0.78	0.75	0.73	0.71	0.69	0.67	0.62	0.58	0.58
0.29										
V_{EEW}	0.37	0.35	0.30	0.25	0.20	0.15	0.10	0.00	0.00	0.00
V_{FW}	0.51	0.54	0.59	0.64	0.69	0.74	0.79	0.88	0.88	0.88
ϕ	0.73	0.72	0.69	0.67	0.64	0.62	0.59	0.54	0.54	0.54
0.35										
V_{EEW}	0.37	0.34	0.28	0.23	0.17	0.11	0.06	0.00	0.34	0.28
V_{FW}	0.70	0.73	0.79	0.85	0.90	0.96	1.02	1.07	1.07	1.07
ϕ	0.67	0.65	0.63	0.60	0.57	0.54	0.52	0.49	0.49	0.49
0.4										
V_{EEW}	0.36	0.32	0.24	0.16	0.08	0.00	0.00	0.00	0.00	0.00
V_{FW}	0.87	0.91	0.99	1.07	1.15	1.23	1.23	1.23	1.23	1.23
ϕ	0.61	0.60	0.56	0.53	0.49	0.46	0.46	0.46	0.46	0.46
0.5										
V_{EEW}	0.35	0.30	0.20	0.10	0.00	0.00	0.00	0.00	0.00	0.00
V_{FW}	1.20	1.25	1.35	1.45	1.55	1.55	1.55	1.55	1.55	1.55
ϕ	0.54	0.52	0.48	0.44	0.40	0.40	0.40	0.40	0.40	0.40
0.6										
V_{EEW}	0.34	0.28	0.17	0.06	0.00	0.00	0.00	0.00	0.00	0.00
V_{FW}	1.52	1.58	1.69	1.81	1.86	1.86	1.86	1.86	1.86	1.86
ϕ	0.47	0.45	0.42	0.38	0.36	0.36	0.36	0.36	0.36	0.36
0.7										
V_{EEW}	0.33	0.27	0.13	0.00	0.00	0.00	0.00	0.00	0.00	0.00
V_{FW}	1.85	1.91	2.05	2.18	2.18	2.18	2.18	2.18	2.18	2.18
ϕ	0.42	0.40	0.36	0.32	0.32	0.32	0.32	0.32	0.32	0.32
0.8										
V_{EEW}	0.30	0.20	0.00	0.00	0.00	0.00	0.00	0.00	0.00	0.00
V_{FW}	2.20	2.30	2.50	2.50	2.50	2.50	2.50	2.50	2.50	2.50
ϕ	0.38	0.35	0.29	0.29	0.29	0.29	0.29	0.29	0.29	0.29

grains present individual ones. All mixing water is existing as AW and EW, namely there is no FW. With the increases in W/C, more cement grains form flocculated structures, and the content of EW rises and reaches to the maximum at W/C of

0.136. When W/C is higher than 0.136, the contents of flocculated structures and EW are little changed by further increase of W/C, while FW appears in the FCPs and its content increases with increased W/C. When low dosage of superplasticizer is added in the FCPs, both the size and amount of flocculated structures are reduced while three types of water AW, EW, FW are found in the FCPs. With the increase in Sp/C, the content of EW drops while that of FW ascends correspondingly. In the case of overdosed superplasticizer in the FCPs, the FW content reaches to the maximum and flocculated structures are no longer influenced by the further addition of superplasticizer. The remaining flocculated structures are usually strongly bonded ones and could be destroyed by the superplasticizer with stronger dispersion capability, the content of which in the FCPs is determined by the superplasticizer type.

In summary, although the contents of the solid phase in the FCPs including cement grains and AW and EW significantly change with the W/C and Sp/C, the volume of FW is still lower than V_{pore}. Hence, these FCPs at W/C $\leq$ 0.15 fail to flow regardless of Sp/C.

On the other hand, Fig. 6.4 presents the microstructure models of the FCPs at W/C > 0.15. Three types of water AW, EW and FW could be found in the blank FCP. With the increase in W/C, the contents of AW and EW stay stable while the FW content keeps ascending evidently. When W/C is larger than 0.33, the FW content increases to be higher than V_{pore} and the blank FCP could free flow. The addition of superplasticizer leads to the decrements in the amount and size of flocculated structures and to an obvious growth in FW content. When the FW content is higher than V_{pore} at one certain Sp/C, the FCPs could flow and the fluidity grows with the Sp/C. When the FW content reaches to the maximum, the flocculated structures are no longer influenced by the superplasticizer and the fluidity stays stable.

6.1.2.3 Verification on the Microstructure Model

Considerable attentions have been paid on correlating the rheological parameters of suspensions with the volume fraction of solid phase. Flatt and Bowen (2006, 2007) deduced a Yodel equation (Eq. 6.9) for concentrated particle suspensions, which could accurately describe the dependence of the yield stress on the volume fraction of solid phase.

$$\tau_0 = m_1 \frac{\phi^2(\phi - \phi_0)}{\phi_M(\phi_M - \phi)} \tag{6.9}$$

where τ_0 is the yield stress of the solid-liquid dispersion; ϕ is the volume fraction of the solid phase; ϕ_M denotes the maximum packing fraction; ϕ_0 represents a percolation threshold; m_1 is introduced for convenience and incorporates everything that is not dependent on the volume fraction of solid phase.

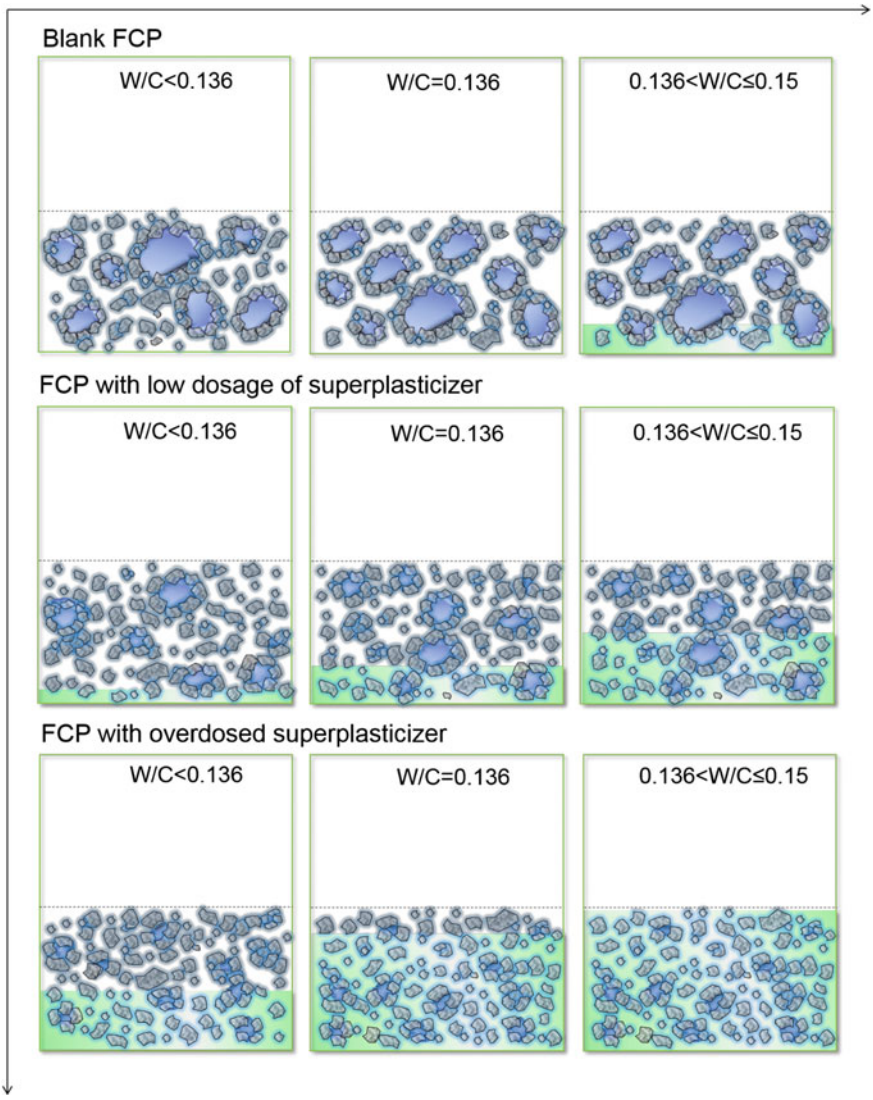

Fig. 6.3 Multi-scale microstructure model of FCPs at W/C $\leq$ 0.15

$$m_1 = \frac{0.15 \times u_{k,k\times} A_0}{\pi^4 H^2} \times \frac{f_{\sigma,\Delta}}{R_{v,50}} \tag{6.10}$$

where A_0 is the Hamaker constant and is 1.7×10^{-21} J for Portland cement (Nawa 2006). $f_{\sigma,\Delta}$ corresponds to a particle size distribution function and $u_{k,k}$ represents a normalization factor that changes the size distribution, which are 1 and 187.63 in fresh cement pastes, respectively (Flatt and Bowen 2006). The median volume

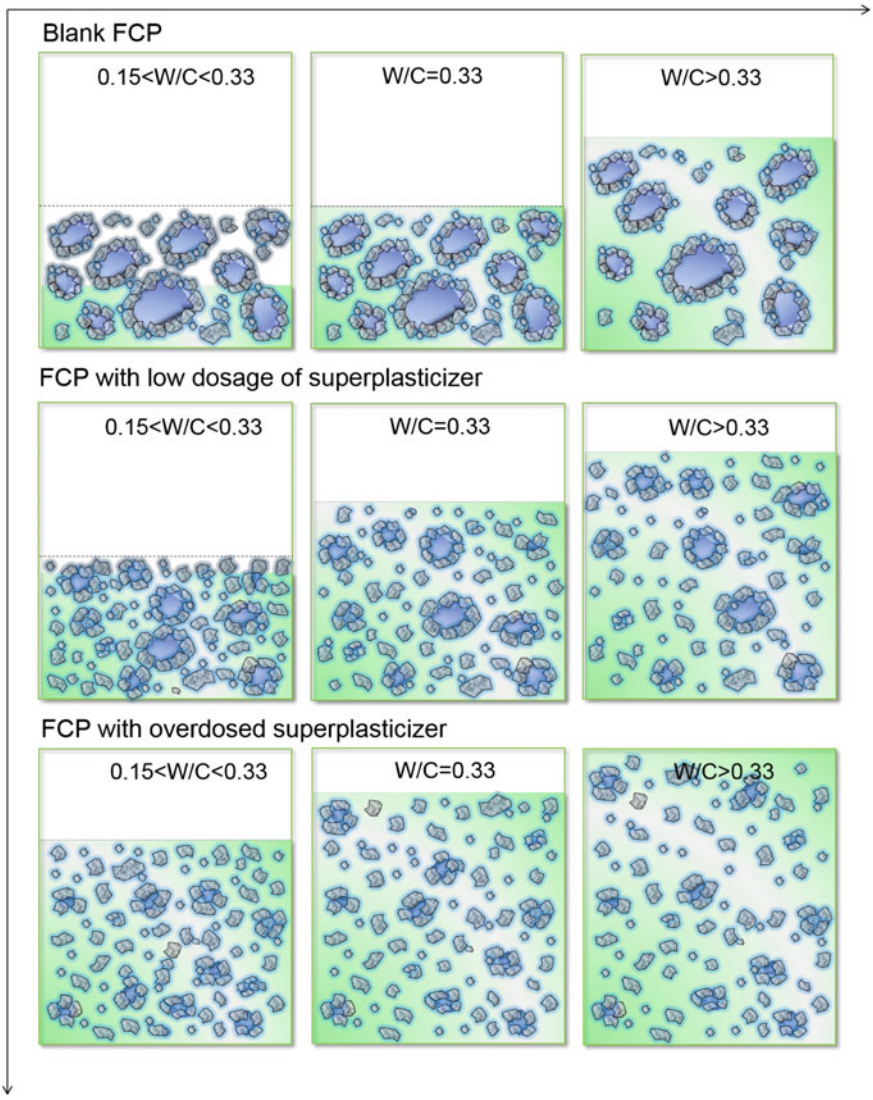

Fig. 6.4 Multi-scale microstructure model of FCPs at W/C > 0.15

radius $R_{v,50}$ is set to 10 μm according to the experimental data. H is the minimum separation distance between cement grains and is 3.2 nm in blank FCP but falls between 6 and 12 nm in the presence of superplasticizers due to the introduction of steric hindrance effect (Kauppi et al. 2003).

On condition that $\phi_M \approx 0.7$ and $\phi_0 \approx 0.03$ in the FCPs, which are slightly influenced by the changes of mix proportion. Combined with ϕ listed in Table 6.3,

the corresponding yield stress of FCPs at varied mix proportions could be calculated. As presented in Fig. 6.5, the calculated yield values are quite close to the experimental ones, which firmly validates the microstructure model.

This microstructure model was established based on the real microstructure of FCPs observed by microscopes with the emphasis of the multi-scaled organization structure of cement grains in the pastes, so the correlation between the rheological behavior and microstructure was clearly revealed. However, we need to emphasize here is that the establishment of this microstructure model is based on the experimental data of this study. When other types of cement and superplasticizers with different dispersion capability are used, the model will surely vary in terms of the contents of different types of water and the solid phase volume due to the changes in the critical water to cement ratio (0.33) and the critical dosage of superplasticizers. Nevertheless, the variation trends and the mechanism reflected in the model should be universal and are applicable for most FCPs.

6.1.3 *Cement-Latex/Asphalt-Water System*

Different from the superplasticizers with a hydraulic radius of nanometer, the polymer particles of submicron and the asphalt particles of micron in the pastes function as the dispersion phase besides affecting the flocculated structures in the FCPs, which further impacts the microstructure of FCPs.

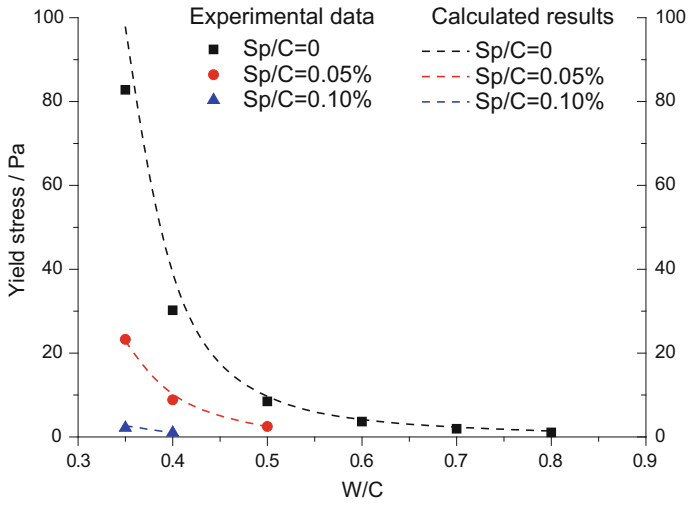

Fig. 6.5 Comparison between the experimental data and calculated results for the yield stress versus W/C of fresh cement pastes at different dosages of superplasticizer

The same hypotheses in Sect. 6.1.2 were applied in the microstructure model of Cement-Latex/Asphalt-Water dispersion system. When the dispersion phase including the cement grains, flocculated structures, entrapped water and adsorption water is in the state of geometrical maximum packing, the incorporation of latexes and asphalt emulsions could fill with the pore volume among the packing particles, and consequently increases the maximum volume fraction, as shown in Fig. 6.6. In other words, the increased value of maximum volume fraction is equal to the volume fraction of polymer or asphalt particles added in the pastes.

The volume fraction of dispersion phases in the Cement-Latex/Asphalt-Water system could also be calculated according to the method described in Sect. 6.1.2.1. Due to the limited space, only the models of the two systems at W/C $\geq$ 0.33 were exhibited in Fig. 6.7. In the models, polymer or asphalt particles, cement grains including the individual ones and the flocculated ones, EW and AW consist of the dispersion phase of the system while FW acts as the dispersion medium. Hereinto, the filling of polymer or asphalt particles in the paste definitely increases the theoretical volume of dispersion phases and a higher dosage leads to a more significant increment. At low dosage of latexes, the adsorption of polymers particles facilitates the formation of flocculated structures due to its neutralizing effects and consequently, the drop of initial fluidity is brought by the increased EW and lessened FW. With further addition, the flocculated structures are reduced due to its plasticizing effects and the fluidity begins to increase. Asphalt emulsion also presents plasticizing effects due to its adsorption on cement surface. When the filling effects of polymer/asphalt particles exceed their plasticizing effects, the initial fluidity of FCPs decreases with the growth of dosage.

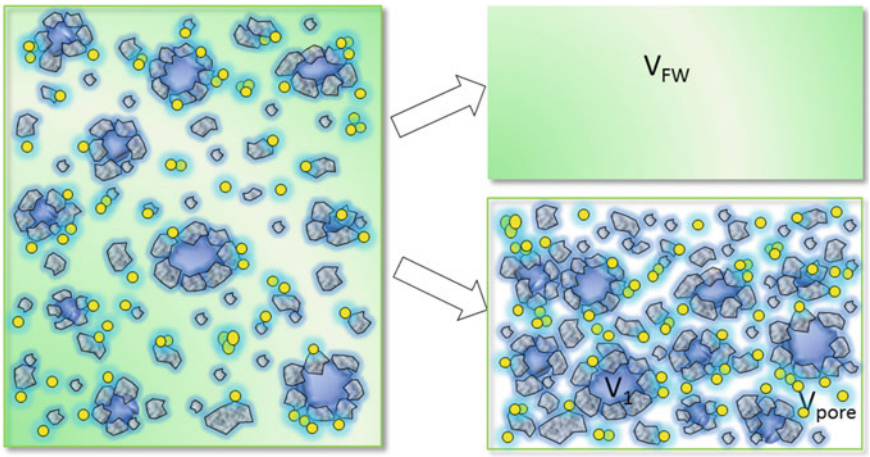

Fig. 6.6 Schematic drawing of fresh cement paste containing polymer latex or asphalt emulsion

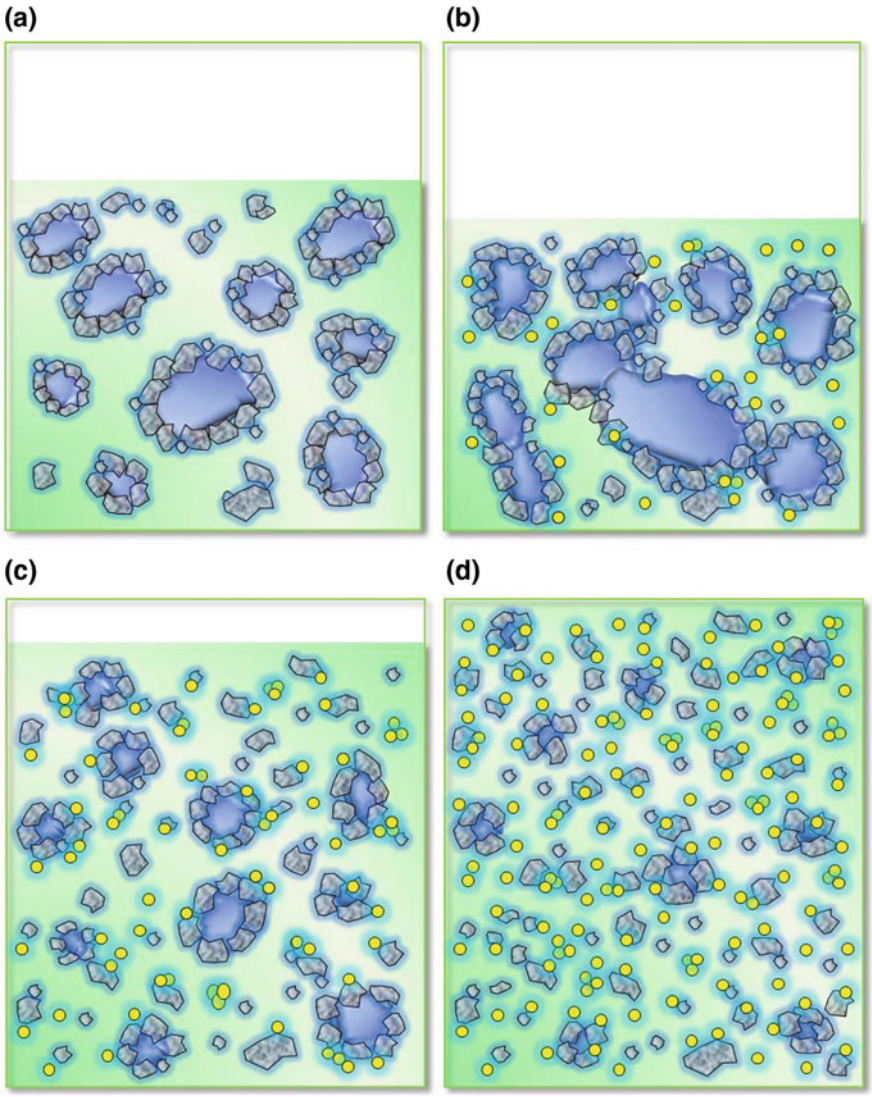

Fig. 6.7 Multi-scale microstructure model of FCPs containing polymer latex or asphalt emulsion at W/C $\geq$ 0.33. **a** Blank FCP, **b** FCP with low dosage of polymer latex or asphalt emulsion, **c** FCP with adequate dosage of polymer latex or asphalt emulsion, **d** FCP with overdosed polymer latex or asphalt emulsion

6.2 Rheological Evolution Model of Fresh Cement Pastes

From the results in Chap. 5, it can be understood that the evolution of rheological parameters over time originates from the cement hydration. During cement hydration, the rheological parameters change over elapsed time due to the continuous growth of the solid volume fraction. The effects of temperature on the development of the rheological parameters over time can be attributed to the effects of temperature on cement hydration. The incorporation of chemical admixtures significantly alters hydration kinetics due to their retardation effects, thereby influencing the development of rheological parameters over time. In summary, in case that the time-changing behavior of rheological properties of FCPs is concerned, relative cement hydration degree is used as one important factor to analyze the effects of mix proportion and temperature on the evolution of rheology behaviors with the elapsed time. Thus, a general expression linking the evolution of rheological parameters and hydration behavior is expected to describe the effects of mix proportion, time and temperature on rheological behavior of FCPs.

6.2.1 Cement-Superplasticizer-Water System

6.2.1.1 Yield Stress

Fresh cement paste is usually considered as a solid-liquid suspension dispersion system with chemical reactivity, whose rheological properties are closely connected to the volume fraction of solid phase. With the progressing hydration, the volume fraction of solid phase gradually ascends. We define the initial volume fraction of solids at any mixing proportion and temperature as ϕ (W/C, Sp/C, 0, T). With the progressing cement hydration, the volume fraction of solids continuously increases. If we denote the volume fraction of solids at any elapsed time as ϕ (W/C, Sp/C, t, T) and the ultimate volume fraction of solids at 100% hydration degree as ϕ (W/C, Sp/C, ∞, T), then the cement hydration degree α at any elapsed time can be defined as:

$$\alpha(W/C, Sp/C, t, T) = \frac{\phi(W/C, Sp/C, t, T) - \phi(W/C, Sp/C, 0, T)}{\phi(W/C, Sp/C, \infty, T) - \phi(W/C, Sp/C, 0, T)} \tag{6.11}$$

Given that a FCP totally loses its fluidity at the time point of initial setting t_{is} because the dense particle packing is caused by cement hydration, the solid volume fraction is supposed to reach a maximum at this moment, namely, ϕ (W/C, Sp/C, t_{is}, T) = ϕ_M. Then, the equation below can be derived:

$$\alpha(W/C, Sp/C, t_{is}, T) = \frac{\phi(W/C, Sp/C, t_{is}, T) - \phi(W/C, Sp/C, 0, T)}{\phi(W/C, Sp/C, \infty, T) - \phi(W/C, Sp/C, 0, T)} \cong \frac{\phi_M - \phi(W/C, Sp/C, 0, T)}{\phi(W/C, Sp/C, \infty, T) - \phi(W/C, Sp/C, 0, T)} \quad (6.12)$$

where α (W/C, Sp/C, t_{is}, T) and ϕ (W/C, Sp/C, t_{is}, T) are the hydration degree and volume fractions of solids at the time point of initial setting t_{is}, respectively. Before the initial setting, the development of rheological parameters with time is considered to be determined by the ratio of the hydration degree at any time point t to the hydration degree at the time point of initial setting.

As stated above, Yodel equation (Eq. 6.9) is usually used to accurately describe the dependence of the yield stress on the volume fraction of solids for concentrated particle suspensions. When $\phi > 0.25$, Eq. (6.13) can be simplified as:

$$\tau_0 \cong m_1 \frac{\phi^3}{\phi_M(\phi_M - \phi)} \quad (6.13)$$

On condition that inter-particle forces are unchanged and the parameters of ϕ_M and m_1 are barely influenced by the changes of mix proportion, elapsed time and ambient temperature, and thus ϕ is the only variable in Eq. (6.13).

Correspondingly, according to Eq. (6.13), the initial yield stress at any mixing proportion and ambient temperature T could be written as Eq. (6.14) and the yield stress at any elapsed time could be expressed by Eq. (6.15).

$$\tau_0(W/C, Sp/C, 0, T) \cong m_1 \frac{\phi(W/C, Sp/C, 0, T)^3}{\phi_M[\phi_M - \phi(W/C, Sp/C, 0, T)]} \quad (6.14)$$

$$\tau_0(W/C, Sp/C, t, T) \cong m_1 \frac{\phi(W/C, Sp/C, t, T)^3}{\phi_M[\phi_M - \phi(W/C, Sp/C, t, T)]} \quad (6.15)$$

Combining Eqs. (6.14) and (6.15), an expression linking the evolution of yield stress and hydration degree is deduced:

$$\frac{\tau_0(W/C, Sp/C, t, T)}{\tau_0(W/C, Sp/C, 0, T)} = \frac{\left[1 + \alpha(W/C, Sp/C, t, T)\left(\frac{\phi(W/C, Sp/C, \infty, T)}{\phi(W/C, Sp/C, 0, T)} - 1\right)\right]^3}{1 - \alpha'} \quad (6.16)$$

in which a non-dimensional hydration index $\alpha' = \frac{\phi(W/C, Sp/C, t, T) - \phi(W/C, Sp/C, 0, T)}{\phi_M - \phi(W/C, Sp/C, 0, T)}$, called relative hydration degree, is employed. The normalized α' is defined as the hydration degree at any elapsed time after the contact of cement with water divided by the hydration degree at the initial setting time, which can be written as follows:

$$\alpha' = \frac{\alpha(W/C, Sp/C, t, T)}{\alpha(W/C, Sp/C, t_{is}, T)} = \frac{Q(W/C, Sp/C, t, T)}{Q(W/C, Sp/C, t_{is}, T)} \tag{6.17}$$

where Q (W/C, Sp/C, t, T) and Q (W/C, Sp/C, t_{is}, T) represent the hydration heat at time t and t_{is}, respectively. They can be obtained from the calorimetry tests, as illustrated in Fig. 6.8.

As shown in Figs. 5.22–5.29, the cement hydration degree within the first 2 h is very low, usually less than 5% (Lin and Meyer 2009). Thus, it is reasonable to approximate the numerator in Eq. (6.17) to be constant 1, namely neglect the item $\alpha(W/C, Sp/C, t, T)\left(\frac{\phi(W/C,Sp/C,\infty,T)}{\phi(W/C,Sp/C,0,T)} - 1\right)$. The Eq. (6.17) can be thus simplified as Eq. (6.18), which quantitatively describes the development of the yield stress of FCPs before the initial setting. All the factors causing the change of the yield stress are integrated into the relative hydration degree.

$$\frac{\tau_0(W/C, Sp/C, t, T)}{\tau_0(W/C, Sp/C, 0, T)} = \frac{\left[1 + \alpha(W/C, Sp/C, t, T)\left(\frac{\phi(W/C,Sp/C,\infty,T)}{\phi(W/C,Sp/C,0,T)} - 1\right)\right]^3}{1 - \alpha'} \cong \frac{1}{1 - \alpha'} \tag{6.18}$$

Based on the results of rheological tests and the calorimetry tests, $\frac{\tau_0(W/C,Sp/C,t,T)}{\tau_0(W/C,Sp/C,0,T)}$ and α' could be calculated. The yield stress tested at 5 min is used to approximate the yield stress at zero time since it is impossible to obtain the rheological parameters at zero time. When $\frac{\tau_0(W/C,Sp/C,t,T)}{\tau_0(W/C,Sp/C,0,T)}$ is plotted in function with $1/(1-\alpha')$, as presented in Fig. 6.9, it is seen that the yield stress develops in a roughly linear fashion with $1/(1-\alpha')$. The slope of fitting curve is 1.02 and the correlation coefficient is 0.95, which fairly validates Eq. (6.18). From the above results, it is concluded that the effects of mix proportion and temperature on the evolution of the yield stress over time can be unified into the relative hydration degree.

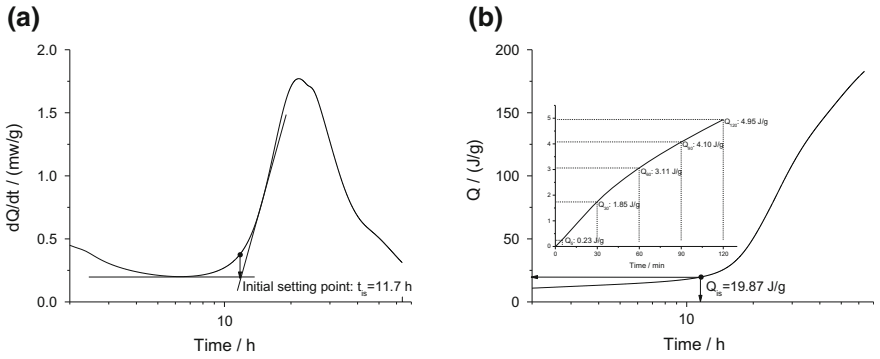

Fig. 6.8 Heat evolution of cement hydration in FCPs with W/C of 0.25 and Sp/C of 0.2% at 20 °C. **a** Differential curve, **b** integral curve

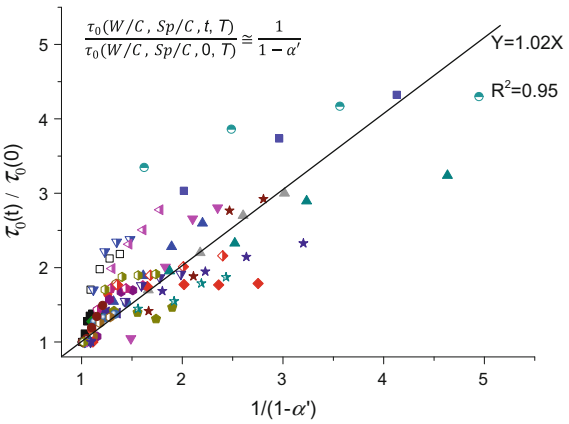

Fig. 6.9 Variation of yield stress with relative hydration degree at various mix proportions and temperatures

6.2.1.2 Plastic Viscosity

Plastic viscosity μ_p is another key parameter for the rheological properties of cement and water mixtures, which reflects the properties of mixing, flowing, pouring, pumping, and compacting of fresh concrete. Similar to yield stress, plastic viscosity of fresh cement pastes also varies with time and temperature. The Krieger–Dougherty equation was proved to be applicable in describing the relationship between the viscosity and the volume fraction of fresh cement pastes. If we assume that both the initial viscosity is $\mu_p(0, T)$ and the viscosity at any time t is $\mu_p(t, T)$, then we have:

$$\frac{\mu_p(0,T)}{\mu_c(0,T)} = \left(1 - \frac{\phi(0,T)}{\phi_M}\right)^{-[\mu]\phi_M} \tag{6.19}$$

$$\frac{\mu_p(t,T)}{\mu_c(t,T)} = \left(1 - \frac{\phi(t,T)}{\phi_M}\right)^{-[\mu]\phi_M} \tag{6.20}$$

When Eqs. (6.19) and (6.20) are combined, assuming that the viscosity of the liquid phase μ_c does not change with time, the following equation can be derived:

$$\ln\frac{\mu_p(t,T)}{\mu_p(0,T)} = -[\mu]\phi_M \ln\left(\frac{\phi_M - \phi(t,T)}{\phi_M - \phi(0,T)}\right) \tag{6.21}$$

Further,

$$\ln\frac{\mu_p(t,T)}{\mu_p(0,T)} = -[\mu]\phi_M \ln\left(1 - \frac{\phi(t,T) - \phi(0,T)}{\phi_M - \phi(0,T)}\right) \tag{6.22}$$

According to the previous definition, $\alpha' = \frac{\phi(t,T)-\phi(0,T)}{\phi_M-\phi(0,T)}$, finally Eq. (6.23) is obtained:

$$\ln\frac{\mu_p(t,T)}{\mu_p(0,T)} = -[\mu]\phi_M \ln(1-\alpha') \tag{6.23}$$

Thus, Eq. (6.23) expresses the link between plastic viscosity and relative hydration degree of fresh cement pastes, which should be independent of mix proportion, time and temperature. Based on the results of plastic viscosity and the calorimetry tests at varied mix proportions, temperature and time, $\ln[\mu_p(t,T)/\mu_p(0,T)]$ versus $\ln(1-\alpha')$ is plotted, as presented in Fig. 6.10. Relatively good linear correlations are found, which validates Eq. (6.23) to some extent. However, the slopes of the fitted curves at varied temperatures vary, which should have remained equal as described in Eq. (6.23). This finding implies that there exist some other factors affecting the evolution of plastic viscosity of fresh cement pastes (Flatt 2004; Morris 2009; Struble and Sun 1995). It has been known that the interactions between particles in solid-liquid dispersion have more significant effects on plastic viscosity than on yield stress (Struble and Sun 1995). The variation in particle interactions at different temperatures may explain why the slopes of the curves are not equal for different temperatures.

Apart from the volume fraction of the solid phase, the microstructure of the solid-liquid dispersion, the changes in the shape of cement grains, and the interactions among particles are also essential for rheological behavior. However, Yodel and K-D models do not consider these factors, which may result in deflection when calculating the yield stress and the viscosity of cement water mixtures. In particular, when it is close to the initial setting time, the microstructure of FCPs including the interlinking and interactions between hydrates and unhydated cement grains as well as the shape of dispersion phases will exert more significant impacts on the rheological properties, thereby increasing the deflection of rheological models and weakening their applicability.

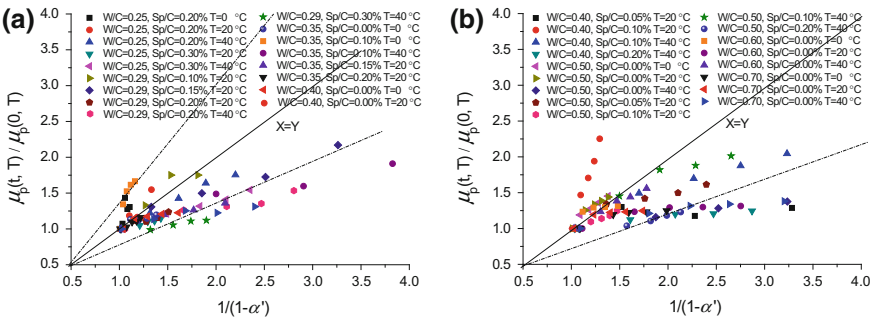

Fig. 6.10 Variation of plastic viscosity with relative hydration degree at various mix proportions and temperatures

6.2.2 *Cement-Asphalt-Water System*

Similar to the Cement-Superplasticizer-Water system, the evolution models of rheological parameters in the Cement-Latex-Water and Cement-Asphalt-Water system could also been described by Eqs. (6.18) and (6.23). Taken the evolution of yield stress of CA pastes as an example, the yield stress at varied temperatures and elapsed time versus relative hydration degree is plotted in Fig. 6.11. The yield stress develops in a roughly linear fashion with $1/(1-\alpha')$ under the coupled effects of time and temperature.

If we look at more details, CA pastes with cationic asphalt emulsion fairly agree with the Eq. (6.18) just with slight deviation for those CA pastes at higher temperatures. The slight increase in τ/τ_0 at high temperatures is believed to result from the demulsification of asphalt emulsion during cement hydration. Conversely, for the CA pastes with anionic asphalt emulsion, the growth rule of τ/τ_0 with relative hydration degree appears to be temperature dependent. For the values obtained at 0 °C, τ/τ_0 versus $1/(1-\alpha')$ satisfactorily fits Eq. (6.18). For the values at 20 and 40 °C, the slope is obviously higher than 1, implying that aside from cement hydration, other mechanisms that determine the evolution of yield stress are involved. During the experiments and as evidenced by Fig. 5.33, the anionic asphalt emulsion is considerably more stable than the cationic asphalt emulsion. That is, after being mixed with the cement, anionic asphalt emulsion exhibits a rather slow demulsification that lasts during cement hydration before setting; cationic asphalt emulsion, on the other hand, is rapidly demulsified after mixing. Consequently, for the CA pastes with cationic asphalt emulsion, the development of the yield stress is caused solely by cement hydration, whereas for the CA pastes with anionic emulsion, the growth of the yield stress is influenced by both cement

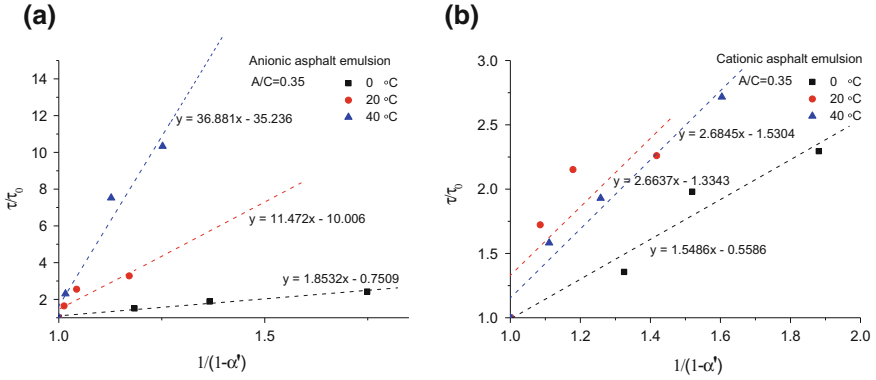

Fig. 6.11 Variation of yield stress of CA pastes with relative hydration degree at varied temperatures. **a** Anionic asphalt emulsion, **b** cationic asphalt emulsion

hydration and asphalt demulsification. A high temperature accelerates the rate of demulsification. Thus, the slope is higher for the CA pastes at high temperatures on the curve $\tau/\tau_0 \sim 1/(1-\alpha')$, as shown in Fig. 6.11a.

6.3 Rheological Models of Fresh Cement Pastes

Many factors contribute to the rheological properties of FCPs, such as water to cement ratio (W/C), the use of chemical admixtures, temperature and elapsed time. These factors are known to change the rheological properties through altering the microstructure of FCPs especially the volume fraction of dispersion phases, which has been discussed in Chap. 5. Specifically, changes in mixing proportions definitely lead to changes in the volume fraction of the solid phase. The volume fraction also continuously changes over time, which majorly originates from the continuous cement hydration after the contact of cement with water. Temperature affects the kinetics of cement hydration, through which it brings the changes in volume fraction of solid phase at a certain elapsed time. Therefore, theoretically speaking, we could derive the relationship linking each factor with the volume fraction of the solid phase ϕ. Then, combined with the existing Yodel and K-D models, the rheological models of the fresh cement pastes incorporating Sp/C, W/C, temperature and time could be deduced.

6.3.1 Yield Stress

As assumed in Fig. 3.1, with the growth of Sp/C, the content of flocculated structures descends and the content of free water increases, thereby reducing the volume fraction of solid phase. At the critical dosage of PCE, the entrapped water in the flocculated structures is completely released and hence the volume fraction of solid phase reaches to a minimum. Considering that the amount of the adsorbed water is far less than the free water and the entrapped water (Table 6.1), the volume fraction of solid phase at time point 0, ambient temperature T and at the critical dosage D_c can be written as:

$$\phi\left(\frac{w}{c}, 0, T, D_c\right) = \frac{V_c}{V_c + V_w} = \frac{m_c \rho_w}{\rho_w m_c + \rho_c m_w} = \frac{\rho_w}{\rho_w + \rho_c (w/c)} \tag{6.24}$$

where ρ_w and ρ_c are the density of water and of cement, respectively. When they are respectively set as 1 and 3 g/cm^3, we get:

$$\phi\left(\frac{w}{c},0,T,D_{\mathrm{c}}\right)=\frac{1}{1+3(w/c)} \tag{6.25}$$

Based on the above analysis, it is not hard to infer that the expression of the volume fraction of solid phase stays the same with Eq. (6.25) if the dosage of superplasticizer is higher than the critical dosage. When Sp/C is lower than the critical dosage, the volume fraction of solid phase could be defined as:

$$\phi\left(\frac{w}{c},0,T,D_{\mathrm{sp}}\right)=\phi\left(\frac{w}{c},0,T,D_{\mathrm{c}}\right)+\mathrm{A}\left(D_c-D_{sp}\right) \tag{6.26}$$

where A is a constant and D_{sp} is superplasticizer dosage. The Eq. (6.26) describes that the volume of solid phase in initial FCPs proportionally decreases with addition of superplasticizer due to the release of entrapped water. It could be inferred that A is a positive value and it represents the dispersing capability of superplasticizer. Larger value of A indicates higher efficiency of the superplasticizer. Based on the experimental results, we noted that the critical dosage is related to the W/C and could be empirically described by Eq. (6.27) based on the experimental data:

$$D_c=i+j\mathrm{e}^{-(w/c)/k} \tag{6.27}$$

With the progressing cement hydration, more free water is consumed and more hydrates are formed; consequently, the volume fraction of solid phase increases. Thus, the volume fraction of solid phase at time t could be defined as follow:

$$\phi\left(\frac{w}{c},t,T,D_{\mathrm{sp}}\right)=\phi\left(\frac{w}{c},0,T,D_{\mathrm{sp}}\right)+\mathrm{Bexp}\left[\frac{-q}{\alpha\left(\frac{w}{c},t,T,D_{\mathrm{sp}}\right)}\right] \tag{6.28}$$

in which B and q are constants, $\alpha\left(\frac{w}{c},t,T,D_{\mathrm{sp}}\right)$ is the hydration degree of cement for FCP with superplasticizer dosage of D_{sp} and a certain W/C at time t and temperature T. Combined the Eq. (6.26) with the Eqs. (6.27) and (6.28), we have:

$$\begin{aligned}\phi\left(\frac{w}{c},t,T,D_{\mathrm{sp}}\right)&=\frac{1}{1+3(w/c)}+\mathrm{A}\left(D_c-D_{sp}\right)+\mathrm{Bexp}\left[\frac{-q}{\alpha\left(\frac{w}{c},t,T,D_{\mathrm{sp}}\right)}\right]\\&=\frac{1}{1+3(w/c)}+\mathrm{A}\left(i+j\mathrm{e}^{-(w/c)/k}-D_{sp}\right)+\mathrm{Bexp}\left[\frac{-q}{\alpha\left(\frac{w}{c},t,T,D_{\mathrm{sp}}\right)}\right]\end{aligned} \tag{6.29}$$

For a blank FCP, the degree of cement hydration is a function of W/C, time and temperature. It may vary between 0 and 100%, which corresponds to the point of hydration start and the point when hydration is fully completed. Previous studies on cement hydration of cement paste without superplasticizers have shown that the

exponential formulation shown in Eq. (6.30) can represent the kinetics of cement hydration (Hansen and Pederson 1985; Pane and Hansen 2002).

$$\alpha\left(\frac{w}{c}, t, T, 0\right) = h\alpha_u \mathrm{e}^{-\left(\frac{C}{t_e}\right)^D} \tag{6.30}$$

where α_u is the ultimate hydration degree and it is strongly affected by W/C, as shown in Eq. (6.31) (Mills 1966). C, D and h are empirical constants which can be determined by experimental data. t_e is the equivalent age at the reference temperature 293 K and it could be expressed as Eq. (6.32) (Hansen and Pedersen 1977).

$$\alpha_u = \frac{1.031w/c}{0.194 + w/c} \tag{6.31}$$

$$t_e = te^{\frac{E}{R}\left(\frac{1}{293} - \frac{1}{273+T}\right)} \tag{6.32}$$

where R = universal gas constant, 8.314 J/molk. Regarding the apparent activation energy E, previous studies have shown that it keeps almost constant, 33,500 J/mol and just changes slightly at early ages (Chanvillard and Laetitia 1997).

During the first 2 h, the incorporation of superplasticizer retards cement hydration and its influence on hydration could be achieved by changing equivalent age t_e.

$$\alpha\left(\frac{w}{c}, t, T, D_{sp}\right) = h\alpha_u \exp\left[-\left(\frac{C}{\frac{t_e}{f\left(D_{sp}\right)}}\right)^D\right] \tag{6.33}$$

where, $f\left(D_{sp}\right)$ is an increasing function correlating with D_{sp} and could be written as Eq. (6.34) at low superplasticizer dosage.

$$f\left(D_{sp}\right) = mD_{sp} + n \tag{6.34}$$

Then, the substitutions of Eqs. (6.31), (6.32) and (6.34) into Eq. (6.33) lead to

$$\begin{aligned}\alpha\left(\frac{w}{c}, t, D_{sp}, T\right) &= h\alpha_u \exp\left[-\left(\frac{C\left(mD_{sp}+n\right)}{te^{\frac{E}{R}\left(\frac{1}{293}-\frac{1}{273+T}\right)}}\right)^D\right] \\ &= h\frac{1.031w/c}{0.194 + w/c} \times \exp\left[-\left(\frac{m'D_{sp}+n'}{te^{\frac{E}{R}\left(\frac{1}{293}-\frac{1}{273+T}\right)}}\right)^D\right]\end{aligned} \tag{6.35}$$

in which, the constants h, m′, n′ and D obtained by fitting the experimental data of hydration degree at low dosages as shown in Fig. 6.12 are 0.00055, 346.41, 0.467 and 1. The fitting coefficient R^2 is 0.88.

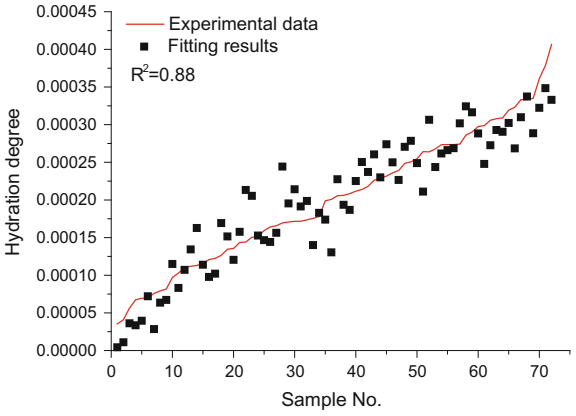

Fig. 6.12 Comparison between experimental data and fitting results

Thus, one might conclude that a model integrating the effects of W/C, time, temperature and superplasticizer dosage, is feasible for predicting the volume fraction, as given in Eq. (6.36).

$$\phi\left(\frac{w}{c},t,T,D_{\mathrm{sp}}\right)=\frac{1}{1+3(w/c)}+\mathrm{A}\left(i+j\mathrm{e}^{-(w/c)/k}-D_{sp}\right)+\mathrm{B}\exp\left\{\frac{-q}{h\frac{1.031w/c}{0.194+w/c}\times\exp\left[-\left(\frac{m'D_{sp}+n'}{te^{\frac{E}{R}\left(\frac{1}{293}-\frac{1}{273+T}\right)}}\right)^{D}\right]}\right\} \tag{6.36}$$

As well known, Yodel equation well establishes the relationship between the yield stress and the volume fraction of solid phase. On condition that $\phi_{\mathrm{M}}=0.7$ and $m_1=3.07$ are barely influenced by the changes of mix design, elapsed time and ambient temperature, ϕ is the only variable in Eq. (6.13). Combined Eq. (6.13) with experimental data of yield stress, we are able to obtain corresponding volume fraction of the solid phase in the FCPs. Then, by fitting the volume fractions of the solid phase at varied W/Cs, D_{sp}, t and T, the constants A, i, j, k, B and q are obtained and are 94.55, 0.00181, 0.0948, 0.0512, 0.182 and 0.000221 respectively. The fitting coefficient R^2 is 0.80. Ultimately, the yield stress as a function of the mix design, temperature and the elapsed time can be roughly predicted by combining Eq. (6.13) with Eq. (6.36).

6.3.1.1 Plastic Viscosity

Similar to the yield stress τ_0, the plastic viscosity of FCPs also varies with mixing design, time and temperature. The μ_p values of FCPs decline with the increase in

W/C and Sp/C as seen in Fig. 3.12. Obvious growths in the viscosity with the elapsed time and ambient temperature are also observed for the FCP with low Sp/C as shown in Figs. 3.14 and 3.16.

The K–D equation was proved applicable in describing the relationship between the viscosity and the volume fraction. Previous studies have shown $[\mu]$ and ϕ_M are 5 and 0.7 respectively for fresh cement pastes (Struble and Sun 1995). Similarly, based on the Eqs. (6.20) and (6.36), we can obtain a viscosity model by fitting the experimental data of plastic viscosity. In the viscosity model, the constants A, i, j k, B and q are 35.85, 0.0037, 0.01, 0.00535, 0.019 and 0.00009 respectively, which are not identical to those in the yield stress model. The microstructure and the interactions between particles in solid-liquid dispersion are not considered in the K–D equation, which may explain why the constants are different in the two models.

Here, only the data of cement pastes with low Sp/C are used because a higher superplasticizer dosage generally brings about obvious deflections when deriving the volume fraction due to the effects of adsorption rate of PCE as well as their interactions. The models of FCPs with high superplasticizer dosages are the subject of on-going studies.

The fitting parameters h, m′, n′, and D and A, i, j, k, B, and q, in the two models are obtained on the basis of the experimental data in this study, and they will surely vary for other cement and superplasticizers. However, we need to emphasize here is that the two models in this study aim at linking the four influencing factors with the rheological properties of FCPs. The mechanism reflected in the models should be universal and they could help to roughly predict the rheological properties. More efforts to put the models into application are underway.

6.4 Summary

(1) Based on the real microstructure of multi-sized particle suspensions and the working mechanism of superplasticizer, the contents of different types of water including free water (FW), adsorption water (AW) and entrapped water (EW) and the volume fraction of dispersion phase in the FCPs were calculated. Finally, a generalized multi-scale microstructure model of FCPs at varied W/Cs and Sp/Cs was established. In the model, the maximum volume of AW and remaining EW in the strongly bonded flocculated structures (V_{AW+REW}) is 0.03. The maximum volume of entrapped water V_{EEW} that could be released by superplasticizer is 0.40. When W/C is lower than 0.136, mixing water is existing as adsorbed water and entrapped water, namely there is no free water in the FCPs. Based on the model, the yield stress of FCPs is calculated and the calculated results are close to the experimental ones, which firmly validates the microstructure model.

(2) Two models to describe the evolution of the yield stress and plastic viscosity over elapsed time after mixing were developed by introducing a relative hydration degree α', which integrated the effects of mix proportion, elapsed time and temperature on the rheological parameters.

$$\frac{\tau_0(W/C, Sp/C, t, T)}{\tau_0(W/C, Sp/C, 0, T)} = \frac{1}{1-\alpha'} \quad \ln\frac{\mu_p(W/C, Sp/C, t, T)}{\mu_p(W/C, Sp/C, 0, T)} = [\mu]\phi_M \ln(1-\alpha').$$

Experimental results show that the development of yield stress over elapsed time is in a roughly linear fashion with $1/(1-\alpha')$ at different temperatures and the slopes are quite close to 1, which validates the model firmly. For the evolution of plastic viscosity, although the fitted curves of viscosity present linear correlation at each temperature, the slopes differ from varied temperatures. It is supposed that the changes in microstructure and the interactions between particles in solid-liquid dispersion may contribute to the deflection of slopes. In addition, the evolution models of rheological parameters concern to rheological properties of FCPs from the beginning of water-cement contact to the initial setting. In particular, when it is close to the setting time, the deflection of rheological models is increased due to the more significant effects of microstructure and the interactions between particles on rheological parameters.

(3) For the Cement-Asphalt-Water system, apart from cement hydration, the demulsification of asphalt emulsion plays an essential role in the evolution of rheological properties of CA paste over time. Under the coupled effects of temperature and time, yield stress increases in a roughly linear fashion with $1/(1-\alpha')$ for all the tested CA pastes. The CA pastes with cationic asphalt emulsion agree well with the equation, regardless of the test temperature. However, for the CA pastes with anionic asphalt emulsion, growth rule τ/τ_0 with a relative hydration degree is rather temperature dependent, which is believed to be derived from the slow demulsification of anionic asphalt emulsion over time.

(4) Based on the Yodel and K-D models, two equations to roughly predict the yield stress and the plastic viscosity of FCPs incorporating Sp/C, W/C, ambient temperature and time as variables were developed. Although the experimental constants in the two models are obtained on the basis of the experimental data of this research, the mechanism reflected in the models should be universal and they could help to approximately foresee the rheological properties. More efforts to put the models into application are underway.

References

Autier C, Azema N, Taulemesse JM et al (2013) Mesostructure evolution of cement pastes with addition of superplasticizers highlighted by dispersion indices. Powder Technol 249(11): 282–289

Banfill PFG, Bowen P, Flatt RJ et al (2007) Improved superplasticisers for high performance concrete: the SUPERPLAST project. Abstract CD ROM of the twelfth international congress on the chemistry of cement, Montreal, Canada, 8–13 July

Chanvillard G, Laetitia D (1997) Concrete strength estimation at early ages: modification of the method of equivalent age. ACI Mater J 94(6):220–227

Ferrari L, Kaufmann J, Winnefeld F et al (2010) Interaction of cement model systems with superplasticizers investigated by atomic force microscopy, zeta potential, and adsorption measurements. J Colloid Interface Sci 347(1):15–24

Flatt RJ (2004) Towards a prediction of superplasticized concrete rheology. Mater Struct 37 (5):289–300

Flatt RJ, Bowen P (2006) Yodel: a yield stress model for suspensions. J Am Ceram Soc 89 (4):1244–1256

Flatt RJ, Bowen P (2007) Yield stress of multimodal powder suspensions: an extension of the YODEL (Yield Stress mODEL). J Am Ceram Soc 90(4):1038–1044

Frankel NA, Acrivos A (1967) On the viscosity of a concentrated suspension of solid spheres. Chem Eng Sci 22(6):847–853

Golaszewski J, Szwabowski J (2004) Influence of superplasticizers on rheological behavior of fresh cement mortars. Cem Concr Res 34(2):235–248

Hansen PF, Pedersen EJ (1977) Maturity computer for controlled curing and hardening of concrete, Nordisk Betong, 41(19):21–25

Hansen FP, Pederson EJ (1985) Curing of concrete structures, Draft DEB-guide to durable concrete structures, Appendix 1, Comite Euro-International du Beton, Lausanne, Switzerland.

Kapur PC, Scales PJ, Boger DV et al (1997) Yield stress of suspensions loaded with size distributed particles. AIChE J 43(5):1171–1179

Kauppi A, Banfill PFG, Bowen P et al (2003) Improved superplasticizers for high performance concrete. In: Proceedings of the 11th international congress on the chemistry of cement, New Delhi, India, 2(LTP-CONF-2003-001), p 8

Kong XM, Zhang YR, Hou SS (2013) Study on the rheological properties of Portland cement pastes with polycarboxylate superplasticizers. Rheol Acta 52(7):707–718

Krieger IM (1972) Rheology of monodisperse latices. Adv Coll Interface Sci 3(2):111–136

Krieger IM, Dougherty TJ (1959) A mechanism for non-Newtonian flow in suspensions of rigid spheres. Trans Soc Rheol (1957–1977) 3(1):137–152

Lin F, Meyer C (2009) Hydration kinetics modeling of Portland cement considering the effects of curing temperature and applied pressure. Cem Concr Res 39(4):255–265

Mills RH (1966) Factors influencing cessation of hydration in water cured cement pastes. Highway research board special report (90), pp 406–424

Morris JF (2009) A review of microstructure in concentrated suspensions and its implications for rheology and bulk flow. Rheol Acta 48(8):909–923

Nawa T (2006) Effect of chemical structure on steric stabilization of polycarboxylate-based superplasticizer. J Adv Concr Technol 4(2):225–232

Pane I, Hansen W (2002) Concrete hydration and mechanical properties under nonisothermal conditions. ACI Mater J 99(6):534–542

Probstein RF, Sengun MZ, Tseng TC (1994) Bimodal model of concentrated suspension viscosity for distributed particle sizes. J Rheol 38(4):811–829

Roncero J, Valls S, Gettu R (2002) Study of the influence of superplasticizers on the hydration of cement paste using nuclear magnetic resonance and X-ray diffraction techniques. Cem Concr Res 32(1):103–108

Sheinn AMM, Ho DWS, Tam CT (2002) Rheological model for self-compacting concrete-paste rheology. In: Proceedings of the 27th conference on our world in concrete and structures, Singapore, pp 28–29

Struble L, Sun GK (1995) Viscosity of Portland cement paste as a function of concentration. Adv Cem Based Mater 2(2):62–69

Wang LJ, Huang FY, Ma XC (2008a) Experimental research on the saturation point of superplasticizers in cement based on fractal dimension. J Wuhan Univ Technol 30(2):28–31 (in Chinese)

Wang LJ, Tan XQ, Cao ML (2008b) Study on flocculated cement based on fractal theory. J Shenyang Jianzhu Univ (Nat Sci) 23(1):82–84 (in Chinese)

Wang DM, Zhang LR, Zhang WL et al (2013) Effects of superplasticizers on multi-level flocculation structure of fresh cement paste. J Build Mater 15(6):755–759 (in Chinese)

Zhang LR, Wang DM, Zhang WL et al (2013) Observation of multi-level flocculation structure of fresh paste using laser scanning confocal microscopy. J Chin Electron Microsc Soc 32(3):231–236 (in Chinese)

Zhou JZQ, Uhlherr PHT, Luo FT (1995) Yield stress and maximum packing fraction of concentrated suspensions. Rheol Acta 34(6):544–561

Chapter 7
Pore Structure and Impermeability of Hardened Cement Pastes

With the development of cement hydration, the modification in the microstructure of FCPs by the addition of chemical admixtures will be persistently extended to the formation of the microstructure during the hardening period of cement pastes, thereby influencing the final properties of hardened cement pastes (HCPs). Although much research on the cement mortars with superplasticizers, polymer latexes and asphalt emulsions have been conducted (Arandigoyen and Alvarez 2007; Beeldens et al. 2005; Czarnecki and Schorn 2007; Gao et al. 2002; Gu et al. 1994; Khatib and Mangat 1999; Knapen and Van Gemert 2009; Ohama et al. 1991; Puertas et al. 2005; Sakai et al. 2006; Song et al. 2006; Xu et al. 2000; Zhang et al. 2011), few studies dwell on their impacts on the pore structure and the impermeability from the viewpoints of microstructure in the fresh state of cement pastes, especially their different impacts originating from the molecular/particle size of the admixtures. Specifically, the formation of the pores may be affected by the addition of these polymers due to their impacts on the microstructure and the rheological properties of fresh pastes, cement hydration, and the shrinkage of hardened pastes. Furthermore, the type of polymers with varied molecular/particle sizes also plays an important role in changing the pore structure and the impermeability.

In this chapter, three types of chemical admixtures commonly used in concrete and mortar (PCE superplasticizer, polyacrylate latexes and asphalt emulsions) which differ in molecular/particle size from nanometer to micron were employed to investigate their effects on the pore structure of hardened cement pastes and the impermeability of hardened mortars. By analyzing the changes in the pore structure and the impermeability with varied polymer dosages and types, the working mechanisms of chemical admixtures with varied sizes were elucidated.

Y. Zhang, *Study on Microstructure and Rheological Properties of Cement-Chemical Admixtures-Water Dispersion System at Early Stage*, Springer Theses, DOI 10.1007/978-981-10-4570-7_7

7.1 Cement-Superplasticizer-Water System

It is well known that for the FCPs without PCE, flocculated structures of cement grains are clearly observed as shown in Fig. 4.13a, whereas for the ones with PCE superplasticizer, as shown in Fig. 4.13b, the cement grains present decent dispersion state. The different organization structures of cement grains in FCPs may lead to different pore structures in HCPs, as schematic drawing in Fig. 7.1. The cement paste with well-dispersed cement grains in the fresh stage might generate finer pore structure after the paste becomes hardened, as described in Fig. 7.1e, f. The so-called inkbottle pore volume may be reduced due to the better dispersion of cement grains in FCPs.

7.1.1 Pore Structure

Traditionally, the pores in HCPs vary in size ranging from a few nanometers to hundreds of microns. Based on their sizes and origins, the pores in HCPs can be subdivided into the following three classes: hydration products pores, capillary pores and air voids (Basheer et al. 2001). Hydration products pores consist of inner C–S–H gel pores (with typical size of 2–4 nm) and outer C–S–H gel pores (also including the pores among various hydrates, with typical size of 20–30 nm). The inner C–S–H gel pores are assumed to be the intrinsic properties of hydrates and should not evolve with W/C in a fully hydrated cement paste. Capillary pores, usually larger than 50 nm, are generally formed by the volume occupied by water that is not consumed in the hydration process. The capillary pores are believed to exert major effects on transporting processes of attacking species in HCPs (Xu et al. 1993a, b). Air voids are formed by air entrainment during the preparation of cement pastes and usually have larger pore size than 1 μm.

From the cumulative curves of MIP, one can obtain some parameters of particular interest like the total pore volume, the critical pore size as well as the threshold pore size (Aligizaki 2005). The total pore volume is the point of maximum intruded volume of mercury, which corresponds to the highest pressure and the smallest equivalent pore size in the cumulative curves. The critical pore size is the most frequently occurring pore size in interconnected pores that allows maximum percolation, corresponding to the steepest slope of the cumulative curve. The threshold diameter is the narrowest path in the interconnected pores, below which commences the great portion of intrusion, corresponding to the sudden inflection point in the injection curve. In the differential curves of MIP, several peaks corresponding to the pores of varied sizes usually can be observed. Vočka et al. (2000) pointed out that the pore size distribution indicated by MIP results depended not only on the pore sizes, but also on the connectivity of pore space. Lower connectivity led to the peak of pore size distribution shifting to smaller size.

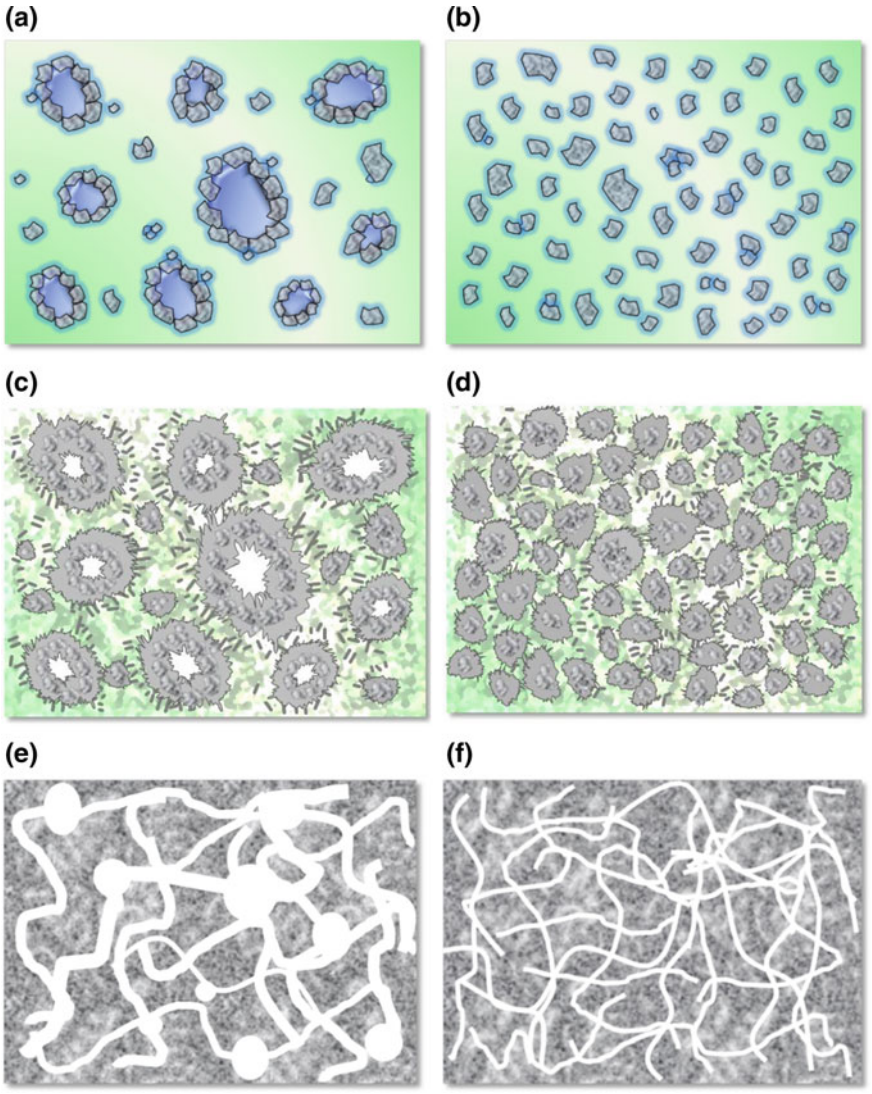

Fig. 7.1 Schematic illustration of the effects of superplasticizer on the microstructure of FCPs and the pore structure of HCPs. **a** Blank FCP; **b** FCP with superplasticizer; **c** blank hydrating cement paste; **d** hydrating cement paste with superplasticizer; **e** blank HCP; **f** HCP with superplasticizer

7.1.1.1 HCPs at W/C of 0.29

The MIP curves of the HCPs cured for 7 and 28 days with varied dosages of PCE are presented in Fig. 7.2 and the pore characteristic parameters of the HCPs are listed in Table 7.1. Figure 7.2a shows a typical inverse S-shaped mercury injection

curve. From Fig. 7.2a, a clear trend is found that the cumulative intrusion volume (i.e. the total pore volume) subsequently declines and the threshold diameter gradually decreases to 50 nm from 200 nm with the increasing addition of PCE. However, at curing age of 28 days, the difference of MIP curves of HCPs caused by the inclusion of PCE becomes rather negligible as seen in Fig. 7.2c.

In Fig. 7.2b, four peaks marked as peak I, II, III and IV can be recognized in the differential pore size distribution curves. According to Vočka et al. (2000), peak I and peak II represent the inner and outer C–S–H gel pores respectively; peak III reflects the capillary pores and peak IV indicates the air voids. With the rise in Sp/C, the position of peak I keeps constant; peak II shifts towards a smaller diameter; peak III and IV disappear. As peak I, centered around 3 nm, reflects the intrinsic nature of C–S–H gel, the position of peak I is unchanged by addition of PCE as well as by the curing age (as seen in Fig. 7.2b, d). Meanwhile, the volume of peak I increases from 0.0088 to 0.0142 mL/g with the increase of Sp/C at 7 days (Table 7.2), while it becomes relatively comparable at 28 days, as shown in Fig. 7.2d. This implies that the cement hydration degree of HCPs at 7 days is increased by the incorporation of PCE. XRD results in Fig. 7.3 and hydration heat

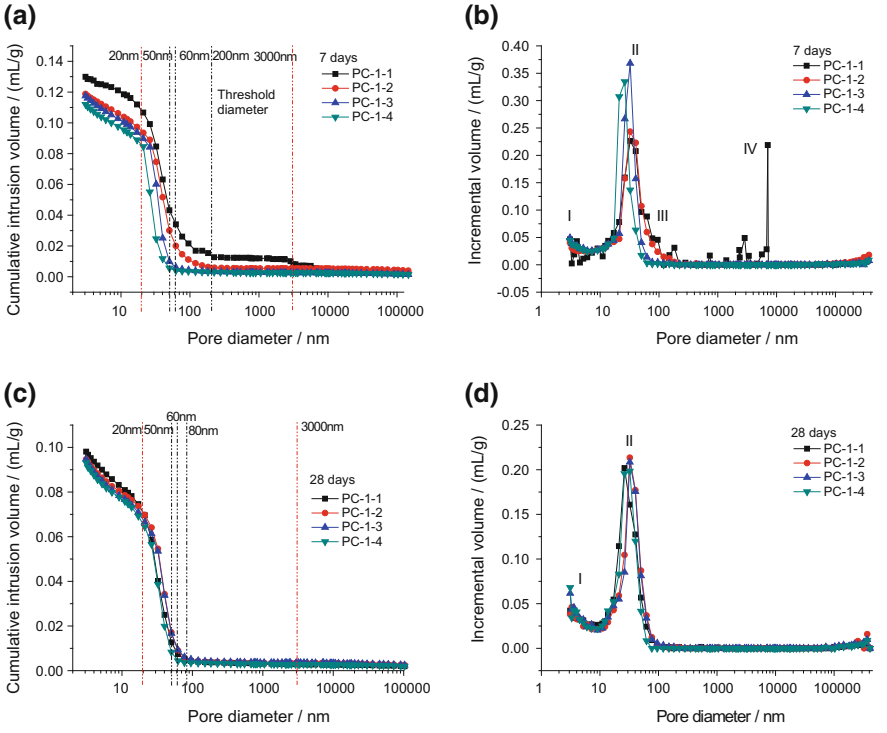

Fig. 7.2 Pore size distribution of the HCPs at W/C of 0.29. **a** Cumulative intruded mercury, 7 days; **b** differential pore size distribution, 7 days; **c** cumulative intruded mercury, 28 days; **d** differential pore size distribution, 28 days

Table 7.1 Pore characteristics of the hardened cement pastes with different superplasticizer dosages at W/C of 0.29

Specimen no.	Pore volume (mL/g)		Porosity (%)		Average pore size (nm)		V_{ib} (mL/g)		*R*f (%)	
	7 days	28 days	7 days	28 days	7 days	28 days	7 days	28 days	7 days	28 days
PC-1-1	0.1299	0.0981	24.50	18.91	25.6	16.5	0.0769	0.0488	59.20	49.75
PC-1-2	0.1188	0.0947	22.52	18.34	21.1	16.3	0.0527	0.0454	44.36	47.44
PC-1-3	0.1175	0.0948	22.35	18.37	18.1	15.9	0.0474	0.0415	40.34	43.77
PC-1-4	0.1119	0.0931	21.60	18.16	16.7	15.4	0.0419	0.0377	37.44	40.49

in Fig. 7.4 confirm that a higher dosage of PCE leads to higher hydration degree at 7 days. This must result from the enhanced contact between water and cement at such low W/C due to the better dispersion of cement grains in FCPs when PCE is added. With the progressing cement hydration, the difference of hydration degree caused by the addition of PCE is diminished at the age of 28 days. For a cement paste without air entraining agent, air voids may be introduced during mixing and casting process when FCP presents poor fluidity. As PCE is added, the fluidity of the FCPs is effectively boosted as presented in Fig. 3.1. Correspondingly, the induced air voids are greatly reduced and consequently, peak IV disappears as shown in Fig. 7.2b.

Looking back at the changes in the total pore volume, the reduced total pore volume at 7 days by the addition of PCE must be a result of higher hydration degree. At 28 days, the total pore volume is less affected by the addition of PCE since the hydration degree is rather comparable as discussed above (Figs. 7.2d and 7.4). Moreover, the increased hydration degree usually leads to the decrease in pore connectivity as more hydration products filling in the capillary pores. Thus, the significant left shifting of peak II, the disappearance of peak III (Fig. 7.2b) and the decrease in threshold pore diameter (Fig. 7.2a) are observed when PCE is added into the pastes.

In addition, the entrapped mercury volume as well as its volume ratio *R*t, obtained from the two cycles of intrusion-extrusion curves as given in Fig. 7.5, presents obvious decline with the incorporation of PCE in cement pastes, as presented in Table 7.2. These results primarily verify the hypothesis described in Fig. 7.1 that FCPs with addition of superplasticizer may develop finer and more homogenously distributed pores after hardened due to the improved dispersion state of cement grains in the fresh pastes.

In summary, at W/C of 0.29, the addition of PCE exerts notable influences on the pore structure of HCPs at early ages. The smaller total porosity and reduced threshold pore size and consequently lower pore connectivity are found in HCPs due to the inclusion of PCE, which results from the dispersing effects of PCE in FCPs and the heightened cement hydration degree. The results are consistent with previous reports of others (Sakai et al. 2006; Khatib and Mangat 1999). The pore size distribution and the pore volume of HCPs cured for 28 days are slightly affected by the addition of PCE, while with the growth in Sp/C, an obvious decrement in the entrapped mercury volume is presented due to the superior dispersion state of cement grains in FCPs.

Table 7.2 Pore volume of the HCPs with W/C of 0.29/(mL/g)

Pore size (nm)	Curing age (days)	PC-1-1 (mL/g)	PC-1-2 (mL/g)	PC-1-3 (mL/g)	PC-1-4 (mL/g)
<10	7	0.0088	0.0126	0.0148	0.0142
	28	0.0149	0.0142	0.0160	0.0154
10–100	7	0.0994	0.0950	0.0983	0.0942
	28	0.0789	0.0760	0.0733	0.0742

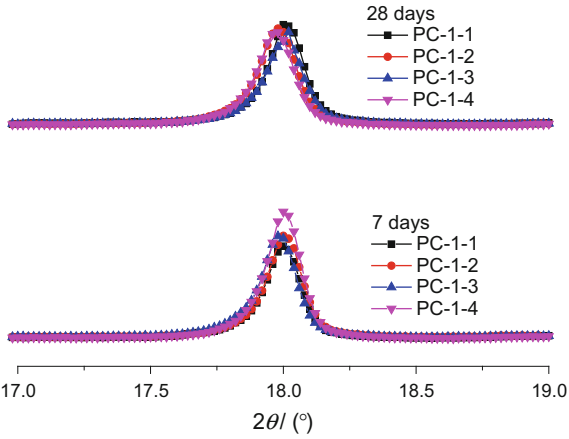

Fig. 7.3 XRD spectra of $Ca(OH)_2$ in HCPs

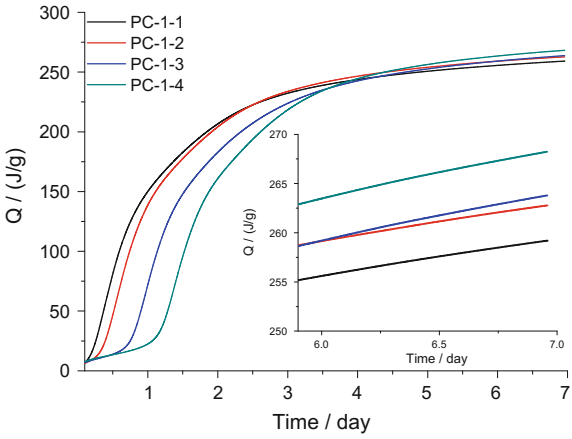

Fig. 7.4 Heat evolution of cement hydration in the HCPs at varied Sp/Cs (W/C = 0.29)

7.1.1.2 HCPs at W/C of 0.4

It has been well reported that the pore structure of HCPs is highly related to W/C (Cook and Hover 1999). Specifically, a higher W/C usually generates larger porosity and higher pore connectivity for a given HCP. On the other hand, a higher W/C may facilitate cement hydration as sufficient water is available surrounding cement grains. Thus, when PCE is added in fresh cement pastes, the enhanced dispersion of cement grains in FCPs at high W/C is expected to have different effects on pore structure of HCPs from that at low W/C.

MIP curves of the HCPs with W/C of 0.4 cured for 7 and 28 days are presented in Fig. 7.6 and the pore characteristic parameters are listed in Table 7.3. As seen from Fig. 7.6a, earlier percolation, i.e., larger threshold diameter, is observed for the HCP with Sp/C of 0.3% and the total pore volumes of HCPs with varied Sp/Cs are almost equal except for the HCP with Sp/C of 0.5%. A clearer trend is found in

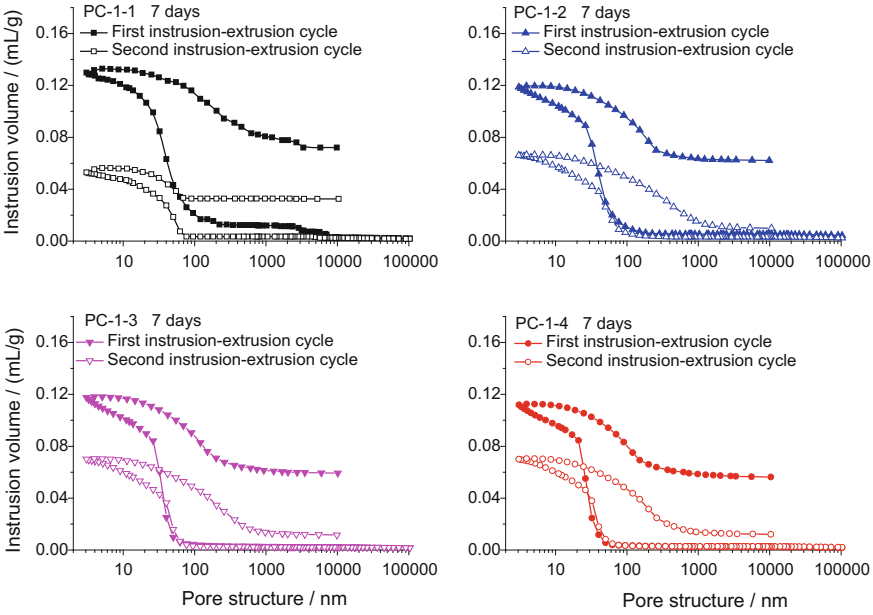

Fig. 7.5 Two cycles of intrusion-extrusion mercury curves of the HCPs at W/C of 0.29

the HCPs at age of 28 days that the increasing PCE dosage in the pastes results in increases of both the total pore volume and the threshold pore size at age of 28 days (see Fig. 7.6c). It should be noted that compared to other HCPs, the HCP with Sp/C of 0.5% (PC-2-4) exhibits notably lower total pore volume and threshold diameter at both ages of 7 and 28 days (see Fig. 7.6a, c). This must originate from severe bleeding during preparation of the FCP, which means that the effective W/C in PC-2-4 is much less than 0.4. Therefore, the HCP with Sp/C of 0.5% is excluded in the following discussion.

In Fig. 7.6b, three marked peaks are visible: inner C–S–H pore peak (peak I), outer C–S–H pore peak (peak II) and capillary pore peak (peak III). As Sp/C increases from 0 to 0.3%, peak I stays at the position of around 3 nm with pore volume rising from 0.0149 to 0.0208 mL/g as shown in Table 7.4. The increase in the corresponding pore volume is again related to the higher hydration degree caused by the incorporation of PCE, as shown by Fig. 7.7. Different from the HCPs with low W/C of 0.29, the enhancement of PCE on cement hydration in HCPs with W/C of 0.4 is even prolonged to the age of 28 days as indicated by the higher volume of peak I in Fig. 7.6d. The cement hydration in HCPs with W/C of 0.29 may stop at a certain age due to insufficient water inside the HCPs and the outer curing water cannot effectively migrate into the hardening cement paste because of its very dense pore structure. Thus the hydration degree in HCPs with W/C of 0.29 reaches almost the same value at 28 days regardless of the addition of PCE, whereas the cement hydration degree still largely differs at W/C of 0.4 due to the

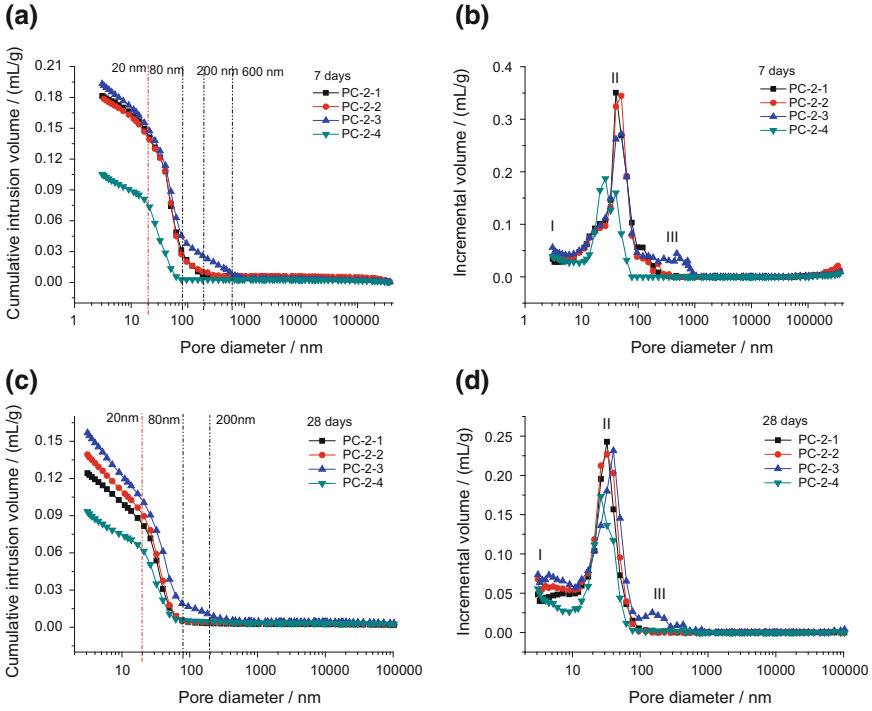

Fig. 7.6 Pore size distribution of the HCPs at W/C of 0.40. **a** Cumulative intruded mercury, 7 days; **b** differential pore size distribution, 7 days; **c** cumulative intruded mercury, 28 days; **d** differential pore size distribution, 28 days

facilitated cement hydration in HCPs by PCE. In the case of HCPs with W/C of 0.4, the addition of PCE leads to a substantial increase in hydration degree even though at age of 28 days. It is believed that the higher capillary pore connectivity enhances the cement hydration during the continuous wet curing.

Different from the results in the 7-day HCPs with W/C of 0.29, peak III shifts towards larger diameters with the addition of PCE in cement pastes at W/C of 0.4 (Fig. 7.6b), which indicates a rise in connectivity of capillary pores or a larger portion of large pores (Vočka et al. 2000). For a blank HCP with high W/C, the capillary pore peak is usually visible in MIP curves at early ages due to the existence of large amount of unconsumed water. When PCE is added, much entrapped water is released from the flocculated structures and sequentially the cement grains are homogenously dispersed in the FCPs. Compared with the low W/C of 0.29, higher W/C of 0.4 facilitates the dispersion of cement grains in greater space which obviously increases with the rise of Sp/C as well. Thus, as hydration proceeds and the paste gets hardened, the throat dimension of an interconnected capillary network is larger for the HCPs with W/C of 0.4 at higher Sp/C. In addition, some dead-end pores or isolated pores in the HCPs may also become connected at high Sp/C due to

Table 7.3 Pore characteristics of the HCPs with different superplasticizer dosages at W/C of 0.4

Specimen no.	Pore volume (mL/g)		Porosity (%)		Average pore size (nm)		V_{ib} (mL/g)		*R*f (%)	
	7 days	28 days	7 days	28 days	7 days	28 days	7 days	28 days	7 days	28 days
PC-2-1	0.1814	0.1243	30.72	25.98	24.3	15.7	0.0698	0.0462	38.48	37.16
PC-2-2	0.1786	0.1393	30.00	24.33	24.3	14.8	0.0688	0.0514	38.52	36.90
PC-2-3	0.1932	0.1568	31.84	26.72	22.5	15.1	0.0756	0.0583	38.41	37.18
PC-2-4	0.1105	0.0933	20.90	18.34	16.8	14.6	0.0328	0.0371	31.15	39.76

Table 7.4 Pore volume of the HCPs with W/C of 0.4/(mL/g)

Pore size (nm)	Curing age (days)	PC-2-1 (mL/g)	PC-2-2 (mL/g)	PC-2-3 (mL/g)	PC-2-4 (mL/g)
<10	7	0.0149	0.0154	0.0208	0.0148
	28	0.0216	0.0268	0.0319	0.0176
10–100	7	0.1447	0.1430	0.1345	0.0878
	28	0.1000	0.1082	0.1100	0.0704

the more homogenous dispersion state of cement grains in the fresh pastes. These effectively increase the connectivity of the pore space in the hardened pastes, which corresponds to the experimentally observed shifts of the capillary pore peak III towards right when PCE is added as well as the increased volume of peak I.

On the other hand, peak II in Fig. 7.6b fails to shift with slight decline in pore volume at 7 days. This is in good agreement with the early findings in literatures that as peak III is visible in the MIP curves, suggesting the capillary pores still form the percolating cluster, the position of peak II is hardly influenced by the changes in the connectivity of capillary pores (Vočka et al. 2000). When the curing age reaches 28 days, the connectivity of capillary pores significantly decreases. Compared with the MIP curves at 7 days (Fig. 7.6b), at 28 days, the peak III disappears and peak II shifts to smaller size for PC-2-1 and PC-2-2, while the position of peak II for PC-2-3 almost keeps stable due to the existence of peak III (Fig. 7.6d).

In a whole, the increases in the total pore volume and the threshold pore size even at age of 28 days (Fig. 7.6c) in the case of higher hydration degree, may again be caused by the boost in the pore connectivity when PCE is added. Similar phenomena could be found in the works of others (Puertas et al. 2005).

Based on the aforementioned results on the pore structure in HCPs with W/C of 0.29, we know that the addition of PCE reduces the entrapped mercury volume due to the disassembly of the flocculated structures in the FCPs. However, for the HCPs

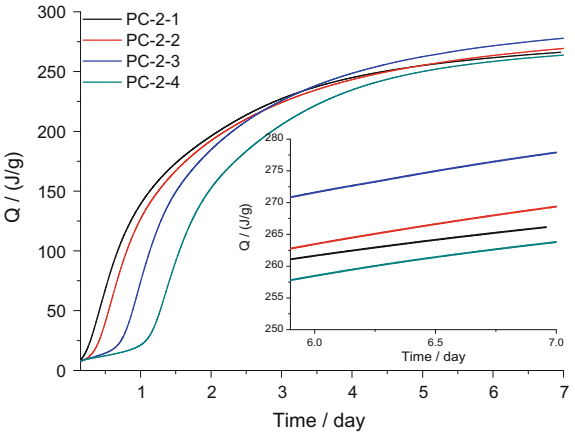

Fig. 7.7 Heat evolution of cement hydration in the HCPs at varied Sp/Cs (W/C = 0.40)

with W/C of 0.4, the entrapped mercury volume at 7 days increases to 0.0756 mL/g (PC-2-3) from 0.0698 mL/g (Blank paste, PC-2-1) by the addition of PCE. At 28 days, the entrapped mercury volume unexceptionally ascends with the increasing Sp/C. From the two cycles intruded mercury curves in Fig. 7.8, it is noted that the intruded mercury curve in the second cycle fails to repeat the section of the curve from 100 to 600 nm after the first intrusion-extrusion cycle, which means that the pores of 100–600 nm induced by the addition of PCE can also entrap mercury. The elevated entrapped mercury volume is supposed to result from the heightened connectivity of the pore space.

From the discussion above, it is found that PCE superplasticizer influences the pore structure of HCPs with varied W/Cs from different aspects. At W/C of 0.29, the dispersion effects of PCE in FCPs facilitate the cement hydration at early age of 7 days and the enhanced cement hydration caused by PCE becomes negligible at 28 days due to the insufficiency of internal curing water and the difficult migration of outer curing water into such dense cement pastes. In this way, at age of 7 days, the total pore volume of HCPs and the threshold pore size are clearly reduced by the addition of PCE, whereas at 28 days, the pore structure of HCPs becomes rather identical regardless of the addition of PCE. On the other hand, in the case of W/C of 0.4, the facilitating effects on cement hydration by the dispersion effects of PCE are prolonged to the age of 28 days, which is believed that the increased pore connectivity in HCPs by the addition of PCE plays a role here. Despite the higher

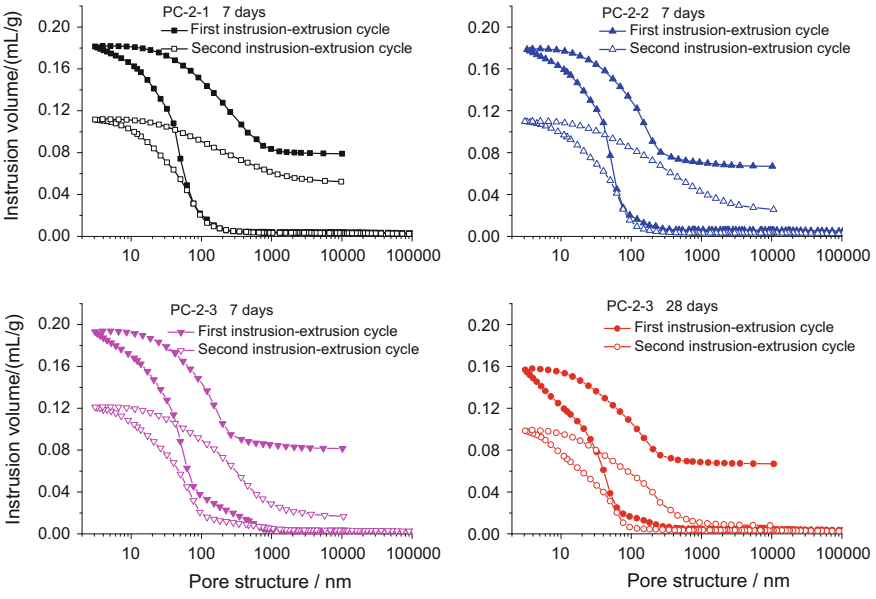

Fig. 7.8 Two cycles of intrusion-extrusion mercury curves of the HCPs at W/C of 0.40

hydration degree, it is interestingly found that even at age of 28 days, the total pore volume and the threshold pore size are apparently increased by the inclusion of PCE, which is believed a result of increased pore connectivity.

7.1.2 Impermeability

AC impedance spectra are often plotted in real ± imaginary complex plane and are parameterized by frequency. This type of parametric plot showing the current response generated at each frequency is known as Nyquist plot. The Nyquist plot for hardened mortars is of the Randles type, which is characterized by a semicircle in high-frequency range and a straight line in low-frequency range, Fig. 7.9a. The diameter of the semicircle is closely related to the microstructure of porous materials and very sensitive to the changes in the microstructure, which increases significantly with the hydration time and compactness (Gu et al. 1993; Song 2000; Wei et al. 1995; Xu et al. 1993a, b). The diameter of the semicircle is also found to be inversely proportional to the porosity and the average pore size of the porous materials (Xie et al. 1993). The left interception of the semicircle on the real axis in high-frequency range is determined by the resistance of the electrolytic solutions in the pores. The resistance is inversely proportional to the porosity (Gu et al. 1993; Xu et al. 1993a, b). The coefficient of diffusion impedance can be calculated from the slope in the resistance versus $\omega^{-1/2}$ plots in the low-frequency curve, which reflects the development of capillary pore structure and is in inverse proportion to diffusion coefficient (Xie et al. 1993). The impedance response of the cement mortars is described by the equivalent circuit illustrated in Fig. 7.9b, where R_0 is the resistance of the electrolytic solution, R_1 is the resistance of the charge transfer, and C_1 is the capacitance of the electrode/mortar specimen interface. All of these electric properties (as shown in Table 7.5) could be simulated using the software Zsimpwin 3.1.

The AC impedance spectra of the hardened mortars cured for 7 and 28 days with varied superplasticizer dosages are shown in Fig. 7.10. The Nyquist plots of AC

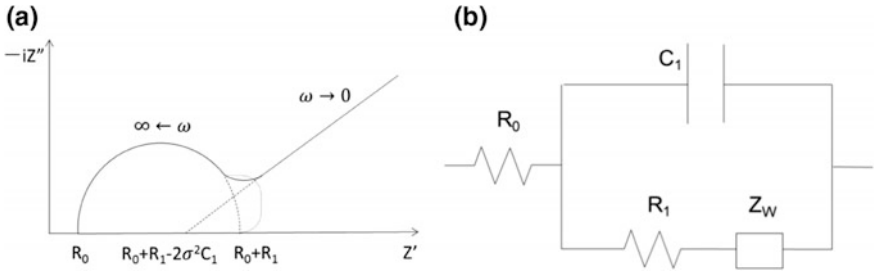

Fig. 7.9 Nyquist plot and equivalent circuit. **a** Nyquist plot of an electrochemical of Randles type; **b** equivalent circuit of Nyquist plot

Table 7.5 Calculated electric properties of the impedance spectroscopy for the mortars with different superplasticizer dosages

Specimens no.	C_1/F		$R_0 + R_1$/Ω		σ/Ω	
	7 days	28 days	7 days	28 days	7 days	28 days
PC-1-1-S	2.290E−11	1.557E−11	815.0	1066.2	1454.51	1958.84
PC-1-2-S	1.765E−11	1.419E−11	900.0	1171.8	1467.93	1982.92
PC-1-3-S	1.634E−11	1.499E−11	1006.6	1216.1	1535.93	1995.41
PC-1-4-S	1.677E−11	1.274E−11	1048.4	1404.1	1647.60	2052.33
PC-2-1-S	3.524E−11	2.693E−11	378.8	486.6	1374.17	1769.95
PC-2-2-B	3.473E−11	2.701E−11	443.3	575.8	1376.57	1792.61
PC-2-3-S	2.792E−11	1.942E−11	496.4	731.6	1405.62	1837.38
PC-2-4-S	2.692E−11	1.859E−11	581.4	886.4	1412.39	1998.46

impedance spectra for the hardened mortars in high-frequency range exhibit typical semicircles and the diameters of the semicircles become larger as Sp/C and curing age increase. Correspondingly, the bulk resistance of the mortars ($R_0 + R_1$) significantly increases with the addition of superplasticizer and with the growth of curing age, which indicates the decreased porosity and pore size. Based on the results of AC impedance spectra in high-frequency region, it is concluded that the addition of superplasticizer and the longer curing age lead to a denser microstructure of the hardened mortars. Therefore, it is expected that the denser microstructure is an indicator for lower permeability of mortars when PCE is incorporated.

In low-frequency region, the Nyquist plots of AC impedance spectra for hardened mortars are straight lines and the coefficient of Warburg impedance σ presents an increase with the growth in PCE dosage and curing age, as listed in Table 7.5, suggesting that the impermeability of the mortars is enhanced due to the inclusion of superplasticizer. In addition, σ of the mortars cured for 28 days is higher than

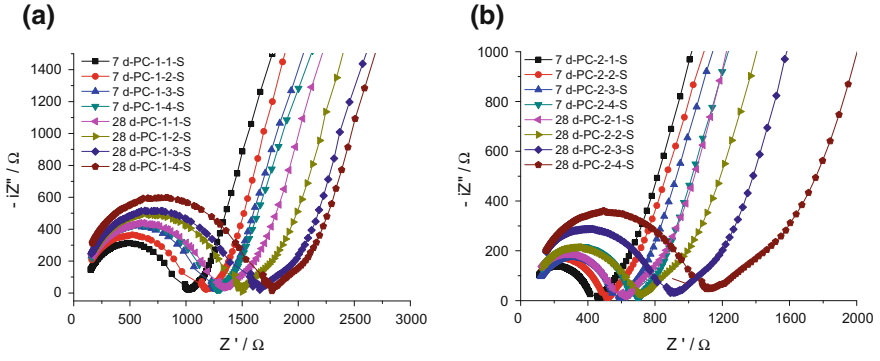

Fig. 7.10 Niquist plots of the mortars with different PCE dosages. **a** W/C = 0.29; **b** W/C = 0.40

that cured for 7 days. These phenomena are compatible with the results of AC impedance in high-frequency range.

It has been well accepted that the impermeability of cement mortars is primarily determined by the pore structure of HCPs as well as the interfacial transition zones (ITZs) between aggregates and cement pastes. As described above, the addition of superplasticizer results in reduced porosity and connectivity in the HCPs at W/C of 0.29 at early ages. All of these are the factors leading to denser structure and lower permeability of the hardened cement mortars. Besides modifying the pore structure of cement paste, PCE superplasticizer could also cause a closer packing of cement grains adjacent to the aggregates due to the improved dispersion state in fresh state, which is essential to reduce the interfacial heterogeneity, i.e., the microstructure and the thickness of transition zone (Xu et al. 2000). In this case, for cement mortars with W/C of 0.4, the increases in impedance and impermeability are mainly attributed to the denser transition zones, whereas for cement mortars with W/C of 0.29, the finer pore structure of cement paste and the significant reduction in interfacial heterogeneity are both responsible for the enhanced impedance and impermeability.

7.2 Cement-Latex-Water System

Based on the previous chapter, it is known that polymer latexes also have plasticizing effects in fresh cementitious mixtures due to the adsorption of polymer particles on the surface of cement grains and consequently better dispersion state of cement grains. For latex L1, the fluidity is markedly increased at high dosages of polymer latexes (L/C > 3%). The addition of latex L2 obviously declines the fluidity at L/C lower than 3% and then the fluidity begins to increase with further addition of polymer latex. Similar to superplasticizers, the influences of polymer latexes on the pore structure of HCPs that originates from the changes in the flocculated structures of cement grains should be expected. On the other hand, different from superplasticizer, polymer particles in latexes exist in a condensed state with particle size of 200–300 nm, which are impossible to be integrated into cement hydrates during cement hydration. During cement pastes hardening, the polymer particles or the polymer films formed by the agglomeration of polymer particles fill in the capillary pores (as schematically described in Fig. 7.11). In this way, the impermeability of HCPs may be more remarkably enhanced by adding polymer latexes than adding superplasticizer due to the combination of plasticizing effects and filling effects.

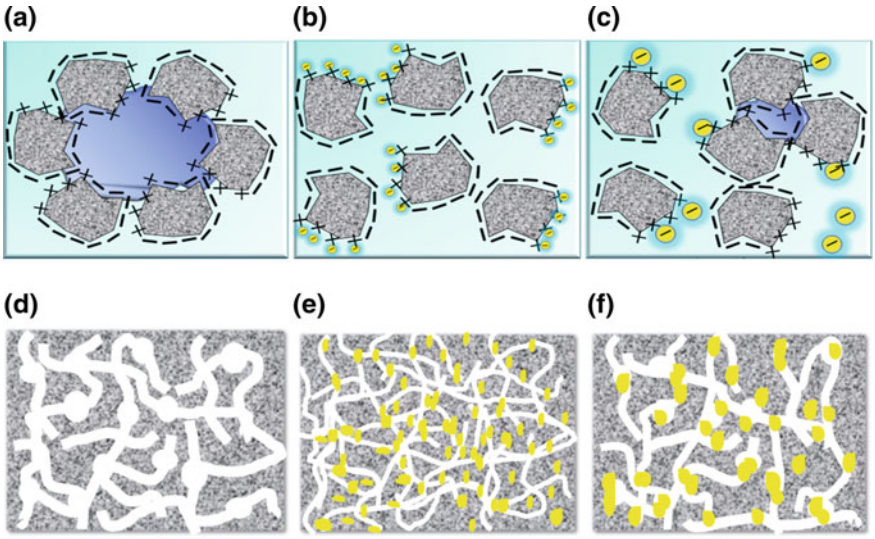

Fig. 7.11 Impact of polymer latexes on the microstructure of cement pastes at the same L/C. **a** Blank FCP; **b** FCP with latex L1; **c** FCP with latex L2; **d** blank HCP; **e** HCP with latex L1; **f** HCP with latex L2 (: cement grain; : free water; : entrapped water; : latex L1; : latex L2; : hardened cement paste; : agglomerated polymer particles)

7.2.1 Pore Structure

The pore size distribution curves of the HCPs with different latex contents are shown in Fig. 7.12. Four peaks corresponding to four families of pores, marked as peak I, II, III and IV, can be recognized in the MIP curves of the HCPs cured for 7 and 28 days. Based on the theory in Sect. 7.1.1, it can be concluded that in

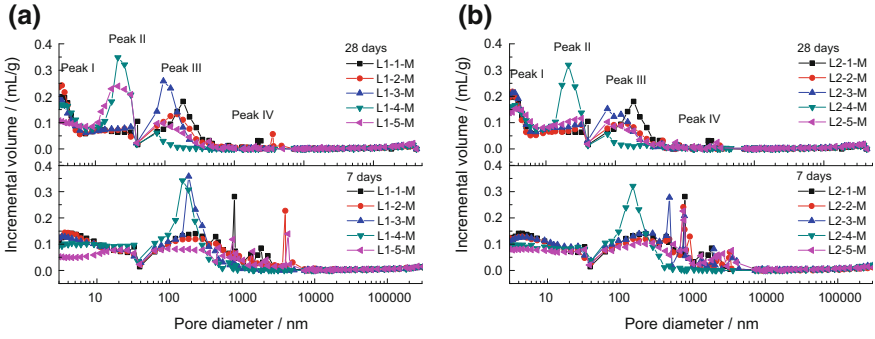

Fig. 7.12 Pore size distribution of the cement pastes with varied latex dosages. **a** HCPs with latex L1; **b** HCPs with latex L2

Fig. 7.12, peak I and peak II represent the C–S–H gel pores, peak III reflects the capillary pores and peak IV indicates the air voids. For the HCPs cured for 7 days, the C–S–H gel pores (peak I and peak II) are very small due to the low hydration degree. The incorporation of polymer latexes in HCPs leads to lowered peak I and left shifting of peak III at L/C larger than 3%. The lowered peak I must result from the reduced hydration degree by the addition of polymer latexes, which is known as the retardation effects of polymer latexes (Li and Kong 2009; Silva and Monteiro 2006). At L/C larger than 3%, the left shifting of peak III implies the decrease in connectivity of capillary pores and the reduced portion of large pores due to the filling effects of polymer particles or films. For 28 days HCPs, the C–S–H gel pores (peak I and peak II) grow significantly with the development of cement hydration. It is noted that a high polymer content (L/C > 3%) results in lower peak I and more pronounced peak II compared with the blank HCP, suggesting that more outer C–S–H gel pores are produced by the incorporation of polymer. Similar to 7 days HCPs, left shifting of peak III (the capillary pores) is also observed in 28 days HCPs with the addition of polymer.

It is known that capillary pores (>50 nm) are the dominating factor for the permeability of HCPs, while the pores with size less than 50 nm play minor roles in the permeability of HCPs (Basheer et al. 2001). Therefore, it is expected that the left

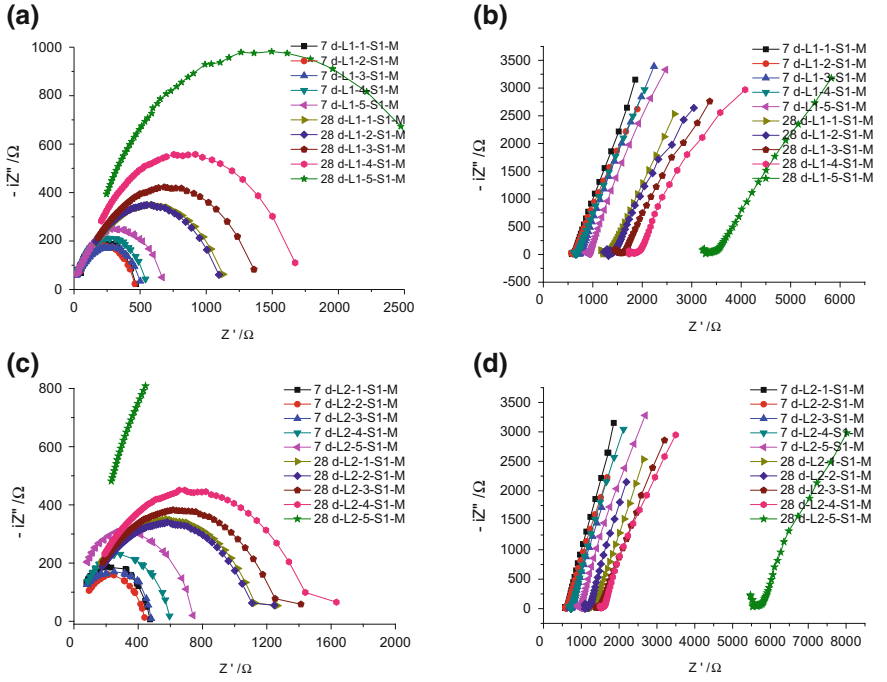

Fig. 7.13 Niquist plots of the hardened mortars with different latex dosages. **a** L1-high frequency; **b** L1-low frequency; **c** L2-high frequency; **d** L2-low frequency

shifting of peak III is an indicator for lower permeability of HCPs when polymer latexes are incorporated. The impacts of polymer on the pore structure of HCPs are similar for both polymer latex L1 and L2 (Fig. 7.12a, b).

7.2.2 *Impermeability*

The Nyquist impedance spectra of the mortars with different latexes contents are shown in Fig. 7.13. The impedance response of the latex modified mortars cured for 7 and 28 days can be described by the equivalent circuits illustrated in Fig. 7.14 (Zhong et al. 2002). R_2 and C_2 are the resistance and the capacitance of polymer respectively. It is seen in Fig. 7.13, at very low L/C (<3%), the diameter of the semicircle is slightly affected by polymer. With more incorporation of polymer latexes in the pastes, the diameter of the semicircle becomes larger. The left interceptions of the semicircles on real axis in high-frequency curves almost remain constant regardless of the addition of polymer latexes. These observations indicate that the incorporation of polymer remarkably increases the compactness of the hardened mortars when L/C is high, and has little effect on the whole porosity. It is also obvious that the diameter of the semicircle grows with the curing age because of the development of cement hydration. Correspondingly, Table 7.6 presents that R_0 makes a trivial fluctuation, R_1 increases constantly after a slight drop, and R_2 significantly increases with the growth in polymer content. The increase in R_1 suggests average pore size declines with the addition of polymer latexes, which is in very good agreement with the left shifting of peak III in MIP curves (Fig. 7.12). The slight drop in R_1 implies average pore size increases when L/C is low, which may result from the poorer dispersion of cement grains in FCPs or the poorer fluidity of FCPs as seen in Fig. 3.24. The mortars cured for 28 days possess higher R_0 and R_1, which indicates that the average pore size decreases with longer curing age due to the enhancements of hydration degree.

The variation of σ presents that low latex contents could slightly degrade the impermeability of mortars while a high latex content is beneficial to enhance the impermeability of mortars, which is consistent with the results of AC impedance in high-frequency range.

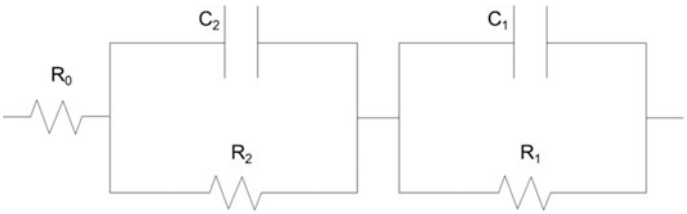

Fig. 7.14 Equivalent circuits of polymer modified mortars

Table 7.6 Calculated electric properties of the impedance spectroscopy for the mortars with different latex contents

Specimens no.	R_0 (Ω)		C_1 (F)		R_1 (Ω)		C_2 (Ω)		R_2 (F)		σ (Ω)	
	7 days	28 days	7 days	28 days	7 days	28 days	7 days	28 days	7 days	28 days	7 days	28 days
L1-1-S1-M	34.63	162.6	2.43E −11	1.74E −11	403.6	703.4	–	–	–	–	1005.41	1027.73
L1-2-S1-M	45.68	160.3	2.57E −11	1.73E −11	383.3	693.8	–	3.50E −10	–	276.0	991.57	1188.01
L1-3-S1-M	46.72	162.6	2.55E −11	1.57E −11	390.3	806.5	–	3.07E −10	–	356.2	1042.90	1262.55
L1-4-S1-M	64.71	165.3	2.40E −11	1.28E −11	453.2	946.8	–	1.43E −10	–	553.4	1071.86	1421.02
L1-5-S1-M	67.19	187.7	2.24E −11	9.77E −12	541.0	1466.0	–	7.17E −11	–	1251.0	1151.72	1613.13
L2-1-S1-M	34.63	162.6	2.43E −11	1.74E −11	403.6	703.4	–	–	–	–	1005.41	1027.73
L2-2-S1-M	37.86	162.9	2.95E −11	1.76E −11	335.7	662.0	–	4.12E −10	–	265.6	953.09	1022.85
L2-3-S1-M	37.80	166.3	2.65E −11	1.66E −11	380.0	732.4	–	3.23E −10	–	331.9	995.79	1208.32
L2-4-S1-M	55.25	166.9	2.47E −11	1.49E −11	436.2	818.6	–	2.31E −10	–	436.3	1043.14	1382.83
L2-5-S1-M	76.54	184.8	1.73E −11	8.63E −12	653.4	2501.0	–	4.12E −11	–	2123.0	1155.75	1626.69

L1 and L2 are two types of latexes and different in particle size and glass transition temperature (T_g). They may lead to different behaviors in cement pastes. In comparison with L2, L1 more significantly decreases the average pore size of the HCPs (indicated by R_1 in AC impedance), and enhances the impermeability of the mortars when L/C is less than 12%. This phenomenon can be explained by the fact that latex L1 leads to better dispersion state of cement grains in FCPs than L2 due to its smaller polymer particle size as suggested in Fig. 7.11. At the same L/C, the number of small polymer particles in L1 is much more than that in L2. Therefore, L1 reduces the flocculated structures more effectively than L2. The schematic illustration of the adsorption of polymer particles with different sizes onto the surface of cement grains is shown in Fig. 7.11.

When L/C is 12%, the pore structure is significantly affected by the filling effects of latex particles in the pores and the transition zones, and also the film formation of polymer particles in these places. The lower impermeability of HCPs with L1 might be due to the poorer film formation ability of L1 due to its higher T_g than L2. L2 is more effective to compact the interfacial zones between phases, so that the impermeability of the HCPs is more enhanced. As presented in Fig. 7.15, it is observed that the microstructure of the HCPs with L2 is more compact than that with L1. All in all, L1 with smaller particle size and poorer film formation ability results in higher impermeability when L/C is low. By contrast, L2 with larger particle size and better film formation ability produces higher impermeability when L/C is higher.

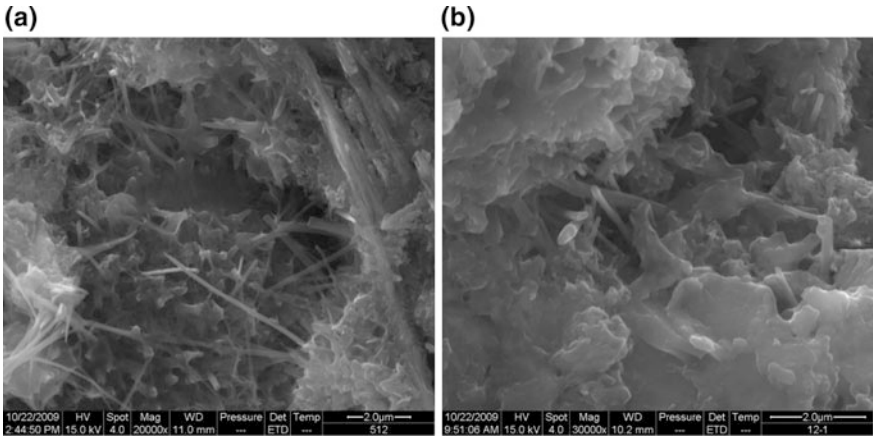

Fig. 7.15 SEM photographs of the HCPs cured for 28 days. **a** HCP with 12% latex L1; **b** HCP with 12% latex L2

7.3 Cement-Asphalt-Water System

Asphalt emulsions can also affect the fluidity of fresh CAMs and the pore structure of hardened CAMs due to their adsorption on cement grains and filling effects. A previous study proved that, at the same W/C, the fluidity of cement pastes can be increased by adding a certain amount of asphalt emulsions (asphalt to cement ratio <20%). In other words, the addition of asphalt emulsions causes a plasticizing effect on the cement paste to some extent. Along with cement hydration, the agglomeration of asphalt particles and film formation adsorbed on cement occur, which effectively changes the microstructure by compacting the interfacial zones among phases. Finally, a structure of dense interpenetrating network is formed, involving cement hydrates, fine aggregates, and asphalt membranes (Yang et al. 2010). In addition, with the increase of asphalt content, the hydrophobic asphalt emulsion gradually becomes the main phase in CAMs. The covering of asphalt membrane on cement grains, hydration products and aggregates resists the penetration of water (Song et al. 2006), which ensures the enhancement in the impermeability of CAMs to a certain extent.

Based upon the above discussions, it is convinced that both the increased fluidity of fresh pastes and the filling effects of polymer latexes and asphalt emulsions have positive effects on the declines of the average pore size and the enhancement in impermeability. The pore structure and the impermeability are primarily determined by the filling effects when their contents are high. In practice, the A/C of a typical CAM is ranging from 0.2 to 1.0, much higher than those of superplasticizers and polymer latexes. As a result, the massive addition of asphalt emulsions results in a sharp decrease in the permeability of CAMs. Therefore, the semicircle diameter of the CAMs in high-frequency curves increases with the rise in A/C, as shown in Fig. 7.16 and Table 7.7. It is noted that, at A/C of 80%, the reduced compactness and impermeability of the CAMs are caused by the increased W/C resulting from the large amount of water associated with the asphalt emulsions.

The findings in Chap. 3 demonstrate that anionic asphalt emulsion enhances the fluidity of cement asphalt pastes more effectively than cationic asphalt emulsion because the former one causes a better dispersion state of cement grains in the fresh pastes. Consequently, the CAMs containing anionic asphalt emulsion should possess more compact structure. The AC impedance results show that the CAMs with anionic asphalt emulsion have relatively denser structure and stronger impermeability than those with cationic asphalt emulsion, as shown in Fig. 7.16a, b.

7.4 Summary

Three types of chemical admixtures (PCE superplasticizer, polyacrylate latexes, and asphalt emulsions) were used to investigate their effects on the pore structure of the hardened pastes and the impermeability of the mortars cured for 7 and 28 days. It is

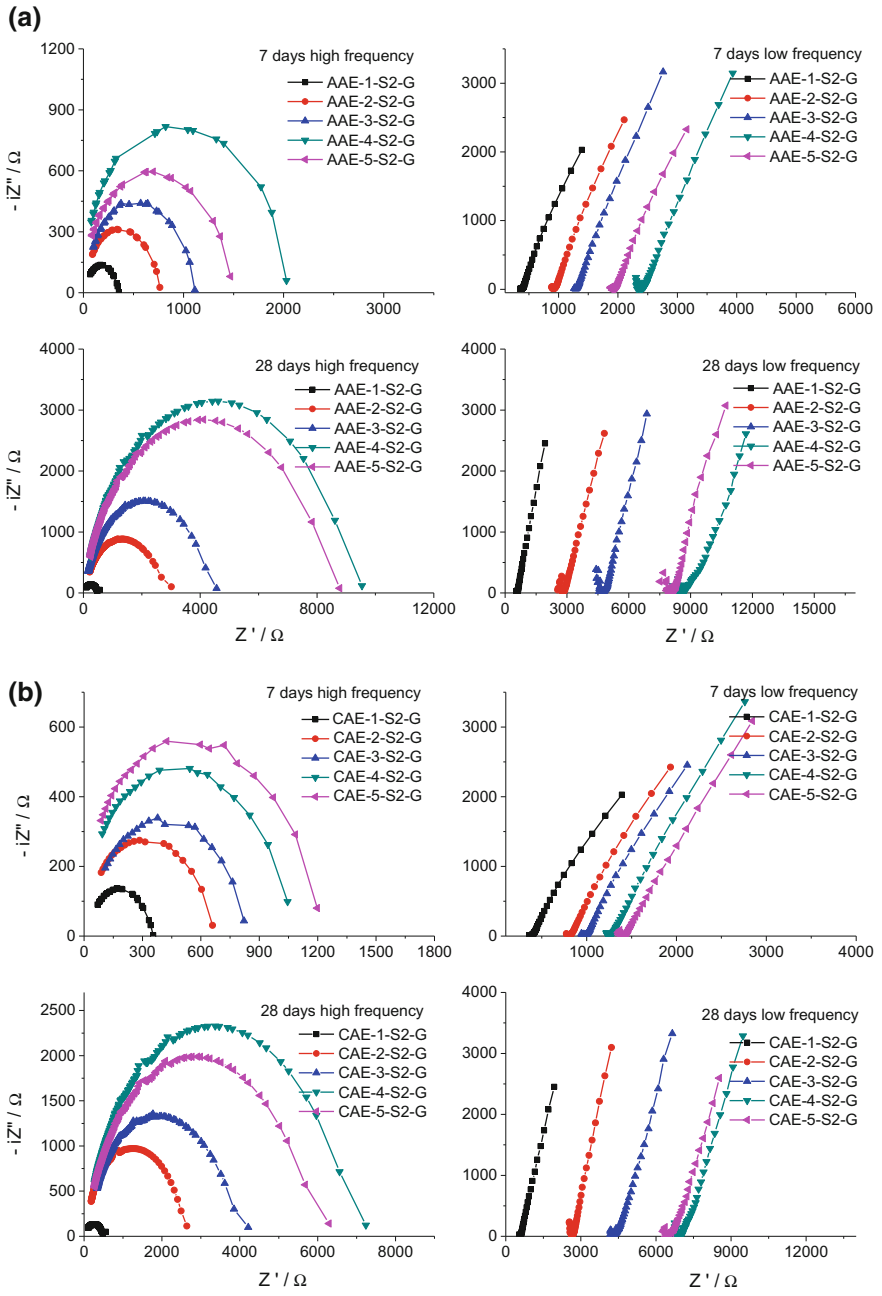

Fig. 7.16 Niquist plots of the CAMs with different asphalt contents. **a** CAMs with anionic asphalt emulsion; **b** CAMs with cationic asphalt emulsion

Table 7.7 Coefficient of diffusion impedance σ (Ω) of the HCPs with different asphalt contents

Specimens no.		AE-1-S2-G	AE-2-S2-G	AE-3-S2-G	AE-4-S2-G	AE-5-S2-G
Anionic asphalt emulsion	7 days	956.57	1003.97	1011.50	1091.11	1072.79
	28 days	963.96	1713.98	1896.27	2665.19	1903.17
Cationic asphalt emulsion	7 days	956.57	957.63	971.25	1021.98	1009.16
	28 days	963.96	1122.56	1813.60	1948.94	1846.16

believed that these admixtures affect the pore structure and the impermeability from three perspectives: (1) changing the flocculation microstructure of cement grains; (2) altering cement hydration process; (3) filling the pores and the cracks in the transition zones and forming films in many cases.

(1) Superplasticizer alters the pore structure of the HCPs due to the improved dispersion of cement grains in FCPs and due to the modified cement hydration kinetics in HCPs. The effects are associated with the W/C and the curing age of the HCPs. In the HCPs with W/C of 0.29, at curing age of 7 days, the total pore volume of HCPs and the threshold pore size are significantly reduced and the gel porosity with size smaller than 10 nm is increased by the incorporation of PCE, whereas at 28 days, the pore structure of HCPs becomes rather identical regardless of the addition of PCE. By contrast, in the case of HCPs with W/C of 0.4, the gel porosity (<10 nm) is significantly heightened in the presence of PCE even at age of 28 days. In spite of the higher hydration degree, the total pore volume and the threshold pore size are apparently increased even at age of 28 days, which indicates the increased pore connectivity by the inclusion of PCE. For cement mortars, the presence of PCE is beneficial to promote the more homogenous dispersion of cement grains in fresh state. Furthermore, the interfacial transition zones of the hardened mortars are densified by adding PCE, which definitely brings a notable increment in the impermeability of the hardened mortars.

(2) The addition of polymer latexes leads to the peak of capillary pores in HCPs shifting to smaller size, and reduces the connectivity of capillary pores due to both plasticizing effects and filling effects. C–S–H gel pore volume presents an obvious drop due to the retardation effects of polymer latexes on cement hydration, especially at early age. For cement mortars with polymer latexes and asphalt emulsions, the impermeability is modified due to the combined effects of plasticizing and filling. At low L/C (<3%), adding polymer latex has little effect on the impermeability. Further addition of polymer latexes leads to a significant enhancement in the impermeability. It is believed that the filling effects play a dominant role in increasing the impermeability when their dosages are high.

(3) At the same L/C, latex L1 is more effective in reducing the average pore size and enhancing the impermeability than L2. This is because latex L1 possesses better plasticizing effects than L2 at the same dosage because of its smaller particle size. Similarly, at the same asphalt content, anionic asphalt emulsion with better plasticizing effects leads to lower permeability of CAMs.
(4) For PCE superplasticizers, which usually have hydraulic radius of 5–20 nm in aqueous solution, the plasticizing effects in FCPs are the main controlling factor for the finer pore structure of HCPs and the enhanced impermeability of mortars. On the other hand, for polymer latexes with particle size in the range of 100 to 1000 nm, their plasticizing effects contribute a lot at low dosages and the filling effects are dominant at high dosages in terms of declining pore size and augmenting impermeability. Regarding asphalt emulsions, filling effects play essential roles in reducing pore size and enhancing impermeability due to larger particle size ranging from 1 to 10 μm.

References

Aligizaki KK (2005) Pore structure of cement-based materials: testing, interpretation and requirements. CRC Press, Boca Raton

Arandigoyen M, Alvarez JI (2007) Pore structure and mechanical properties of cement-lime mortars. Cem Concr Res 37(5):767–775

Basheer L, Kropp J, Cleland DJ (2001) Assessment of the durability of concrete from its permeation properties: a review. Constr Build Mater 15(2):93–103

Beeldens A, Van Gemert D, Schorn H et al (2005) From microstructure to macrostructure: an integrated model of structure formation in polymer-modified concrete. Mater Struct 38(6):601–607

Cook RA, Hover KC (1999) Mercury porosimetry of hardened cement pastes. Cem Concr Res 29 (6):933–943

Czarnecki L, Schorn H (2007) Nanomonitoring of polymer cement concrete microstructure. Restor Build Monum 13(3):141–152

Gao JM, Qian CX, Wang B et al (2002) Experimental study on properties of polymer-modified cement mortars with silica fume. Cem Concr Res 32(1):41–45

Gu P, Xie P, Beaudoin JJ et al (1994) Investigation of the retarding effect of superplasticizers on cement hydration by impedance spectroscopy and other methods. Cem Concr Res 24(3): 433–442

Gu P, Xu Z, Xie P et al (1993) Application of AC impedance techniques in studies of porous cementitious materials: (I): influence of solid phase and pore solution on high frequency resistance. Cem Concr Res 23(3):531–540

Khatib JM, Mangat PS (1999) Influence of superplasticizer and curing on porosity and pore structure of cement paste. Cement Concr Compos 21(5):431–437

Knapen E, Van Gemert D (2009) Cement hydration and microstructure formation in the presence of water-soluble polymers. Cem Concr Res 39(1):6–13

Li QH, Kong XM (2009) Properties and microstructure of polymer modified mortar based on different acrylate latexes. J Chin Ceram Soc 1:024

Ohama Y, Demura K, Kobayashi K et al (1991) Pore size distribution and oxygen diffusion resistance of polymer-modified mortars. Cem Concr Res 21(2):309–315

Puertas F, Santos H, Palacios M et al (2005) Polycarboxylate superplasticiser admixtures: effect on hydration, microstructure and rheological behaviour in cement pastes. Adv Cem Res 17(2): 77–89

Sakai E, Kasuga T, Sugiyama T et al (2006) Influence of superplasticizers on the hydration of cement and the pore structure of hardened cement. Cem Concr Res 36(11):2049–2053

Silva DA, Monteiro PJM (2006) The influence of polymers on the hydration of portland cement phases analyzed by soft X-ray transmission microscopy. Cem Concr Res 36(8):1501–1507

Song G (2000) Equivalent circuit model for AC electrochemical impedance spectroscopy of concrete. Cem Concr Res 30(11):1723–1730

Song H, Do J, Soh Y (2006) Feasibility study of asphalt-modified mortars using asphalt emulsion. Constr Build Mater 20(5):332–337

Vočka R, Gallé C, Dubois M et al (2000) Mercury intrusion porosimetry and hierarchical structure of cement pastes: theory and experiment. Cem Concr Res 30(4):521–527

Wei DF, Chatterjee I, Jones DA (1995) Evaluation of corrosive degradation in coated steel using alternating current impedance spectroscopy. Corrosion 51(2):97–104

Xie P, Gu P, Xu Z et al (1993) A rationalized A.C. impedence model for microstructural characterization of hydrating cement systems. Cem Concr Res 23(2):359–367

Xu G, Beaudoin JJ, Jolicoeur C et al (2000) Interfacial transition zone characterization of Portland cement mortars containing relatively high dosages of polynaphthalene sulfonate superplasticizers. Concr Sci Eng (Fr) 2(7):150–157

Xu Z, Gu P, Xie P et al (1993a) Application of A.C. impedance techniques in studies of porous cementitious materials, (II): relationship between ACIS behavior and the porous microstructure. Cem Concr Res 23(4):853–862

Xu Z, Gu P, Xie P et al (1993b) Application of A.C. impedance techniques in studies of porous cementitious materials (III): ACIS behavior of very low porosity cementitious systems. Cem Concr Res 23(5):1007–1015

Yang JB, Yan PY, Kong XM et al (2010) Study on the hardening mechanism of cement asphalt binder. Sci China Technol Sci 53(5):1406–1412

Zhang YR, Kong XM, Zhang ZL et al (2011) Impermeability of polymer modified mortar with different acrylate latexes. Sci Technol Commer Mortar 11:86–91 (in Chinese)

Zhong S, Shi M, Chen Z (2002) A study of polymer-modified mortars by the AC impedance technique. Cem Concr Res 32(6):979–982

Chapter 8
Conclusions of the Research

This chapter presents the conclusions of the research based on the main findings stated in the previous chapters. The original contributions to the knowledge and the practical applications in real cases are also discussed. Future work arising from the research with regards to the impacts of chemical admixtures on cement mortars and concrete as well as a more general outlook are proposed.

8.1 Conclusions of the Research

The workability and/or the rheological properties of fresh concrete is one of the most important properties of concrete both for casting at initial stage and even for performance during a long-term service. In recent years, the rheological properties of fresh concrete could be tuned in a wide range in virtue of the advanced chemical admixture technology. Water soluble superplasticizers like polycarboxylate type superplasticizer, and water dispersible admixtures such as polymer latexes, asphalt emulsions were within the scope of investigation as chemical admixtures. However, for a long time, the research on these chemical admixture has been significantly lagged behind the development of industry, where the influence mechanisms of various chemical admixtures on the rheological properties and workability of cementitious materials have not been fully investigated and clarified. This becomes a main obstacle to both further development of chemical admixture technology and the practical applications of chemical admixtures in the concrete industry.

Rheology is highly governed by the microstructure of the cementitious materials. Therefore, in the research, the rheological properties and the microstructure of fresh cement pastes (FCPs) containing various chemical admixtures are investigated. Superplasticizers, polyacrylate latexes and asphalt emulsions, which differ in molecular/particle size from nanometer to micron, were incorporated into the FCPs

Y. Zhang, *Study on Microstructure and Rheological Properties of Cement-Chemical Admixtures-Water Dispersion System at Early Stage*, Springer Theses, DOI 10.1007/978-981-10-4570-7_8

to evaluate their effects and working mechanisms, corresponding to Cement-Superplasticizer-Water system, Cement-Latex-Water system and Cement-Asphalt-Water system respectively. Fluidity, yield stress and plastic viscosity of FCPs at varied superplasticizer to cement ratios (Sp/Cs), water to cement ratios (W/Cs), temperature (T) and elapsed time (t) were measured. The viscoelastic properties were also estimated by a microrheometer. The microstructure of FCPs was characterized by a combination of different microscopes and a clear correlation of microstructure with fluidity of FCPs was correspondingly established. Polymers with different molecular structures were chosen to investigate their adsorption by total organic carbon, zeta potential tests and their retardation effects by isothermal calorimetry, and eventually the working mechanisms of various chemical admixtures involving adsorption, hydration and rheology were elucidated. Based on the microstructure observation and the working mechanisms, a generic multi-scale microstructure model of FCPs was proposed. Furthermore, two models were developed by introducing a relative hydration degree α' to describe the evolution of the rheological parameters, and two equations with incorporation of the above important influencing factors were deduced to quantitatively reflect the correlation of microstructure with the key rheological parameters of FCPs, which can roughly predict the yield stress and the plastic viscosity of FCPs. In addition, the impacts of these admixtures on the pore structure of hardened cement pastes (HCPs) and the impermeability of hardened cement mortars were also discussed from the viewpoint of microstructure in the fresh state of cement pastes.

Based on the experimental results, the main conclusions can be drawn as below:

1. **Rheological Properties of FCPs in the Presence of the Chemical Admixtures**

   (1) Cement-Superplasticizer-Water system

   The initial fluidity of the FCPs rises linearly with the increase of Sp/C and reaches to a maximum value at a critical dosage. Beyond the critical dosage, the initial fluidity is scarcely affected by the further addition of superplasticizers. The maximum fluidity increases with the increased W/C in FCPs and reaches a maximum value at the W/C of 0.35, whilst the critical dosage shows a declining trend with the growth of W/C. On the other hand, the fluidity retention over elapsed time is enhanced by adding superplasticizers due to their retardation effects. Compared to the FCPs with NSF superplasticizer, the pastes with PCE superplasticizer present higher initial fluidity and stronger fluidity retention.

   A higher temperature generally leads to a sharper drop in the initial fluidity and the fluidity retention of FCPs over elapsed time. At high Sp/C or W/C, the impacts of temperature on the initial fluidity and the fluidity retention are weakened.

   Yield stress and plastic viscosity, the two key parameters of the rheological properties of FCPs, show similar variation trends to the fluidity under different influencing factors.

A microrheology analyzer was adapted to in situ follow the development of viscoelastic properties of FCPs for the first time. Results indicate that rheological behavior of FCPs transforms from a slightly liquid-like behavior to a strongly solid-like behavior in the first minutes due to the establishment of the "network structure". The incorporation of PCE superplasticizer significantly weakens the elastic feature of the FCPs due to its effects of improving the dispersion of cement grains and retarding cement hydration. The effects of superplasticizer are more pronounced at lower water to cement ratio.

(2) Cement-Latex-Water system

With the incorporation of polymer latexes in the FCPs, the initial fluidity of pastes declines at first and then increases to the maximum values at the critical dosage of polymer latexes. The maximum initial fluidity is respectively achieved at 9% L1 and 12% L2. Beyond the critical dosages, the further addition of latex particles leads to a decrease of the initial fluidity due to the filling effects of polymer latexes. On the other hand, a higher dosage of latexes is beneficial to the fluidity retention of FCPs. Compared to the FCPs with latex L2, the ones with latex L1 show a larger initial fluidity and a stronger fluidity retention.

At elevated temperatures, the initial fluidity and the fluidity retention for all the FCPs containing latexes are decreased in most circumstances. The impacts of temperature on the initial fluidity are strengthened as the dosage of L1 is increased. By contrast, for the FCPs with latex L2, the impacts of temperature on initial fluidity are weakened at high dosages. The effects of temperature on the fluidity retention of FCPs are obviously reduced at larger L/C.

(3) Cement-Asphalt-Water system

The initial fluidity of CA pastes reaches maximum at asphalt dosage of 20%. When A/C is larger than 20%, the initial fluidity of CA pastes starts to decrease. Moreover, the fluidity retention of the CA pastes over time is visibly improved with the increase in asphalt content. Compared with the cationic asphalt emulsion, anionic asphalt emulsion more strongly increases the initial fluidity and the fluidity retention of the CA pastes because of its favorable adsorption onto cement surface and greater retardation effect. The variation trends of yield stress are compatible with those of the fluidity of CA pastes.

An elevated temperature results in a lower initial fluidity and weaker fluidity retention of CA pastes. The effects of temperature on the initial fluidity are weakened at high A/C. For the CA pastes with anionic asphalt emulsion, a higher asphalt content leads to a lower temperature effect on the fluidity retention. For the CA pastes containing cationic asphalt emulsion, an increase in asphalt content leads to a strong temperature effect because of its instability at high temperatures.

2. **Mesostructure of FCPs in the Presence of the Chemical Admixtures**
The changes on the microstructures of pastes directly reflect the effects of chemical admixtures on the rheological properties of FCPs. The structural parameters including particle size, granular shape and fractal dimension of spatial distribution (Dpd) were used to quantitatively characterize the organization of cement grains in varied media at a mesoscopic scale and to establish the correlation of mesostructure with rheological properties. Specifically, higher fluidity corresponds to larger Dpd and circularity as well as a lower mean particle size. Moreover, mean particle size and Dpd are more sensitive to the change of the fluidity of FCPs.

   (1) Cement-Superplasticizer-Water system
   The addition of superplasticizers in the cement suspensions evidently diminishes the amount and size of flocculated structures of cement grains. That means that a higher Sp/C corresponds to a lower mean particle size and a larger circularity and Dpd. According to the level of difficulty to be disassembled, the flocculated structures can be roughly sorted into three classes from easy to difficult order, i.e., cluster I, II, and III, corresponding to S-S structures, L-M-S structures and L-L structures respectively. Compared to NSF superplasticizer, PCE superplasticizer with stronger dispersing capability facilitates the disassembly of strongly bonded flocculated structures (L-L structures).

   (2) Cement-Latex-Water system
   In the presence of 3% L1, separated cement grains with clear edges and hard corners, and a small amount of flocculated structures are found. By contrast, the addition of 3% L2 leads to the formation of a large amount of flocculated structures. With the growth of L/C, the latex particles fill in the pores between the cement grains besides being adsorbed on cement surface. Compared to L2, L1 more significantly strengthens the dispersion degree of cement grains.

   (3) Cement-Asphalt-Water system
   In the case of the FCPs containing asphalt particles of microns, the flocculated structures are broken into small pieces and asphalt emulsion is uniformly distributed in the continuous cement paste at low A/C (<35%). With the increment of A/C, asphalt emulsion functions as the continuous phase and enwraps all the cement grains. With the progressing cement hydration, the agglomeration of asphalt particles including adsorption onto the cement surface, packing and condensation, and the formation of a partly continuous asphalt membrane wrapping around the cement grains are clearly observed.

3. **Mechanisms of Chemical Admixtures for Modifying Rheological Properties**
The adsorption of organics on cement surface is closely related to both the charge density of organics and the entropic loss upon adsorption, whilst the driving forces of adsorption mainly lie in the electrostatic attractive forces and chelating effects. Specifically, in the premise of the same dosage of charging groups, organic monomers AA, SSS and MAPTAC do not show visible adsorption on cement surface and thus exert scarce influences on cement hydration. By contrast, their corresponding homo-polymers PAA, PSSS and PMAPTAC can be adsorbed on cement surface to different extents. The adsorption amounts of anionic polymers are higher than that of cationic polymer because of the dominant positive charges on cement surface, and the adsorption ratio of PAA is larger than that of PSSS due to the complexation effect of $-COO^-$ with Ca^{2+}. Their retardation effects on cement hydration are in the order of PAA > PSSS > PMAPTAC. Similarly, for the comb-shaped co-polymers, the charge characteristics of the main chain also strongly determine their adsorption behaviors and retardation effects, in the order of $-COO^- > -SO_3^- > \equiv N^+-$.

   (1) Cement-Superplasticizer-Water system
   NSF exhibits a typical mono-layer adsorption on cement surface, which enhances the fluidity of FCPs and retards cement hydration by covering on cement surface. A larger coverage ratio of NSF on cement surface leads to higher initial fluidity and a lower hydrating rate. After full coverage, namely the saturation of the adsorption on cement grains, the initial fluidity of FCPs and the fluidity retention reach the maximum.
   PCE presents a multi-layer (double-layer) adsorption on cement surface. At high W/C, the increase of the initial fluidity of FCPs with PCE is solely proportional to the surface coverage of the first adsorption layer and the second layer does not contribute to the fluidity of FCPs. At low W/C, more adsorbed PCE molecules are required to disassemble the flocculated structures and increase the initial fluidity. Both the adsorbed PCE and the PCE remaining in the aqueous phase actively participate in retarding cement hydration. A higher superplasticizer dosage leads to a lower hydration rate and thus stronger fluidity retention of FCPs.

   (2) Cement-Latex-Water system
   At low dosage of latexes (<3%), the initial fluidity decreases with the adsorption of polymer particles on cement surface due to their neutralizing effects. With further addition of latexes, more coverage of latex particles on cement surface brings about better dispersion state of cement grains and higher initial fluidity of FCPs. Moreover, the presence of latexes in the pastes brings about significant retardation on cement hydration and thereby stronger fluidity retention of FCPs. Compared to L2, L1 with smaller size could effectively increase the initial fluidity and the fluidity retention of FCPs due to its larger adsorption amount on cement surface.

(3) Cement-Asphalt-Water system
The adsorption and coverage of asphalt particles on cement surface lead to an increment of initial fluidity. However, the initial fluidity starts to decrease due to the increased volume fraction of the solid phases. The fluidity retention of the CA pastes over time visibly improves with the increase in asphalt content due to the retardation effects on cement hydration. In comparison to the cationic asphalt emulsion, anionic asphalt emulsion more strongly increases the fluidity of the CA pastes and retards cement hydration because of its favorable adsorption onto the surface of cement grains.
The effects of temperature on the initial fluidity of Cement-Chemical admixtures-Water systems are closely related to the adsorption amount of chemical admixtures on cement surface. Specifically, a larger adsorption amount at elevated temperatures weakens the temperature effects. The impacts of temperature on the fluidity retention are determined by cement hydration in Cement-Superplasticizer-Water system. For the other two systems, both the cement hydration and the stability of latexes or asphalt emulsions are responsible for temperature effects on fluidity retention.

4. **Microstructure Model and Rheological Model of Fresh Cement Pastes**
A generic multi-scale microstructure model of FCPs at varied dosages of PCE and water to cement ratios was established based on the microstructure of cement suspensions and the working mechanism of superplasticizer, in which the contents of different types of water, including free water (FW), adsorption water (AW) and entrapped water (EW) in FCPs, were calculated. The maximum volume of AW and remaining EW in the strongly bonded flocculated structures (V_{AW+REW}) is 0.03. The maximum volume of entrapped water V_{EEW} that could be released by PCE used in this research is 0.40, which is in positive proportion to the dispersing capability of superplasticizers.
By introducing a relative hydration degree α', two models were developed to describe the evolution of the rheological parameters, which integrated the effects of mix proportions, elapsed time and environmental temperature on the rheological properties.

$$\frac{\tau_0(W/C, Sp/C, t, T)}{\tau_0(W/C, Sp/C, 0, T)} = \frac{1}{1-\alpha'} \ln \frac{\mu_p(W/C, Sp/C, t, T)}{\mu_p(W/C, Sp/C, 0, T)} = [\mu]\phi_M \ln(1-\alpha').$$

The evolution models of rheological parameters are concerned with the rheological properties of FCPs from the beginning of water-cement contact to the initial setting. In particular, when it is close to the setting time, the deflection of rheological models is increased due to the more significant effects of microstructure and the interactions between particles on rheological parameters. In addition, two equations incorporating Sp/C, W/C, ambient temperature and time as variables were developed to roughly predict the yield stress and the plastic viscosity of FCPs, in which the constants are obtained on the basis of the experimental data of FCPs at low Sp/C. More efforts to put the models into application are underway.

5. **Pore Structure and Impermeability of Hardened Cement Pastes**

(1) Cement-Superplasticizer-Water system
The effects of PCE superplasticizer on the pore structure are associated with W/C and curing age of cement pastes. At W/C of 0.29, an increasing superplasticizer dosage results in obvious declines in total pore volume at early ages and reduces pore connectivity. By contrast, an increase in total pore volume and higher pore connectivity are found when PCE is incorporated in the paste at W/C of 0.4. Moreover, the inclusion of PCE brings about a denser structure and enhanced impermeability of hardened mortars. It is believed that the enhanced impermeability is related to the reduced interfacial heterogeneity and the compacted interfacial zone when PCE is added.

(2) Cement-Latex-Water system
The addition of polymer latexes reduces the size and connectivity of capillary pores in HCPs due to both their plasticizing effects and filling effects. Meanwhile, C-S-H gel pore volume presents an obvious drop due to the retardation effects of polymer latexes on cement hydration, especially at early age. At low L/C (<3%), adding polymer latex has little effect on the impermeability. Further addition of polymer latexes leads to a significant enhancement in the impermeability. It is believed that the filling effects play a dominant role in increasing the impermeability when the dosages of latexes are high. At the same L/C, latex L1 with smaller particle size is more effective in reducing the pore size and enhancing the impermeability than L2 because of its better plasticizing effects.

(3) Cement-Asphalt-Water system
For cement mortars with asphalt emulsions, the impermeability is modified due to the combined effects of plasticizing and filling. At high asphalt dosages, filling effects play significant roles due to the particle size of micron of asphalt particles. At the same asphalt content, CAMs with anionic asphalt emulsion show stronger impermeability than those with cationic one because of the superior plasticizing effect of anionic asphalt emulsion.

8.2 Contribution to Knowledge

This work has presented the microstructure and rheological properties of Cement-Chemical admixtures-Water dispersion system. With achievement of the main research aim, the research has made the following original contributions to the knowledge in the field:

(1) The research has provided detailed and comprehensive analysis on the impacts of crucial influencing factors including W/C, Sp/C, T and t on the rheological behaviors of FCPs through the studies on the microstructure of FCPs and the interactions between chemical admixtures and cement grains. Two equations incorporating these influencing factors as variables were developed to roughly predict the yield stress and the plastic viscosity of FCPs, which reflect the correlation of microstructures with the key rheological parameters of FCPs.
(2) For the first time, Morphologi G3 was adopted to in situ identify and differentiate the structural organization of cement grains in suspensions by providing high-quality images and structural parameters. Three structural parameters including particle size, circularity and fractal dimension of particle spatial distribution allow to quantitatively characterize the organization of cement grains in suspensions at a mesoscopic scale, through which the relationship between the mesostructure and the rheological behavior of FCPs was established.
(3) The adsorption behaviors of polycarboxylate polymers with different functional groups and their effects on cement hydration were elucidated. This is expected to bring novel insights into the influences of PCE superplasticizers on cement hydration and to lay a theoretical basis for the development of new superplasticizers with more efficient and robust performance.
(4) This research reveals how the working mechanism of NSF differs from that of PCE superplasticizers, which improves and enriches the current theory of working mechanisms of chemical admixtures in FCPs.
(5) A generic microstructure model was developed based on the microstructure observation and the working mechanisms of chemical admixtures. The relative hydration degree was introduced to indicate the evolution of rheological properties, based on which, two models were developed to indicate the coupled effects of the temperature and elapsed time on rheological properties.
(6) This research confirms that a non-disturbing measurement provided by the microrheology analyzer is a novel and powerful technique to in situ follow the development of the viscoelastic properties of fresh cement pastes, which provides abundant information about the rheological properties as well as the viscoelastic properties of the FCP samples. Information of cement hydration and setting of FCPs could also be obtained by following the evolution of those parameters provided by the microrheology analyzer. In addition, the impacts of chemical admixtures, including viscosity modifier and superplasticizer on properties of FCPs could be easily investigated with this method. Compared to the traditional rheology testing methods, the most important advantages of this method are non-disturbing and easy operation.

8.3 Limitations and Recommendations for Future Work

In this research, several research gaps in existing knowledge have been closed, but there is an opportunity to extend some of topics to the more general area of cementitious materials with chemical admixtures. Specifically, future works in the following areas could be further conducted:

(1) This research only focuses on the rheological properties of fresh cement pastes. However, cement mortars and concrete are much more widely used in practice. The impacts of chemical admixtures, temperature and elapsed time on the rheology of mortars and concrete require a further investigation.
(2) In this research, all the fresh cement pastes were regarded as Bingham fluids and the effects of chemical admixtures on the fluid types were neglected. Further studies to explore the relationship of shear stress and shear rate of cementitious materials in the presence of chemical admixtures could be conducted.
(3) The impacts of $-COO^-$, $-SO_3^-$ and $\equiv N^+-$ on adsorption and retardation behaviors of polymers have been elucidated in this research. The investigation on other functional groups, such as phosphate groups and silanes, could be a possibility for future research.
(4) The interactions between particles in solid-liquid dispersion system have significant effects on plastic viscosity, which were not considered in the K-D equations, so that evident deflections were found in the evolution model of plastic viscosity. This suggests that it would be valuable to choose or even establish a reasonable viscosity model in the future research in order to accurately simulate the changes of rheological properties over elapsed time.
(5) In the two rheological models, only the data of cement pastes with low Sp/C were used since a higher superplasticizer dosage generally brings about obvious deflections on the volume fraction due to the effects of adsorption rate of PCE as well as their interactions. Although the mechanism reflected in the models should be universal, there is still a possibility to further adjust the mechanism based on more findings in real-case studies.

Appendix A
Typical Morphology of Particles in C-E System

Y. Zhang, *Study on Microstructure and Rheological Properties of Cement-Chemical Admixtures-Water Dispersion System at Early Stage*, Springer Theses, DOI 10.1007/978-981-10-4570-7

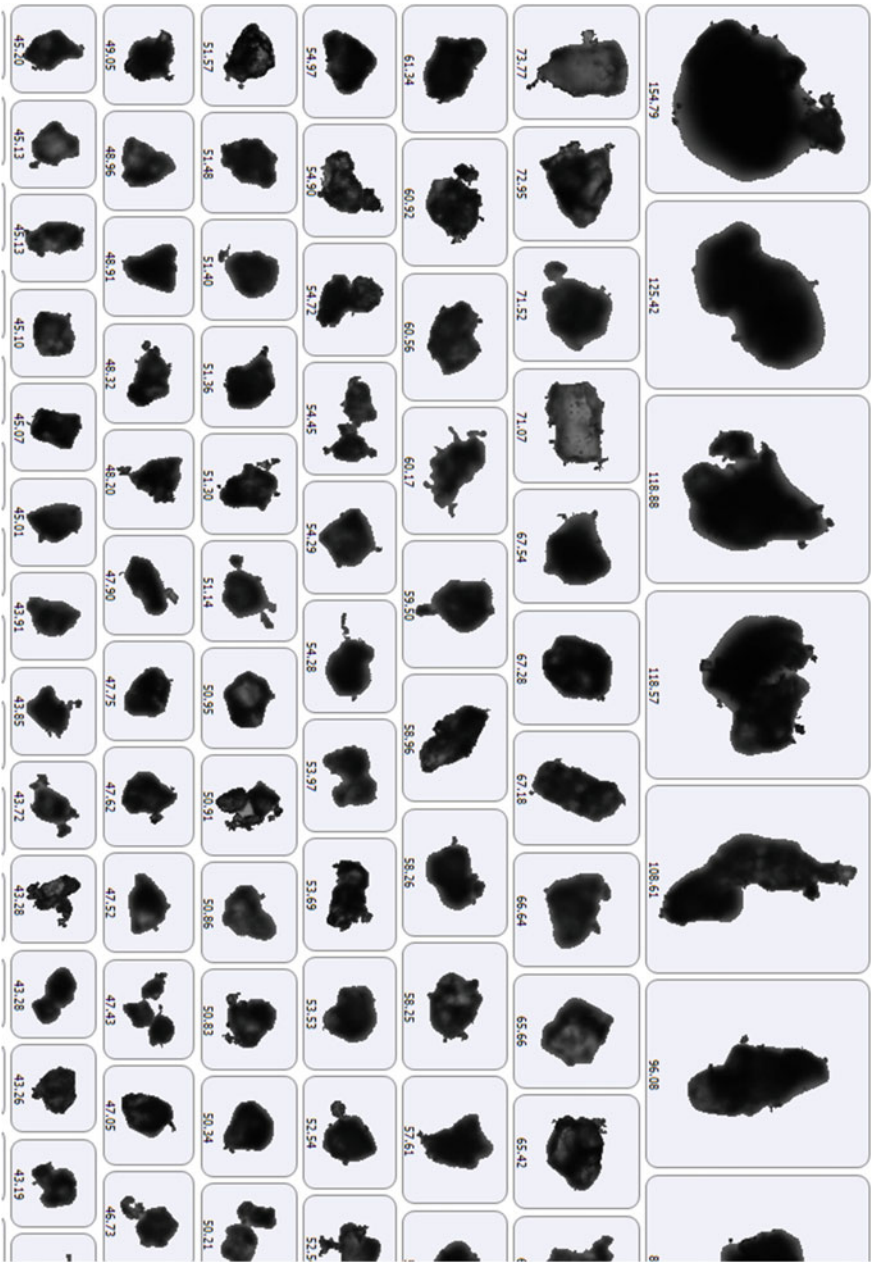

Appendix B
Typical Morphology of Particles in C-W System

Y. Zhang, *Study on Microstructure and Rheological Properties of Cement-Chemical Admixtures-Water Dispersion System at Early Stage*, Springer Theses, DOI 10.1007/978-981-10-4570-7

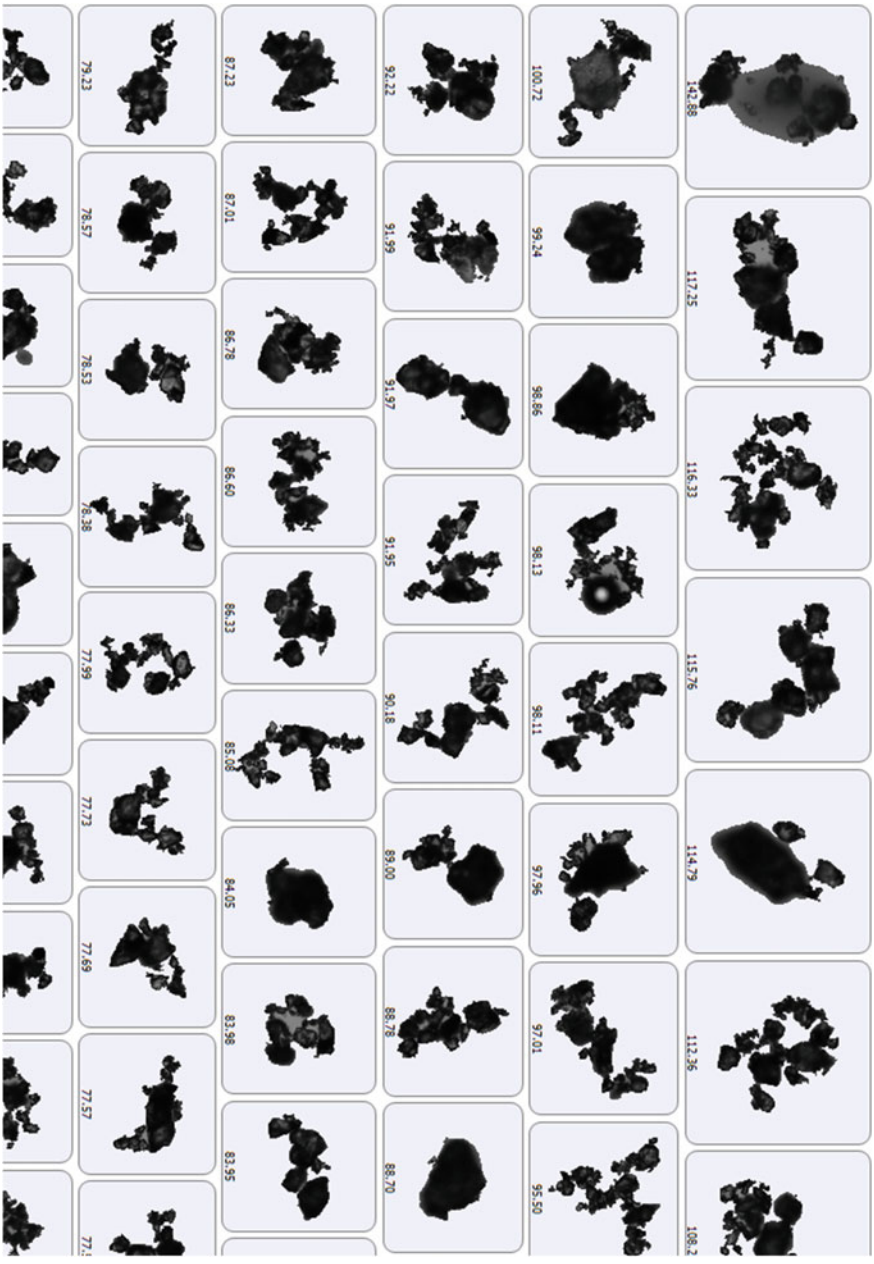

Appendix C
Typical Morphology of Particles in C-EW System

Y. Zhang, *Study on Microstructure and Rheological Properties of Cement-Chemical Admixtures-Water Dispersion System at Early Stage*, Springer Theses, DOI 10.1007/978-981-10-4570-7

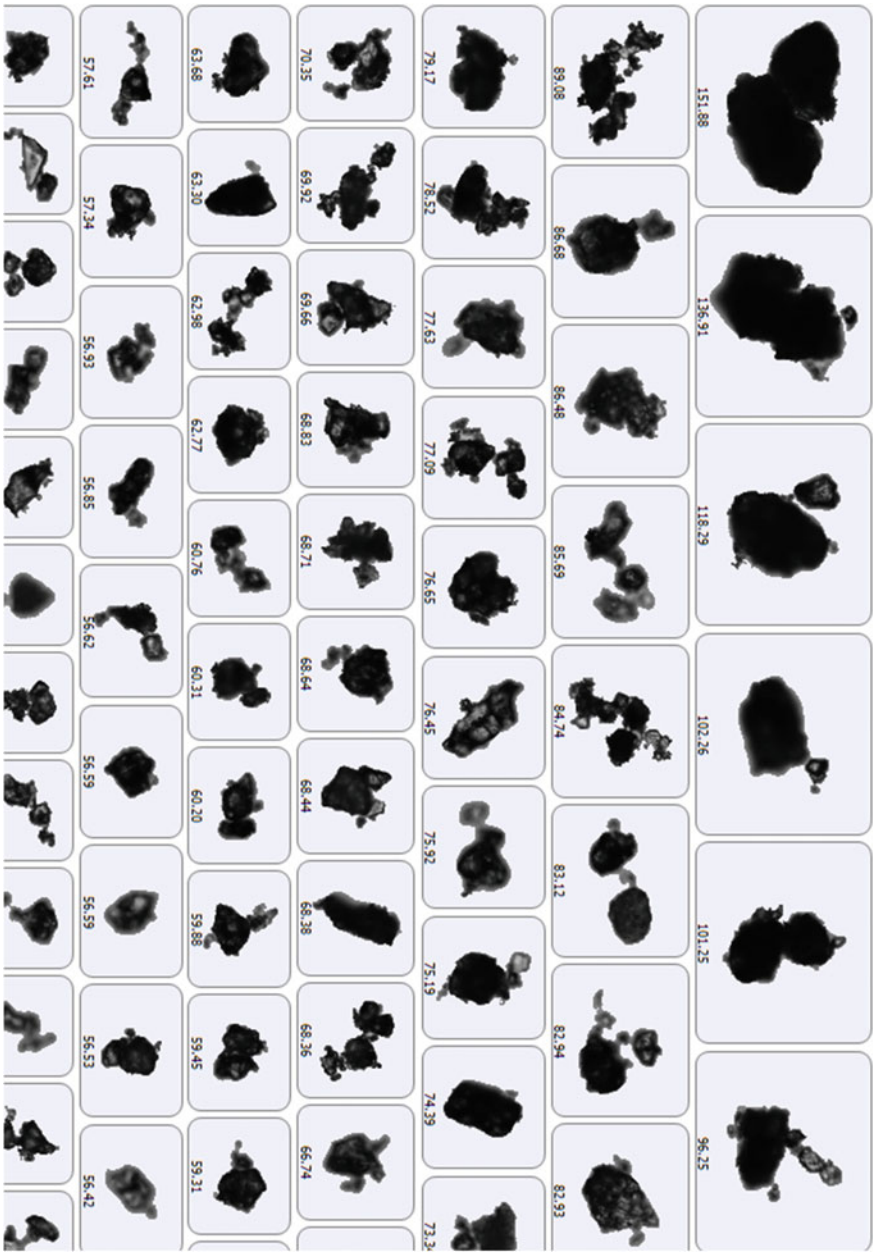

Appendix D
Typical Morphology of Particles in C-E + C-W System

Y. Zhang, *Study on Microstructure and Rheological Properties of Cement-Chemical Admixtures-Water Dispersion System at Early Stage*, Springer Theses, DOI 10.1007/978-981-10-4570-7

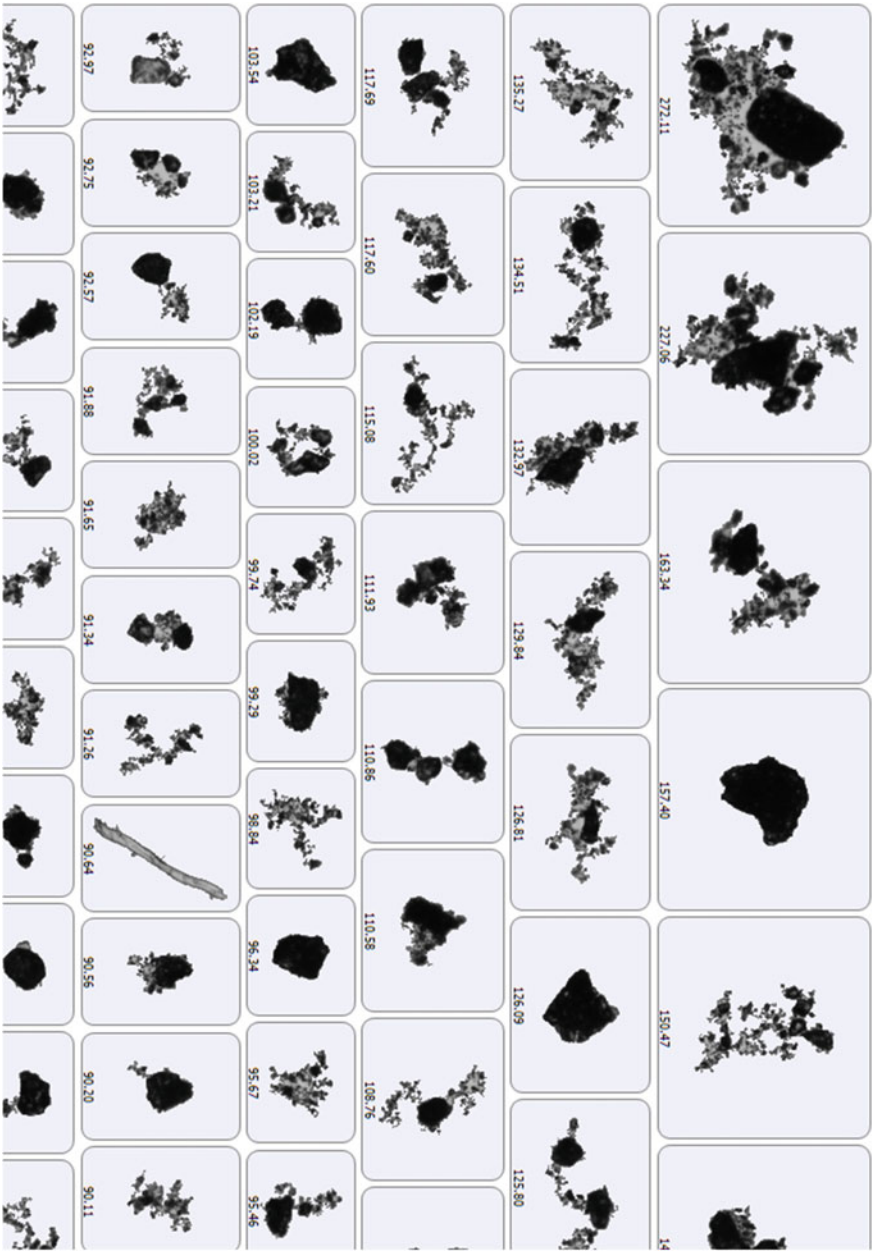

Appendix E
Typical Morphology of Particles in C-W-P0.1 System

Y. Zhang, *Study on Microstructure and Rheological Properties of Cement-Chemical Admixtures-Water Dispersion System at Early Stage*, Springer Theses, DOI 10.1007/978-981-10-4570-7

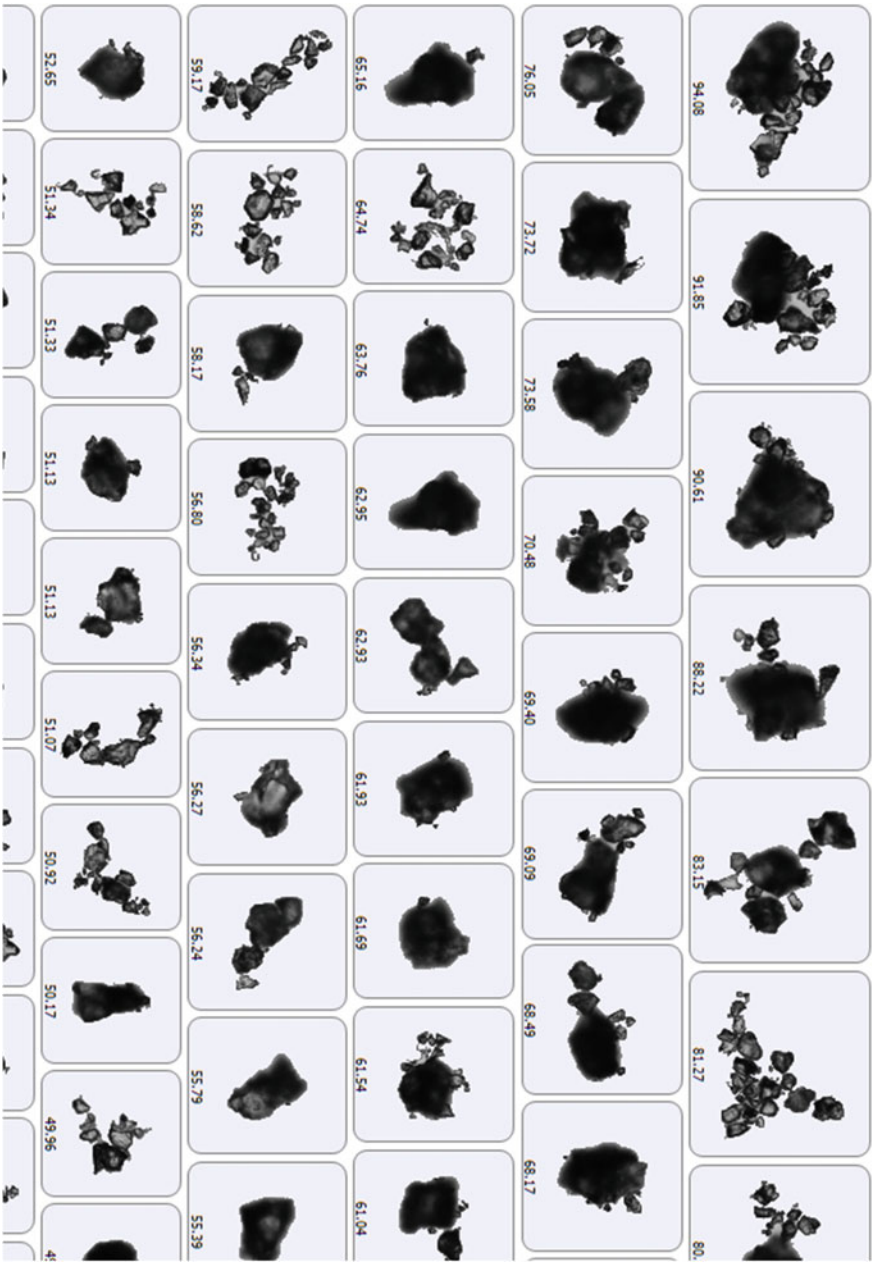
94.08
91.85
90.61
88.22
83.15
81.27
80.
76.05
73.72
73.58
70.48
69.40
69.09
68.49
68.17
65.16
64.74
63.76
62.95
62.93
61.93
61.69
61.54
61.04
59.17
58.62
58.17
56.80
56.34
56.27
56.24
55.79
55.39
52.65
51.34
51.33
51.13
51.13
51.07
50.92
50.17
49.96

Appendix F
Typical Morphology of Particles in C-W-P0.3 System

Y. Zhang, *Study on Microstructure and Rheological Properties of Cement-Chemical Admixtures-Water Dispersion System at Early Stage*, Springer Theses, DOI 10.1007/978-981-10-4570-7

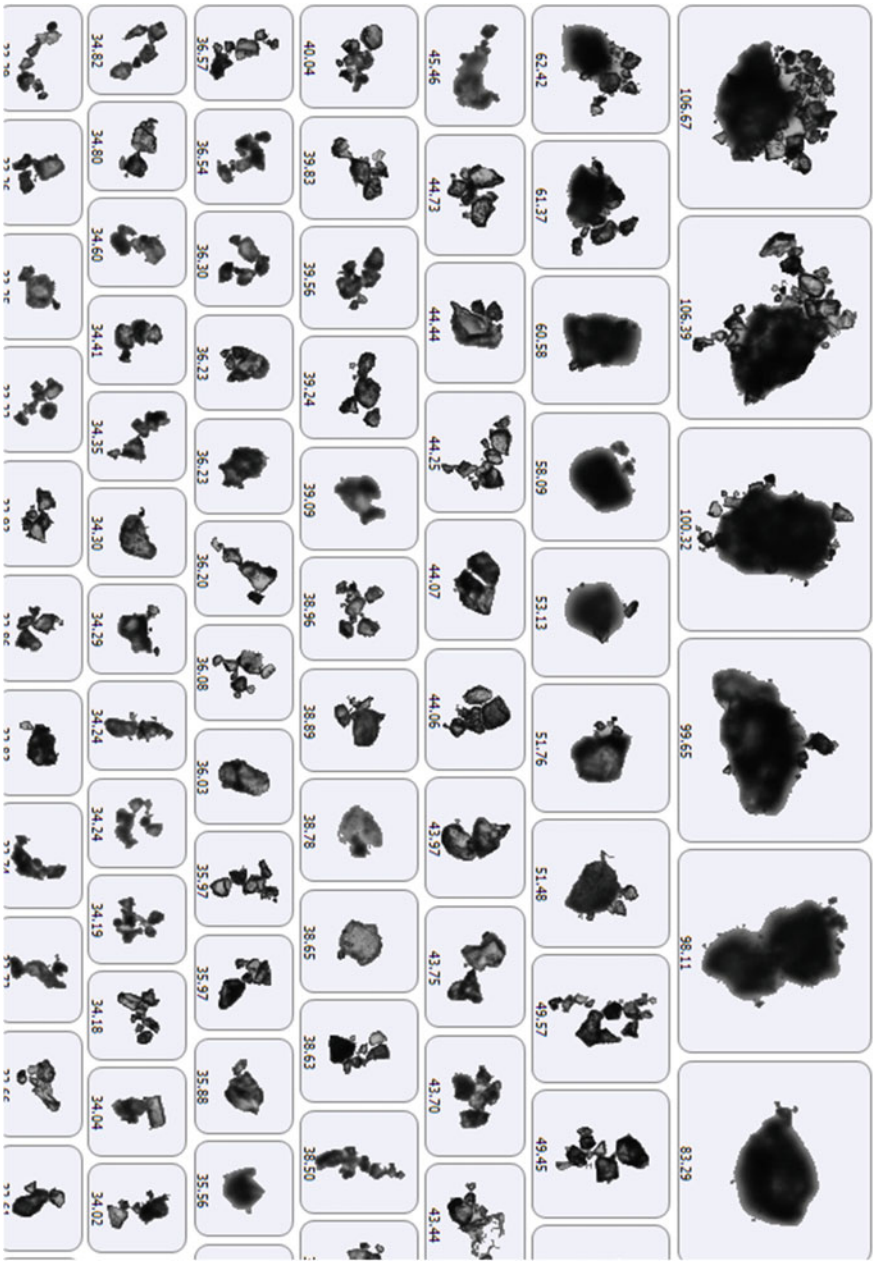

Appendix G
Typical Morphology of Particles in C-W-P0.5 System

Y. Zhang, *Study on Microstructure and Rheological Properties of Cement-Chemical Admixtures-Water Dispersion System at Early Stage*, Springer Theses, DOI 10.1007/978-981-10-4570-7

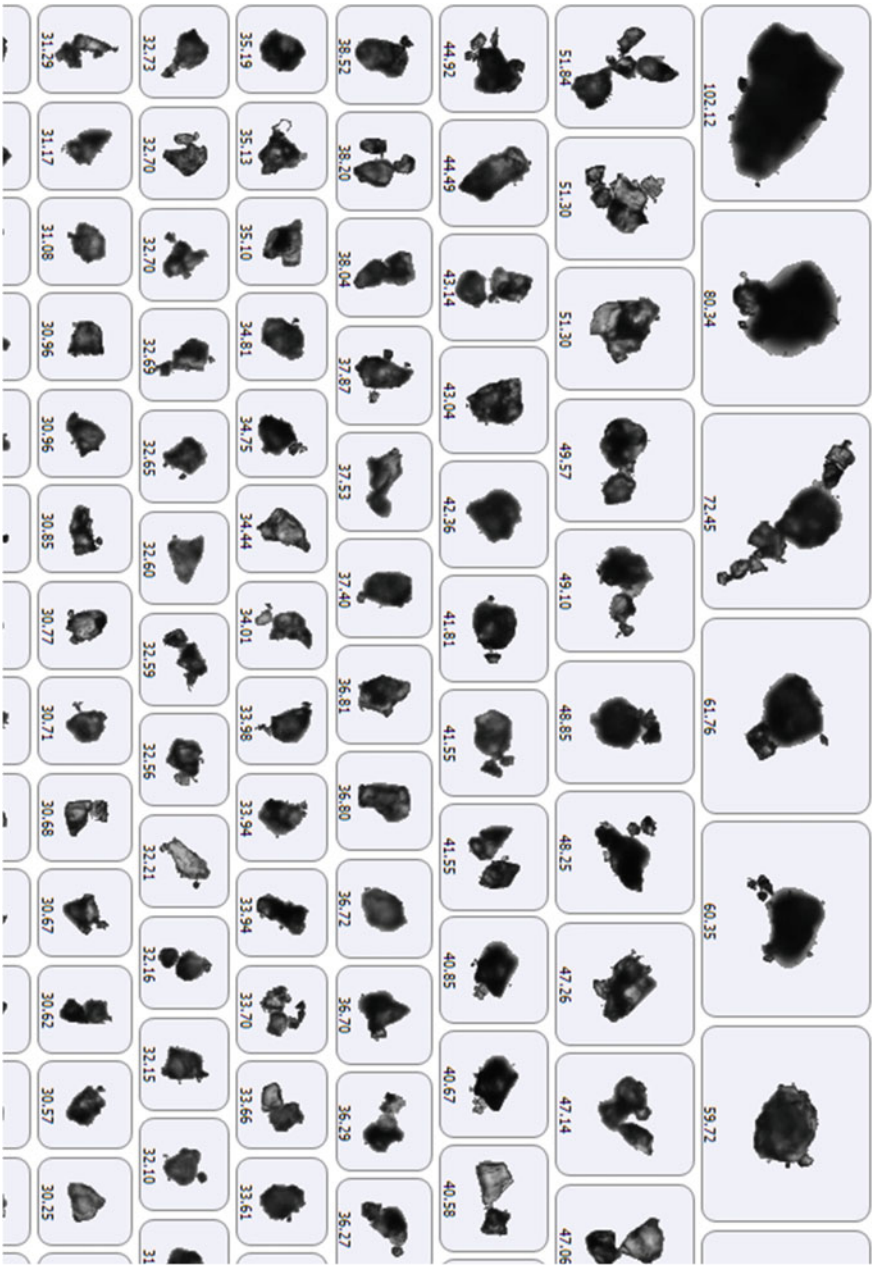

Appendix H
Typical Morphology of Particles in C-W-N0.5 System

Y. Zhang, *Study on Microstructure and Rheological Properties of Cement-Chemical Admixtures-Water Dispersion System at Early Stage*, Springer Theses, DOI 10.1007/978-981-10-4570-7

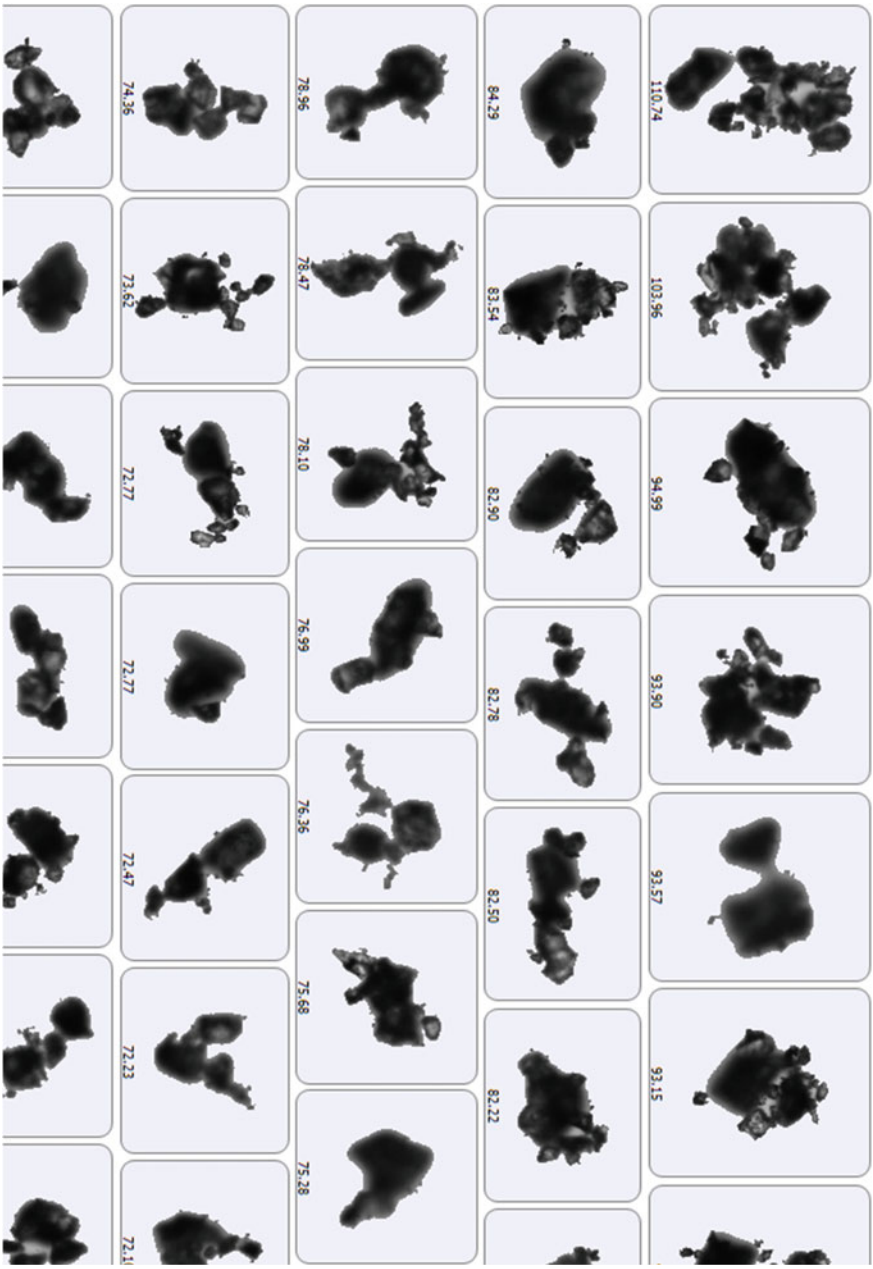
110.74
103.96
94.99
93.90
93.57
93.15
84.29
83.54
82.90
82.78
82.50
82.22
78.96
78.47
78.10
76.99
76.36
75.68
75.28
74.36
73.62
72.77
72.77
72.47
72.23